# Studies of Orientationally-Disordered Organic and Inorganic Molecular Solids

by

Ralph Michaël Paroli

*A thesis submitted to the Faculty of Graduate Studies and Research in partial fulfillment of the requirements for the degree of Doctor of Philosophy*

Department of Chemistry
McGill University
Montreal, Quebec, Canada

October 1988

63 characters

short title

Studies of Orientationally-Disordered Solids (Plastic Crystals)

*To my greatest fans:*

*My Parents*

## Abstract

The phase transitions of some orientationally-disordered solids (plastic crystals) have been studied by DSC, and variable-temperature-IR and -Raman spectroscopy. The adamantane derivatives, 1-bromoadamantane (1-$C_{10}H_{15}Br$) and 2-chloroadamantane (2-$C_{10}H_{15}Cl$) were found to have two phase transitions, at 283 K and 312 K for the former and 227 K and 242 K for the latter; 2-bromoadamantane (2-$C_{10}H_{15}Br$) and 1-chloroadamantane (1-$C_{10}H_{15}Cl$) only exhibited one phase transition each, at 281 K and 245 K, respectively. Only one phase transition was found for 9-bicyclononanone (9-$C_9H_{14}O$) at 299 K. Oxanorbornane ($C_6H_{10}O$), a liquid, was found to have three phase transformations (192, 234, and 245 K), with the 234 K transition being metastable. Another phase transition, which is both time dependent and rate-of-cooling dependent, was found for *o*-carborane (*o*-$C_2B_{10}H_{12}$) by variable-temperature infrared spectroscopy. The infrared and Raman spectra of the adamantane derivative, 2-adamantanone (2-$C_{10}H_{14}O$), revealed that a new low-temperature phase was present after cycling.

Micro-Raman pressure spectroscopy was used for the first time in the study of phase transitions of plastic crystals. The same phase transformation of 1-chloroadamantane that occurred at 245 K and 1.0 bar was found to occur at 295 K and ~5 kbar. The *o*-carborane phase transition which took place at 274 K and 1.01 bar also takes place at 295 K and ~10 kbar. Finally, 2-chloroadamantane, which exhibited two phase transitions (227 K and 242 K) at atmospheric pressure, also underwent phase transformations at room temperature and 3 and 11 kbar, respectively.

## Résumé

Les transitions de phase de certains cristaux plastiques ont été étudiées par calorimétrie différentielle programmée (CDP) ainsi que par spectroscopie vibrationnelle (spectroscopie infrarouge et Raman). Deux transitions de phase ont été trouvées pour les dérivés de l'adamantane, bromure-1-adamantane (1-$C_{10}H_{15}Br$) et chlorure-2-adamantane (2-$C_{10}H_{15}Cl$), soit 283 K et 312 K pour 1-$C_{10}H_{15}Br$, et 227 K et 242 K pour 2-$C_{10}H_{15}Cl$. Une seule transformation de phase a été trouvée pour le bromure-2-adamantane (2-$C_{10}H_{15}Br$) à 281 K et le chlorure-1-adamantane, 1-$C_{10}H_{15}Cl$, à 245 K. Il a aussi été démontré que le bicyclononanone-9 (9-$C_9H_{14}O$) n'avait qu'une transition de phase et ce à 299 K. Trois transformations de phase ont été trouvées pour le liquide oxanorbornane ($C_6H_{10}O$), une à 192 K, une autre à 234 K (phase métastable), et la dernière à 245 K. Une autre transition de phase, qui varie selon le taux de chauffage, a été trouvée pour l'*o*-carborane par infrarouge à température variable. Les spectre vibrationnels de l'adamantanone-2, ont démontré qu'après le cyclage, une nouvelle phase existait à basse température.

La spectroscopie sous-pression micro-Raman a été utilisée pour la première fois à fin d'étudier les transitions de phase des cristaux plastiques. La même phase qui était présente à 245 K et 1.01 bar pour le 1-$C_{10}H_{15}Cl$ est aussi présente à 295 K et ~5 kbar. Pour l'*o*-$C_2B_{10}H_{12}$, la transition de phase à 274 K et 1.01 bar se produit à 295 K et ~10 kbar. Finalement, deux transition de phase ont été trouvées pour le dérivé 2-$C_{10}H_{15}Cl$, à température ambiante et 3 kbar ainsi qu'à 11 kbar.

## Acknowledgements

I would like to express my heartfelt thanks and gratitude to Dr. Ian S. Butler for his support and guidance while under his supervision for this PhD project.

I would also like to thank Dr. D. F. R. Gilson for his criticisms throughout this project. I wish to thank Drs. J. F. Harrod, J. J. Hogan, and A. G. Shaver for their interest and suggestions given during the annual Inorganic Division Reviews.

I also wish to thank:

- Dr. H. B. R. Cole for her introducing me to the variable-temperature infrared and Raman technique, as well as for her continuing encouragement.
- Dr. G. Lord for his aid in the pressure work, Dr. V. Benham for the pictures of the diamond-anvil-cell, and Ms. N. T. Kawai for her assistance on the 2-chloroadamantane project.
- Messrs. A. Kluck, R. Gaulin, B. Bastian, and G. di Ridolfo for their technical assistance with regards to the instrumentation used in this thesis.
- Dr. D. G. Peters of Analect for permission to use the AQS-18 FT-IR spectrometer diagram.
- Mr. R. Trincinelli of Instruments S. A. for the authorization to use the schematic diagrams of the J.-Y. Ramanor U-1000 Raman spectrometer.
- The office staff, Ms. C. Brown, A. Charade, R. Charron, G. Clarke, J. Heaton, P. Hénault, and C. Marotte, for always providing me with help and assistance when needed.
- My laboratory co-workers, Ms. M. Doyon, Ms. J.-P. Gao, Mr. J. Haines, Mr. Y. N. Huang, Ms. D. Lafleur, Ms. H.-Q. Li, Dr. I. Wharf, and Mr. Z.-H. Xu, for the interesting discussions.

- My co-workers at C.N.R.C.-I.G.M. division, Dr. J.-J. Hechler, Mr. J. B. Boulanger, Dr. K. C. Cole, Dr. D. Noël, and the late Dr. C. P. Vijayan, for giving me the opportunity to work with them over the last five years, and for the use of the SETARAM differential scanning calorimeter.
- The governments of Canada and Quebec for financial support (N.S.E.R.C., and F.C.A.R.), McGill University for the McGill Special Fellowship, and the Chemistry Department for the T. S. Hunt awards.

I wish to express my gratitude to Ms. Haewon L. Uhm for the fruitful discussions and her constant help during the last two years. I also wish to thank Ms. D. C. Maher for her help with PC-MODEL and for her humour.

Last, but not least, I wish to express my deepest gratitude and appreciation to my Parents for their continuous support and encouragement throughout all these years.

## Note on Units

As specified in the *Guidelines Concerning Thesis Preparation*, from the Faculty of Graduate Studies and Research, the use of SI units must be used except when for historical reasons or for reasons of clarity other units are preferrable. This thesis utilizes units which are generally used by other researchers in the same field. The following table is therefore given for the benefit of the readers which prefer using SI units at all times.

| Parameter | Symbol | SI Unit | Other Units |
|---|---|---|---|
| Wavelength | $\lambda$ | m | $10^{10}$ Å |
| Pressure | P | Pa (N $m^{-2}$) | $10^{-2}$ kbar<br>$9.8692 * 10^{-6}$ atm<br>$7.5006 * 10^{-3}$ mm Hg<br>$1.0206 * 10^{-2}$ lb $in^{-2}$ |
| Temperature | T | K | $^{o}C + 273.15$ |
| Wavenumber | $\nu$ | $m^{-1}$ | 100 $cm^{-1}$ |
| Enthalpy | $\Delta H$ | kJ $mol^{-1}$ | 0.239 kcal $mol^{-1}$ |
| Entropy | $\Delta S$ | J $K^{-1}$ $mol^{-1}$ | 0.239 cal $deg^{-1}$ $mol^{-1}$ |

## Table of Contents

# CHAPTER 1
# ORIENTATIONALLY-DISORDERED SOLIDS (PLASTIC CRYSTALS)

## A. INTRODUCTION

Solids are usually thought of as materials that are not easily deformed and possessing very little internal molecular motion. Furthermore, a high entropy of fusion is expected upon melting a solid. This is not always the case, however, as some molecules undergo almost complete free rotation and are even known to self-diffuse to nearly the same extent as liquids. Although, Timmermans[1,2] was not the first to realize that molecules might rotate in the solid state, he was the first to notice some interesting trends in the physical properties of certain globular organic compounds. These molecules are highly symmetric and have very small entropies of fusion. Moreover, although they have very sharp melting points, the solid phases are not crystalline, and flow under moderate pressures. All of these observations prompted Timmermans to name this group of "molécules globulaires", ***plastic crystals***.[1-3] These materials are definitely not liquids nor are they true solids; they are somewhere in between and therefore this additional solid phase has become known as the ***plastically-crystalline*** phase or state. Figure 1.1 shows the different phases that can appear in a regular solid, a plastic crystal, and a liquid crystal. The main distinction between solids and liquids can be considered in terms of viscosity - low for liquids, higher for orientationally-disordered solids and very high for normal solids.

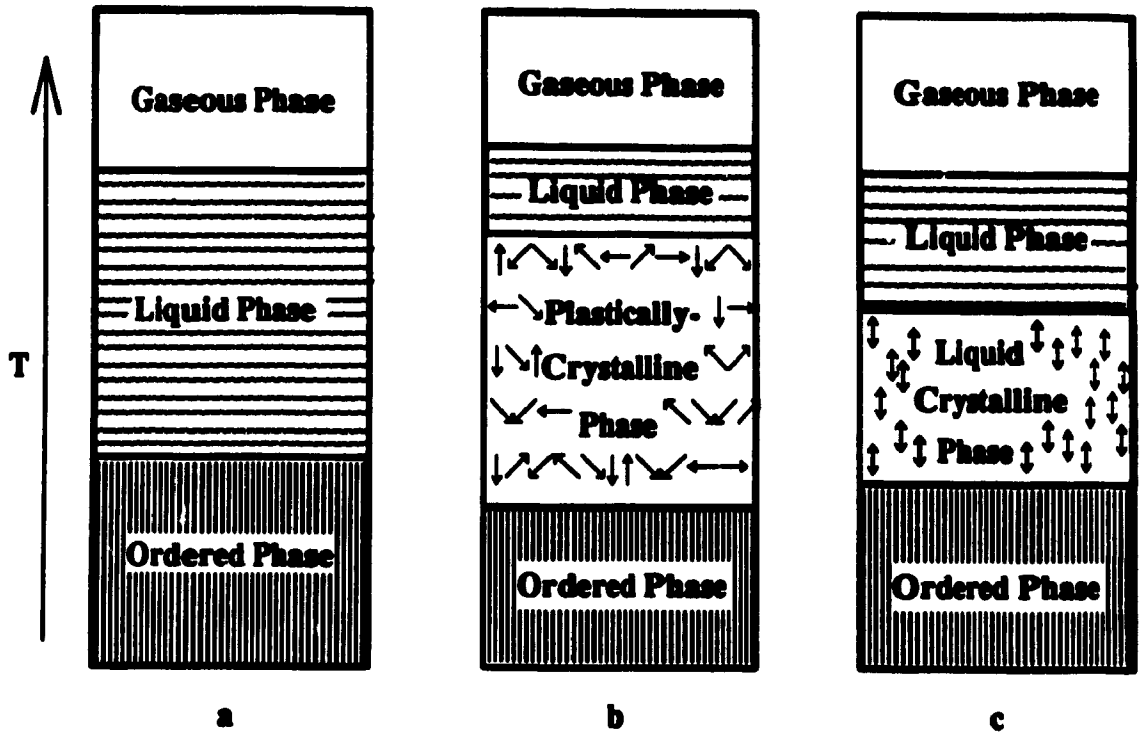


Figure 1.1 Phases for (a) an ordinary solid, (b) a plastic crystal, (c) a liquid crystal.

Thus liquids flow under gravity, plastic crystals require much force, while "true" solids will fracture.

## I. Nomenclature

The term plastic crystals is in reality a misnomer but, until recently, no new name was considered acceptable, and since this earlier nomenclature has been used for the last 50 years it is doubtful if it will ever be eliminated. Obviously this name seems appropriate due to a chief physical characteristic associated with this class of compounds, i.e., it depends upon a mechanical property; the ability to flow under pressure or stress. This does, however, lead to confusion since the term plastic is usually associated with polymers, and plastic crystals are not necessarily polymers and vice versa. Moreover, such a name would imply that plasticity is only involved with plastic crystals whereas even metals are

"plastic" to a certain extent. Although the name might seem to be a trivial matter, it is believed to be one of the main reasons for there being relatively so little information on plastic crystals even after 50 years. There are many similarities between liquid crystals and plastic crystals, yet in general those working on liquid crystals have tended to shy away from plastic crystals simply because of the name.[4,5] The main differences between plastic and liquid crystals are that the former are generally globular, compact and have positional but no orientational order, while the latter are less viscous, long, sometimes rigid, and have no postional order but do have orientational order. As a result of these differences, it is easily conceivable that plastic crystals can reorient themselves with greater ease than their liquid counterparts. Based on these observations, some researchers have preferred the name ***plastic liquid crystals***.[4]

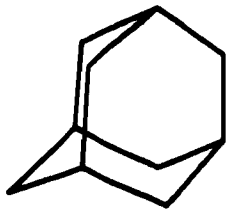

Adamantane

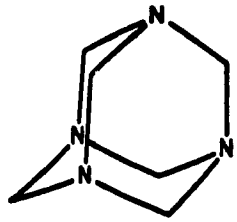


Hexamethylenetetramine

The other name that had been proposed by Timmermans was ***globular molecules***. This is not a proper name because, although many globular molecules are plastic crystals, not all plastic crystals are globular, and nor do all globular molecules belong to the class of plastic crystals. Consider hexamethylenetetramine, which has the same basic molecular structure as adamantane and yet is not a plastic crystal.[6] *Isotropic molecules* was also put forward as a possible name; however, even though cubic crystals are isotropic, not all cubic

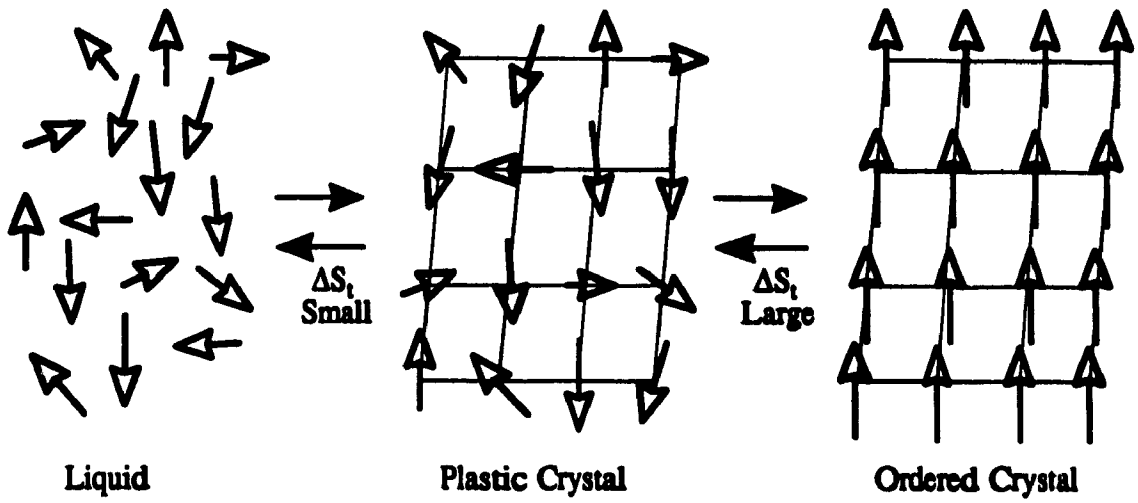


Figure 1.2 Different orientations of molecules in a plastic crystal in various phases.

crystals are plastic (e.g., hexamethylenetetramine) and, more importantly, not all plastic crystals are cubic.[7] The terms currently in vogue are ***orientationally-disordered solids*** (ODIS) and ***orientationally-disordered crystals*** (ODIC). These two names are essentially equivalent and stem from a well-known characteristic of plastic crystals - their orientational disorder (see Figure 1.2).

## II. General Characteristics

X-ray studies on this class of compounds have shown that very few, if any, lattice reflections are observed. There are two possible explanations for this situation. Firstly, there are many equivalent allowed orientations or secondly, there is a great deal of

orientational mobility. Furthermore, based on the small observed lattice parameters, only restricted, as opposed to free, molecular reorientation is taking place.[8]

Plastic crystals have other particular properties associated with them which clearly distinguish them from ordinary solids, the most prominent one being the entropy of melting. Timmermans had observed that, in general, $\Delta S_m \leq 2.5R$, where R is the gas constant.[3] This relationship is due to the nature of the plastically-crystalline phase, i.e., considerable disorder is present in the solid, so much so, that it has very little to gain by melting. However, this is only a rule-of-thumb, and consequently there are exceptions. For example, $SF_6$ is a plastic crystal and yet its entropy of melting is actually 2.6R.[9] Postel and Reiss[9] have suggested using another approach, namely, the ratio of the minimum distance between molecular centers within a crystal lattice to the maximum diameter of the molecule. Any value greater than 0.77 (the value associated with hexamethylenetetramine) would indicate a plastic crystal.[9] Many exceptions can, however, be found for this parameter since it applies solely to globular molecules.[10,11] Moreover, since not all plastic crystals are globular, it cannot be used as a general criterion; therefore, for the lack of a better method, $\Delta S_m$ is still an acceptable means of determining whether a compound belongs to this class of compounds or not.

Another interesting physical characteristic associated with plastic crystals is the relatively high melting points observed when comparing two isomers, one of which is a plastic crystal and the other which is not. For example, consider neopentane, $C(CH_3)_4$, a plastic crystal, and its structural isomer *n*-pentane, $CH_3(CH_2)_3CH_3$, an ordinary solid. The melting point of neopentane is 257 K, while that of *n*-pentane is 132 K.[3] As was the case for the entropy, very little additional disorder is gained by melting, therefore the melting point of the plastic crystal is higher.

The observed volume of melting of a plastic crystal is very small. This is also due to the degree of disorder which is already present in the solid state, therefore upon melting,

there is very little expansion. Moreover, since the intermolecular forces are weakened, the degree of mobility in the solid state is high and, the vapour pressures of plastic crystals are higher than those for ordinary solids.

As pointed out above, plastic crystals are solids that appear to behave very much like liquids. This raises the question, should they be treated as solids or as liquids? Michels[12] conceived extrusion experiments based on the assumption that plastic crystals should be considered as liquids. His results, however, led him to conclude that based on the observed deformations, plastic crystals are more like ordinary solids than liquids. The same conclusion was attained from NMR results.[13]

Lastly, orientationally-disordered solids must have at least one solid-solid phase transformation occurring at temperatures below their melting points. If one considers the case of cooling, during a transition the solid must lose its orientational order and this generally involves large enthalpy and entropy changes. Below the transition temperature, all molecular rotation and/or migration in the solid state is halted. Many different techniques can be used to probe the phase transformations.

## III. Methods of Analysis

Among the many methods that can be used to study the solid-solid phase transitions occurring in orientationally-disordered solids is calorimetry.[3,14-18] This is an obvious method since an important property of plastic crystals is that $\Delta S_m \leq 2.5R$. Differential scanning calorimetry or differential thermal analysis are very convenient methods through which both enthalpies and entropies of melting and transition can be obtained. With the aid of these methods the thermodynamic order of the reaction can be established. An interesting characteristic of plastic crystals that was noted from thermal analysis studies is that they are often easily supercooled (but not easily superheated) to form *glassy* states in

which stable phases are never formed. It is for this reason that the phases labelled in this thesis refer to the heating rather than the cooling cycles.

When there is interest in discerning the structure of a solid, x-ray analysis immediately comes to mind. Unfortunately, plastic crystals cannot be cleaved or easily powdered, and yield few diffracted x-ray beams.[18-20] As a result structure determination is extremely difficult and usually no definite conclusion can be reached. This fact has actually helped in determining which crystals are disordered and a molecule is considered orientationally-disordered if its site symmetry is higher than its point-group symmetry.[18] Neutron diffraction is also employed in molecular structure determination,[18,19,22] whereby, geometrical information as well as dynamic information on the re-orientation process can be obtained.[19]

Two extremely useful techniques for studying solids are infrared and Raman spectroscopy. Variable-temperature and -pressure IR and Raman spectroscopy yield data regarding to the structure of the molecules under investigation. Much information can be obtained these techniques because the crystal symmetry and the vibrational selection rules vary as the phase changes. It is therefore expected that the spectra of each phase will be different. More importantly, monitoring the spectral changes while varying both the pressure and temperature permits construction of a phase diagram.

In 1936, Smyth *et al.* found that unlike normal crystallization, when a polar liquid crystallizes to a plastically crystalline phase, the dielectric constant (also known as relative permitivity) does not decrease sharply.[18-22] Not only does it not decrease, but in several cases, it actually increases.[18] Further cooling, i.e., into the ordered phase, ultimately yields the anticipated sharp drop in dielectric constant.[21]

Other techniques that are used to probe these systems include those that monitor molecular motion. Two such techniques are self-diffusion using radiotracer techniques and nuclear magnetic resonance (NMR) spectroscopy.[18-21] In the case of self-diffusion (also

known as creep studies), radiotracers, such as $^{14}C$ or $^{3}H$, are utilized to measure the rate of penetration of a radioactively-labelled molecule into the bulk of the material being studied.[19] Based on these experiments, it was found that the self-diffusion coefficient, D, is much higher for a plastic crystal than for a regular solid but it is very close to that for a liquid, once again suggesting that motion in a plastic crystal is nearly the same as that in a liquid.[19,21] The other technique which monitors molecular motion, NMR spectroscopy, has been applied quite extensively in order to obtain information on the type of motion taking place and the associated kinetics.[18,19] As in the case of self-diffusion, it was found that a liquid which forms a plastic crystal upon freezing displays less line-broadening effects than does a liquid which can be crystallized into an ordered phase. This observation implies that rotation is still taking place in the disordered solid. When the plastic crystal is cooled down further so that it becomes ordered, the observed line-broadening effects are the same as those for an ordinary solid. This again indicates that there is no rotation taking place in the ordered phase of the plastic crystal. The best method available to study this rotational motion is that of the spin-relaxation. These measurements include $T_1$, $T_{1\rho}$, $T_{1D}$ and $T_2$ studies in which the spin-lattice relaxation times in the laboratory frame, rotating frame, dipolar relaxation time, and spin-spin relaxation times, respectively, can be determined.

## IV. Applications of Plastic Crystals

The solid-solid phase transitions occurring in plastic crystals involve large changes in entropy and enthalpy that are normally only associated with liquid-solid phase changes. It is the large enthalpy changes that has aroused the interest of industry since such compounds could possibly be used for energy storage. Obviously, before a compound can be used as a *phase change material*,[23] it must fulfill a series of conditions, namely: (1) the

phase transition temperature of the material must be within the range of the desired operating temperature of the heating or cooling system; (2) the $\Delta H_m$ or $\Delta H_t$ values must be as large as possible so that energy storage can be maximized; (3) a well-characterized phase diagram would facilitate usage of the compound; (4) the material must be easily contained and the container should be strong enough to resist the expansions and contractions generated by the phase changes occurring in the material; (5) the higher the density of the compound the better since more heat can be stored in a smaller volume; (6) the compound must not be too susceptible to supercooling since this has been found to interfere, if not completely suppress, heat transfer; (7) the substance should be chemically stable and not react with the container in which it is being held; (8) the material should not be toxic, have a foul smell, or corrode easily and should be readily disposable; (9) the material should be cost effective, i.e., things like production, shipping and handling costs, etc., should be reasonable. Based on the above criteria, plastic crystals are anticipated to be very good candidates for energy storage devices, and in fact some have already been used for this purpose.[24-30]

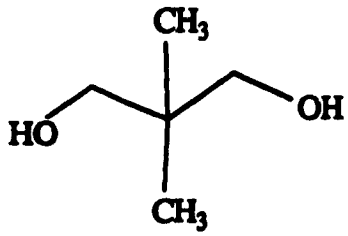


2,2-dimethyl-1,3-propanediol

(DMP or NPG)

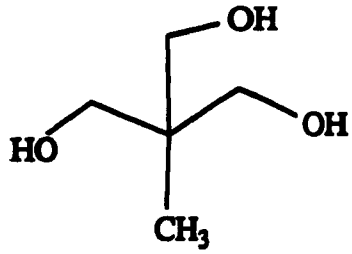


2-hydroxymethyl-2-methyl-1,3-propanediol

(HMP)

One plastic crystal used in solar heat storage devices is neopentylglycol (NPG) also known as 2,2-dimethyl-1,3-propanediol (DMP);[29] it is maintained at 313 K (40 °C), and

absorbs heat during the day and releases it at night. The main advantages of DMP are that it is a solid thereby eliminating leakage problems, it undergoes expansion and contractions to a lesser degree than do water-based systems, it is inexpensive, and it will only need to be replaced about every 25 years.

Aside from solar heating, plastic crystals are being used in what is termed *temperature-adaptable fabrics*.[24-30] Vigo and Frost found that the best plastic crystals for this purpose were DMP and one of its derivatives, 2-hydroxymethyl-2-methyl-1,3-propanediol (HMP).[24-26] The idea behind these fabrics is to treat the fibers with the plastic crystal and then make a piece of clothing with those fibers. The use of such a garment is obvious - protective clothing when temperature extremes are met. One could easily imagine using these fibers to fabricate clothing to protect humans from hypothermia (life jackets) or to protect fire-fighters from the excessive heat, or even to protect animals and plants from sudden temperature changes. These materials could also be used to cover food during shipping thereby limiting spoilage and lowering transportation costs since special bulk containers would no longer be required. It has been proposed that HMP-treated fibers could be used in the 320-375 K range since between 345 and 375 K energy is stored, while it is released between 320 K and 347 K.

## B. THESIS OBJECTIVES

The main objective of this study was to probe the phase transitions in plastic crystals of different symmetries, by various methods. The compounds studied are shown in Figure 1.3, and include some adamantane derivatives, a carborane derivative and other cyclic hydrocarbons. Chapter 2 contains a brief review and description of thermal analysis and the results obtained using differential scanning calorimetry. Chapter 3 describes the

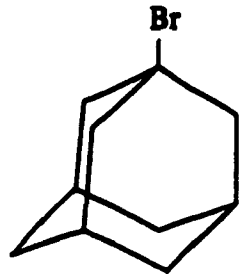


**1**

1-bromoadamantane

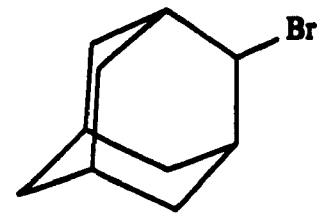


**2**

2-bromoadamantane

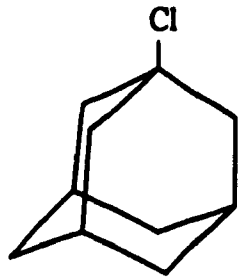


**3**

1-chloroadamantane

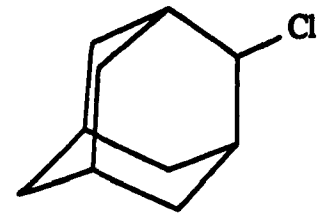


**4**

2-chloroadamantane

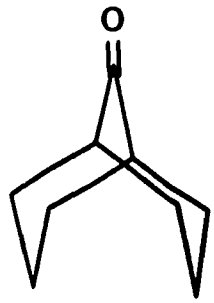


**5**

bicyclononanone

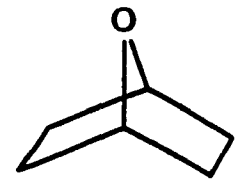


**6**

oxanorbornane

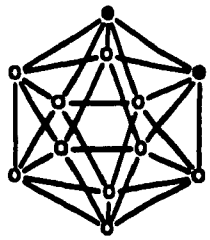

**7**

*o*-carborane

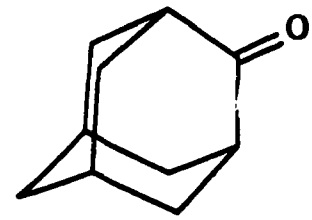


**8**

adamantanone

**Figure 1.3** Compounds studied in this thesis. Note in compound 7, o = B, ● = C, and the H atoms have been omitted for the sake of clarity.

experimental set-up for variable-temperature IR and Raman spectroscopic measurements and the proposed vibrational assignments for these orientationally-disordered solids. The results of the high pressure-Raman studies on three typical plastic crystals, 1-$C_{10}H_{15}Cl$, 2-$C_{10}H_{15}Cl$, and *o*-$C_2B_{10}H_{12}$ are presented in Chapter 4; this work is especially interesting as it appears to be the first time that microRaman spectroscopy system has been used for the analysis of plastic crystals under external pressure. The thesis concludes with a summary and contributions to knowledge.

## V. References


(1) J. Timmermans, *Bull. Soc. Chim. Belg.*, **44**, 17 (1935)

(2) J. Timmermans, *J. Chim. Phys.*, **35**, 331 (1938)

(3) J. Timmermans, *J. Phys. Chem. Solids*, **18**, 1 (1961)

(4) G. W. Gray, P. A. Winsor, *Mol. Cryst. Liq. Cryst.*, **26**, 305 (1974)

(5) V. K. Pershin, Vi. K. Pershin, S. A. Skopinov, *Mol. Cryst. Liq. Cryst.*, **84**, 213 (1982)

(6) H. A. Resing, *Mol. Cryst. Liq. Cryst.*, **9**, 100 (1969)

(7) W. J. Dunning, *J. Phys. Chem. Solids*, **18**, 21 (1961)

(8) G. W. Smith, *Adv. Liq. Cryst.*, **1**, 189 (1975)

(9) M. Postel, J. G. Reiss, *J. Phys. Chem.*, **81**, 2634 (1977)

(10) H. Szwarc, *J. Phys. Chem.*, **84**, 1997 (1980)

(11) M. Postel, J. G. Reiss, *J. Phys. Chem.*, **84**, 1998 (1980)

(12) A. Michels, *Bull. Soc. Chim. Belg.*, **57**, 575 (1948)

(13) B. S. Shah, J. N. Sherwood, *Trans. Farad. Soc.*, **67**, 1200 (1971)

(14) E. F. Westrum, *NATO ASI Ser., Series C*, **119**, 671 (1984)

(15) W. B. Daniels, P. E. Cladis, P. A. Keyes, *High Press. Sci. Tech., Proc. Inter. AIRAPT Conf. 7th*, **2**, 655 (1980)

(16) B. Wunderlich, J. Grebowicz, *Poly. Mater. Sci. Eng.*, **50**, 114 (1984)

(17) G. M. Schneider, *Thermochim. Acta*, **88**, 159 (1985)

(18) N. G. Parsonage, L. A. K. Staveley, *Disorder in Crystals*, Clarendon Press, Oxford, Great Britain, 1978

(19) J. N. Sherwood, *The Plastically-Crystalline State: Orientationally-Disordered Crystals*, John Wiley and Sons, Chichester, England, 1979

(20) G. P. Johari, R. K. Chan, *Can. Chem. Educ.*, **10**, 8 (1975)

(21) G. P. Johari, R. K. Chan, *Can. Chem. Educ.*, **10**, 10 (1975)

(22) M. Bee, *J. Chim. Phys. (JCPBAN)*, **82**, 205 (1985)

(23) G. A. Lane, "The Science of Phase Change Materials", in *Solar Heat Storage: Latent Heat Materials*, vol. I, George A. Lane, Ed., CRC Press, Inc., Boca Raton, Florida, 1983

(24) T. L. Vigo, C. M. Frost, *Thermochim. Acta*, **76**, 333 (1984)

(25) T. L. Vigo, C. M. Frost, *J. Text. Res.*, 743 (1985)

(26) T. L. Vigo, C. M. Frost, *J. Coated Fabrics*, **12**, 243 (1983)

(27) *Pop. Sci.*, "Hot/Cold Threads", 73 (February 1988)

(28) *Chem. Engr. News*, "Fabrics Given Enhanced Thermal Properties", 15 (October 20, 1986)

(29) *Chem. Week*, "'Plastic Crystals' That Store and Release Heat", 22 (August 1, 1984)

(30) *Chem. Engr. News*, "Fibers with Enhanced Thermal Storage Made", 31 (April 30, 1984)

# CHAPTER 2
# DIFFERENTIAL SCANNING CALORIMETRIC STUDIES OF ORIENTATIONALLY-DISORDERED SOLIDS (PLASTIC CRYSTALS)

## A. INTRODUCTION

### I. General

Thermal analysis has been defined by the International Confederation of Thermal Analysis (ICTA) as a general term which covers a variety of techniques that record the physical changes occurring in a substance as a function of temperature.[1,2] This term therefore encompasses many techniques such as thermogravimetry (TG), evolved gas analysis (EGA), differential thermal analysis (DTA), and differential scanning calorimetry (DSC), just to name a few. The application of thermal analysis to the study of plastic crystals stems from the properties of these crystals. Timmermans was the first to notice that many spherical and globular organic molecules had entropies of fusion, $\Delta S_f$, of 21 J $K^{-1}$ $mol^{-1}$ or $\Delta S_f/R$ of 2.5.[3] It was found, for example, that bromocamphor (a non-spherical molecule) had a $\Delta S_f$ of 115.5 J $K^{-1}$ $mol^{-1}$, while the globular and spherical camphor had a $\Delta S_f$ of 11.7 J $K^{-1}$ $mol^{-1}$.[4] Moreover, these types of compounds are known to undergo at least one solid-solid phase transformation below their melting point. It is therefore obvious that thermal analysis is useful in the study of plastic crystals and since

the two techniques associated with energy changes occurring in a substance are DTA and DSC, it is these two which will be discussed in detail.

Ever since the invention of DSC, there has been much confusion over the difference between DTA and DSC. The exact ICTA definition of DTA is a method that monitors the temperature difference existing between a sample and a reference material as a function of time and/or temperature assuming that both sample and reference are subjected to the same environment at a selected heating or cooling rate.[1,2] The plot of $\Delta T$ as a function of temperature is termed a DTA curve and endothermic transitions are plotted downward on the y-axis, while temperature (or time) is plotted on the x-axis. DSC, on the other hand, has been defined as a technique that records the energy (in the form of heat) required to yield a zero temperature difference between a substance and a reference, as a function of either temperature or time at a predetermined heating and/or cooling rate, once again assuming that both the sample and the reference material are in the same environment.[1,2] The plot obtained is known as a DSC curve and shows the amount of heat applied as a function of temperature or time. As can be seen from the above definitions, the two techniques are similar but not the same. The two yield the same thermodynamic data such as enthalpy, entropy, Gibbs' free energy, and specific heat, as well as kinetic data. It is only the method by which the information is obtained that differentiates the two techniques. A brief history on the development, and a comparison of the two techniques is therefore in order.‡

## II. DTA AND DSC

A little over a hundred years ago, two papers were published by Le Châtelier dealing with the measurement of temperature in clays; the first entitled "On the action of heat on clays" and the second "On the constitution of clays".[22,23] The experiment

‡ For a more detailed history, comparison and theoretical description, consult the references listed in references 5-21.

described in these papers was not a truly differential one since the difference in temperature between the clay and reference material was not measured. The apparatus consisted of a Pt-Pt/10% Rh thermocouple embedded in a clay sample, which in turn was packed into a 5-mm diameter Pt crucible. The crucible was then placed in a larger crucible, surrounded with magnesium oxide and inserted into an oven. Le Châtelier used a heating rate of 120 K $min^{-1}$ and recorded the electromotive force of the thermocouple on a photographic plate at regular time intervals. As long as no phase change occurred in the clay, the temperature rose evenly and the lines on the plate were evenly spaced. If, however, an exothermic transformation took place, then the temperature would rise more rapidly and therefore the lines would be unevenly spaced and closer together. An endothermic transition, on the other hand, would cause the measured temperature to rise more slowly and the spacing between the lines would be much larger. In order to ensure that the measured temperatures were correct, he calibrated his instrument with the aid of boiling points of known materials such as water, sulfur, and selenium, as well as the melting point of gold. Since Le Châtelier's experiment does not fit the ICTA definition of DTA, his main contribution to the development of DTA was the automatic recording of the heating curve on a photographic plate. True differential thermal analysis was actually developed twelve years later (in 1899) by Roberts-Austen.[24]

Roberts-Austen connected two Pt-Pt/10% Ir thermocouples in parallel which in turn, were connected to a galvanometer. One thermocouple was inserted into a reference sample consisting of a Cu-Al alloy or of an aluminium silicate clay (fireclay). The other thermocouple was embedded into a steel sample of the same shape and dimensions as the reference. Both the sample and reference were placed in an evacuated furnace. A second galvanometer monitored the temperature of the reference. The purpose of the experiments was to construct a phase diagram of carbon steels and, by extension, railway lines. Since his method was a true differential technique, it was much more sensitive than

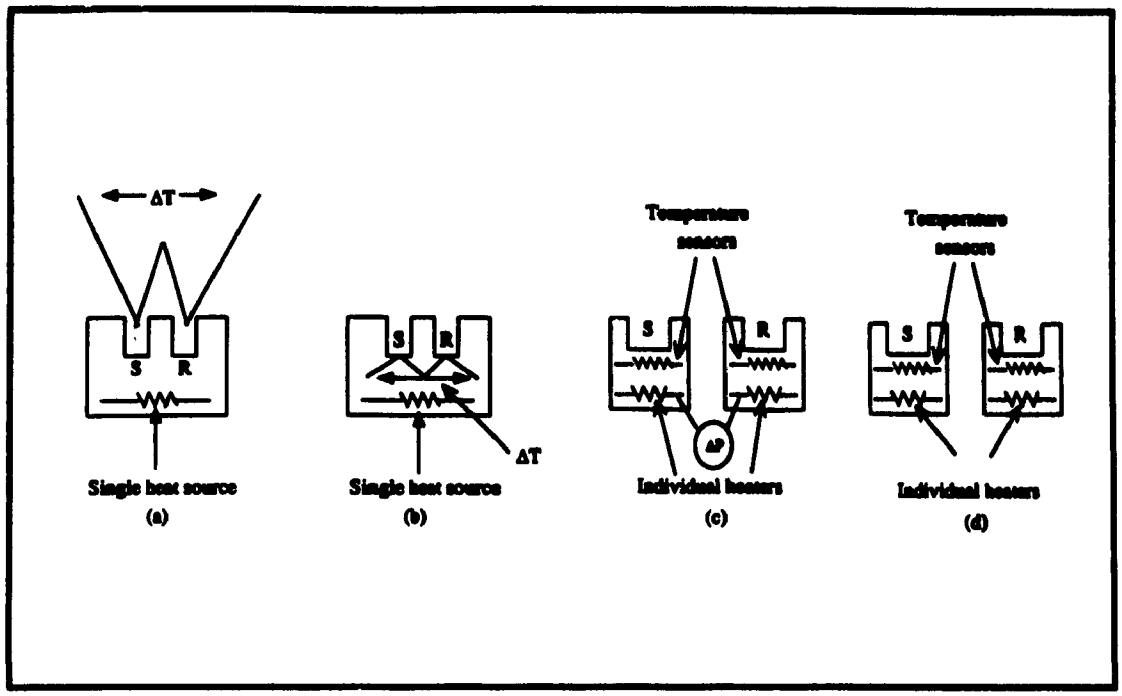


Figure 2.1 Schematic diagrams of different instruments used in thermal analysis to detect energy changes occurring in a sample. (a) Conventional DTA; (b) *Boersma* DTA; (c) Power-compensation DSC and (d) Heat-flux DSC.

Le Châtelier's. The DTA design used today is only a slight modification of Roberts-Austen's and the only major improvements are in the electronics of temperature control and in the data processing, which is now handled by computers (see Figure 2.1a).

It took about fifty years for the DTA technique to be considered not only qualitative but also as a quantitative means of analyzing and characterizing materials. Moreover, it was only then that the Roberts-Austen set-up was modified by Boersma.[25] The modification was in the placement of the thermocouples. Rather then placing the thermocouples into either the sample or the reference, Boersma suggested that they be fused onto cups and that sample and reference be placed into these cups. This modification eliminated the necessity of diluting the sample with reference materials, and reduced the importance of sample size. The vast majority of today's DTA instruments are based on the Boersma principle in that only the crucibles are in contact with the thermocouples.

Boersma's DTA configuration, Figure 2.1b, can be considered as the missing link between differential thermal analysis and differential scanning calorimetry. Some even feel that this configuration is in fact a DSC instrument. This is the major reason behind the confusion as to the differences between DTA and DSC.

The two most crucial differences between the two techniques are: (a) in DSC, the sample and reference have their own heaters and temperature sensors as compared to DTA where there is one common heater for both; (b) DTA measures $\Delta T$ vs temperature and therefore, must be calibrated to convert $\Delta T$ into transition energies, while DSC obtains the transition energy directly from the heat measurement. The confusion is also partly due to the fact that there are at least three different types of DSC instruments; a DTA 'calorimeter', a heat-flux type (Figure 2.1c), and a power compensation (Figure 2.1d) one. This in turn arises from the fact that some define calorimetry as quantitative-DTA. As opposed to conventional DTA, the thermocouples in a DSC instrument do not come into contact with either the sample or reference. Instead, they either surround the sample (thermopiles) or are simply outside the sample (thermocouples). Furthermore, the sample and reference weights are usually under 10 mg.

The DTA calorimeter, sometimes called DSC, was developed by David in 1964.[26,27] The term DTA calorimeter is more appropriate since this system actually measures $\Delta T$ directly from the experiment. Unlike conventional DTA however, the experiment is performed at quasi-equilibrium conditions, i.e., sample mass is less than 10 mg, slow cooling/heating rate, and only one calibration coefficient needs to be measured for the entire temperature range. This therefore yields quantitative data but by definition remains a DTA instrument.

The other two categories of DSC apparatus are true calorimetric instruments in that the calorimetric information is obtained directly from the measurement, i.e., no conversion factor is required to convert $\Delta T$ into readily used energy units as the thermometric data is

obtained directly. A constant is still required to convert the energy term into more suitable units. The main goal of any enthalpic experiment, which is to determine the enthalpy of a sample as a function of temperature, is attained by measuring the energy obtained from a sample heated at a constant rate with a linear temperature or time programming. These two DSC instruments are based on the method developed by Sykes in the mid-1930's.[28,29] Sykes' apparatus was designed so that the temperature of the metal block, which contained the sample, was slightly lower than the temperature of the sample itself. To maintain the sample at the same temperature as the block, power was supplied to the sample. The main disadvantage of this apparatus was that a correction factor had to be applied to account for the heat transfer between the surrounding medium and the block. Both the heat flux and power-compensation DSC instruments overcome this drawback because, as the name suggests, they are *differential* instruments. The heat-flux instruments measure the flux across a thermal resistance, whereas the power compensating differential scanning calorimeters measure the energy applied to the sample (or the reference) by an electrical heater in order to maintain a zero-temperature differential.

The first commercial DSC instrument was introduced by Watson and his co-workers at Perkin-Elmer (Model DSC-1) in 1964.[30] Watson *et al.* also appear to be the first to have used the nomenclature *differential scanning calorimetry*. Their instrument, a power-compensating DSC, maintained a zero temperature difference between the sample and the reference by supplying electrical energy (hence, the term "*power-compensation*") either to the sample or to the reference, as the case may be, depending on whether the sample was heated or cooled at a linear rate. The amount of heat required to maintain the sample temperature and that of the reference material isothermal to each other is then recorded as a function of temperature. Moreover, in power-compensation DSC, an endothermic transition, which corresponds to an increase in enthalpy, is indicated as a peak in the upward direction (since power is supplied to the sample), while an exothermic

transformation, a decrease in enthalpy, is shown as a negative peak. This therefore differs from the DTA curve since the peaks are in opposite direction and that the information obtained is heat flow, rather than $\Delta T$, as a function of temperature (see Figure 2.2). Also, as will be shown later, the integration of a DSC curve is directly proportional to the enthalpy change.

The heat-flux DSC instrument is very often based on the Tian-Calvet calorimeter. The original calorimeter, built in the early 1920's by Tian[31], consisted of single compensation vessel and the measurement was via a thermopile. Calvet then modified this set-up about twenty-five years later by making it a twin calorimeter, i.e., applying the differential technique.[31] The energy measuring device is a thermopile consisting of approximately 500 Pt-Pt/10% Rh thermocouples which are equally spaced and connected in series. This arrangement enables the electromotive force (emf) to be directly proportional to the amount of heat lost by the sample and reference holders. Essentially, this type of calorimeter measures the difference in temperature between the sample and reference as a function of time, and since the temperature varies linearly with time, as a function of temperature as well. The heat-flux is actually derived from a combination of the $\Delta T(t)$ curve and the $d\Delta T(t)/dt$, both of these are transparent to the user since the electronics used yield a direct heat flux value from these terms. If temperature compensation is required, then it is done by Joule heating (for an endothermic process) or by Peltier effect (for an exothermic process). As in the DTA case, an endothermic signal is in the negative direction, while an exothermic signal is the upward direction (see Figure 2.2).

Both the heat-flux calorimeters and power-compensation calorimeters have their advantages and disadvantages, but, the end result is the same, the two will yield the same information. The advantage of the heat-flux type is that it can accommodate larger sample volumes, has a very high sensitivity, and can go above 1100 K. The disadvantage is that it

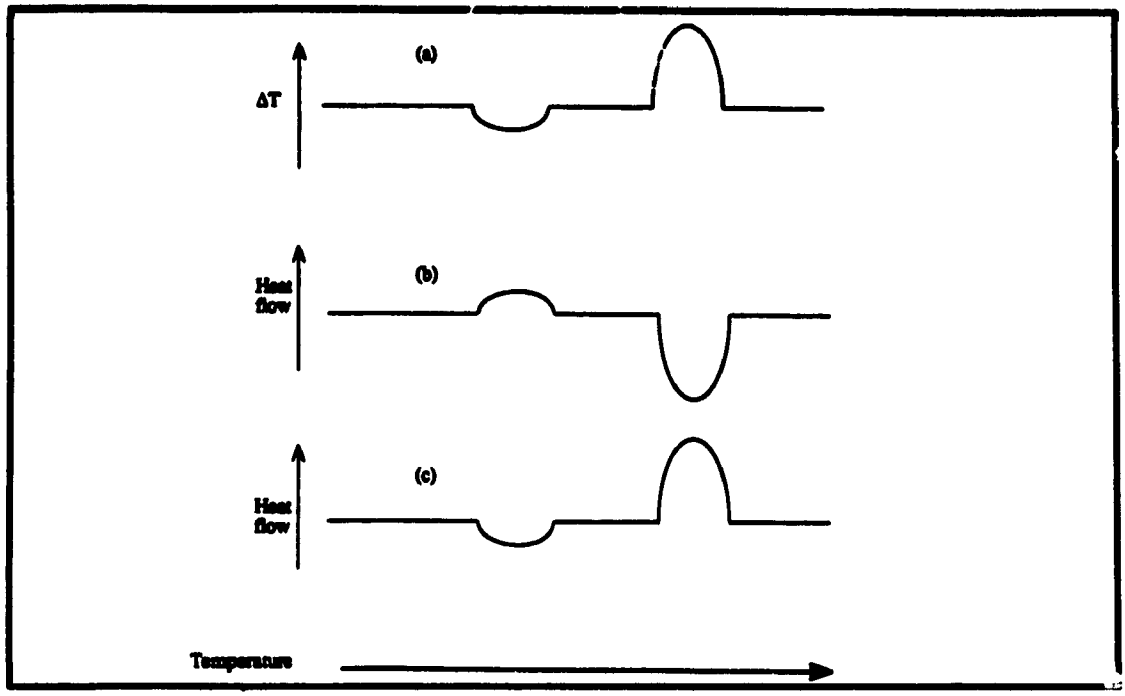


Figure 2.2 Comparison of curves obtained on heating by (a) DTA, (b) Power-compensating DSC, and (c) heat-flux DSC.

cannot be scanned at rates faster than 10 K $min^{-1}$ at high temperatures and not faster than 3 K $min^{-1}$ at sub-ambient temperatures. The main advantage of the power-compensation calorimeter is that it does not require a calibration in that the heat is obtained directly from the electrical energy supplied to the sample or reference compartment (a calibration is still necessary however, to convert this energy into meaningful units) and that very fast scanning rates can be obtained. The disadvantage of this system is that the electronic system must be of extremely high sensitivity and large fluctuations in the environment must be absent so as to avoid compensating effects which are not due to the sample, also, the complexity of the electronics prevents the system from being used above ~1100 K.

The calibration of a DSC or DTA instrument is crucial for various reasons. Firstly, for the determination of the temperature and secondly, to convert the dissipated power into useful energy units, e.g., joules or calories. The temperature calibration is of vital

importance since in most cases a calibrated thermometer cannot be used for the temperature measurement. As for the calibration of energy, it too is important as in many cases the amplitude of the signal of dissipated power is affected by the heating and cooling rates. Based on these facts, it is obvious that the accuracy of the measurement is generally lower than the degree of reproducibility.

There are quite a few different methods for the calibration of DSC instruments, of which the most popular are: (a) calibration by Joule-effect and (b) calibration by heats of fusion.[14,17,32] The Joule-effect calibration is relatively simple and straight-forward in that it consists of an electrical heater inserted into the sample and reference compartments. A pulse of predetermined duration and intensity is sent to the sample and the dissipated power is then measured. The disadvantage of this method is that some heat flux can be dissipated in the heater wires and therefore not truly measured and furthermore, the electrical heater is not necessarily composed of the same material as the sample and reference holders. Still, the accuracy of this calibration technique is better that 0.2%.

The heats of fusion calibration method affords two simultaneous calibrations. Pure substances which undergo phase transformations at very well-characterized temperatures are used. Since the enthalpy of fusion and temperature of fusion of the calibrant are well known, both a temperature and enthalpic calibration can be performed with the same substance. Ideally, more than one compound and more than one scanning rate should be utilized (or if only one scanning rate is employed, then the scanning rate should correspond to that which will be used for the experiment) since the sensitivity of the measurement is not only temperature dependent, but also scan rate dependent. Since the thermal conductivity might play an important role in the measured response, the mass of the calibrant should be as close as possible to the sample mass. The following criteria should be used when choosing a calibrant:

(a) the substance must be available in high purity; (b) the transition temperature and enthalpy of transition should be known with a high degree of accuracy; and, (c) the substance should not show any tendency to super-heating.[6,7,14]

The major drawback of this method is that since transitions are very temperature specific, one substance might be suitable for only one temperature range, hence the need to use more than one calibrant (or one must assume that the calibration will hold for the entire range being studied).

Another calibration method is with the use of radioactive materials since they generate constant heat (i.e., power) which is independent of temperature. Some of these materials, however, are not suitable at high temperatures as they might diffuse through the sample holder. The most often used radioactive material as a calibrant appears to be plutonium.[33]

The integration of a DSC (and a DTA) curve is directly proportional to the enthalpy change,[34]

$$\text{Area} = Km\Delta H \qquad [2.1]$$

where K is the calibration coefficient, m the sample mass, and $\Delta H$ the heat of transition. Unlike DTA, however, in DSC, K is temperature independent. As is the case for DTA†, the term dH/dt for DSC is given by three measured quantities,[34]

$$dH/dt = -(dq/dt) + (C_s - C_r)dT_p/dt + RC_s d^2q/dt^2 \qquad [2.2]$$

where dq/dt is the area, $(C_s - C_r)dT_p/dt$ is the baseline contribution, and $RC_s d^2q/dt^2$ is the peak slope. The differences between the two techniques are quite apparent; firstly, the area under the curve is $\Delta q = -\Delta H$, i.e., the enthalpy and secondly, the thermal resistance, R, only shows up in the third term of the equation. Although a calibration coefficient, is still

† In DTA[34]: $R(dH/dT) = (T_s - T_r) + R(C_s - C_r)dT_r/dT + RC_s d(T_s - T_r)/dt$

required it is only needed as a means of converting the area (heat flow) into an acceptable energy unit, such as joules or calories, and it is not a thermal constant.[28]

Phases which are thermodynamically stable have a finite number of degrees of freedom. Each phase is separated by a boundary where the phase change occurs. As one crosses the boundary, a new phase appears to the detriment of the other and, since the overall free energy of the process is zero, the thermodynamic parameters such as $\Delta S$, and $\Delta H$ must change in a quantitative manner at the border. Since different types of phase boundaries are encountered, different types of enthalpies are obtained, for example, $\Delta H_f$ entropy of fusion, enthalpy of transition $\Delta H_t$, etc.

The previous discussion shows that a great deal information can be obtained from a DSC curve and that the interpretation of such a curve can yield valuable insight into the nature of the material being investigated. It is important to be able to identify what type of phase transition is occurring in the substance by looking at the curve itself and therefore what follows is a brief explanation on phase transformations in general, and how they can be identified from a DSC (or DTA) curve.

## III. Polymorphic Transitions

Different phases arise when a body of matter has properties which differ, such as, chemical composition, density, crystalline form, refractive index and, of course, a change in physical state (solid, liquid, or gas). Phases are considered polymorphs of each other if they give rise to the same solid, liquid or gas by a simple phase transformation, e.g., there are nine known crystalline phases of ice. The least likely polymorph to exist is one in the vapour phase as pure substances have only one vapour phase. Liquid substances which yield polymorphic phases are known as *liquid crystals*. Solid polymorphs are distinguished by physical differences such as crystalline form, density, refractive index, and solubility,

etc. Two categories of crystalline substances exist: monotropic and enantiotropic. Monotropic crystals have only one stable form (the other forms being metastable) over the entire solid phase range and therefore exhibit only one irreversible solid-solid phase transformation. Enantiotropic materials, however, have at least one reversible and stable phase transformation (i.e., two stable forms) at a very definite temperature.[35]

It is important to realize that at a transition temperature both phases can exist for an unlimited period and therefore polymorphic transition temperatures will depend on whether a heating or cooling cycle is used. Generally, the observed temperature of a phase transition will be above the true value during a heating cycle and below, during a cooling cycle. Moreover, since the result obtained is dependent on the rate of reaction it will also depend on the heating (or cooling) rate. As many substances are known to undergo supercooling, but few undergo superheating, it is preferable to specify the transition temperature on heating rather than on cooling, or the median of the heating and cooling cycles.

Phase transitions can be classed into two categories; those that are first-order and those that are second- or higher-order.[36,37] First-order transformations are characterized by discontinuities in the change in energy, volume, and structure. In second- and higher-order modifications, there is a gradual change in volume and energy at the phase transition. There is apparently no physical significance to transformations greater than second-order and some even claim that second-order transitions are actually pseudo-first-order.[36,37]

The thermodynamics of phase transitions can be described as follows: At a transition point, two phases are in equilibrium, therefore, their Gibbs free energies are equal and hence, at constant pressure, the free energy curves must intersect. The thermodynamic description for a one-component system has been demonstrated to be:[36,37]

$$G = H - TS \quad [2.3]$$

$$(\partial G/\partial T)_p = -S \quad [2.4]$$

$$(\partial G/\partial p)_T = V \quad [2.5]$$

$$(\partial^2 G/\partial T^2)_p = -Cp/T = -(\partial S/\partial T)_p \quad [2.6]$$

$$(\partial^2 G/\partial p^2)_T = -KV = -(\partial V/\partial p)_T \quad [2.7]$$

$$(\partial^2 G/\partial p \partial T) = \alpha V = (\partial V/\partial T)_p \quad [2.8]$$

where G is the Gibbs free energy, T the temperature, S the entropy, p the pressure, V the volume, K the isothermal compressibility, $\alpha$ the thermal expansion, and $\Delta H$ the heat of reaction where the subscripts p and T denote constant pressure and temperature conditions, respectively. As shown in eq. [2.4] and [2.5], first-order transitions have derivatives of G which are discontinuous. Furthermore, the phase transition itself, which occurs upon a change in temperature with either the absorption or release of latent heat, is accompanied by both a sudden increase in entropy and volume. The relationship between $\Delta S$ and $\Delta V$, as well as the effect of pressure on the transition temperature, has been shown to be:

$$\partial p/\partial T = \Delta S/\Delta V = \Delta H/T\Delta V \quad [2.9]$$

where $\Delta H$ represents the latent heat of reaction. The above equation is better known as the Clausius-Clapeyron equation, and shows that a phase change associated with a change in volume will have its transformation temperature affected by pressure.

The main difference between first-order solid-solid transitions and physical transformations such as melting, freezing, etc., is the latter have large energy barriers and smaller latent heats of transition. The exact temperature of transition can be difficult to obtain since some of these transitions are quite sharp and thus their peak widths can be rather narrow. It is for this reason that some prefer to use the peak temperature (i.e., peak maximum or peak minima as the case may be) as the transformation temperature. This, however, does not actually represent any physical phenomena and consequently, some people prefer to use the onset temperature as the transition temperature since this point does represent the start of the transition.

Unlike first-order transitions, second- and higher-order transformations do not display any discontinuity in the first-derivative of the Gibbs function. This arises from the fact that both the free energy and the first-derivatives curves of the two phases touch. This situation results in no sudden change in volume ($\Delta V = 0$) or entropy ($\Delta S = 0$), and no absorption or release of latent heat as the second-order phase change occurs; however, discontinuities do occur in higher derivatives (eq. [2.6]-[2.8]). One can therefore use the second-derivatives to characterize second-order transformations. One of the most obvious parameters to explore is the specific heat, $C_p$. When $C_p$ is plotted as a function of temperature, a sharp rise occurs for second-order transitions. This is followed by a return to the baseline. Such a curve resembles the Greek letter $\Lambda$, and the transitions are termed *lamda-point* or $\Lambda$-transitions. The appearance of a $\Lambda$-transition does not, however, guarantee that a second-order transition is taking place.[38]

Since second-order transitions have no change in entropy or volume, it is obvious that the Clausius-Clapeyron equation (eq. [2.9]) will not hold. Yet, these transitions are still pressure sensitive and their transition temperatures are affected by pressure as well.[39] The pressure-temperature dependence for these transformations can be obtained by:[36,37]

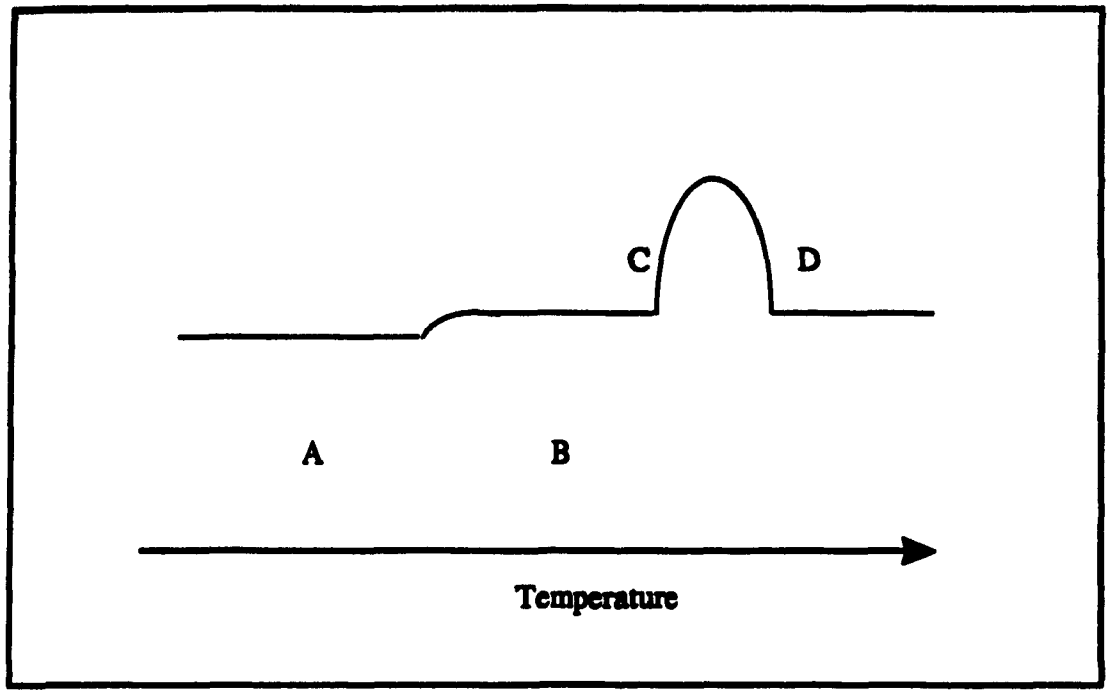


Figure 2.3 Simulated DSC curve showing a second-order transition (between A and B) and a first-order transition (between C and D).

$$\partial p/\partial T = \Delta C_p/VT\Delta\alpha = \Delta\alpha/\Delta K \qquad [2.10]$$

The term $\Delta K$ is the most difficult one to obtain and so the exact physical-meaning of a second- or higher-order transition is still not fully understood. It is, however, believed that the onset of superconductivity, glass-transitions, as well as some order-disorder transitions may very well be second-order or a combination of both a first- and second-order process.[40]

The shape and appearance of DSC curves can give a clue as to the type of transition taking place. Figure 2.3, displays a simulated DSC curve containing both a first-order transition (between phases I and II) and a second-order transformation (between phases II and III). The second-order transition simply appears as a shift in baseline while the first-order transformation is represented by a distinct peak.

As previously mentioned, plastic crystals undergo at least one solid-solid phase modification below their melting-point. This transition usually entails a disorder → order; transition, however, it could also be a disorder → less disorder transformation. Either one tends to signify the beginning of molecular reorientation, i.e., hindered rotation or other motions of the molecule. Aside from their low entropies of fusion, these crystals are also known to have high enthalpies of transition. These transitions may either be first- or second-order and there appears to be no method by which one could predict which type will prevail.

It is quite apparent from the above discussion and brief history on DTA/DSC that this type of thermal method is a prerequisite to the study of phase transitions in disordered solids as well as any other unknown material. With this in mind, the compounds listed in Table 2.I have been studied by variable-temperature DSC in the present work.

## B. EXPERIMENTAL

### I. Purification

All solid samples listed in Table 2.I were purified immediately prior to use by slow vacuum sublimation (21°C, $10^{-3}$ torr). The liquid sample, oxanorbornane 6, was purified by double-distillation over $CaH_2$ and its purity was determined by GC.

**Table 2.I Compounds studied by DSC.**

| Compound | CAS Registry Number | Number | MW g/mole | MP K |
|---|---|---|---|---|
| 1-Bromoadamantane[¥] 1-$C_{10}H_{15}Br$[*] | 768-90-1 | 1 | 215.14 | 390 |
| 2-Bromoadamantane 2-$C_{10}H_{15}Br$[*] | 7314-85-4 | 2 | 215.14 | 412 |
| 1-Chloroadamantane 1-$C_{10}H_{15}Cl$[*] | 935-56-8 | 3 | 170.67 | 438 |
| 2-Chloroadamantane 2-$C_{10}H_{15}Cl$[**] | 7346-41-0 | 4 | 170.67 | 458 |
| Bicyclo[3.3.1]-nonan-9-one (Bicyclononanone) 9-$C_9H_{14}O$[*] | 17931-55-4 | 5 | 138.21 | 429 |
| 7-oxabicyclo-[2.2.1]heptane (oxanorbornane) (1,4-epoxycyclohexane) $C_6H_{10}O$[*] | 279-49-2 | 6 | 98.15 | 245 |
| *o*-Carborane (1,2-dicarbado-decarborane[12]) *o*-$C_2B_{10}H_{12}$[**] | 16872-09-6 | 7 | 144.23 | 559 |

[*] Aldrich Chemical Co. [**] Alfa Products

[¥] The formal name of adamantane is tricyclo[3,3,1,1]decane

## II. Power-Compensation DSC

Differential scanning calorimetric experiments for compounds 1-7, were performed on a Perkin-Elmer DSC-7 calorimeter. The temperature and enthalpy calibrations were based on the phase and melting transitions of cyclohexane (Aldrich Chemical Co. "gold" grade). The sample weights were typically 5-10 mg, and the samples were hermetically sealed in aluminium pans. All samples were scanned at 5 K $min^{-1}$, and 2.5 K $min^{-1}$ before cycling and after cycling. The cycling of the samples was done at 20 K $min^{-1}$ for approximately one hour or five complete cycles (one cycle = cooling + heating). Unless otherwise mentioned, the phase transition temperatures and enthalpies did not show any dependence on scan rate (2.5 and 5 K $min^{-1}$).

## III. Heat-Flux DSC

A SETARAM DSC-111 was used for the heat-flux DSC measurements of compounds **1, 5, 6, 7**. The temperature and enthalpy calibrations were based on the $C_p$ of $Al_2O_3$, melting transitions of various metals, as well as the Joule-effect. The sample weights were typically 5-10 mg, and the samples were carefully sealed in stainless-steel pans with nickel o-rings. All samples were scanned at 3 K $min^{-1}$, and 2 K $min^{-1}$. The cycling of the samples was done at 4 K $min^{-1}$. The results obtained were similar (within experimental error) to those obtained by the Perkin-Elmer instrument. Also, for the sake of clarity, the results presented in this chapter (including DSC curves) are those obtained from the DSC-7.

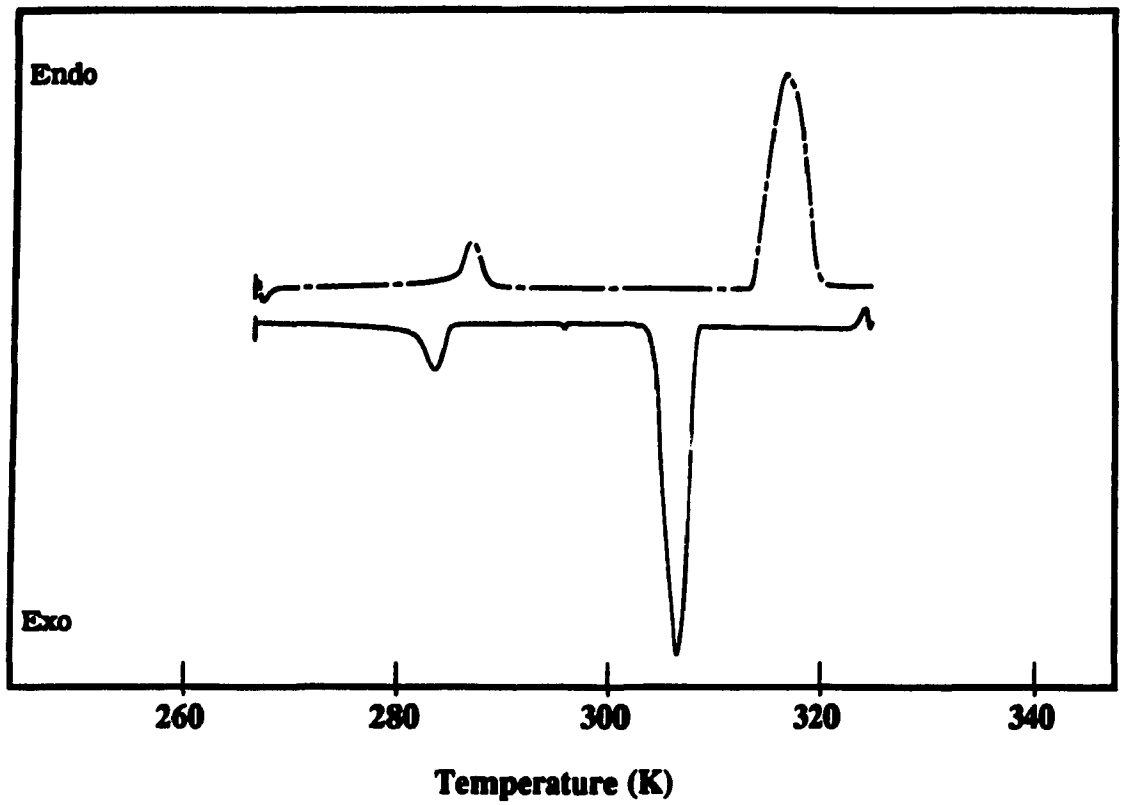


Figure 2.4 DSC curve of 1-bromoadamantane 1-$C_{10}H_{15}Br$ after cycling, scanned at 5 K $min^{-1}$ in the 240-346 K region. Cooling:solid line, heating:dashed line.

## C. RESULTS AND DISCUSSION

### I. Results

The DSC curves obtained on heating and cooling for the compounds listed in Table 2.I are shown in Figures 2.4 to 2.13. The transition temperatures as well as their associated enthalpies and entropies are given in Tables 2.II and 2.III. Although Table 2.II lists both onset and peak transition temperatures, only the onset temperatures will be used

in the discussion of phase transformations. Also, unless otherwise specified, all the samples were examined between 120 K and 300 K.

### *i. 1-Bromoadamantane (1-$C_{10}H_{15}Br$)*

The compound 1-$C_{10}H_{15}Br$ was studied between 120 K and 350 K. The DSC curve (Figure 2.4) indicates that on heating, the compound undergoes two phase transformations one at 282 K and the other at 312 K. The associated enthalpies are 0.873 kJ $mol^{-1}$ and 7.31 kJ $mol^{-1}$ with entropies of 3.12 J $K^{-1}$ $mol^{-1}$ and 23.4 J $K^{-1}$ $mol^{-1}$ for transitions I and II, respectively. These values compare very well with those obtained by Clark *et al.*[41] ($\Delta H$ = 6.93 kJ $mol^{-1}$, $\Delta S$ = 22.32 J $K^{-1}$ $mol^{-1}$) and McCormick and co-workers.[42] Neither of the previous groups, however, reported any hysteresis.

The three solid phases exhibited by 1-$C_{10}H_{15}Br$ can be described by Scheme a:

$$\text{Phase I} \underset{282\ \text{K}}{\overset{283\ \text{K}}{\rightleftarrows}} \text{Phase II} \underset{306\ \text{K}}{\overset{312\ \text{K}}{\rightleftarrows}} \text{Phase III} \qquad [a]$$

The phase I to phase II transformation temperature shows no hysteresis while that for phase II to phase III shows a 6 K hysteresis. The hysteresis is characteristic of a first-order transitions and can be attributed to many factors which will be discussed later.

Another interesting phenomenon seen from the DSC curve is that on heating, the peak associated with the phase II to phase III transition is asymmetric. This could be indicative of a transition which proceeds in at least two steps. Scanning at 2.5 K $min^{-1}$ did not yield a different curve; however it is still possible that scanning at an even slower rate would have resulted in a separation of the two processes.

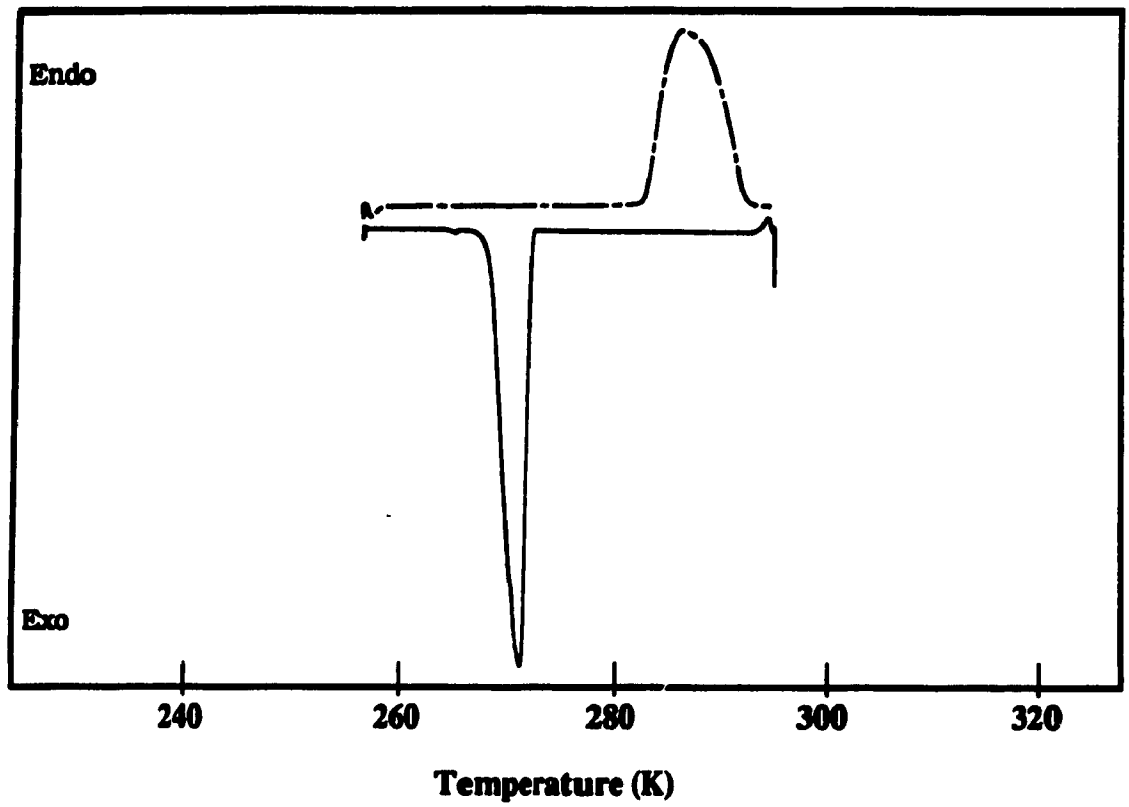


Figure 2.5 DSC curve of 2-bromoadamantane (2-$C_{10}H_{15}Br$) after cycling, scanned at 5 K $min^{-1}$ in the 220-326 K region. Cooling:solid line, heating:dashed line.

### *ii. 2-Bromoadamantane (2-$C_{10}H_{15}Br$)*

The DSC curve for 2-$C_{10}H_{15}Br$ (Figure 2.5) shows that only one solid-solid phase transition is encountered between 120 K and 350 K. The transition temperature is 281 K and 270 K on heating and cooling, respectively. The enthalpy associated with this transformation is 11.4 kJ $mol^{-1}$ while the entropy is 40.6 J $K^{-1}$ $mol^{-1}$. Although the transition temperature is similar to that found by Hara *et al.*, both the enthalpy and entropy of transition are higher than theirs ($\Delta H$ = 15.0 kJ $mol^{-1}$, 51.3 J $K^{-1}$ $mol^{-1}$).[43] 2-Bromoadamantane has one of the largest entropies encountered in the series of

**Table 2.II Transition temperatures (after cycling) for compounds 1 → 7.**

| | Transition Temperature (K) | | | | |
|---|---|---|---|---|---|
| | Cooling | | Heating | | Enthalpy |
| Compound and Transition | Onset | Peak | Onset | Peak | kJ mol$^{-1}$ |
| 1-$C_{10}H_{15}Br$ | | | | | |
| Phase I→II | 282 | 281 | 283 | 284 | 0.873 |
| Phase II→III | 306 | 304 | 312 | 315 | 7.31 |
| 2-$C_{10}H_{15}Br$ | | | | | |
| Phase I→II | 270 | 269 | 281 | 284 | 11.4 |
| 1-$C_{10}H_{15}Cl$ | | | | | |
| Phase I→II | 240 | 237 | 245 | 248 | 5.35 |
| 2-$C_{10}H_{15}Cl$ | | | | | |
| Phase I→II | 178 | 175 | 227 | 231 | 0.470 |
| Phase II→III | 231 | 228 | 242 | 244 | 8.31 |
| 9-$C_9H_{14}O$ | | | | | |
| Phase I→II | 283 | 282 | 299 | 304 | 13.9 |
| $C_6H_{10}O$ | | | | | |
| Phase I'→I | *** | *** | 189 | 190 | 0.555 |
| Phase I→II | 175 | 174 | 192 | 194 | 5.00 |
| Phase II→III | 210 | 210 | 234 | 235 | 1.28 |
| Phase III→liq | 246 | 244 | 245 | 249 | 0.746 |
| *o*-$C_2B_{10}H_{12}$ | | | | | |
| Phase I→II | 271 | 269 | 274 | 276 | 3.88 |

compounds studied, and is comparable to the value obtained for 2-adamantanone[44] and 1-adamantanol[45] which are greater than 35 J $K^{-1}$ $mol^{-1}$.

Scheme b, describes the two phases displayed by 2-$C_{10}H_{15}Br$:

$$\text{Phase I} \underset{270\ \text{K}}{\overset{281\ \text{K}}{\rightleftarrows}} \text{Phase II} \qquad [b]$$

and as can be seen a hysteresis of 11 K is observed between the reversible phases. Surprisingly, Hara and coworkers[43] did not report any temperature hysteresis but found a pressure hysteresis of only 0.10-0.13 kbar, which is quite low compared to the temperature hysteresis which we obtained.

As in the case of 1-$C_{10}H_{15}Br$, a broad asymmetric peak is observed on heating. Once again this could be due to a transition which proceeds in two steps or more.

### *iii. 1-Chloroadamantane (1-$C_{10}H_{15}Cl$)*

Figure 2.6 shows that the DSC curve for 1-$C_{10}H_{15}Cl$ contains only one solid-solid phase transformation in the region studied. The transition temperature is 245 K on heating while on cooling, the transformation occurs at 240 K. The related enthalpy and entropy are 5.35 kJ $mol^{-1}$ and 22.0 J $K^{-1}$ $mol^{-1}$, respectively, and are in excellent agreement with those reported by Clark *et al.*[41] ($\Delta H$ = 6.01 kJ $mol^{-1}$, $\Delta S$ = 24.61 J $K^{-1}$ $mol^{-1}$).

As can be seen from Scheme c, 1-$C_{10}H_{15}Cl$ has a hysteresis of only 5 K. Clark *et al.* did not apparently observe any temperature hysteresis.[41]

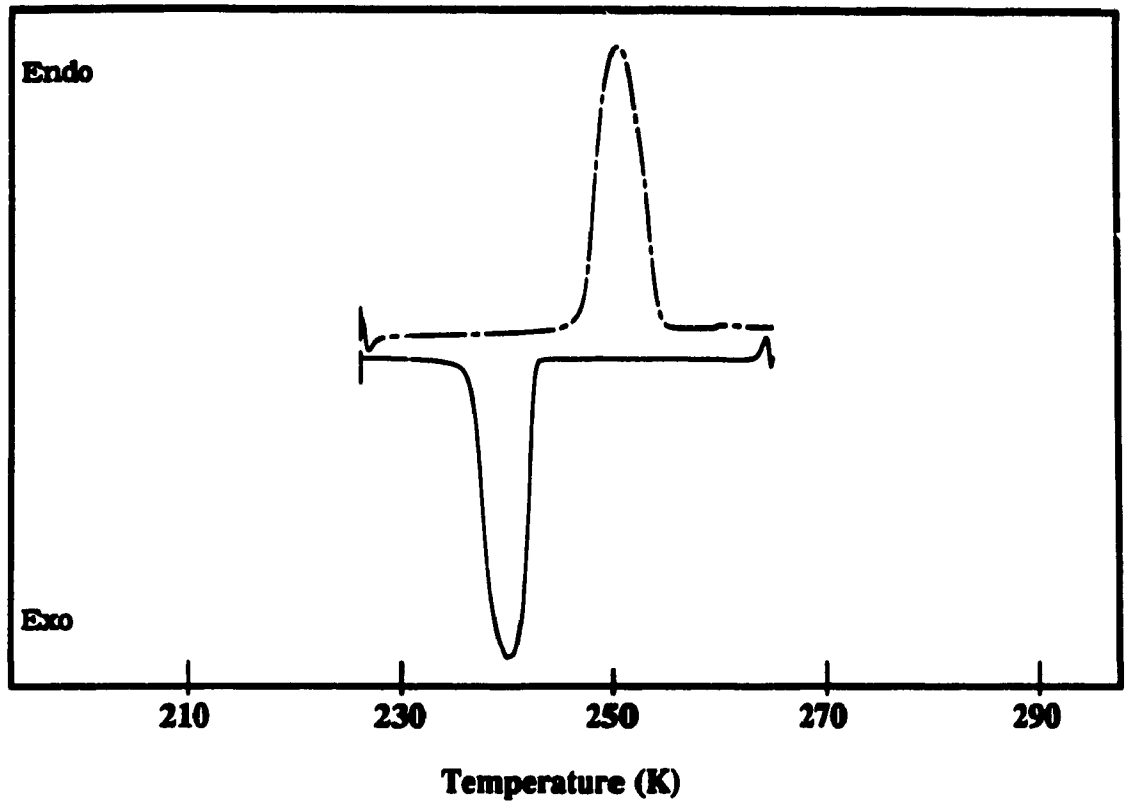


Figure 2.6 DSC curve of 1-chloroadamantane (1-$C_{10}H_{15}Cl$) after cycling, scanned at 5 K $min^{-1}$ in the 190-296 K region. Cooling:solid line, heating:dashed line.

$$\text{Phase I} \underset{240\,\text{K}}{\overset{245\,\text{K}}{\rightleftarrows}} \text{Phase II} \qquad [c]$$

Once again, this compound displays a broad asymmetric peak on heating which could be attributed to transformation which proceeds in more than one step.

### *iv. 2-Chloroadamantane (2-$C_{10}H_{15}Cl$)*

Two phase transitions were detected by DSC (Figure 2.7). The transition temperatures were 227 and 242 K on heating, and 231 and 178 K on cooling, with enthalpies of 8.31 kJ $mol^{-1}$ for the first transition and 0.470 kJ $mol^{-1}$ for the second.

**Table 2.III Thermodynamic data for compounds 1 → 7 (after cycling).**

| | Hysteresis (K) | | | |
|---|---|---|---|---|
| Compound<br>Transition | Onset<br>($\Delta T_o$) | Peak<br>($\Delta T_p$) | Entropy Change<br>J K$^{-1}$ mol$^{-1}$ | $\Delta S \Delta T_o$<br>J mol$^{-1}$ |
| 1-$C_{10}H_{15}Br$ | | | | |
| Phase I→II | 1 | 3 | 3.1 | 3.1 |
| Phase II→III | 6 | 11 | 23.4 | 140.4 |
| 2-$C_{10}H_{15}Br$ | | | | |
| Phase I→II | 11 | 15 | 40.6 | 446.6 |
| 1-$C_{10}H_{15}Cl$ | | | | |
| Phase I→II | 5 | 11 | 22.0 | 110.0 |
| 2-$C_{10}H_{15}Cl$ | | | | |
| Phase I→II | 49 | 56 | 2.1 | 102.9 |
| Phase II→III | 11 | 14 | 34.3 | 377.3 |
| 9-$C_9H_{14}O$ | | | | |
| Phase I→II | 16 | 22 | 46.5 | 744.0 |
| $C_6H_{10}O$ | | | | |
| Phase I'→I | ** | ** | 3.0 | ** |
| Phase I→II | 17 | 20 | 26.0 | 442.0 |
| Phase II→III | 24 | 25 | 5.6 | 134.4 |
| Phase III→liq | 1 | 5 | 3.1 | 3.1 |
| *o*-$C_2B_{10}H_{12}$ | 3 | 7 | 14.2 | 42.4 |

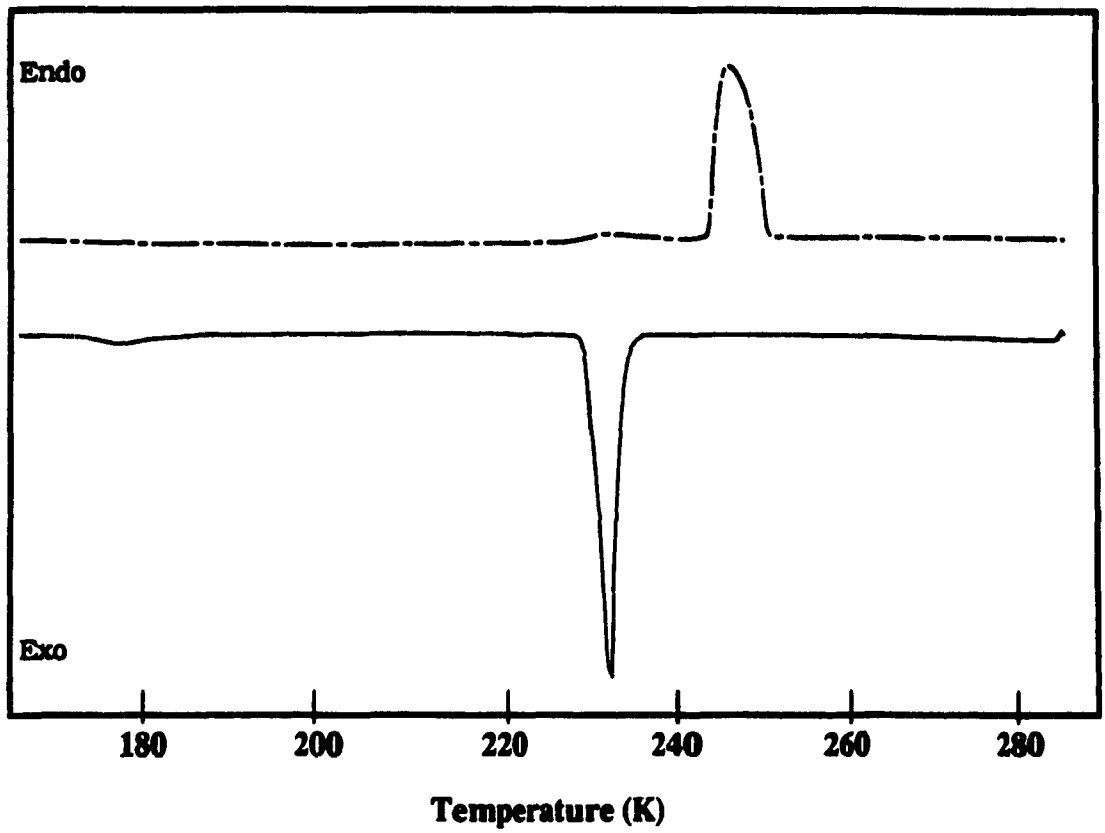


Figure 2.7 DSC curve of 2-chloroadamantane (2-$C_{10}H_{15}Cl$) after cycling, scanned at 5 K $min^{-1}$ in the 160-286 K region. Cooling:solid line, heating:dashed line.

The two solid-solid transitions can be described as three phases shown in Scheme d:

$$\text{Phase I} \underset{178\ \text{K}}{\overset{227\ \text{K}}{\rightleftarrows}} \text{Phase II} \underset{231\ \text{K}}{\overset{242\ \text{K}}{\rightleftarrows}} \text{Phase III} \qquad [d]$$

Although large hystereses are observed (~10 K for the phase II to phase III transformation and ~50 K for the phase I to phase II), 2-chloroadamantane did not exhibit any memory effects, i.e., the phase transition temperatures and enthalpies were not dependent on the previous thermal history of the sample. Rapid quenching, cycling at 20 K $min^{-1}$, did not reveal any exotherms on heating, hence no glassy state was formed. The entropies of transitions are 2.3 and 35 J $K^{-1}$ $mol^{-1}$ for the first and second phase transition,

respectively. The entropy of the first phase transition is much larger than that of adamantane itself and of various 1-substituted halo-derivatives which have entropies less than 25 J $K^{-1}$ $mol^{-1}$, but is similar to the entropies of 2-bromoadamantane, 1-adamantanol,[45] and 2-adamantanone.[44]

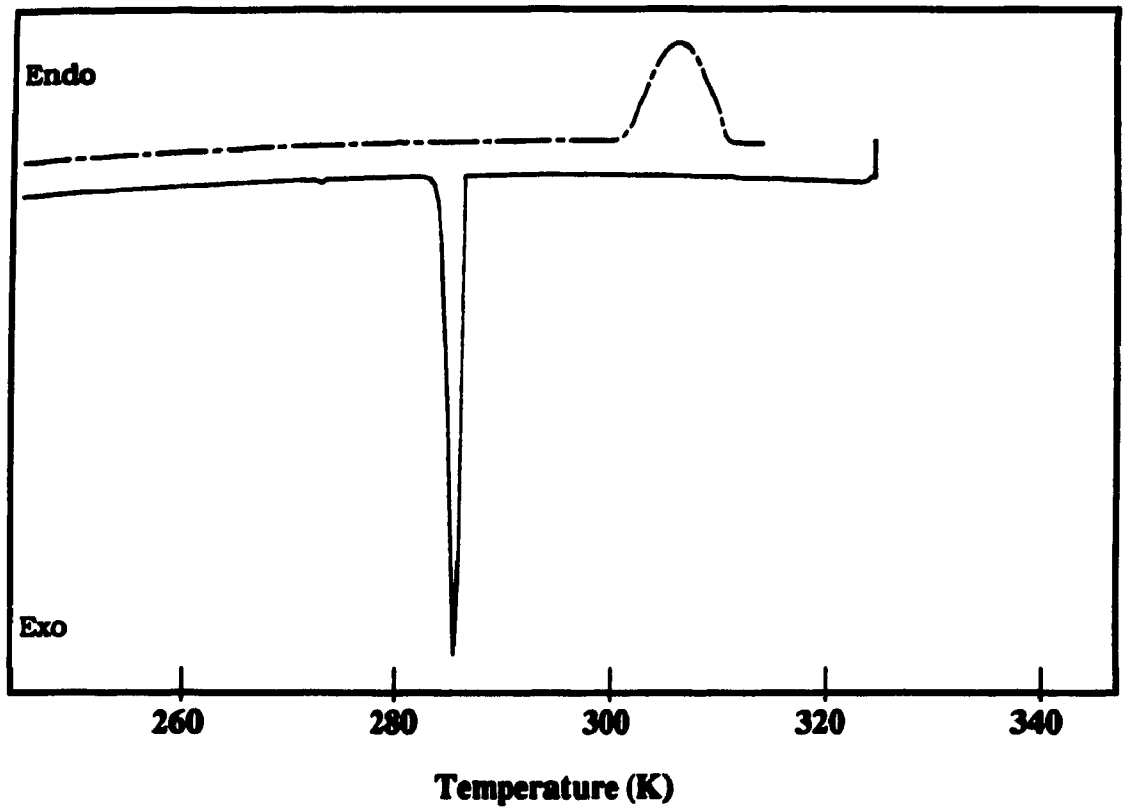


Figure 2.8 DSC curve of 9-bicyclononanone (9-$C_9H_{14}O$) after cycling, scanned at 5 K $min^{-1}$ in the 240-346 K region. Cooling:solid line, heating:dashed line.

### *v. Bicyclo[3.3.1]nonan-9-one (9-$C_9H_{14}O$)*

Only one solid-solid phase transition was detected by DSC, Figure 2.8, at 299 K on heating and 283 K on cooling with an enthalpy of 13.9 kJ $mol^{-1}$. The entropy associated with this transition is 46.5 J $K^{-1}$ $mol^{-1}$ and is the largest for the compounds studied in this

series. Although a large hysteresis of 16 K was found for 9-$C_9H_{10}O$ (Scheme e), no exotherm was observed on heating, after cycling, and therefore no glassy state was formed.

$$\text{Phase I} \quad \underset{283\ \text{K}}{\overset{299\ \text{K}}{\rightleftarrows}} \quad \text{Phase II} \qquad [e]$$

*vi. 7-oxabicyclo[2.2.1]heptane ($C_6H_{10}O$)*

This cage hydrocarbon exhibited three phase transitions, prior to cycling, of which one was a change-of-state and two were solid-solid phase transformations (Figure 2.9). On heating, the transition temperatures obtained were 191 K, and 231 K for the solid-solid transformation and 243 K for the melting transition. The cooling curve shows that melting occurs at 244 K, while the solid-solid transformations occur at 206 K and 170 K. The enthalpies (and entropies) prior to cycling were 5.14 kJ $mol^{-1}$ (26.9 J $K^{-1}$ $mol^{-1}$) for the first transition, 1.05 kJ $mol^{-1}$ (4.53 J $K^{-1}$ $mol^{-1}$) for the second, and 0.640 kJ $mol^{-1}$ and (2.61 J $K^{-1}$ $mol^{-1}$) for the melting transition. As seen from Scheme f, both solid-solid phase transitions exhibit large hysteresis effects. The melting transition showed no hysteresis which is indicative of a pure sample. Moreover, since only one peak is observed on melting, the melting transition is said to be congruent, i.e., the liquid and the crystal coexist. An incongruent melting point would show a minimum of two peaks on melting due to decomposition of the compound into a liquid and a new crystalline solid. Since the entropy of fusion (3.05 J $K^{-1}$ $mol^{-1}$) is less than the gas constant (8.314 J $K^{-1}$ $mol^{-1}$), it can be said that the plastic phase is a solid with free molecular rotation. In other words, the freedom of rotation was already present in the solid plastic phase and all that was gained from melting was translational freedom.

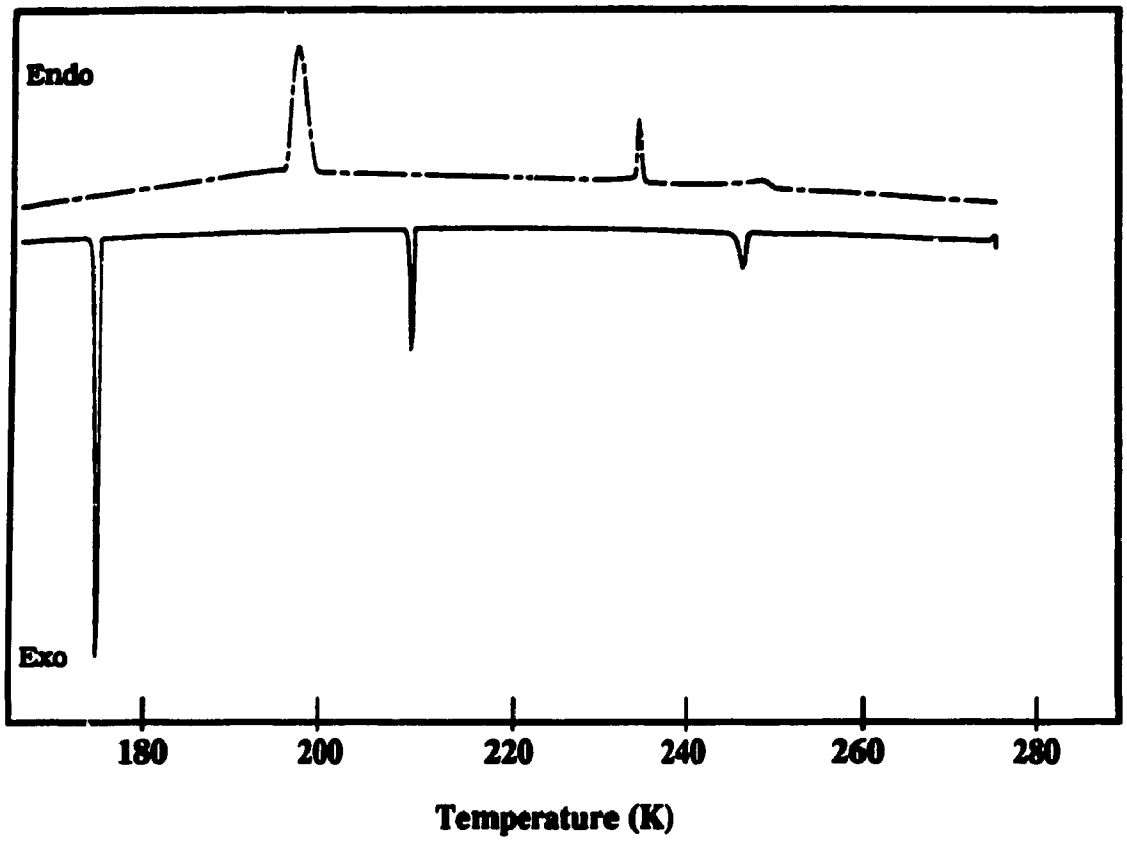


Figure 2.9 DSC curve of oxanorbornane scanned at 5 K $min^{-1}$ in the 160-286 K region, before cycling. Cooling:solid line, heating:dashed line.

$$\text{Phase I} \underset{170\,\text{K}}{\overset{191\,\text{K}}{\rightleftarrows}} \text{Phase II} \underset{206\,\text{K}}{\overset{231\,\text{K}}{\rightleftarrows}} \text{Phase III} \underset{244\,\text{K}}{\overset{243\,\text{K}}{\rightleftarrows}} \text{Liquid} \qquad [f]$$

During cycling at 20 K $min^{-1}$ (Figure 2.10), three peaks are observed on heating and on cooling. The peculiar aspects of the curves are that on heating, the phase I to phase II transformation shows a broad asymmetric peak probably due to a process involving two or more steps. Also, on cooling, the phase II to phase I transition displays a lot of movement as it travels in between cycles, until the fourth cycle when it remains at the same position. This is characteristic of a metastable state; hence, phase II is believed to be a metastable

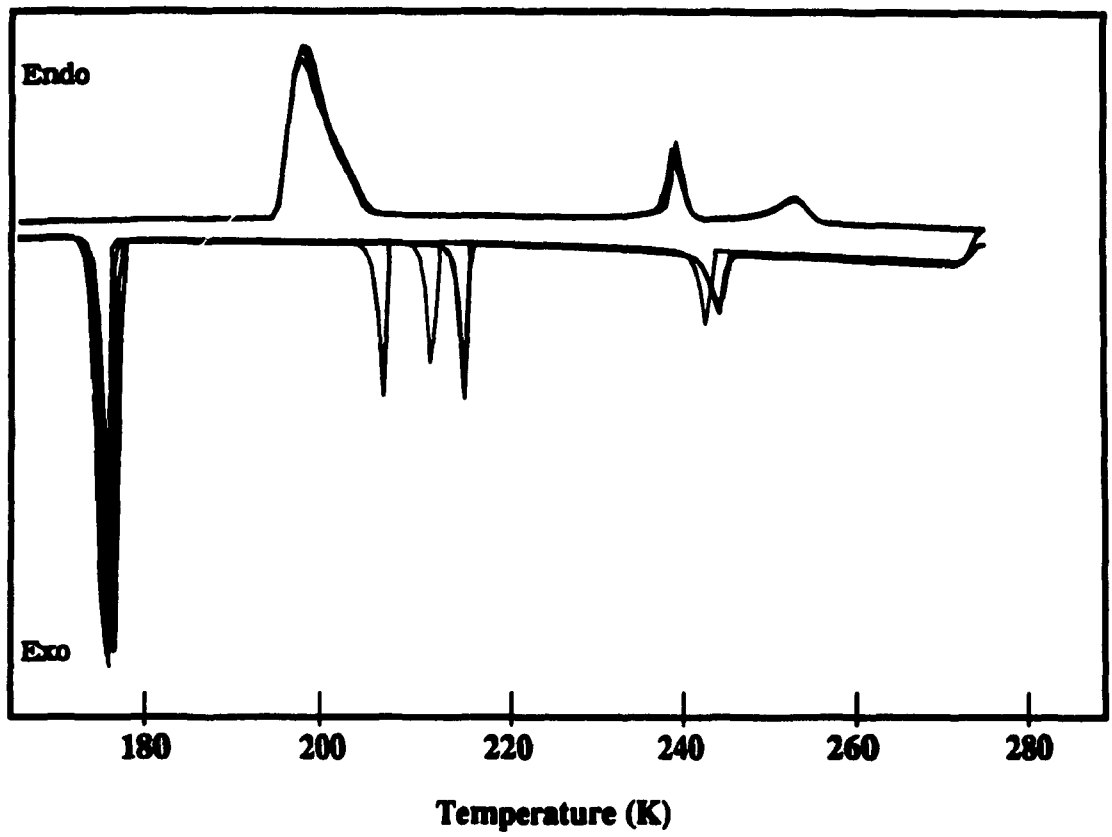


Figure 2.10 DSC curve of oxanorbornane ($C_6H_{10}O$) on cycling at 20 K $min^{-1}$, in the 160-286 K region.

one. Since this treatment did not reveal any exotherms on heating, it can be concluded that a glassy state was not formed.

Once the cycling was terminated, the sample was rescanned at 5 K $min^{-1}$. The cooling curve did not change except for sharpening of the peaks. On heating, however, the phase I to phase II transition was now composed of two sharp peaks (Figure 2.11). In other words, a total of five phases were present; four solid phases (see Scheme g) plus a liquid state. The related enthalpies (and entropies) of transition were 0.555 kJ $mol^{-1}$ (2.93 J $K^{-1}$ $mol^{-1}$), 5.00 kJ $mol^{-1}$ (26.0 J $K^{-1}$ $mol^{-1}$), 1.28 kJ $mol^{-1}$ (5.47 J $K^{-1}$ $mol^{-1}$), and 0.746 kJ $mol^{-1}$ (3.05 J $K^{-1}$ $mol^{-1}$), for transitions I', I, II, III, and melt, respectively. Since phase I' is so near phase I, it is quite possible that former is the same phase but with a

different nucleation site. Figure 2.12, shows a DSC curve for $C_6H_{10}O$ obtained on heating at 2.5 K $min^{-1}$, phase I' has nearly completely disappeared; this is probably due to slower scan speed which allows the crystals to nucleate from the same site. Alternatively, phase I' could possibly be a metastable phase.

$$\text{Phase I'} \underset{?????}{\overset{189\text{ K}}{\rightleftarrows}} \text{Phase I} \underset{175\text{ K}}{\overset{192\text{ K}}{\rightleftarrows}} \text{Phase II} \underset{231\text{ K}}{\overset{234\text{ K}}{\rightleftarrows}} \text{Phase III} \underset{244\text{ K}}{\overset{245\text{ K}}{\rightleftarrows}} \text{Liq} \qquad [g]$$

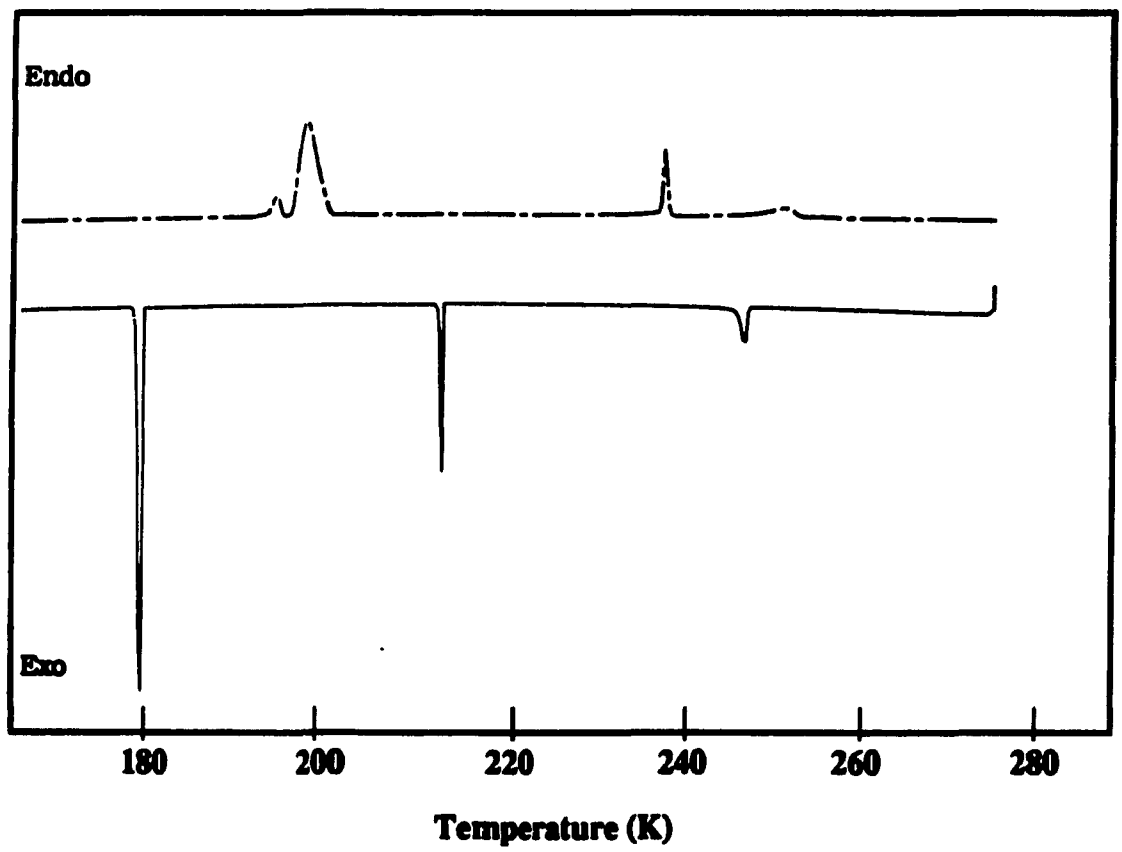


Figure 2.11 DSC curve of oxanorbornane after cycling, scanned at 5 K $min^{-1}$ in the 160-286 K region. Cooling:solid line, heating:dashed line.

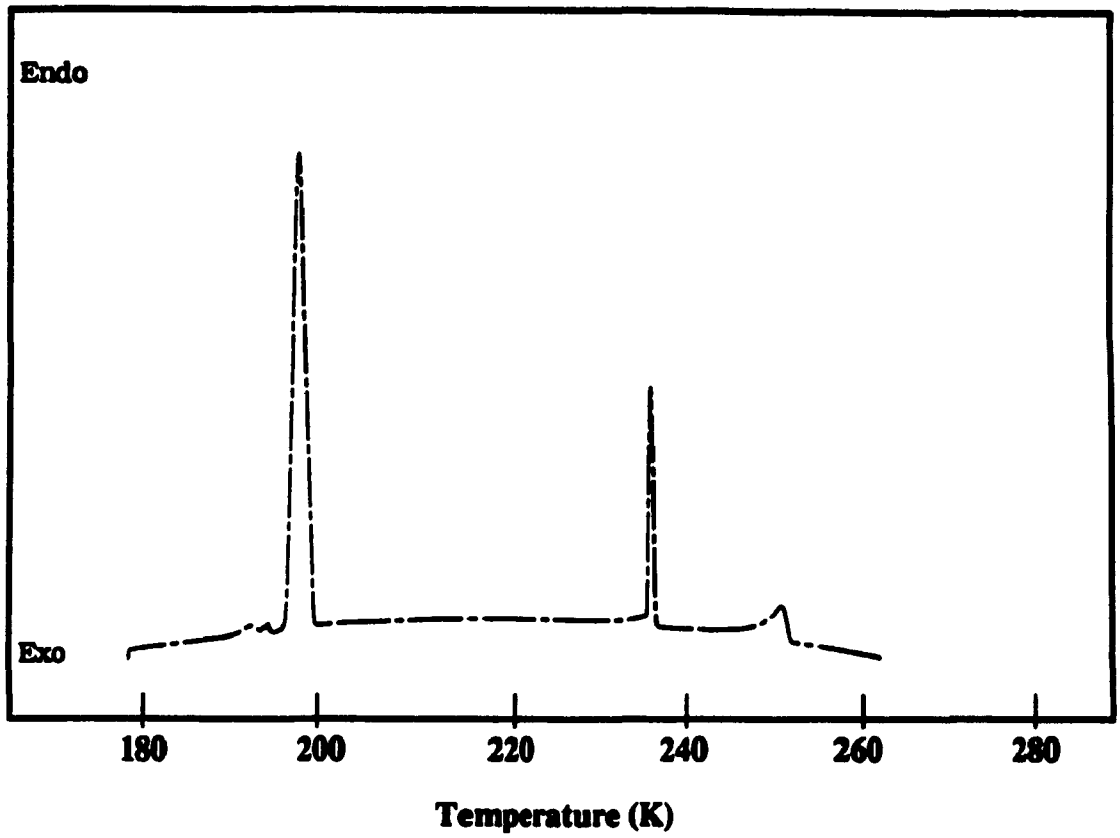


Figure 2.12 DSC curve of oxanorbornane on heating, after cycling, scanned at 2.5 K $min^{-1}$ in the 160-286 K region.

### *vii. o-Carborane ($o$-$C_2B_{10}H_{12}$)*

The DSC curves (Figure 2.13) revealed only one phase-transition in the temperature range of 330-100 K, with onset temperatures of 273 K on heating and 271 K on cooling (see Scheme h). The enthalpy and entropy of transition were 3.25 kJ $mol^{-1}$ and 12.0 J $K^{-1}$ $mol^{-1}$, respectively. These results are in excellent agreement with those cited in the literature.[46,47] However, no phase-transition was observed at 158 K as had been reported by Westrum and Henriquez (using adiabatic calorimetry).[47] This discrepancy is most probably due to differences in sample preparation and history, and possibly the scanning rate used (*vide infra*).

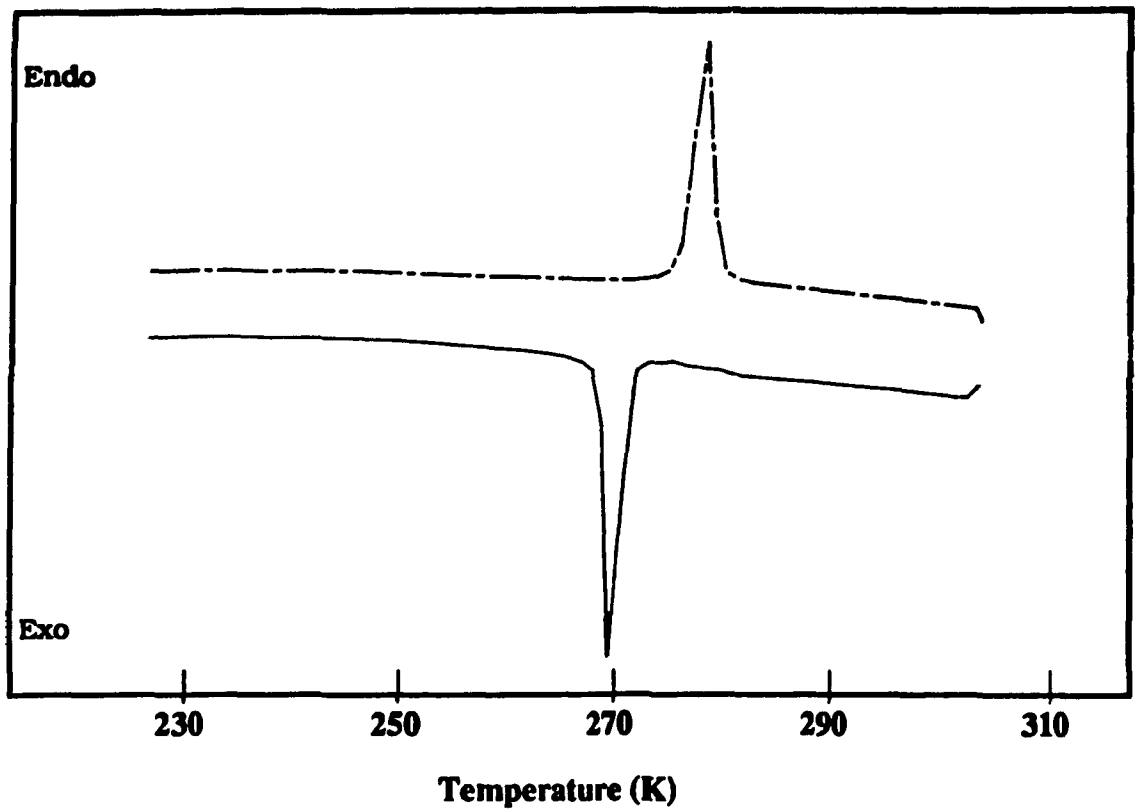


Figure 2.13 DSC curve of *o*-carborane ($o$-$C_2B_{10}H_{12}$) after cycling, scanned at 5 K min-1 in the 230-316 K region. Cooling:solid line, heating:dashed line.

$$\text{Phase I} \underset{271\ \text{K}}{\overset{273\ \text{K}}{\rightleftarrows}} \text{Phase II} \qquad [h]$$

## II. Discussion

### *i. Hysteresis*

The data in Tables 2.II and 2.III clearly indicate that for all of the reversible transformations, the transition temperatures for all the compounds, were dependent on whether cooling or heating was taking place. From a thermodynamic point of view, this

should not be observed if the process is truly reversible. This dependence is termed *hysteresis* from the Greek word *hysterein* meaning to be late.[48] By definition, the delay is caused by different forces, such as internal friction, acting on the substance being studied. A great deal of research has been carried out on this effect in order to more fully understand the reasons and the implication of hysteresis in general.[49-56]

One theory as to the cause of hysteresis is that rather than looking at the whole crystal, one should concentrate on a small region. This region, often referred to as the domain, would contain only a few molecules and a crystal can contain many domains which are similar but different. The size and properties of the crystal will then be controlled by the domain which is present in majority. When the sample is first cooled, many of the small domains are generated at a certain transition temperature. Eventually, these small domains migrate towards each other and merge, thus forming a larger domain which requires more energy (higher temperature) to undergo a phase transition.[54]

Another theory is based on regional densities of the two phases. Assuming that each phase has different densities, then, since one phase "gives birth" to the other, strain is induced. It is this strain or strain energy which based upon the Clausius-Clapeyron equation gives rise to the hysteresis.[50]

A third theory is that for a transformation to take place, nucleation must occur. Complete transformation, however, requires a nucleus of critical size to be present. This nucleus in turn depends on the strain to which the growing phase is exposed, and, as the strain varies so does the transition temperature. This theory seems to be a combination of the first two as it takes into account both strain and size of different regions.[50]

On the basis of the above theories, the domain which is present in greater proportions will dictate the behaviour of the crystal, and therefore, unlike liquid to solid crystallizations, small amounts of impurities should not affect solid-solid transformation.

The information which can be obtained from the temperature hysteresis is a rough estimate of the change in volume and strain energy. Staveley and Thomas found that the temperature hysteresis is, in general, proportional to the change in volume.[50] Rao and Rao found that the temperature hysteresis multiplied by the entropy of transition i.e., $\Delta T_0 \Delta S$, gives a general indication of the strain energy.[54] The calculated $\Delta T_0 \Delta S$ values for all the compounds studied can be found in Table 2.III.

The magnitude of $\Delta T$ varies from compound to compound and for a given compound, from transition to transition. The order of increasing $\Delta T_0$ (and thus $\Delta V$) is:

$$o\text{-}C_2B_{10}H_{12} < 1\text{-}C_{10}H_{15}Cl < 1\text{-}C_{10}H_{15}Br < 2\text{-}C_{10}H_{15}Br < 9\text{-}C_9H_{14}O < C_6H_{10}O < 2\text{-}C_{10}H_{15}Cl$$

The larger and more positive the $\Delta V$ value, the greater the strain energy since it implies that nuclei of lower density are growing out of nuclei with higher density. The $o\text{-}C_2B_{10}H_{12}$ would thus appear to have little if any strain involved in its phase transition, therefore the density of the two crystals should be the same, while $2\text{-}C_{10}H_{15}Cl$ has a lot of strain energy associated with the phase transformation, thus the density of the phases are very different.

The order of increasing $\Delta T_0 \Delta S$ is:

$$o\text{-}C_2B_{10}H_{12} < 1\text{-}C_{10}H_{15}Cl < 1\text{-}C_{10}H_{15}Br < 2\text{-}C_{10}H_{15}Br < 2\text{-}C_{10}H_{15}Cl < C_6H_{10}O < 9\text{-}C_9H_{14}O$$

The two previous trends, which take into account the total solid-solid phase transformation for a compound, are roughly similar as would be expected, since the strain energy is related to both $\Delta V$ and $\Delta T_0 \Delta S$.[54]

**Table 2.IV Calculated values for the excess entropy, $\Delta S_{xs}$, the conformational entropy, $R\ln(N_1/N_2)$, and entropy of transition, $\Delta S^{calc}$.**

| Compound | Symmetry | $N_1/N_2$ | $R\ln(N_1/N_2)$ J K$^{-1}$ mol$^{-1}$ | $\Delta S_{xs}$ J K$^{-1}$ mol$^{-1}$ | $\Delta S^{calc}$ J K$^{-1}$ mol$^{-1}$ |
|---|---|---|---|---|---|
| 1-$C_{10}H_{15}Br$ | $C_{3v}$ | 8 | 17.3 | 16.6 | 33.9 |
| | | 4 | 11.5 | 16.7 | 28.2 |
| 2-$C_{10}H_{15}Br$ | $C_s$ | 24 | 26.4 | 14.4 | 40.8 |
| 1-$C_{10}H_{15}Cl$ | $C_{3v}$ | 8 | 17.3 | 11.5 | 28.8 |
| | | 4 | 11.5 | 11.5 | 23.0 |
| 2-$C_{10}H_{15}Cl$ | $C_s$ | 24 | 26.4 | 11.2 | 37.6 |
| 9-$C_9H_{14}O$ | $C_{2v}$ | 12 | 20.7 | 14.4 | 35.1 |
| | | 48 | 32.2 | 14.4 | 46.6 |
| $C_6H_{10}O$ | $C_{2v}$ | 12 | 20.7 | 27.3 | 48.0 |
| | | 4 | 11.5 | 27.3 | 38.9 |
| *o*-$C_2B_{10}H_{12}$ | $C_{2v}$ | 12 | 20.7 | 10.5 | 31.2 |
| | | 2 | 5.7 | 10.5 | 16.2 |

The hysteresis involved in the phase II to phase III of oxanorbornane should be noted. As previously mentioned, the hysteresis varied with each cycle; sometimes it became larger and sometimes smaller, until after four cycles it was constant. Originally the hysteresis was 25 K while after cycling it was 17 K. A similar situation has been observed for 2-adamantanone by Butler and co-workers.[44] They attributed the hysteresis to a crystal containing impurities and defects, and that, after cycling, these factors were equally distributed over the entire crystal. They do however point out that if this was the sole reason for the hysteresis, then the hysteresis should diminish with cycling and not get larger as was the case for 2-adamantanone. Another possible explanation is that originally the

crystals are broken up into many small units, as cycling progresses, the crystal units might get larger thereby generating a larger hysteresis. The opposite had been theorized by Staveley and Thomas for the condition where the hysteresis gets smaller i.e., the original crystal units are large and as cycling takes place, they break up into smaller domains thus changing the transition temperatures and reducing the hysteresis.[50] Initially, in the case of oxanorbornane, cycling gives rise to a larger hysteresis and, hence, large crystals are involved; after cycling, the hysteresis gets smaller and so smaller crystals should be present. That phase, however, can still be said to be metastable.

### *ii. Guthrie And McCullough Entropies*

The Guthrie and McCullough equation for the interpretation of conformational entropies of transition in plastic crystals is:[57]

$$\Delta S_{tr} = R \ln(N_1/N_2) \qquad [2.11]$$

where $N_1/N_2$ is the ratio of the number of distinguishable positions on going from the ordered ($N_2$) to the disordered ($N_1$) phase. The calculated $N_1/N_2$ ratio, based on this equation, would range from 6 to 269, the latter being unreasonably high. Clark and co-workers have examined the entropies of transition for several cage hydrocarbons and proposed an empirical equation involving an excess entropy, which depends upon the temperature range of the disordered phase, eq. [2.12]:[41,58]

$$\Delta S_{tr} = R \ln(N_1/N_2) + 10.3 + 45 \exp\{-[0.0183(T_m-T_{tr})]\} \qquad [2.12]$$

where $10.3 + 45 \exp\{-[0.0183(T_m-T_{tr})]\}$ is the excess entropy and $(T_m-T_{tr})$ is the temperature range of the plastically crystalline phase. When more than one solid-solid transformation is present, the total entropy change between ordered and disordered

structures is given by the sum of all the transition entropies, plus a small, negligible term for the heat capacity. The values for $N_1/N_2$ listed in Table 2.IV are based on the assumption that phase I is face-centered-cubic (fcc), which is typical for these materials. Table 2.IV contains the calculated data using eq. [2.12], where $T_m$, the melting temperature, is listed in Table 2.I, and $T_{tr}$, the onset temperature of transformation for phase I obtained on heating, can be found in Table 2.II.

A comparison of the experimental $\Delta S$ (Table 2.III) with the calculated $\Delta S^{calc}$ (Table 2.IV), shows that the Clark *et al.*[40,58] equation applies quite well to some of the compounds and rather poorly in other cases. This could be due to the fact that the equation is based on a limited series of compounds as well as lattice expansion effects. For the compounds where the $\Delta S^{calc}$ did not correspond to the experimental value, the $N_1/N_2$ ratio was varied until a more reasonable comparison was obtained.

As shown in Table 2.IV, the excess entropy, $\Delta S_{xs}$, is approximately the same for the bromoadamantanes but larger than that for the chloroadamantanes (although the chloroadamantanes do have similar $\Delta S_{xs}$). $\Delta S_{xs}$ is the entropy due to lattice slackening or lattice expansion and other effects such as dipolar interactions. This would indicate that larger substituents increase the slackening of the lattice and, since the 1-substituted adamantanes have a slightly larger $\Delta S_{xs}$ than their 2-substituted counterparts, that perhaps the 1-position has a greater lattice expansion effect then the 2-position.

## D. REFERENCES


1. R. C. Mackenzie, *Talanta*, **16**, 1227 (1969).
2. R. C. Mackenzie, C. J. Keattch, D. Dollimore, J. A. Forrester, A. A. Hodgson, J. P. Redfern, *Talanta*, **19**, 1079 (1972).
3. J. Timmermans, *J. Chim. Phys.*, **35**, 331 (1938).
4. J. Timmermans, *J. Phys. Chem. Solids*, **18**, 1 (1961).
5. H. Arntz, G. M. Schneider, *Farad. Discuss. Chem. Soc.*, **69**, 139 (1980).
6. E. M. Barrall, J. F. Johnson, "Differential Scanning Calorimetry Theory and Applications" in *Techniques and Methods of Polymer Evaluation*, 1970, Vol. 2, Chap. 1.
7. M. D. Judd, M. I. Pope, *J. inorg. Nucl. Chem.*, **33**, 365 (1971).
8. R. C. Mackenzie "Basic Priciples and Historical Development", in *Differential Thermal Analysis*, R. C. Mackenzie, ed., Academic Press, New York, 1970, Vol. 1, Chap. 1.
9. R. C. Mackenzie, P. G. Laye, *Chemistry in Britain*, 1005 (1986).
10. R. C. Mackenzie, B. D. Mitchell, "Technique", in *Differential Thermal Analysis*, R. C. Mackenzie, ed., Academic Press, New York, 1970, Vol. 1, Chap. 4.
11. R. C. Mackenzie, B. D. Mitchell, *Analyst*, **87**, 420 (1962).
12. T. Meisel, *J. Thermal Anal.*, **29**, 1379 (1984).
13. J. P. Redfern, "Low-Temperature Studies", in *Differential Thermal Analysis*, R. C. Mackenzie, ed., Academic Press, New York, 1972, Vol. 2, Chap. 30.
14. J. Rouquerol, P. Boivinet, "Calorimetric Measurements", in in *Differential Thermal Analysis*, R. C. Mackenzie, ed., Academic Press, New York, 1972, Vol. 2, Chap. 27.
15. S. N. Pennington, *Rev. Anal. Chem.*, **1**, 113 (1972).
16. J. Sestak, P. Holba, G. Lombardi, *Ann. Chim. (Rome)*, **67**, 73 (1977).
17. H. A. Skinner, "Theory, Scope, and Accuracy of Calorimetric Measurements" in *Biochem. Microcalorimetry*, H. D. Brown, ed., Academic Press, New York, 1969, Chap. 1.
18. H. Suzuki, B. Wunderlich, *J. Thermal Anal.*, **29**, 1369 (1984).
19. M. J. Vold, *Anal. Chem.*, **21**, 683 (1949).
20. M. A. White, *Thermochim. Acta*, **74**, 55 (1984).
21. R. C. Wilhoit, "Thermodynamic Properties of Biochemical Substances", in *Biochem. Microcalorimetry*, H. D. Brown, ed., Academic Press, New York, 1969, Chap. 2.
22. H. Le Châtelier, *Compt. Rend. hebd. Séanc. Acad. Sci. Paris*, **104**, 1443 (1887).

23. H. Le Châtelier, *Bull. Soc. Fr. Mineral. Cristallogr.*, **10**, 204 (1887).

24. W. C. Roberts-Austen, *Proc. Inst. Mech. Eng.*, **35** (1899).

25. S. L. Boersma, *J. Am. Ceram. Soc.*, **38**, 281 (1955).

26. D. J. David., *Anal. Chem.*, **36**, 2162 (1964).

27. E. Murrill, L. W. Breed, *Thermochim. Acta*, **1**, 409 (1970). and P. Pacor, *Anal. Chim. Acta*, **37**, 200 (1967).

28. E. E. Sidorova, L. G. Berg, "Determination of Thermal Constants", in *Differential Thermal Analysis*, R. C. Mackenzie, ed., Academic Press, New York, 1972, Vol. 2, Chap. 26.

29. M. J. O'Neill, *Anal. Chem.*, **36**, 1238 (1964).

30. E. M. Watson, M. J. O'Neill, J. Justin, N. Brenner, *Anal. Chem.*, **36**, 1233 (1964).

31. E. Calvet, *J. Chim. Phys.*, **59**, 319 (1962).

32. J. E. Callanan, S. A. Sullivan, *Private Communication*

33. A. Radenac, C. Berthaut, *Bull. Inform. Sci. Tech., Commis. Energ. At. (Fr.)*, **180**, 43 (1973).

34. A. P. Gray, "A Simple Generalized Theory for the Analysis of Dynamic Thermal Measurement", in *Analytical Calorimetry*, R. S. Porter, J. F. Johnson, eds., PLenum Press, 1968, pp. 209-218.

35. *CRC Handbook of Chemistry and Physics*, R. C. Weast, M. J. Astle, eds., CRC Press, Boca Roca, Florida, 1982, pp. F-92 and F-106.

36. A. R. Ubbelhode, *Quart. Reviews*, **11**, 246 (1957).

37. A. R. Ubbelhode, *The Molten State of Matter Melting and Crystal Structure*, John Wiley and Sons, Ltd., U.S.A. (1978), Chap. 4.

38. A. J. Majumdar, H. A. McKinistry, R. Roy, *J. Phys. Chem. Solids*, **25**, 1487, (1964).

39. N. G. Parsonage, L. A. K. Stavely, *Disorder in Crystals*, Oxford University Press, Great Britain (1978).

40. W. Gutt, A. J. Majumdar, "Phase Studies", in *Differential Thermal Analysis*, R. C. Mackenzie, ed., Academic Press, New York, 1972, Vol. 2, Chap. 29.

41. T. Clark, T. M. Knox, H. Mackle and M.A. McKervey, *J. Chem. Soc., Faraday Trans. I*, **73**, 1224 (1977).

42. D. G. McCormick, L. R. Sherman, T. J. Klingen, *Radiat. Phys. Chem.*, **15**, 677 (1980).

43. K. Hara, Y. Katou and J. Osugi, *Bull Chem. Soc. Jpn.*, **54**, 687 (1981).

44. I. S. Butler, H. B. R. Cole, D. F. R. Gilson, P. D. Harvey, J. D. McFarlane, *J. Chem. Soc., Faraday Trans. II*, **82**, 535 (1986).

45. P. D. Harvey, D. F. R. Gilson, I. S. Butler, *Can. J. Chem.*, **65**, 1757 (1987).

46. R. H. Baughmann, *J. Chem. Phys.*, **53**, 3781 (1970)

47. E. F. Westrum, S. H. Henriquez, *Mol. Cryst. Liq. Cryst.*, **32**, 31 (1976)

48. *Webster's Ninth New Collegiate Dictionary*, Mirriam-Webster Inc., U.S.A. (1986), p. 595.

49. P. Dinichert, *Helv. Phys. Acta*, **17**, 389 (1944).

50. D. G. Thomas, L. A. K. Staveley, *J. Chem. Soc.*, 2572 (1951).

51. A. R. Ubbelhode, *Nature (Lond.)*, **169**, 832 (1952).

52. L. A. K. Staveley, *Ann. Rev. Phys. Chem.*, **13**, 351 (1962).

53. C. J. Schneer, R. W. Whiting, *Amer. Mineral.*, **48**, 737 (1963).

54. K. J. Rao, C. N. R. Rao, *J. Mater. Sci.*, **1**, 238 (1966).

55. J. S. Ingman, G. J. Kearley, S. F. A. Kettle, *J. Chem. Soc. Faraday Trans., I*, **78**, 1817 (1982).

56. E. B. Smith, *J. Phys. Chem. Solids*, **9**, 182 (1959).

57. G. B. Guthrie, J. P. McCullough, *J. Phys. Chem. Solids*, **18**, 53 (1961).

58. T. Clark, M. A. McKervey, H. Mackle and J. J. Rooney, *J. Chem. Soc., Faraday Trans. I*, **70**, 1279 (1974).

# CHAPTER 3
# VARIABLE-TEMPERATURE FT-IR AND RAMAN STUDIES OF ORIENTATIONALLY-DISORDERED SOLIDS (PLASTIC CRYSTALS)

## A. INTRODUCTION

### I. General

The infrared (IR) and Raman spectroscopic techniques have been used routinely for about 50 years in molecular structure determination. Both methods of analysis, however, have undergone significant changes over the last twenty years. In the case of the IR spectroscopy, the advent of computers and the incorporation of a Michelson-type interferometer have led to a considerable gain of popularity under the name of Fourier transform-infrared (FT-IR) spectroscopy. This technique has some definite advantages associated with: (1) Fellgett's advantage, also known as the multiplex advantage, which, as the name suggests, allows for the spectrum to be gathered from a single scan since all the frequencies are detected simultaneously; (2) Jacquinot's advantage, where the optical throughput of the system is increased and thus, so is the signal-to-noise ratio; and (3) Connes' advantage, where all the frequencies are calibrated as a function of the He-Ne laser. These three advantages together with the interfacing of a micro- or minicomputer permit the acquisition of much more sensitive spectra in shorter time periods than when

using a conventional dispersive IR spectrometer. The Raman technique increased in popularity in the late 1960's when CW lasers first began to be used as excitation sources, and is constantly undergoing changes. Most recently, FT-Raman spectroscopy has been developed and once the major bugs are taken out of this system, Raman spectroscopy will become a very important industrial tool. FT-Raman spectroscopy will not, however, be able to completely replace conventional Raman spectroscopy for a very long time, if ever. For a more complete theoretical and historical review on IR and Raman spectroscopy, see references 1 to 16.

Interactions between a photon and a molecule can give rise to three different phenomena. Firstly, absorption can come about if $E = h\nu$ is equal to the difference between two energy levels of a molecule. Secondly, if the energy of the photon corresponds to the difference between a true energy level and a virtual one, then scattering occurs. This is a two-photon effect which cannot be broken into two single steps, i.e., absorption and emission. Two different effects, Rayleigh and Raman scattering, can be observed from scattering. If the incident photon either loses or gains energy i.e., inelastic scattering, then the effect is known as Raman scattering otherwise it is labelled Rayleigh (elastic) scattering. Rayleigh line is several orders of magnitude ($\sim 10^4$) more intense than Raman scattering and since,

$$h\nu_{Rayleigh} = h\nu_0 \qquad [3.1]$$

it is possible to use the Rayleigh line as a means of verifying the frequency of the laser line being used to excite the sample. (This is accomplished by closing the slits to ~50 μm, reducing the laser power to ca. 50 mW, and scanning from -10 to +10 $cm^{-1}$). The third effect that can arise from the interaction of a photon with a molecule is emission and is a direct consequence of absorption.

The three effects listed above give rise to spectra from which it is possible to determine vibrational energies. In IR spectroscopy (an absorption technique),

$$\nu_{vib} = \nu_0 = \nu_{IR} \qquad [3.2]$$

where $\nu_0$ is the frequency of the incident beam with which the vibrating molecule interacts coherently and $\nu_{IR}$ is the frequency of the absorbed radiation. As previously noted, Raman spectroscopy can yield two possible energies,

$$\nu_{vib} = \nu_0 - \nu_{Stokes} \qquad [3.3a]$$

$$\nu_{vib} = \nu_{anti\text{-}Stokes} - \nu_0 \qquad [3.3b]$$

where $\nu_{Stokes}$, and $\nu_{anti\text{-}Stokes}$ are the Stokes and anti-Stokes frequencies and $\nu_0$ is the excitation wavelength. In theory, one can employ either Stokes or anti-Stokes scattering and observe the same Raman bands on a single Raman spectrometer. Unfortunately, this is not truly possible due to the loss of sensitivity of the detector in the anti-Stokes region and due to the low-intensity of the anti-Stokes bands which are governed by the Boltzman distribution function. Thus, in general, it is the Stokes Raman scattering that is analyzed. Lastly, the energy calculation for fluorescence, an emission process, is governed by:

$$\nu_{vib} = \nu_0 - \nu_{emission} \qquad [3.4]$$

and it is dependent on the excitation wavelength.

The basic difference between Raman and fluorescence spectroscopy is that in Raman scattering a transfer of energy occurs without the formation of an excited electronic state while in fluorescence, an excited electronic state is formed. Raman scattering arises from molecular motions that generate polarizability changes in the molecule, whereas IR absorptions are due to interactions between normal modes, which undergo changes in

dipole moment, and the incident radiation. This difference in selection rules gives rise to different spectra and it is for this reason that both techniques are used in the vibrational analysis of a molecule. Bands that appear strongly in the IR may be very weak in the Raman spectrum and *vice-versa*. Moreover, as the symmetry of the molecule increases, Raman active bands are often IR inactive and likewise for IR active peaks.

The effect of temperature on a vibrational spectrum is well-known and is governed by the Boltzman distribution function and therefore, lowering the temperature reduces, if not eliminates, the occurrence of "*hot bands*". Sometimes, however, the spectral changes are much more dramatic and it is obvious that the changes are not due only to the Boltzman effect but rather to some other factor. This is another application of variable-temperature FT-IR and Raman spectroscopy, namely probing phase transitions. It had been shown, in the previous chapter, that DSC can be used to determine whether a phase change is taking place and if so, of what order it is (i.e., first or second-order). It is not, however, possible to ascertain whether the transformation is of the order-disorder type or if some other phenomenon is taking place. Variable-temperature vibrational spectroscopy thus supplements the DSC results by allowing the researcher to judge, based on the observed IR and/or Raman bands, what type of phase is present. This is rendered possible because as the temperature is reduced, the lattice contracts and if a phase transformation occurs, then the crystal symmetry varies and invariably so will the selection rules, hence, a different spectrum should be obtained. Furthermore, as will be shown in this chapter, variable-temperature Raman and IR can sometimes detect phase transitions which cannot easily be observed by DSC measurements. It will also be demonstrated that certain vibrational regions are more susceptible to changes as the molecule undergoes a phase transformation and that, as previously indicated, these changes are not merely due to temperature effects.

The primary aim of this chapter is not to do a complete and thorough band analysis for the compounds studied (although some band analyses will be presented), but rather, to

demonstrate the usefulness of variable-temperature IR and -Raman phase studies in identifying phase transitions.

## B. EXPERIMENTAL

### I. Raman Measurements

The Raman spectra were obtained using an Instruments S.A. spectrometer with a Jobin-Yvon U-1000, 1.0-m double monochromator that was interfaced to a Columbia Commandor 964 microcomputer. The 514.532-nm (green) and 487.987-nm (blue) lines of a Spectra-Physics model 164, 5-W (all-line-power) argon-ion laser were used to excite the samples. The power levels were measured on a Coherent Radiation model 201 power-meter; the laser powers varied between 100 and 300 mW at the sample. The Raman studies were done on samples sealed in glass capillary tubes which were mounted on to the cold finger of a cryostat (see Section 3.B.III.i) using indium foil as the conducting junction. The resolution employed was dependent on the slit-width and on the argon-ion line used and varied between 1 and 3 $cm^{-1}$. The resolution was obtained by constructing a curve based on some information provided by I.S.A. The following equation was determined by fitting the above curve (see Figure 3.1):

$$\text{Res.} = \{(0.2254 - 1.436*10^{-3}*\lambda + 3.959*10^{-6}*\lambda^2 - 5.645*10^{-9}*\lambda^3 + 4.073*10^{-12}*\lambda^4 - 1.177*10^{-15}*\lambda^5)*\mu\} \quad [3.5]$$

where the resolution is given in $cm^{-1}$, $\lambda$ is the wavelength in nm and $\mu$ is the slit-width in $\mu$m. The equation governs the range of the U-1000 monochromator from 300.0 to

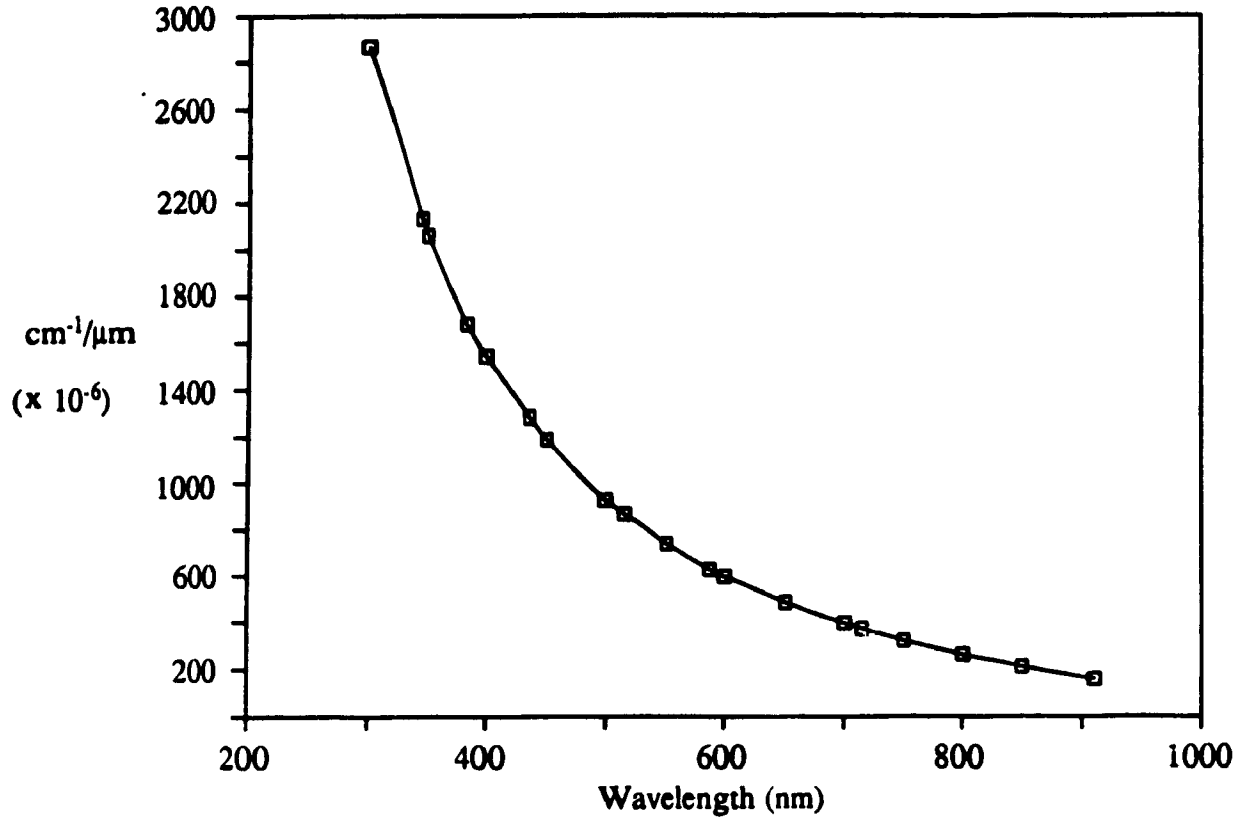


Figure 3.1 Double dispersion as a function of wavelength for the I.S.A. Ramanor U-1000 Raman Spectrometer.

909.1 nm when equipped with two 1800 grooves $mm^{-1}$ holographic gratings. The resolutions for commonly used wavelengths and slit-widths are given in Table 3.I. Unless otherwise mentioned, the spectra were not smoothed. In the cases where spectral smoothing (Savitsky-Golay algorithm) was employed, the resolution of the spectrum could be calculated from eq. [3.6]:

$$\text{Res(smoothed)} = \sqrt{[\text{Res(experimental)}^2 + \{(\#\text{ pts. smoothing})/2\}^2]} \qquad [3.6]$$

Therefore, a 9-point smoothing on a spectrum experimentally acquired at 2 $cm^{-1}$, yields a resolution of 5 $cm^{-1}$.

**Table 3.I** Resolution as a function of commonly used wavelengths and slit-widths for the U-1000 monochromator.

| λ (nm) (in air) | Slit-width (μm) | Resolution ($cm^{-1}$) |
|---|---|---|
| 487.986 (argon-ion) | 100 | 0.98 |
| | 300 | 2.95 |
| | 500 | 4.92 |
| 514.531 (argon-ion) | 100 | 0.87 |
| | 300 | 2.62 |
| | 500 | 4.36 |
| 520.832 (krypton-ion) | 100 | 0.85 |
| | 300 | 2.54 |
| | 500 | 4.24 |
| 530.866 (krypton-ion) | 100 | 0.81 |
| | 300 | 2.44 |
| | 500 | 4.06 |
| 568.189 (krypton-ion) | 100 | 0.69 |
| | 300 | 2.08 |
| | 500 | 3.46 |
| 645.629 (krypton-ion) | 100 | 0.50 |
| | 300 | 1.50 |
| | 500 | 2.50 |

The filtering of the laser lines was achieved by two methods: (a) Pellin-Broca premonochromator or (b) Fabry-Pérot interference type filter (514.5-nm and 488.0-nm). The advantage of the Pellin-Broca system is twofold. Firstly, unlike interference filters which must be changed based on the wavelength used, the premonochromator is applicable over a wide range of wavelengths, e.g., 300 to 900 nm. Secondly, the power-throughput on a Pellin-Broca premonochromator is close to 80%, whereas interference filters yield only

~50% throughput. The disadvantage of the Pellin-Broca system is that the alignment is extremely critical if high-throughput is desired.

*i. Optical alignment of the Pellin-Broca premonochromator*

The alignment of the optical components is crucial in obtaining a good Raman spectrum. It is essential that the following procedure be used when power at the sample and spectral resolution are important.

(a) Remove all optical components (except the Brewster angle prisms) between the laser and the monochromator - simply trying to correct the laser beam path by adjusting various lenses in the optical path will not yield good results (see Figure 3.2a).

(b) Measure the height of the laser beam immediately after the upper prism (prism #2) and immediately before entering the sample compartment set-up (at M3). If the heights are not equal, then move the bottom prism (prism #1) up or down until a straight line is obtained.

(c) Once a straight beam is obtained, place both lenses back onto the optical rail, pushing them in completely so that only the set screws are being skimmed by the beam (i.e., if the beam is straight then the set screws represent the center reference point).

(d) Place the pin-hole on the optical rail, making certain that the 100–μm aperture is centered with the beam. Position the 300-mm focal length lens, (lens #1) nearest to prism #2, so that the laser beam is passing through its center and simultaneously ensuring that the beam is still going through the 100–μm aperture.

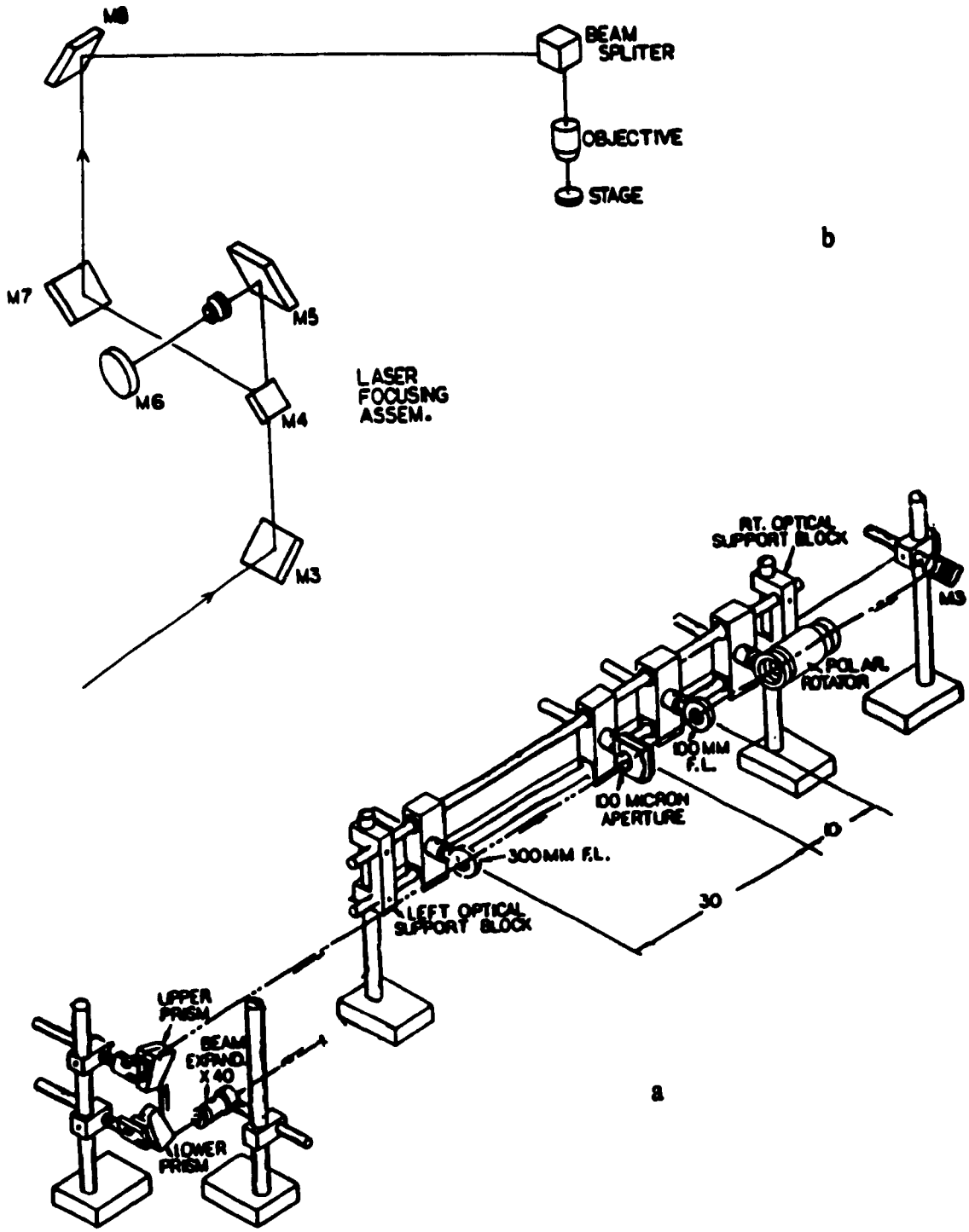


Figure 3.2 (a) Optical components of the Pellin-Broca filtering system and (b) optical configuration of the macrochamber and the microscope. (Taken in part, with permission from Instruments S.A., Metuchen, New Jersey, U.S.A.)

(e) Position the 100-mm focal-length lens (lens #2), so that the beam passes through its center. At this point, the distance between the 300-mm lens and the pin-hole should be ~30 cm and that between the pin-hole and the 100-mm lens ~10 cm.

(f) Install the 40X beam expander (between the laser and prism #1) so that the beam passes through its center (19.5 cm from table, and 7.7 cm from stand to center of expander). If the position is correct, then the beam should still be passing through the center of the 300-mm lens and the 100-μm aperture (pin-hole).

(g) Adjust the beam expander in order to obtain a spot the size of a dime (~10 mm-20 mm diameter) on the 300-mm focal length lens.

(h) If all the above is correct, then proceed with maximizing power through the pin-hole by moving the pinhole towards, or away from, the 300-mm lens. At this stage it might also be necessary to adjust the prism #2 with the micro-adjustment mount. Also, adjust the 100-mm focal length lens so as to collimate the beam as it enters the sample compartment.

(i) Install the rotator polarizer and set it at $0^{o}$.

### *ii. Macrochamber alignment*

Since it is more difficult to align the microscope than the macrochamber, it is preferable that the macrochamber be aligned prior to aligning the microscope. **Note: unless steps (a) to (i) of the previous section are optimized, it will be extremely difficult to align the macrochamber and even more so, the microscope.**

(a) Rotate the macro/micro mirror (M4) so that the beam can reach the macrochamber (see Figure 3.2b).

a

b

c

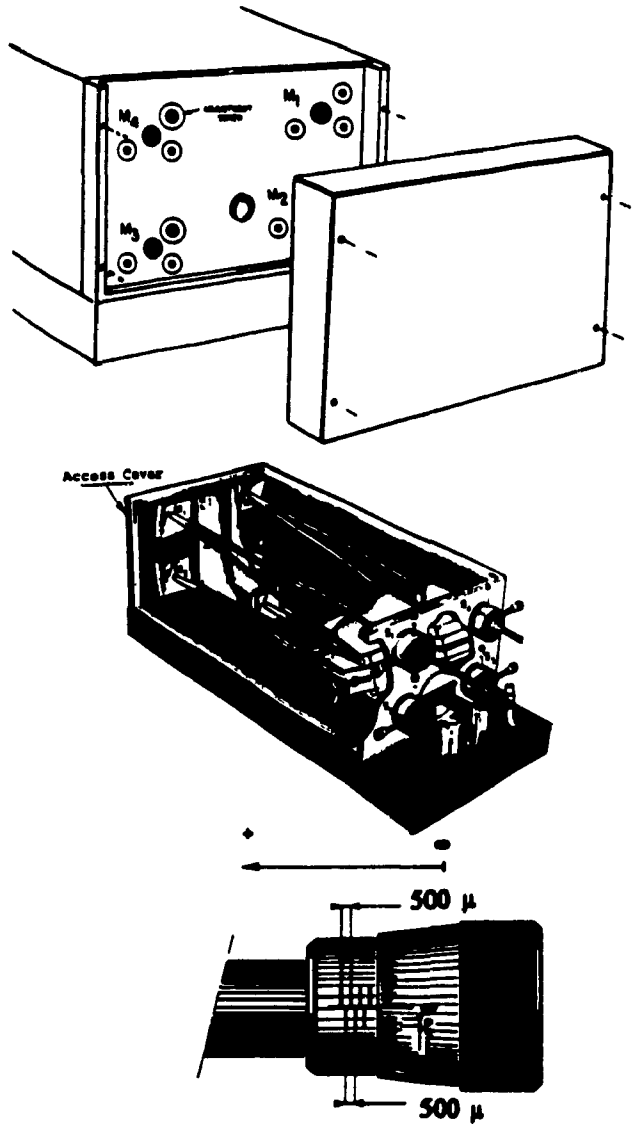


Figure 3.3 (a) Inside of access cover (b) U-1000 Raman Spectrometer and (c) Vernier scale for slit adjustment. (Taken in part, with permission from Instruments S.A., Metuchen, New Jersey, U.S.A.)

(b) Remove the lens at the entrance of the macrochamber and place a target mask in its place as well as over the mirror directly across from it.

(c) Adjust table top mirror (M3) so that the beam is hitting the center of the macro entrance mirror (M5).

(d) Adjust M5 so that the beam is passing through target mask #1.

(e) The laser beam should also be passing through the center of target mask #2 (seated on M6). If this is not the case then proceed with the following.

(i) Adjust M3 until the beam is further away from the center of target mask #2

(ii) Readjust M5 in order to have beam pass through the center of target #1.

(iii) If the beam is still not passing through the center of target #2, then repeat steps (i) and (ii).

(f) Remove target mask #1 and replace the lens at the entrance of the macrochamber. Adjust it so the beam is still passing through the center of target mask #2.

(g) The macrochamber is now aligned, **do not touch M3 again**; if necessary, use M5 to align the beam with a sample.

### *iii. Microscope alignment*

With the macrochamber now aligned it is possible to align the microscope without too much difficulty.

(a) Rotate M4 so as to have the beam enter the microscope.

(b) Place a piece of Si wafer on the microscope stage.

(c) If the beam entering the microscope is not hitting the center of mirror of M7 (never touch mirror M7), then adjust M4 with Allen keys (do not touch M3).

(d) Adjust M4 until the beam intensity on the Si wafer is visibly at a maximum.

(e) Using the GOTO program, set the monochromator at 524 $cm^{-1}$ and maximize the signal by adjusting both M4 and the microscope stage. The maximum intensity for the Si wafer is obtained when the wafer is positioned at 45° on the stage. The slit width should be set to 200-μm and an intensity between 7 000 and 8 000 counts per second is considered acceptable with an 80X microscope optic.

(f) If steps (a) through (e) do not yield acceptable results, then it will be necessary to remove the microscope cover as well as the plate covering the microscope optics. The beam should be hitting the center of the beam splitter. If it is not, then adjust M4 until it does. If at this point acceptable results are still not obtained, then move mirror M3; however, it is highly probable that the overall alignment is off.

### *iv. Coupling and calibration of the U-1000 double monochromator*

If high-resolution Raman spectra are required then it is imperative to couple the two monochromators in order to ensure that they both detect the same wavelengths. Furthermore, it is necessary to calibrate the spectrometer so that the accuracy of the instrument may be determined. Many methods exist for the calibration of spectrometers; it is possible to use (1) the mercury lines (1122.6 $cm^{-1}$ at 514.532 nm and 2179.8 $cm^{-1}$ at 487.987 nm) from fluorescent lighting (which will sometimes appear in a spectrum if light from the room gets into the monochromators), (2) the argon-ion laser lines by removing the

appropriate filter or pin-hole, or (3) a neon lamp. The neon lamp is easy to use as its lines are very sharp and well-known. More recently, Kim *et al.*[17] have tabulated the neon peak positions with respect to the 487.987-nm (blue) line and the 514.532-nm (green) line of the argon-ion laser.

In order to couple the spectrometer, slits 1 and 2 were set at 10-μm while slits 3 and 4 were set at 100-μm (see Figure 3.3). The 585.249-nm line of the neon lamp was used (2348.39 $cm^{-1}$ at 514.532-nm or 3405.64 $cm^{-1}$ at 487.987-nm). Assuming the green-line, the GOTO routine was used to position the monochromator at 2348.39 $cm^{-1}$; if this did not correspond to the maximum intensity then the spectrometer was moved to the maximum intensity by scanning the region until the maximum was found. The cover at the end of the spectrometer (parallel to the prisms) was removed from the U-1000. The knob at the center was then turned to obtain a maximum signal. Once the intensity was at its maximum, $S_3$ was closed until $S_3 = S_2 = S_1 = 10$ μm. If no loss of intensity was observed, then the coupling was deemed correct. However, if a loss of intensity occurred then, the signal was maximized with $S_2$ and $S_3$ at 10 μm and, at this point $S_3$, was reopened to 100 μm. The intensity was then monitored as $S_3$ was closed down to 10 μm and no signal-loss was observed. If a loss of signal is still detected, however, then it might be necessary to adjust the concave mirror (top left with respect to the knob) to maximize the signal. This can be achieved by closing $S_4$ and $S_1$ to 10 μm, setting $S_2 = S_3 = 100$ μm and adjusting the concave mirror to obtain maximum intensity.

Once the coupling was considered to be correct, it was possible to calibrate the spectrometer in order to ensure that the accuracy was indeed ± 1 $cm^{-1}$. The calibration was accomplished with the aid of six lines from the neon lamp. The six lines scanned were (with respect to the 514.532-nm line): 2348.39, 2433.82, 2613.81, 3031.38, 3350.94, and 3815.62 $cm^{-1}$. If the observed lines were off by more than 1 $cm^{-1}$ in the same direction, then the back-plate (behind the absolute $cm^{-1}$ counter) was removed and the ridged belt on

the counter-pulley was detached. The absolute counter $cm^{-1}$ was turned by the amount by which it was offset, the belt was repositioned on the pulley and the lines were rescanned. If the lines appeared within the $\pm 1\ cm^{-1}$ tolerance level, then the calibration was deemed complete. (If, however, the offset was dependent on the line being scanned, i.e., $2\ cm^{-1}$ at $2348.39\ cm^{-1}$, $-3\ cm^{-1}$ at $3350.94\ cm^{-1}$, $-1\ cm^{-1}$ at $3815.62\ cm^{-1}$, etc., then I.S.A. should be called since the cosecant bar most probably needs to be adjusted. This situation was never encountered.

## II. FT-IR Measurements

The IR spectra were recorded on an Analect AQS-18 spectrometer equipped with a KBr beam splitter ($4400\text{-}450\ cm^{-1}$) and a triglycine sulfide (TGS) detector. The cryostat was coupled to the FT-IR instrument by modifying the sample cover (see Figure 3.4). The data acquisition was performed with the standard program provided with the AQS-18, but some macros were written by the author of this thesis to do repetitive scanning and storing of spectra.

Several sampling techniques were attempted: KBr pellets, diffuse reflectance, sublimation on to KBr windows, and pressing into thin layer films. Since similar spectra were obtained in each case (including the large hystereses observed in phase transition temperatures), the KBr pellet technique was used (5 mg sample in 750 mg KBr powder) as it proved to be the most convenient. In the future, however, it would be of interest to use diffuse reflectance since no sample preparation is required and the results obtained would be more easily compared to the Raman data. The effect of KBr pelleting on phase transitions has been studied previously and was shown to possibly increase the degree of the hysteresis at a phase transition[18]. In the case of samples which, due to their *plasticity*, were difficult to grind, the samples were cooled down with liquid nitrogen prior to

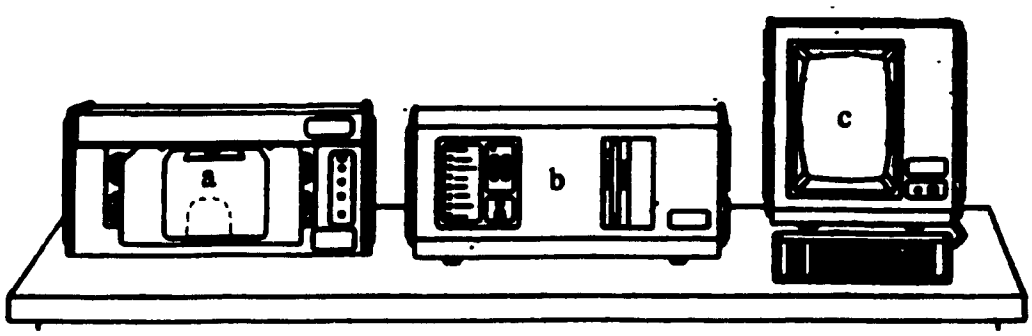


Figure 3.4 Analect AQS-18 FT-IR spectrometer with modified sample cover. (a) spectrometer, (b) MAP-67 computer and (c) monitor. (Reproduced with permission from Analect Instruments, Utica, New-York, U.S.A.)

grinding. In all cases, the samples were allowed to relax for at least one month prior to measurement of spectra.

## III. Variable-Temperature Apparatus

### *i. Cryosystems Cryostat*

Variable-temperature FT-IR and Raman spectra were recorded with the aid of a CTI Cryodyne Model 21 (CTI-Cryogenics, Kelvin Park, Waltham, Massachusetts, U.S.A. 02254) double-stage cryocooler. The system operates by compressing the 99.999% pure He gas and allowing it to expand as it reaches the cold head which is theoretically at room temperature. Since the cryocooler is a closed system, the gas returns to the compressor unit at which point it is re-compressed. In order to reach the low temperatures, it was necessary

to refill the compressor with He gas and the disposable adsorber was replaced. The lowest temperature reached with no load was 29 K, while with a load, the temperature attained was 35 K. The helium pressure in the compressor was 145 psi when not in use and 95 psi when in use. The temperature was controlled by a Palm Beach Cryophysics, Inc. (P.O. Box 2786, West Palm Beach, Florida, 33402), Model 4025 controller (range 400-4 K) equipped with an IEEE-488 interface and a calibrated silicon-diode (SDT-102) temperature sensor.

The sample temperatures remained essentially constant (± 0.5 K). The temperature accuracy, however, varied depending upon the technique used i.e., FT-IR or Raman spectroscopy. The IR KBr pellet holder was small and the distance between the pellet and the thermocouple was small. Moreover, the He-Ne alignment laser emits very little power therefore, the accuracy was about ± 2 K.

The temperature accuracy of the Raman data, however, was ± 5 K due to local heating by the laser. Even when relatively low-power (< 100 mW) was used, local heating effects took place. Calibration of the temperature reading was attempted but to no avail as the temperature was dependent on the placement of the temperature-sensor, the power used and the compound itself. Temperature-determination via the Stokes/anti-Stokes peak area ratio (eq. [3.2]):[6]

$$T = (-\nu_k * 1.43879)/[\ln\{I_{as}/I_s\} + 4\ln\{(\nu_0 - \nu_k)/(\nu_0 + \nu_k)\}] \qquad [3.2]$$

where T is in units of K, $\nu_0$ is the laser line in $cm^{-1}$, $\nu_k$ is the band originating from the sample in $cm^{-1}$, $I_s$, $I_{as}$ are the Stokes and anti-Stokes peak areas (unlike in IR measurements, Raman peak intensities are influenced by laser power, the detector response, as well as many other factors and therefore cannot really be easily used) associated with peak $\nu_k$, and 1.43879 is hc/k where h is Plank's constant, c the speed of light and k the Boltzmann constant, was unsuccessful due to the low-intensity of the anti-Stokes lines

below ~200 K. Many of the possible internal standards contain peaks that could overlap bands originating from the compound under study and significant band shifts could occur if a chemical reaction between the internal standard and the sample takes place. There is, however, one internal standard which might be useful: ruby powder. Ruby has been used quite extensively as a pressure calibrant (see Chapter 4) but its temperature-dependence is also well known.[19] A possible sample preparation method would then be to grind the sample with some ruby-powder and then place the sample in a capillary tube. The sample can then be scanned as before and the ruby-region, which does not interfere with most compounds (~5000 $cm^{-1}$ on the green line), would be scanned to determine the exact temperature of the sample.

In both the IR and Raman experiments, the sample holders were made of brass and coated with indium metal at the junction between the cold-finger and the sample holder to increase conductivity. The windows used for the cryostat head during the Raman experiments were constructed from quartz. Since quartz does not transmit throughout the mid-IR region, two 49 x 6 mm KBr windows (International Crystal Laboratories, 11 Erie St., Garfield, N.J. 07026) were used. The cryostat was mounted on a X-Y translation stage adapted to a pseudo-Z mount by Mr. A. Kluck (McGill University) in order to facilitate the optimization of the Raman signal. For the IR experiments, the cryostat was mounted on to a X-Y translation stage.

The cycling of adamantanone and oxanorbornane in the Raman experiment was achieved with the aid of a program written in BASICA by the author of this thesis for an IBM-PC interfaced via an RS-232 serial card and connected to a Black Box Technology IEEE-488 to RS-232 convertor which in turn, was connected to the temperature controller.

### *ii. Home-made Cryostat*

FT-IR data for oxanorbornane could not be obtained with the previously discussed cryostat because oxanorbornane is a very volatile liquid and the cryostat had a relatively large volume which required some time for it to be evacuated completely. This therefore resulted in the sample being pumped off as well. It is for this reason that another cryostat was designed by the author of this thesis with the aid of Mr. A. Kluck, Mr. B. Bastien, and Mr. R. Gaulin (McGill University). This cryostat had a much smaller volume and could therefore be evacuated in a shorter time period. The sample was contained in a liquid sample IR cell holder and was cooled by pouring liquid nitrogen down the neck of the cryostat. The temperature of the sample was monitored by two type T thermocouples (Omega Products) linked to a ten-channel thermocouple reader. The sample temperature was controlled with the aid of a Variac voltage regulator; since the heaters were melting-point heaters, the voltage applied to them never exceeded 50 V. The same KBr windows described in the previous section were used for this cryostat.

## C. RESULTS AND DISCUSSION

### I. Results

### *i. 1-Bromoadamantane (1-$C_{10}H_{15}Br$)*

The isolated 1-$C_{10}H_{15}Br$ molecule has $C_{3v}$ symmetry for which 40 IR/Raman active bands are predicted: $\Gamma_{vib} = 16a_1 + 8a_2 + 24e$, where $a_1$ and e are both IR/Raman

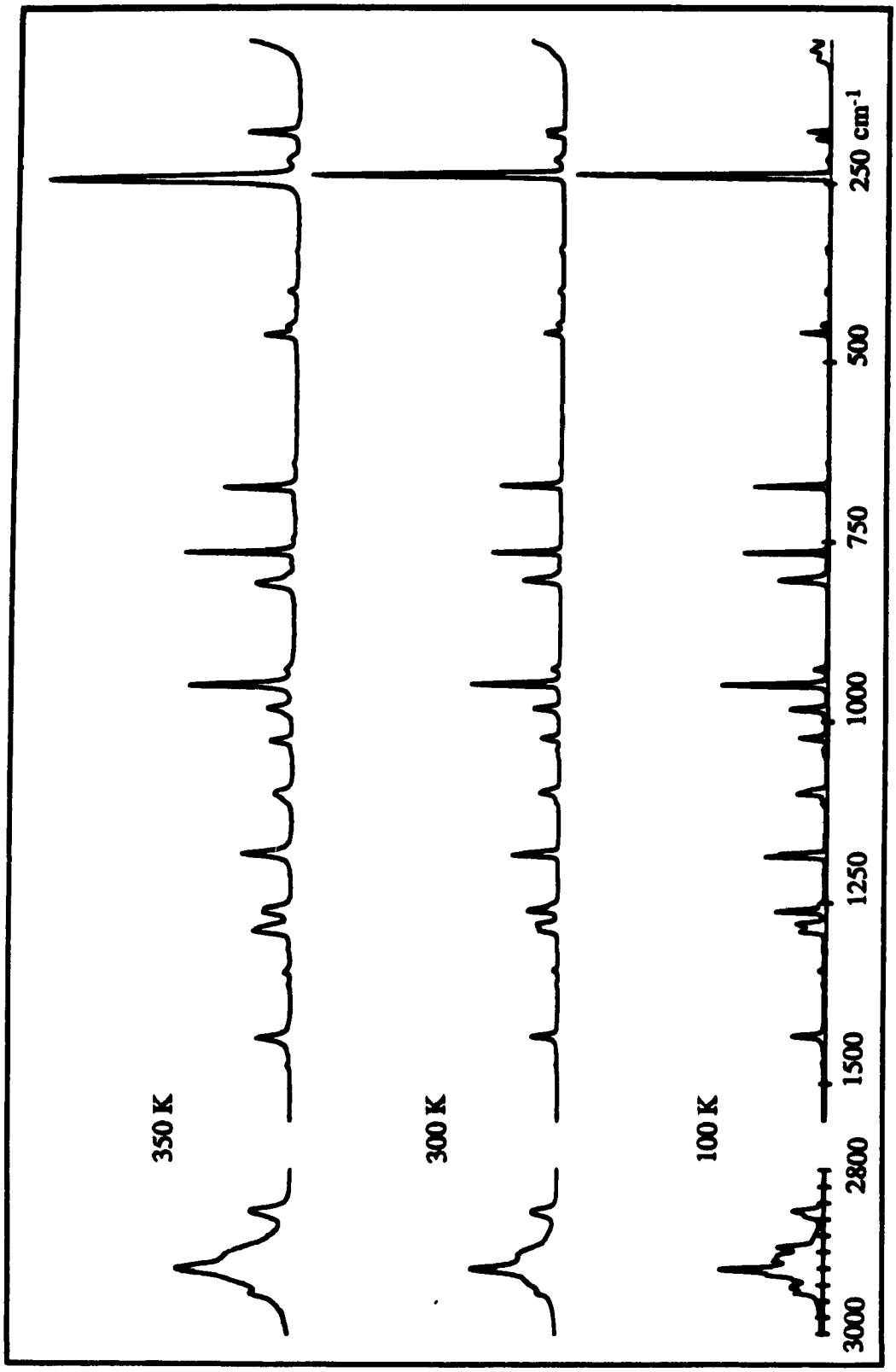


**Figure 3.5** Raman spectra of 1-bromoadamantane: phase I (100 K), phase II (300 K), and phase III (350 K)

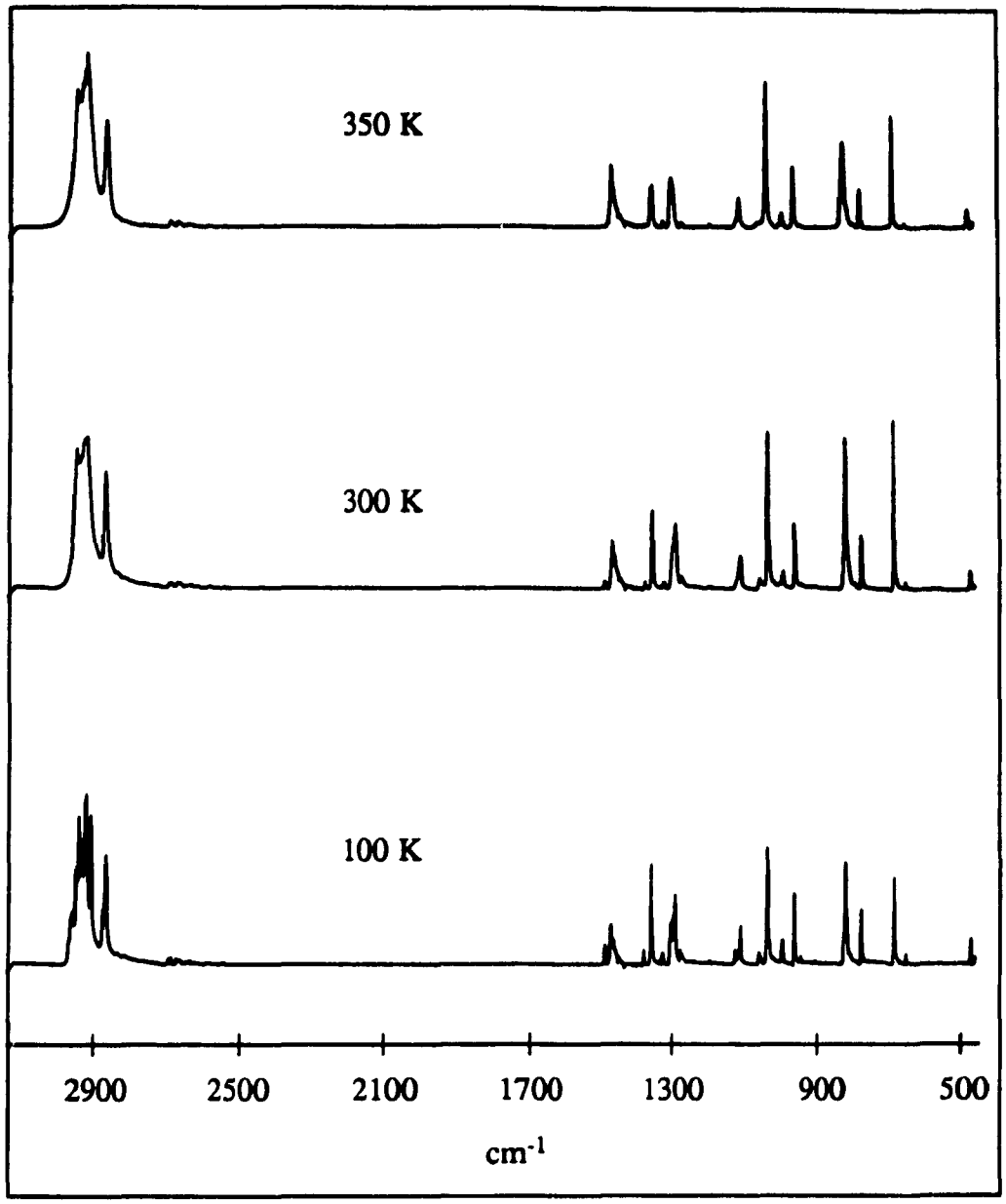


Figure 3.6 IR spectra of 1-bromoadamantane: phase I (100 K), phase II (300 K) and phase III (350 K).

active and $a_2$ is IR/Raman inactive. There were 38 Raman peaks and 36 IR peaks detected at room temperature; however, it is possible that some of these bands were overtones and/or combinations. Furthermore, it is quite probable that some bands are not observed due to the overlapping of certain peaks.

The Raman and IR spectra of 1-bromoadamantane revealed the presence of three phases as noticed in the DSC study. The spectra of phases III to I are shown in Figures 3.5 and 3.6, while the observed peak positions and band assignments are listed in Table 3.II. All of the assignments are based on literature values for various adamantane derivatives.[20-29] As would be expected, the plastic phase (phase III) contains many broad, featureless bands indicating that considerable motion is present in this phase. In phase II, some of the peaks begin to split, but the lattice mode is still broad and rather featureless, thus suggesting the presence of a more ordered phase than that present in phase III, but still disordered. Finally, as phase I (the lowest temperature phase) is approached, more splitting occurs, the peaks become better resolved and lattice modes appear. The spectra imply that phase I is the most ordered phase. Moreover, it can be seen that the bands that undergo splitting are split into two components. Based on the vibrational splittings observed in phases I and II, the ordered phases have at least two molecules per unit cell.

One of the more interesting regions is the CH stretching region (3000 - 2800 $cm^{-1}$) which lacks detail and is broad in phases III and II. As the sample is cooled down to phase I, the peaks sharpen dramatically and many new peaks appear. It is not possible, however, to explain this region solely on ν(CH) modes as it too might contain overtones and combinations.

Zielinski and Foulon[30] have studied the x-ray structure of 1-$C_{10}H_{15}Br$ and found that the crystal structure for the plastic phase belongs to the space group Fm3m and there are four molecules per unit cell. The only acceptable symmetry site would be $O_h$ as is the factor group. However, due to the nature of the plastic phase, i.e., orientationally-

**Table 3.II** Vibrational data ($cm^{-1}$) for 1-bromoadamantane

| Phase I (197 K) | | Phase II (290 K) | | Phase III (340 K) | | |
|---|---|---|---|---|---|---|
| Raman | IR | Raman | IR | Raman | IR | Assignments |
| 2950vs | 2950sh | 2950s | 2950sh | 2950s | | $a_1$ |
| 2943m | 2944m | | | | | |
| | | | 2936sh | | 2936vs | CH str. |
| 2930sh | 2935vs | 2930sh | 2930vs | | | |
| 2925sh | 2928vs | | | | 2927sh | $a_1$,e |
| 2922vs | 2922vs | 2921vs | | 2921vs | 2921sh | |
| | 2918sh,s | | | | 2917s | $CH_2$ |
| 2910sh | 2910vs | | 2913s | | 2913s | anti- |
| 2905s | | | 2907vs | | 2906s | symmetric |
| | | 2900s | | 2900sh | | str. |
| 2895vs | 2895vs | | | | | |
| | 2860sh | | | | | $a_1$,e |
| 2855sh | | | 2854s | | 2854s | $CH_2$ |
| 2851m | 2852s | 2852m | | 2851m | | symmetric |
| | 2820vw | | 2820vw | | 2820vw | str. |
| | 2680vw | | 2680vw | | | |
| | 2670vw | | 2670vw | | 2670br,vw | overtones |
| | 2650vw | | 2650br,vw | | 2650br,vw | and |
| | 2640vw | | | | | combinations |
| 1470w | 1472w | 1470w | 1475vw | 1470vw | | |
| | 1457m | 1456w | | | | $a_1$,e |
| | 1451w | | 1451sh | | | $CH_2$ Def. |
| 1435m | | 1435m | 1434sh | 1434m,br | 1436m | |
| 1370vw | 1365vw | 1370vw | 1364vw | 1370vw | 1370vw | $a_1$,e |
| 1345vw | 1345s | 1344vw | 1343m | 1346vw | 1343m | $CH_2$ wag |
| 1315vw | 1318vw | 1315vw | 1315vw | | | and |
| 1310vw | 1311vw | 1310vw | 1311vw | 1310vw | 1310vw | CCH def. |
| 1289sh | 1289w | 1289sh,w | 1289m | 1287w | | |
| | | | 1286sh | | | |
| 1280w | 1281sh | 1281w | 1280sh,vw | 1281sh,w | | CC str. |
| | 1278m | | 1277m | | 1278m | |
| 1262m | 1262vw | 1261m | 1261w | 1261m | 1261vw,br | e |
| | 1258vw | | | | | |
| 1250sh,vw | | 1250sh,vw | | | | e, C-C str. |
| 1205vw | | 1205vw | | | | $CH_2$ def. |
| 1185m | | | | | | $CH_2$ twist |
| 1183m | 1180vw | 1183m | 1180sh,w | 1181m | 1180vw | and CCH def. |
| | | | | | | $a_1$,e |
| 1110vw | 1113vw | | | | | |
| | | | | | | CCH def. |
| 1100sh,vw | | 1104sh | 1105sh | 1105sh | | |
| 1099m | 1097w | 1098m | 1099w | 1099m,br | 1100w | and |
| 1090sh | | | | | | |
| 1050sh,vw | | | 1050br,vw | | | $CH_2$ rock |
| 1045vw | 1048w | | 1048br,vw | | 1048br,vw | |
| 1023w | 1024s | 1023w | 1025s | 1026w | 1025s | and |
| 1005vw | | 1005vw | 1010vw | | 1010vw,sh | |
| | | | 990vw,sh | | 990sh | CCC bend |
| 983m | 982w | 982m | 982w | 981w | 982w | |
| 949vs | 948m | 948vs | 948m | 949vs | 948m | and |
| 928vw | | 927vw | 928vw | 927vw | 927vw | |
| | | | | | | C-C str. |

**Table 3.II** Vibrational data ($cm^{-1}$) for 1-bromoadamantane

| Phase I (197 K) | | Phase II (290 K) | | Phase III (340 K) | | |
|---|---|---|---|---|---|---|
| Raman | IR | Raman | IR | Raman | IR | Assignments |
| | 808w | | | 809m | | $a_1$,e |
| 804s | 805s | 804s | 805s | | 805s | C-C str. |
| | 800sh | | | | | and |
| 782vw | 782sh | 782vw | 782vw | 782vw | 782vw | C-C-C |
| 766s | 764m | 766s | 764m | 766s | 764m | bending |
| 673s | 675s | 673s | 675s | 675m | 675s | $a_1$ C-Br str. |
| 640vw | 641vw | 640vw | 641vw | 640vw | 641vw,br | |
| 560vw | | 560vw | | 560vw | | $a_1$,e |
| 460w | 461w | 461w | 462vw | 463w | 462w | |
| 448vw | | 449vw | | 451vw | | skeletal |
| 402vw | | 402vw | | 402vw | | modes |
| 348vw | | 348vw | | | | |
| 344vw | | 344vw | | 344vw | | |
| 241vs | | 240vs | | 245vs | | e |
| 230w | | 230w | | 232sh,w | | C-C-Br |
| 188w | | 184w | | | | bending |
| 178w | | 178w | | 179w | | |
| 77w | | | | | | e |
| 75sh | | | | | | skeletal |
| 64w | | | | | | modes |
| 60sh | | | | | | |

**Table 3.III** Factor group analysis of the ordered phase (phase I = $P2_1/c$) of 1-bromoadamantane and 1-chloroadamantane.

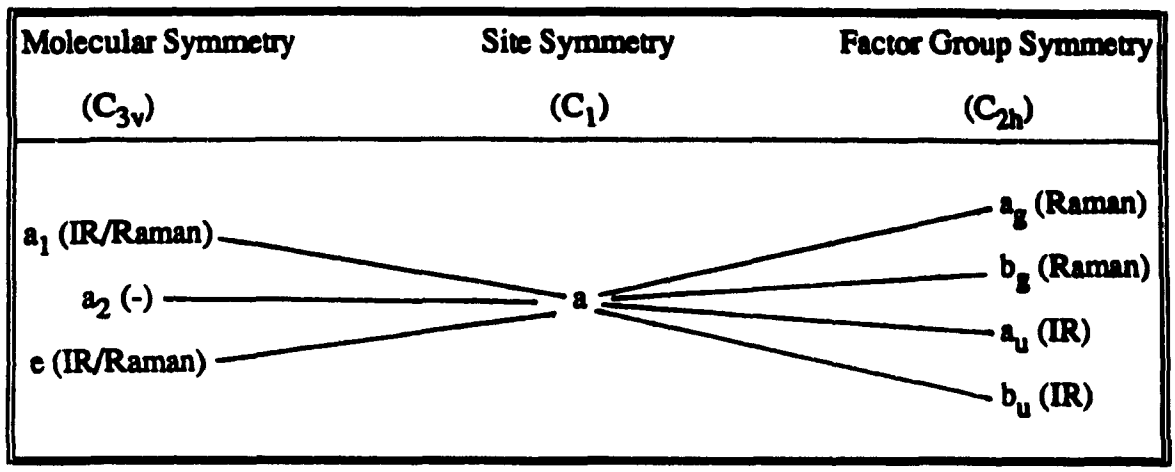


disordered, a correlation diagram cannot be constructed. The partially-ordered phase (phase II) was also found to have four molecules per unit cell with a Pmcn (or Pmna) crystal structure. Since no $C_2$ axis is present in the molecule and the site symmetry is $C_s(4)$, the only possible factor group must be $D_{2h}$. The lower temperature (and most ordered) phase was observed to be $P2_1/c$, once again with four molecules per unit cell. The site symmetry for this phase must be $C_1$ with a factor group of $C_{2h}$. They observed what might be another phase transition below 150 K which possibly has a space group of $P2_1/c$. This last phase was not observed in the present work by either vibrational spectroscopy or DSC. The correlation diagrams for phases I, and II are shown in Tables 3.III, and 3.IV.

### *ii. 2-Bromoadamantane (2-$C_{10}H_{15}Br$)*

The isolated 2-bromoadamantane molecule has $C_s$ symmetry for which 72 normal modes of vibration are predicted (40a' and 32a''). Since the a' and a'' modes are both Raman and IR active, 72 peaks should appear in both the Raman and the IR spectra.

**Table 3.IV** Factor group analysis of the semi-ordered phase (phase II = Pmna) of 1-bromoadamantane.

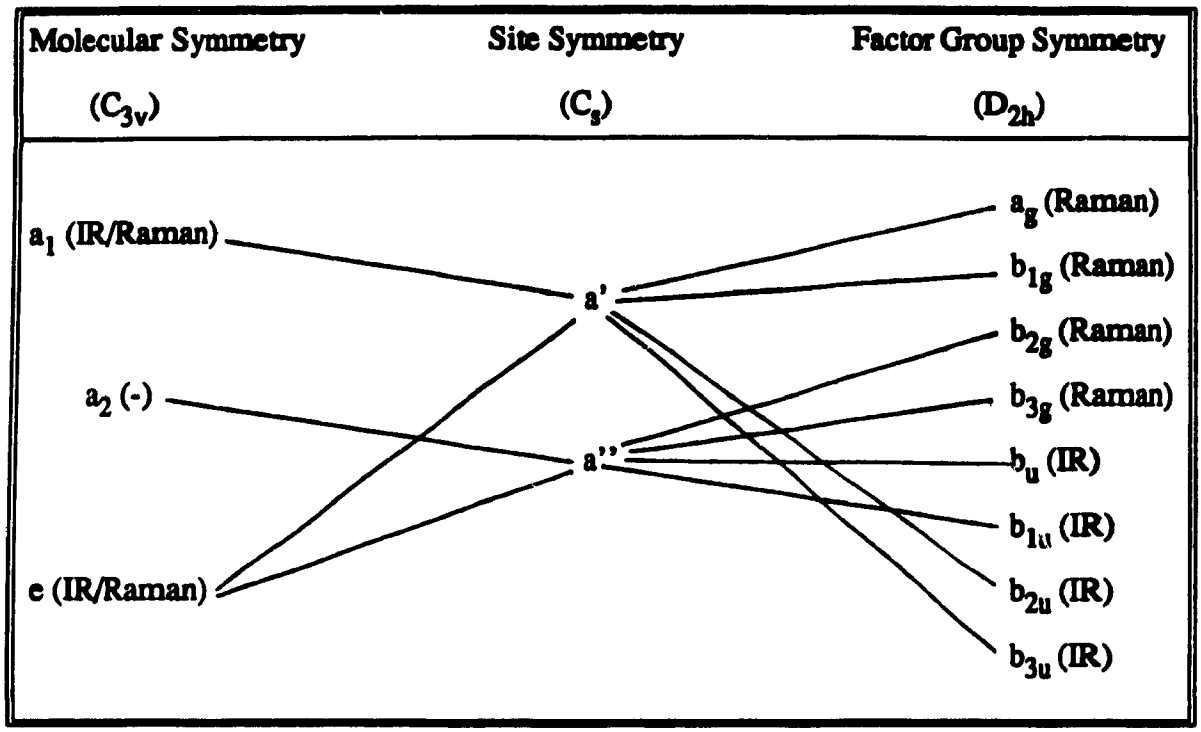


Two phases were detected by both variable-temperature Raman and IR spectroscopy. This correlates well with the DSC results obtained for this compound. The proposed vibrational assignments, as well as the observed peak positions, are tabulated in Table 3.V. Figures 3.7 and 3.8 display the Raman and IR spectra acquired at 160 K and 300 K for 2-$C_{10}H_{15}Br$. Instead of observing 72 peaks, only 40 were detected at room temperature. This can, once again, be attributed to band overlaps which are likely to occur as the bands are quite broad. The broad and featureless bands can be ascribed to the plastic, and hence totally disordered, phase of 2-$C_{10}H_{15}Br$. Although the lattice region of 2-$C_{10}H_{15}Br$, contained no very distinct features in phase II, there were some weak

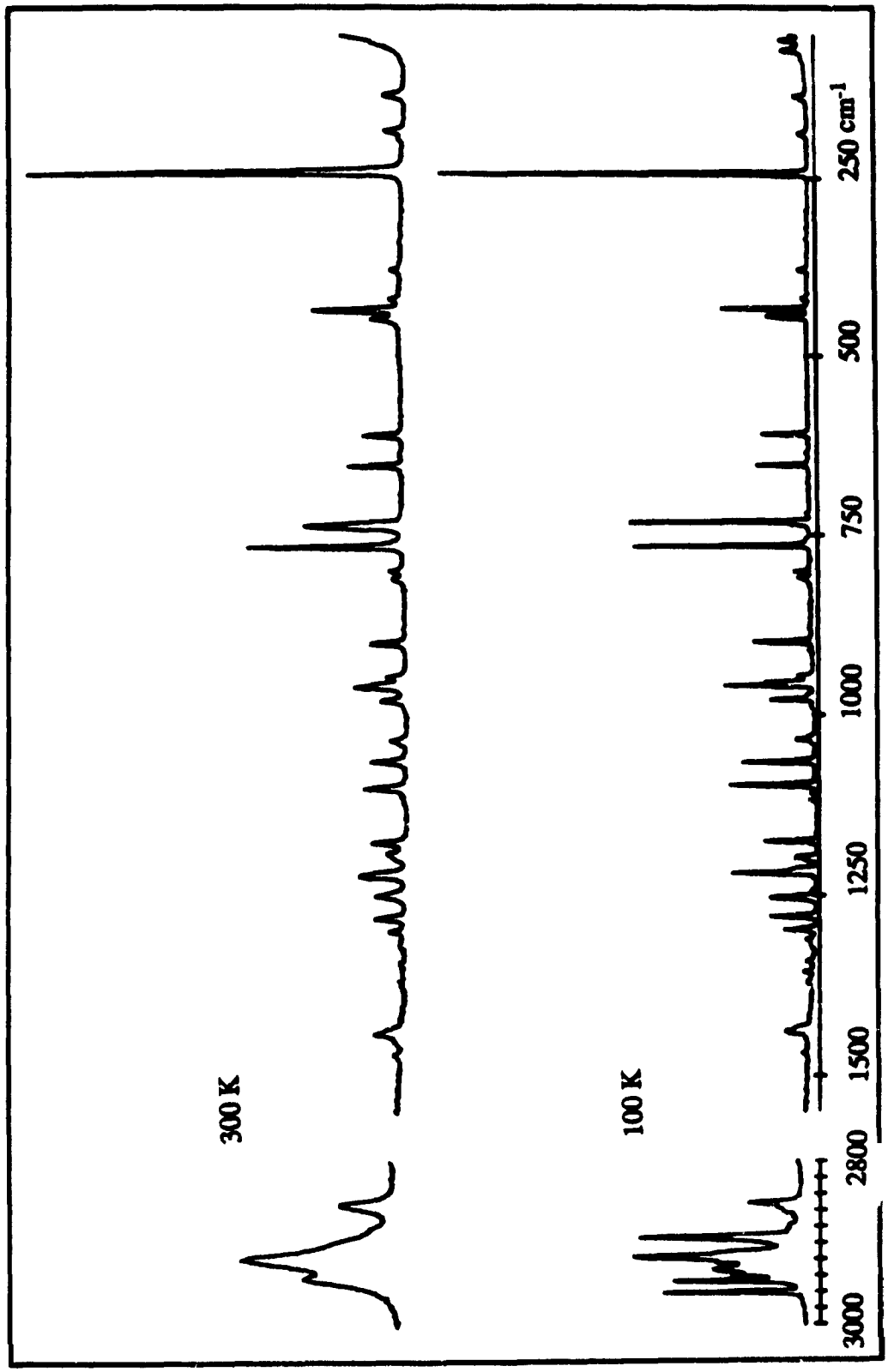


Figure 3.7 Raman spectra of 2-bromoadamantane: phase I (100 K), and phase II (300 K).

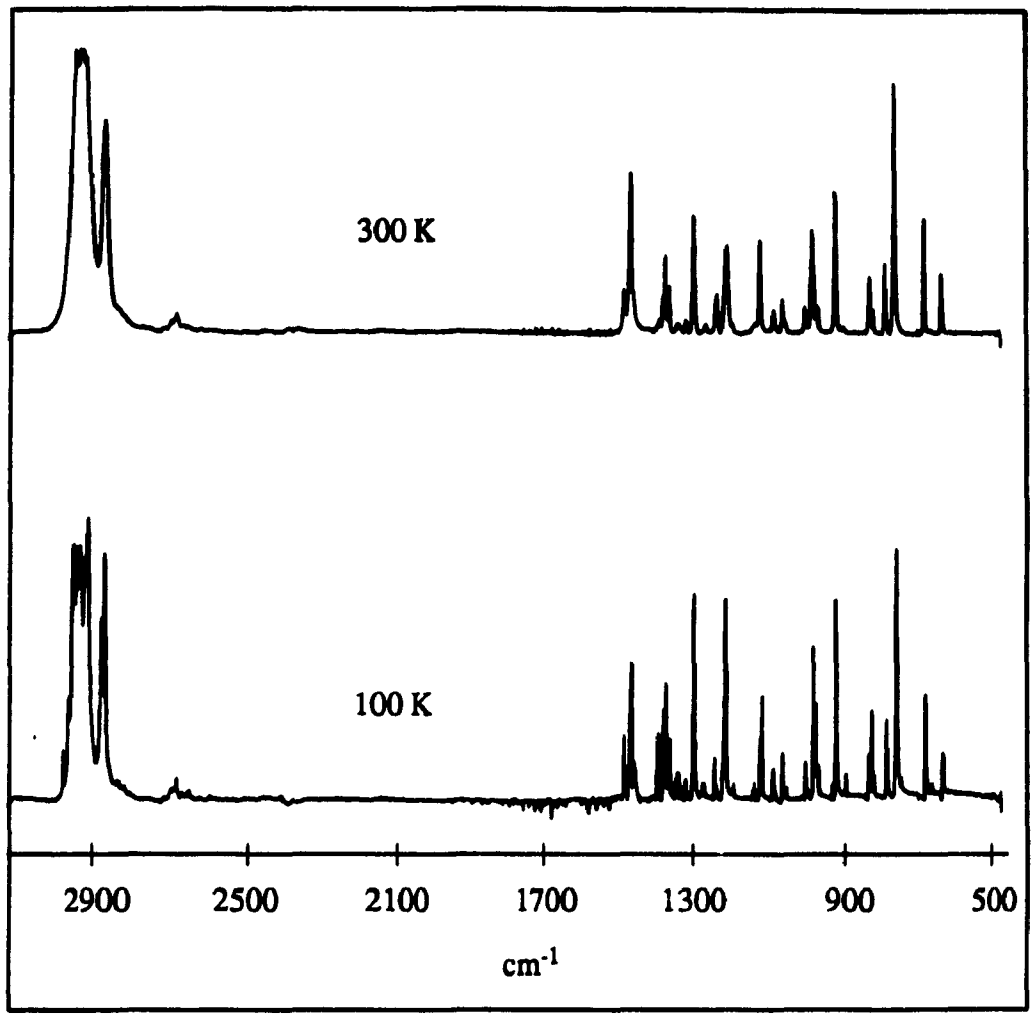


**Figure 3.8** IR spectra of 2-bromoadamantane: phase I (100 K), and phase II (300 K).

**Table 3.V** Vibrational data ($cm^{-1}$) for 2-bromoadamantane

| Phase I (157 K) | | Phase II (299 K) | | |
|---|---|---|---|---|
| Raman | IR | Raman | IR | Assignments |
| 2961vs | 2960w | | | a' CH str. |
| 2947vs | 2945s | | | |
| 2940s | | 2941s | | |
| 2933s | 2933vs | | | |
| | 2930vs | | 2930vs,br | a'' $CH_2$ anti-symmetric str. |
| 2921sh | 2922vs | | | |
| 2917vs | 2914vs | 2918vs,br | 2916vs,br | |
| 2910sh | | | | |
| | 2898s | | | |
| 2894vs | 2894sh | | | |
| | 2892vs | | | |
| 2860sh | 2857vs | | | a'' $CH_2$ symmetric str. |
| 2852s | 2850vs | 2852s,sh | 2852vs | |
| 1469vw | 1467w | 1470w | 1468w | a' $CH_2$ Def. |
| | 1463vw | | | |
| | 1447m | | 1450m | |
| 1440m | 1440br,vw | 1440m | 1440sh | |
| 1372vw | 1370w | 1367vw | 1370vw | a'' $CH_2$ wag and CCH def. |
| 1358vw | 1356w | | 1358w | |
| | 1350m | | 1352w | |
| 1343vw | 1340w | 1344vw | 1341w | |
| | 1322vw | | 1320vw,br | |
| | 1318vw | | | |
| 1313w | | 1313br | | |
| 1299m | 1300w | 1299m | 1300vw | a' C-C str. |
| 1280m | 1280m | 1281m | 1278m | |
| 1254m | 1252vw | 1249m | 1250vw | a'' C-C str. $CH_2$ def. $CH_2$ twist and CCH def. |
| | 1223vw | | | |
| 1219s | 1218vw | 1221m | 1216w | |
| 1198w | 1193s | | | |
| 1175m | 1175vw | 1175m | 1178sh,vw | |
| 1119vw | 1120vw | | | CCH def. |
| 1109vw | 1110vw | | 1110sh,vw | |
| 1098s | 1099w | 1100s | 1098w | a'' CCH def. |
| | 1094w | | | |
| 1066s | 1064vw | 1064m | 1068w | |
| | | | 1061w | |
| 1035w | 1040vw | 1035w | 1039vw,br | a' CCH def. |
| 989vw | | | | a'' $CH_2$ rock and CCC bend and C-C str. |
| 979w | 978w | 979w | 977vw | |
| | 975sh | | | |
| 959s | 957s | 959m | 958w | |
| 950s | 951m | | | |
| 940m | 945vw | 940w,sh | 944vw | |
| 911vw | 910vw | | | |
| 899m | 899s | 900w | 899m | |
| | 875vw | | 875vw | |
| | 820w | | | |
| | 818sh | | | |

**Table 3.V** Vibrational data (cm-1) for 2-bromoadamantane

| Phase I (157 K) | | Phase II (299 K) | | |
|---|---|---|---|---|
| Raman | IR | Raman | IR | Assignments |
| 811w | 814w | 810vw | 808vw | a' C-C str. |
| 802w | 800vw | 800vw | 798vw | |
| 766vs | 761w | 766s | 763w | |
| 738sh | | | | |
| 732vs | 733vs | 737m | 736s | |
| | 720vw | | | |
| 653m | 657m | 653m | 652m | C-Br str. |
| 637vw | 633vw | | | CCC bending |
| 610m | 608vw | 610w | 610vw | |
| 446w | | 447w | | a'' skeletal modes |
| 435m | | 435m | | |
| 420vw | | 420vw | | |
| 380vw | | 379vw | | |
| 245vs | | 242vsw | | C-C-Br str. |
| 189w | | 185w | | |
| 140sh | | | | |
| 137w | | 135w | | |
| 71vw | | | | skeletal modes |
| 69sh | | | | |
| 57w | | 60sh | | |

shoulders which were present. This could indicate that although it is a plastic crystal some degree of order is present in the molecule. Phase I did show two very sharp and well resolved peaks thereby indicating that it is a more ordered phase. Interestingly, aside from the CH stretching region, very few bands undergo splitting in the Raman spectra as the sample is cooled down from the plastic to the ordered phase. The peaks which were split include the 732, 959, and the 1219 $cm^{-1}$ bands. Those three regions correspond to CCH deformations and bending as well as to C-C stretching. There were, however, some bands which underwent changes in relative intensity, e.g., the 435 $cm^{-1}$ doublet, and the 737 $cm^{-1}$ and 766 $cm^{-1}$ peaks, which are essentially due to C-C stretching and skeletal modes. Since this molecule has $C_s$ symmetry, it is not surprising that the same observations were noticed in the IR spectra - although much band narrowing was observed, few actually split into two or more components. The 1468, 1098, 977, 957, and 808 $cm^{-1}$ peaks were split in the low-temperature phase. Many of the other peaks present appear to be due to band narrowing since some of them were seen as shoulders on a prominent peak. As for the Raman spectra, a few bands changed in relative intensity. The 1194 and 1279 $cm^{-1}$ peaks which were less intense than the 1450 $cm^{-1}$ peak are now more intense than it, as well as being much sharper. The 899 $cm^{-1}$ band also increased in amplitude relative to the most intense peak at 733 $cm^{-1}$. The 808 $cm^{-1}$ band, which had undergone considerable splitting in the ordered phase, is now as intense as the 761 $cm^{-1}$ band. Since most of the bands occur at the same frequencies in both the Raman and IR spectra, the unit cell is most probably not centrosymmetric.

### *iii. 1-Chloroadamantane (1-$C_{10}H_{15}Cl$)*

As in the case of the 1-$C_{10}H_{15}Br$ molecule, the vibrational representation for the 48 modes of the free 1-$C_{10}H_{15}Cl$ molecule ($C_{3v}$ symmetry) results in $\Gamma_{vib} = 16a_1 + 8a_2 + 24e$,

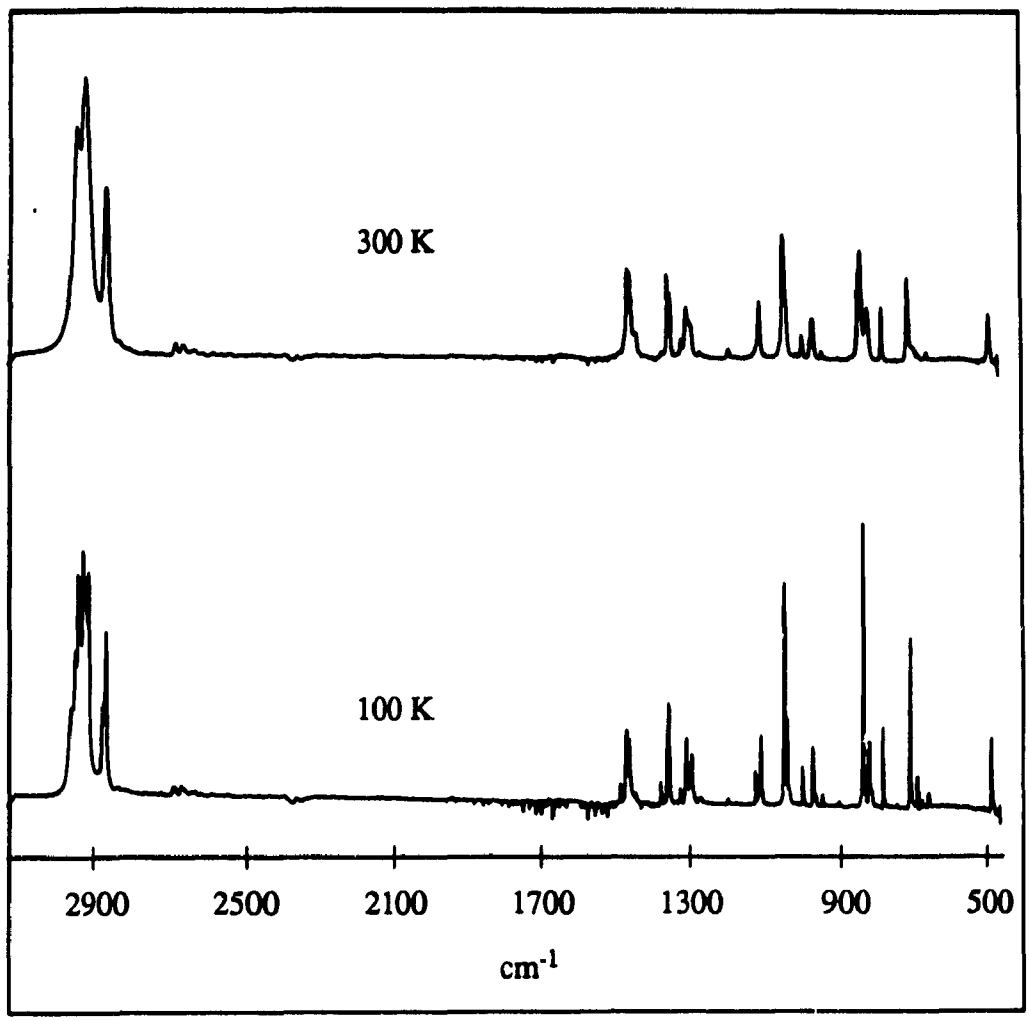


**Figure 3.9** IR spectra of 1-chloroadamantane: phase I (100 K), and phase II (300 K).

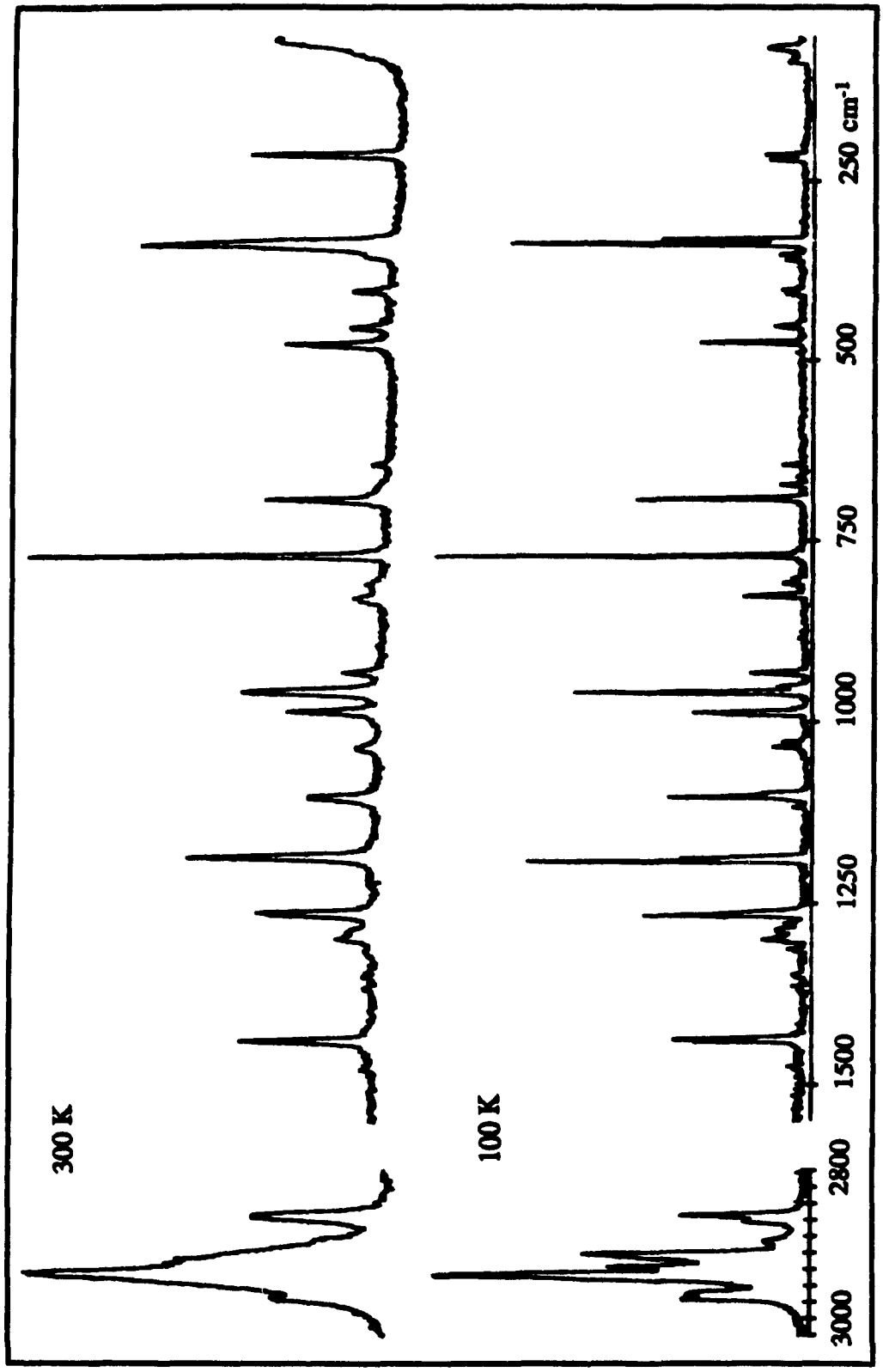


Figure 3.10 Raman spectra of 1-chloroadamantane: phase I (100 K), and phase II (300 K).

where $a_1$ and e are both IR/Raman active and $a_2$ is IR/Raman inactive and therefore, it is possible to predict a total of 40 IR/Raman active bands. In all, 29 Raman and 26 IR peaks were detected at room temperature (see Table 3.VI for peak tabulation and assignments). This low count can be attributed to broad peaks which most likely overlap some of the other weaker bands. Also, it is possible that some of the observed bands are overtones and/or combinations, thus, the number of "true" peaks might actually be even lower.

The DSC curve for 1-$C_{10}H_{15}Cl$ had shown that only two phases were present. This was also apparent from the variable-temperature vibrational data (Figures 3.9 and 3.10). Once again, the high-temperature phase contains many broad and featureless peaks, characteristic of a totally-disordered or plastic phase.

In the IR spectra (Figure 3.9), the broad CH stretching region once again reveals many components when the molecule is cooled down from the plastic phase (phase II) into its ordered phase (phase I). In other regions of the spectrum, most of the peaks split into doublets. There is, however, one notable exception; the bands at 1343 and 1350 $cm^{-1}$, corresponding to $a_1$ + e modes and the $CH_2$ wag and CCH deformation, collapse into just one peak (1346 $cm^{-1}$) in the ordered phase. The relative intensities also change, and as in the two previous adamantane derivatives, it is the CCC bending and the CC stretching which are affected (1036 $cm^{-1}$) as well as the $CH_2$ wagging and CCH deformation (1459 $cm^{-1}$, 1346 $cm^{-1}$), and the symmetric C-Cl stretch (828 $cm^{-1}$).

Most of the peaks in the Raman spectra (Figure 3.10) also undergo splitting into two components. The spectrum of the low-temperature phase contains lattice modes and has sharper peaks than the high-temperature phase. This once again implies an ordered phase for the low-temperature (phase I) phase and a disordered phase for the high-temperature (phase II). Not many peaks have changes in relative intensities. The most distinct change occurs in the 215 $cm^{-1}$ peak (C-C-Cl str.) which upon splitting exhibits a dramatic decrease

**Table 3.VI** Vibrational data ($cm^{-1}$) for 1-chloroadamantane

| Phase I (190 K) | | Phase II (300 K) | | |
|---|---|---|---|---|
| Raman | IR | Raman | IR | Assignments |
| 2960s | | | | $a_1$ |
| 2954s | | 2954s | | |
| | 2947sh | | | CH str. |
| 2940s,sh | 2939s | | 2934vs | |
| 2927vs | 2928vs | 2927vs | | $a_1$,e |
| 2920vs | 2920sh | 2920sh | | |
| | 2915vs | | | $CH_2$ |
| 2910sh | 2906vs | 2910sh | 2908vs | anti- |
| 2902vs | 2900vs | 2900s | | symmetric |
| 2887m | | | | str. |
| 2870s,sh | | | | $a_1$,e |
| | 2861vs | | | $CH_2$ |
| 2855s | 2855s | 2855s | 2854s | sym. str. |
| 1476vw | | 1477vw | | |
| | 1459w | | 1460m | $a_1$, e |
| | 1451w | | 1450m | $CH_2$ def. |
| 1440sh | | | 1440sh | |
| 1439s | 1434sh | 1439s | | |
| 1380vw | | 1380vw | | $a_1$, e |
| 1370vw | 1367w | 1370vw | | $CH_2$ wag |
| | | | 1352vw | and |
| | | | 1350m | CCH def. |
| | 1346m | | 1343m | |
| 1320vw | 1318vw | 1320vw | | $a_1$, e |
| | 1314vw | | 1313vw | CH def. |
| 1300w | 1298m | 1298br,w | 1299br,w | |
| 1290w | 1287w | | | |
| 1280w | 1282m | | | e |
| 1266s | | | 1268vw | |
| 1265sh | | 1264s | | C-C str. |
| | 1257vw | | | |
| 1191vs | | | 1190vw | e |
| 1186s | 1186vw | 1186s | | CH def |
| 1110vw | 1113w | | | |
| 1104s | 1105w | 1103br,s | | $a_1$, e |
| 1100sh | 1099m | | 1102w | |
| 1035w | 1035s | 1036w,br | 1036m | CCC bend |
| 1030w | | | | |
| | 1026m | | | and |
| | | | 1000vw | C-C str. |
| 990sh | | | | |
| 988sm | 984w | 985s | 985s | |
| 960vs | 955w | 958s | 953w | |
| 950w | 950sh | | | |
| 933m | 931vw | 932vw | | |

**Table 3.VI** Vibrational data ($cm^{-1}$) for 1-chloroadamantane

| Phase I (190 K) | | Phase II (300 K) | | |
|---|---|---|---|---|
| Raman | IR | Raman | IR | Assignments |
| 828m | 825vs | 829m,br | 827m | $a_1$ C-Cl str |
| 810w | 810w | 810w,br | 809w | $a_1$, e $CH_2$ anti-symmetric def. |
| 806vw | 806w | | | |
| | 801w,sh | | | |
| 772vs | 770sh | 772vs | | |
| | 768m | | 767m | |
| 693s | 690s | 694s | 691m | $a_1$, e C-C-C bending |
| | | | 680sh | |
| 673w | 670vw | | | |
| | | | 650vw | |
| 645w | 643vw | 645w | 645vw | |
| 476m | 474w | 479m,br | 477w | e C-Cl bend |
| 453w | | 455w | | |
| 404w | | 404br,w | | skeletal modes |
| 360w | | | | |
| 355w | | | | |
| 339vs | | 339s,br | | |
| 330s | | | | C-C-Cl str. |
| 221m | | | | |
| 215m | | 215m | | |
| 83vw | | | | skeletal modes |
| 65w | | | | |
| 64w | | | | |
| 60sh | | | | |

in intensity. The other peak of interest is the 1104 $cm^{-1}$ (C-C-C bending and C-C stretching) which in the ordered phase undergoes a sudden increase in intensity.

Zielinski and Foulon[30] have also studied the x-ray structure of 1-chloroadamantane and they observed the same crystal structure for phase II as that of phase III of 1-bromoadamantane, notably Fm3m (Z = 4) for the plastic phase. The site symmetry and factor group are $O_h$. As for the most ordered phase of 1-bromoadamantane, the low-temperature ordered phase of 1-$C_{10}H_{15}Cl$ was found to be $P2_1/c$ (Z = 4). The site symmetry for this phase must be $C_1$ with a factor group of $C_{2h}$. The correlation diagram for phase I is therefore the same as for the 1-bromoadamantane and is shown in Table 3.III.

### *iv. 2-Chloroadamantane (2-$C_{10}H_{15}Cl$)*

As for the 2-bromoadamantane molecule, the isolated 2-chloroadamantane molecule has $C_s$ symmetry for which 72 normal modes of vibration ($\Gamma_{vib}$ = 40a' and 32a'') are predicted. Moreover, since the a' and a'' modes are both Raman and ir active, 72 peaks should be observed in both the Raman and the ir spectra.

The Raman and IR spectra of phases I-III are shown in Figures 3.11 and 3.12; the measured peak positions and the proposed vibrational assignments are given in Table 3.VII. These assignments are based on literature values for various adamantane derivatives[20-29] and on Raman spectra of 2-$C_{10}H_{15}Cl$ in $CCl_4$ and $CS_2$ solution. Only 58 bands out of a possible 72 have been clearly identified, probably as a result of the overlapping of peaks. Even amongst those observed, it is possible that some may be combinations and/or overtones.

Many interesting changes were observed in the Raman spectra (Figure 3.11) as the sample was cooled and then heated between 298 K and 150 K. Consider the lattice region (100-20 $cm^{-1}$); the tail extending to 100 $cm^{-1}$ in phase III is featureless. However, in

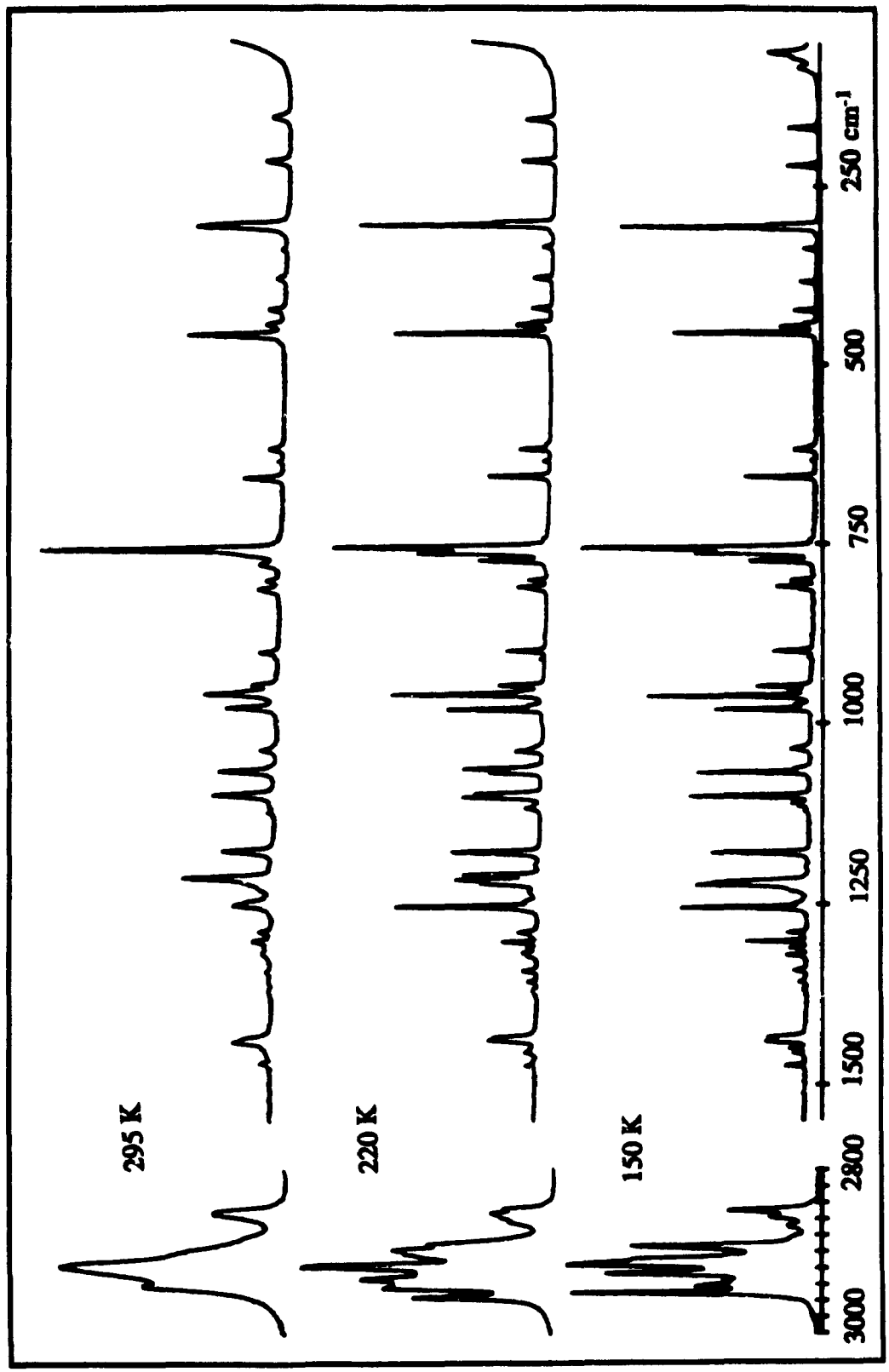


**Figure 3.11** Raman spectra of 2-chloroadamantane: phase I (150 K), phase II (220 K), and phase III (295 K).

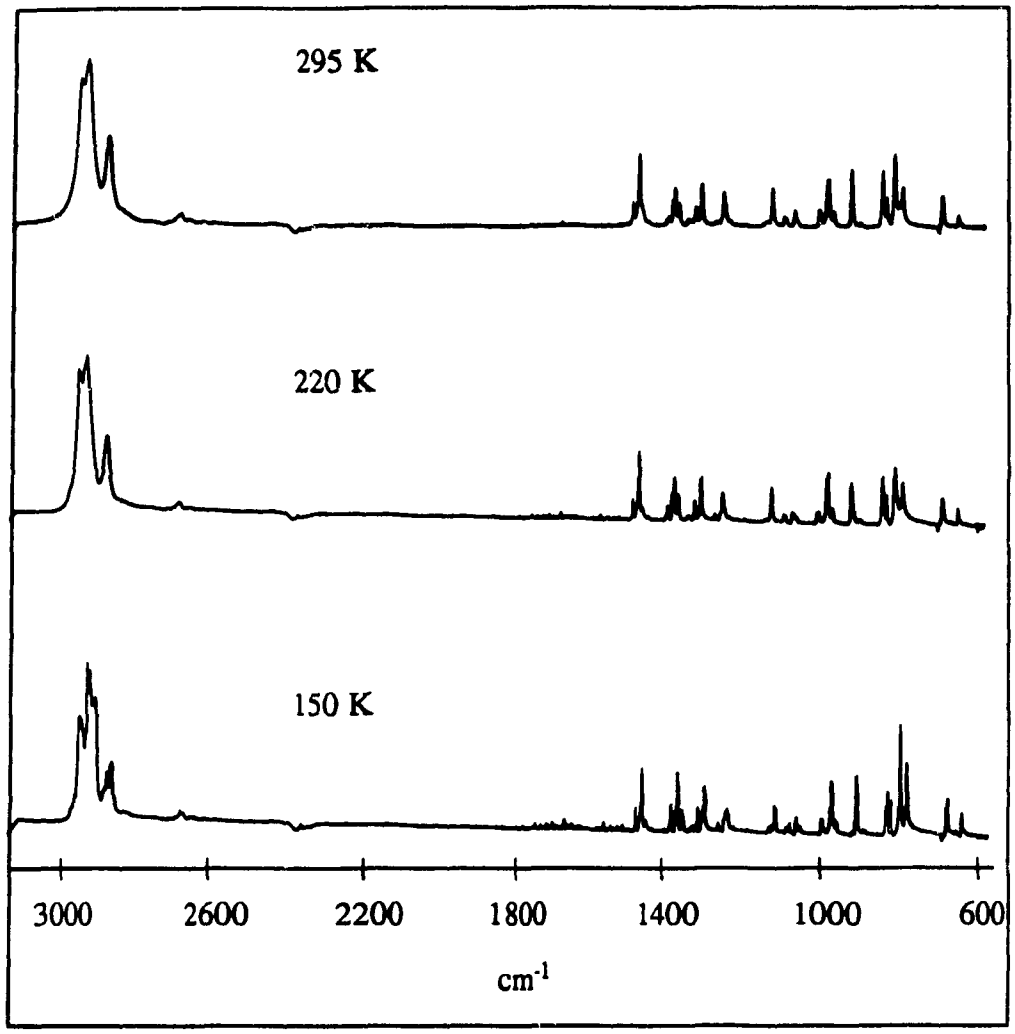


**Figure 3.12** IR spectra of 2-chloroadamantane: Phase I (150 K), phase II (220 K) and phase III (295 K).

phase II, some weak features develop at ~60 and 80 $cm^{-1}$, and in phase I some very distinctive peaks appear. These results corroborate those of the DSC measurements, i.e., phase III is the completely disordered phase since it exhibits a total absence of lattice modes. The weak, broad peaks observed in this region for phase II indicate that it is orientationally disordered, while the sharp peaks in phase I show that it is a completely ordered phase.

In Figure 3.11, the changes that occur in the Raman for the C-C-Cl bending mode are shown. In phase III, the peak appears at 156 $cm^{-1}$. As the sample is cooled down towards phase II, the peak width narrows and the peak shifts to slightly higher wavenumber (159 $cm^{-1}$) once in phase II. However, on going from phase II to phase I, a new peak appears at 167 $cm^{-1}$ and the 159 $cm^{-1}$ peak decreases in intensity. The 167 $cm^{-1}$ peak eventually shifts to 169 $cm^{-1}$ and becomes a sharp singlet for phase I, while the peak at 159 $cm^{-1}$ disappears completely.

The symmetric C-C stretching mode also undergoes distinct changes as the sample proceeds from phase III to phase I. In the plastic phase, the peak occurs as a singlet at 760 $cm^{-1}$ with a smaller peak at 780 $cm^{-1}$. In phase II, the 760 $cm^{-1}$ peak is split into a doublet at 757 and 764 $cm^{-1}$. Furthermore, the 780 $cm^{-1}$ peak sharpens and increases in intensity moving finally to 775 $cm^{-1}$. Little change occurs as the sample progresses from phase II to phase I. Since this spectral region is solely due to C-C stretching, i.e., cage skeletal stretching, the observed changes must result from a change in crystal structure.

The C-C stretching and $CH_2$ twisting modes at 1067 $cm^{-1}$ and the C-C-H deformation and $CH_2$ wag at 1100 $cm^{-1}$ alternate between singlets and doublets as the sample goes from phase III to phase I. The doublets in phase III collapse to singlets in phase II which then split into doublets in phase I. Since the C-C and $CH_2$ modes contribute to the two bands, it is not surprising that the bands are sensitive to crystal structure (C-C) as well as to orientational ($CH_2$) changes. The same is true for the 3000-2800 $cm^{-1}$

**Table 3.VII** Vibrational data ($cm^{-1}$) for 2-chloroadamantane

| Solution[a] | Phase I (39 K) | | Phase II (280 K) | | Phase III (290 K) | | |
|---|---|---|---|---|---|---|---|
| Raman | Raman | IR | Raman | IR | Raman | IR | Assignments |
| | | 2960w | 2956s | 2959w | | | |
| | | 2953s | | 2952sh | | | a' |
| | 2950vs | 2951m | | | | | |
| 2940s,p | 2942m | | 2943s | | 2941s | | CH str. |
| | | 2939vs | 2939s | 2938sh | | | |
| | 2935sh | 2935vs | 2934s | 2933s | | | |
| | | 2930vs | | | | 2930s | a'' |
| | 2928vs | 2926vs | 2926sh | 2926s | | 2926s | |
| 2918s | 2915vs | 2913vs | 2918vs | 2917s | 2918vs | 2916sh | $CH_2$ |
| | 2909sh | | | 2910s | | 2910sh | anti- |
| | | 2905vs | | 2906vs | | 2906vs | symmetric |
| | | | 2903sh | | | 2903sh | |
| | | 2896s | 2899s | 2899s | | | str. |
| | 2894vs | 2890s | 2891s | 2895sh | | | |
| | | 2871sh | | | | | |
| | 2868m | 2867m | 2865sh | 2867sh | | | a'' |
| | 2857m | 2859s | 2858sh | 2859s | | | $CH_2$ |
| 2852m | 2850m | 2851s | 2854m | 2853s | 2853m | 2853s | symmetric |
| | | 2847s | 2848m | 2849s | | | str. |
| | | 2665w | | 2667w | | 2660w | |
| | 1474w | | 1474w | | | | |
| 1471w,p | | 1469w | 1469vw | 1469w | 1470w | 1468w | a' |
| | 1457vw | | 1456vw | | | | |
| | 1450vw | | 1454vw | | | | $CH_2$ |
| | | 1451m | | 1451m | | 1450m | |
| 1443m,p | 1440m | 1441br,w | 1438m | 1442br,w | 1441m | 1442w | Def. |
| | 1435w | | 1435sh | | 1435sh | | |
| | | 1373vw | | 1374vw | | 1374w | |
| | | 1370w | | 1370w | | 1368w | a'' |
| 1356w | 1359w | 1358w | 1359vw | 1358w | | 1358w | |
| | | 1353m | | 1353m | | 1353m | $CH_2$ wag |
| 1345w | 1344vw | 1344w | 1344vw | 1343w | 1344vw | 1343w | |
| | 1322w | 1323br,w | 1321vw | 1321w | | 1321w | and |
| | | 1320br,w | | | | | |
| 1319w | 1319vw | 1318w | 1319vw | 1316w | 1319w | | CCH def. |
| | 1312w | | 1310vw | | | 1313w | |
| 1304w | 1303m | 1303m | 1304w | 1302m | 1302w | 1301m | |
| | 1295vw | 1295w | 1294sh | 1295vw | | | a' |
| 1290w,p | 1290w | 1290vw | 1290w | 1291sh | 1289w | 1290sh | C-C str. |
| | | 1287m | | 1287m | | 1287m | |
| 1252w | 1256s | 1251w | 1255s | 1251w | 1252m | 1251w | a'' |
| | | 1237sh | | 1236sh | | 1234sh | C-C str. |
| | | 1232w | | 1231w | | 1230m | $CH_2$ def. |
| | 1223s | 1225sh | 1220sh | 1225sh | 1228sh | 1226sh | |
| 1215s | 1221sh | | 1218m | | 1214s | | a'' |
| | | 1213vw | 1211m | 1213vw | | 1212vw | $CH_2$ twist |
| 1178m | 1179m | 1175vw | 1179m | 1175vw | 1177m | 1175vw | and |
| 1123w | | 1118br,vw | 1118w | 1118vw,br | 1123w | | CCH def. |
| | 1115vw | | | | 1114w,br | | |
| | 1112w | 1111sh | 1112sh | | | | CCH def. |
| | | 1107vw | | 1108vw | | | |
| | 1102s | 1102sh | 1103m | 1104sh | | | a'' |
| 1101m | | 1100w | 1098m | 1100w | 1100m | 1099m | CCH |
| | | 1070vw | | | | | def. |
| 1068m | 1069s | 1066vw | 1068w | 1066w | 1067m | 1066w | |
| | 1063sh | 1061w | 1063m | 1061w | | 1061w | |

Table 3.VII Vibrational data ($cm^{-1}$) for 2-chloroadamantane

| Solution[a] | Phase I (30 K) | | Phase II (260 K) | | Phase III (290 K) | | |
|---|---|---|---|---|---|---|---|
| Raman | Raman | IR | Raman | IR | Raman | IR | Assignments |
| | | 1045sh | | 1045sh | | 1040sh | a' |
| | | 1043w | | 1043w | | 1038w | |
| 1039w,p | 1036w | 1039br,w | 1039w | 1037vw | 1037w | 1035sh | CCH def. |
| | | 1032vw | | 1032vw | | 1032sh | |
| | 982m | 982w | 982m | 982w | | | |
| 980m | | | 976sh | 979sh | 979m | 978w | a'' |
| | 975w | 975vw | | 975vw | | | |
| | | 960sh | | 960sh | | 960sh | $CH_2$ rock |
| 961m | 963s | 958m | 961s | 958m | 960m | 958m | |
| | 955w | 953w | 955sh | | 955sh | | and |
| 948m | 949m | 950sh | 949w | 950sh | 947m | 949sh | |
| | | 947w | | 946w | | 945w | CCC bend |
| | 911vw | 909vw | 911vw | 910vw | 910sh | | |
| 903m | 900w | 899m | 901w | 900m | 902w | 901m | and |
| | | 881vw | | 880vw | | 878vw | |
| | | 876vw | | 876vw | | | CC str. |
| | | | | | | 822sh | |
| 815w | | 814sh | 813w | 814w | 815w | 813m | |
| | 811w | 810m | | 810m | | | |
| 803w,p | 802w | 801w | 802w | 801w | 803w | 801w | a' |
| 781vw,p | 775m | 774m | 775m | 774m | 780w | 779m | |
| | 762s | 761w | 764s | 761w | 764sh | 764br,w | C-C str. |
| 760vs,p | 757vs | 756m | 757vs | 756m | 760vs | 756m | and |
| 660m | 658m | 657m | 658m | 657m | 660m | 659m | C-C-C |
| | 634vw | 634vw | 636vw | 634vw | 637vw | 635vw | bending |
| 621w | 620w | 617w | 620w | 618w | 620w | 619w | |
| | | 614br,vw | | 614br,vw | | | |
| | 458s | 462m | 459s | 462m | 462s | 462m | C-Cl |
| | 448w | 445w | 446w | 445w | 446w | 445w | str. |
| | 442vw | | 443sh | | | | |
| | 425w | | 424w | | 425w | | a'' |
| 380w | 385w | | 381w | | 381w | | skeletal |
| 340w | 339vw | | 338vw | | 341vw | | modes |
| 309m | 309s | | 308s | | 309s | | |
| | 305sh | | 303sh | | | | |
| 220w | 222w | | 218w | | 218w | | C-C-Cl |
| | 169w | | | | | | str. |
| 157w | | | 159w | | 156w | | |
| | | 84w | | | | | skeletal |
| | | 62sh | | | | | def. |
| | | 29w | | | | | |

a in $CCl_4$ and $CS_2$ solutions

(symmetric and asymmetric CH stretching) region, which also undergoes dramatic changes as the sample transforms from phase III to I.

Figures 3.12 show some variable-temperature FT-IR spectra obtained for 2-chloroadamantane. As expected for a $C_s$ symmetry molecule, all the changes parallel those observed in the Raman spectra. Again, phase I contains many sharp, well-resolved peaks indicating an ordered phase, whereas phase III has mostly broad, featureless bands implying a high degree of disorder. The 765 $cm^{-1}$ peak is broad but well resolved in phase III. As the sample approaches phase II, the peak decreases in intensity until the transition to phase II is reached, at which point the peak becomes a shoulder. In phase I, the band reappears as a sharp, well-defined peak. The major differences between the IR and Raman data are that the effects observed in IR are gradual, as would be expected when using a KBr matrix [18], whereas in the Raman they are sudden. Also, some IR peaks were not observed in the Raman spectra, probably due to narrower peaks and better signal-to-noise ratio available for the FT-IR measurements.

Based on the vibrational splittings observed in phases I and II, the ordered phases have at least two molecules per unit cell.

### *v. 2-Adamantanone (2-$C_{10}H_{14}O$)*

This adamantane derivative has $C_{2v}$ symmetry and its 69 vibrational modes transform into $\Gamma_{vib} = 21a_1 + 13a_2 + 18b_1 + 17b_2$, where all the modes are IR/Raman active save for $a_2$ which is Raman active only. The vibrational spectra of 2-$C_{10}H_{14}O$ had been previously studied in our laboratory by Harvey[31] and therefore some of the proposed band assignments are based on his work (Table 3.VIII). The reason for taking further look at this compound is that in the previous study it had not been subjected to cycling about the phase

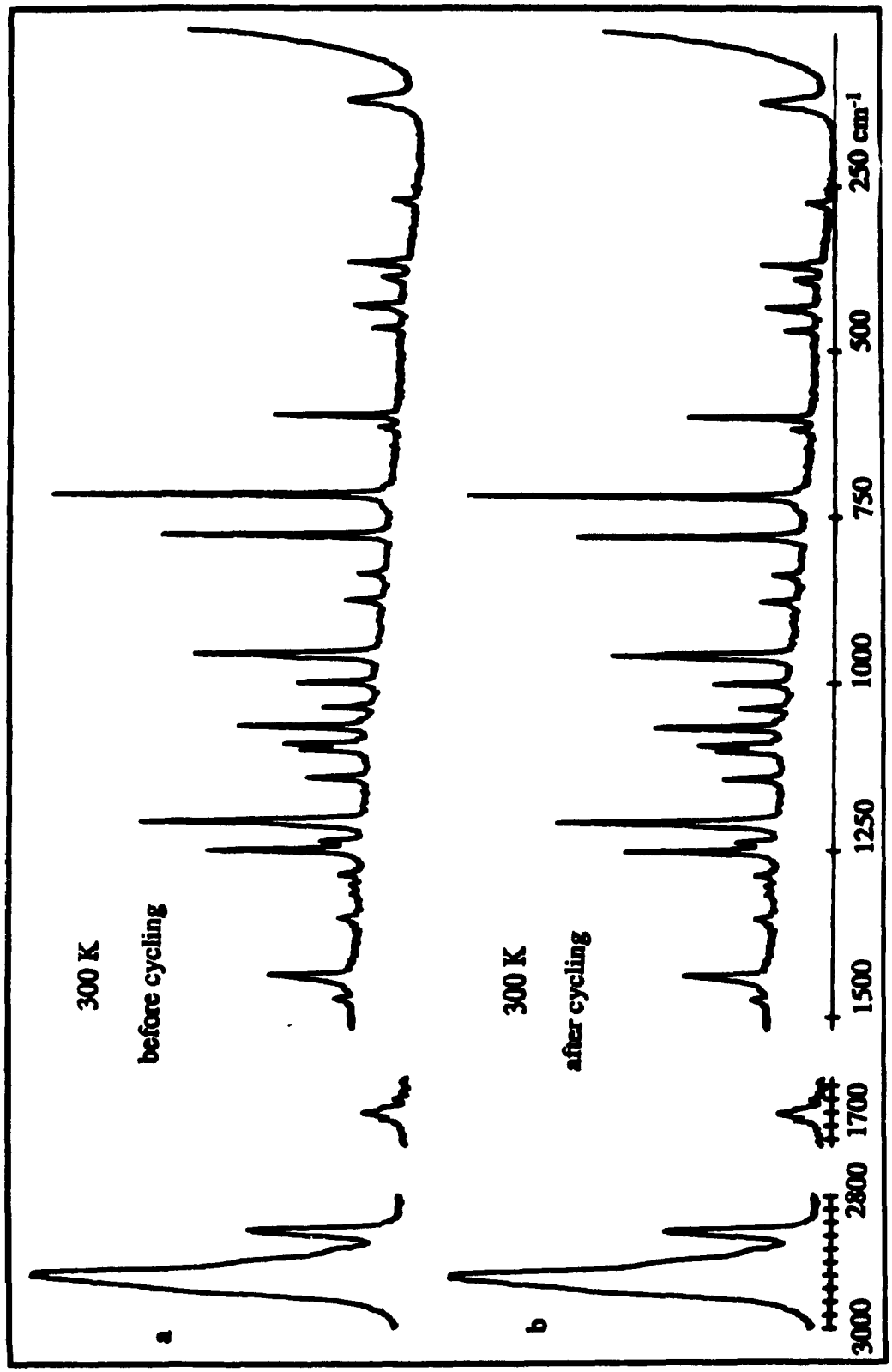


**Figure 3.13** Raman spectra of 2-adamantanone at 300 K (phase II) before and after cycling.

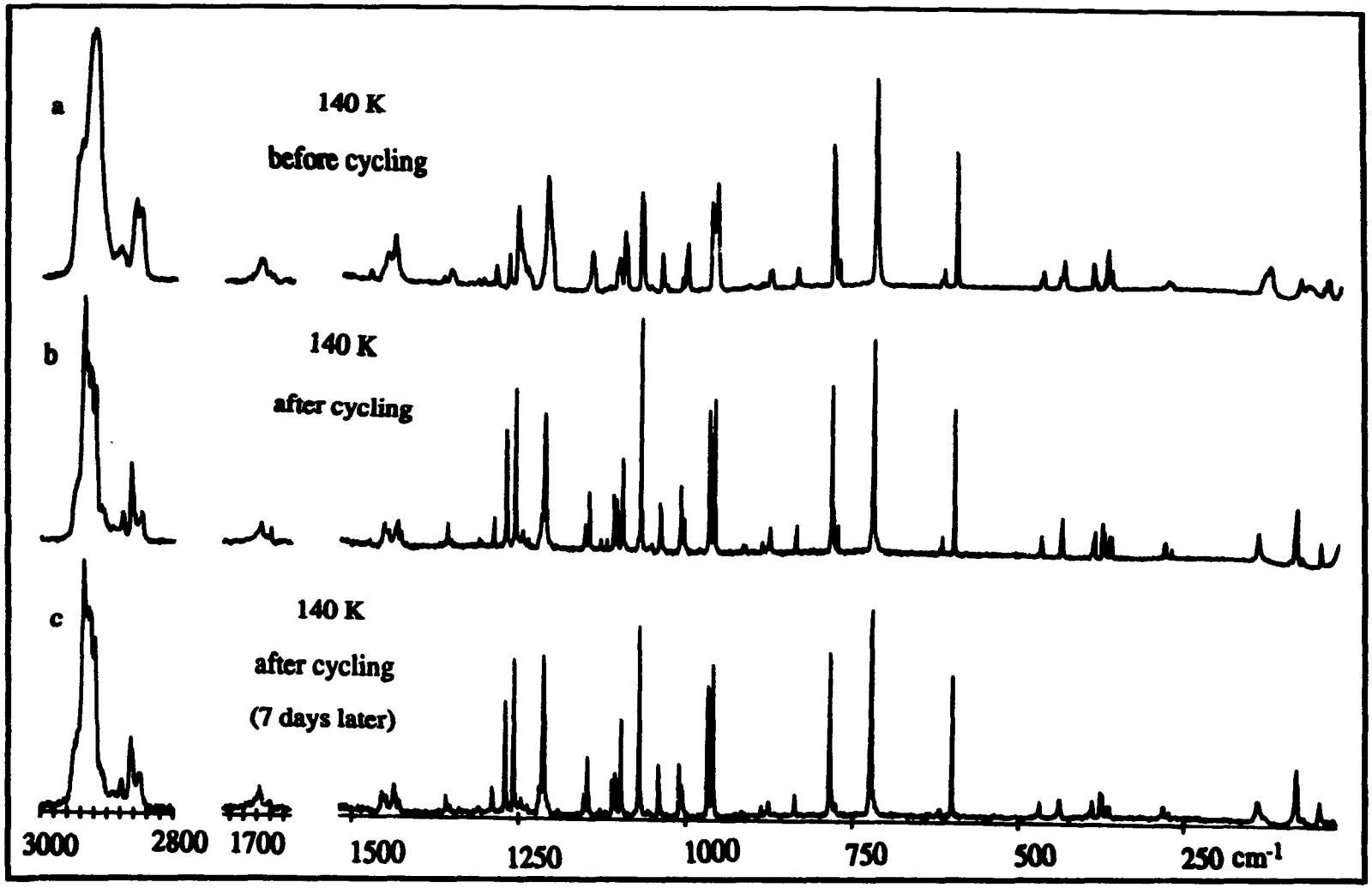


Figure 3.14 Raman spectra of 2-adamantanone at 140 K (phase I) before, immediately after cycling (phase I'), and 7 days after cycling.

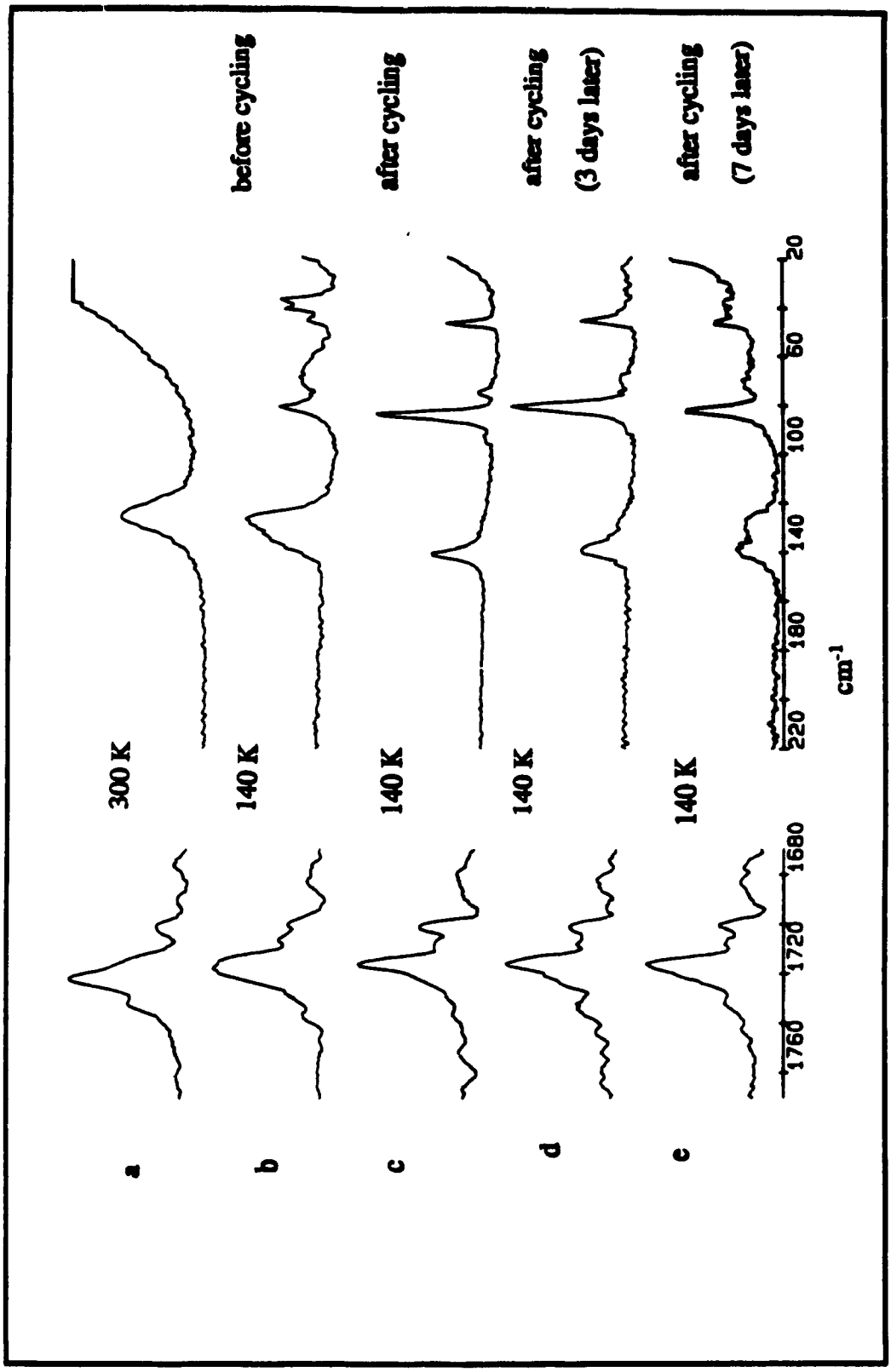


**Figure 3.15** Raman spectra of the lattice region and C=O region at 300 K and 140 K before and after cycling.

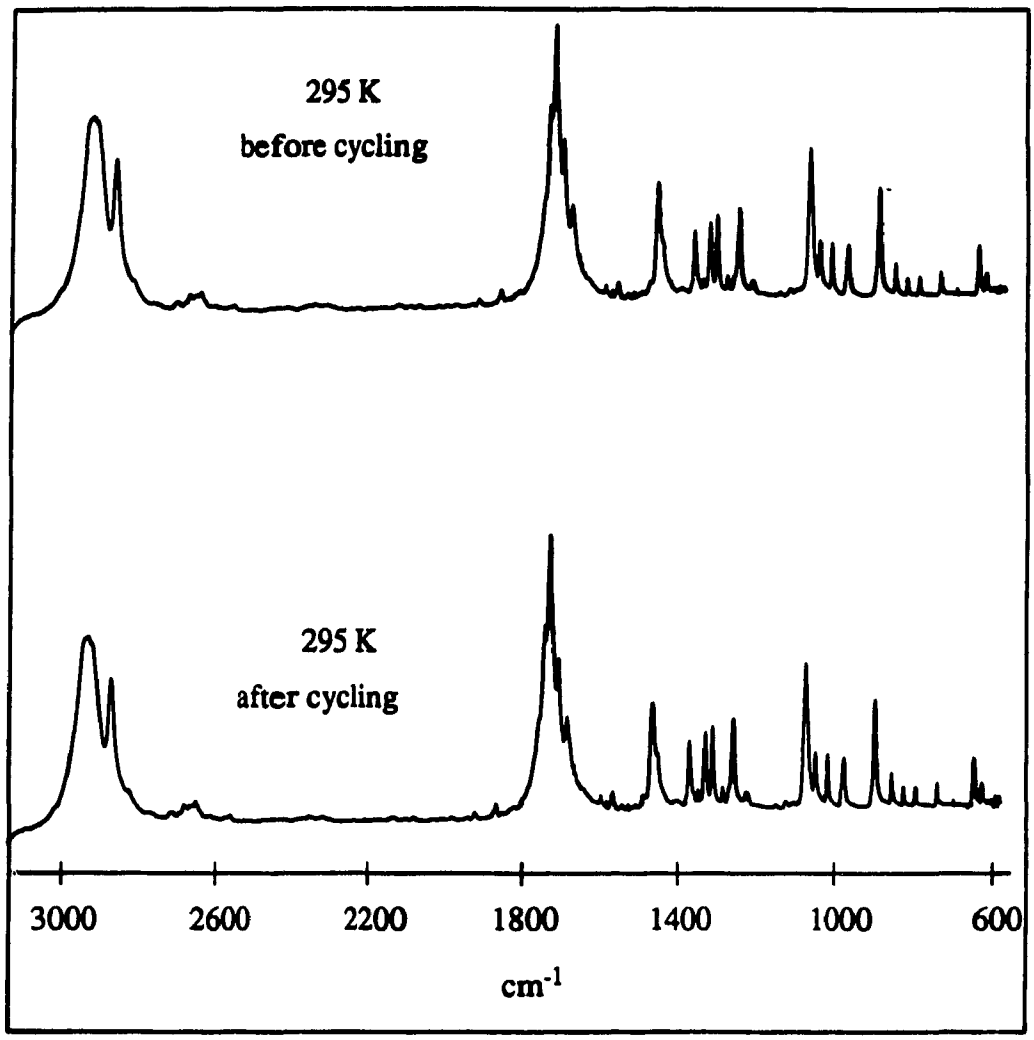


**Figure 3.16** IR spectra of 2-adamantanone at 295 K (phase II) before and after cycling.

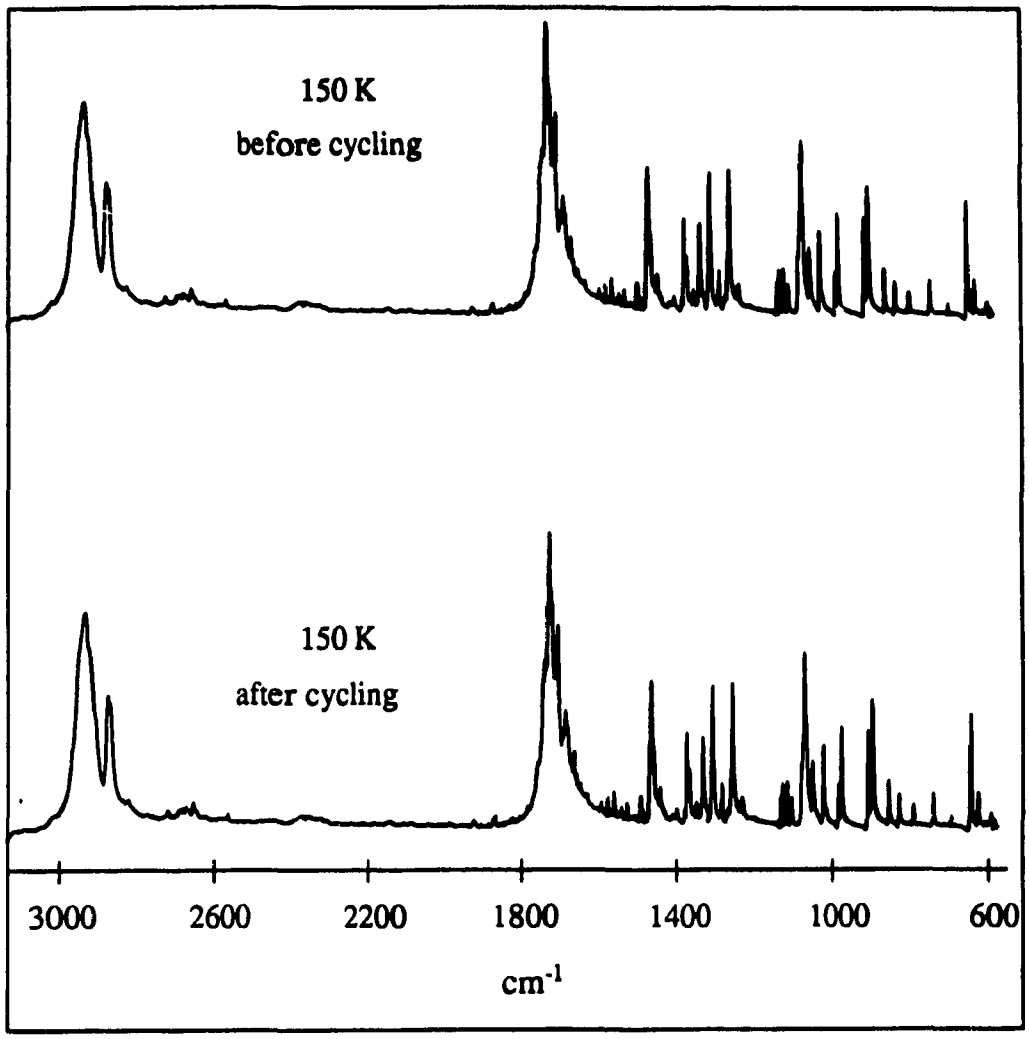


**Figure 3.17** IR spectra of 2-adamantanone at 150 K (phase I) before cycling and (phase I') after cycling.

transformation and it had been shown by Butler and co-workers[32] that 2-adamantanone has a new low-temperature phase which appears after cycling.

In this investigation, only 40 Raman peaks and 45 IR bands were observed (see Figures 3.13 and 3.16). This total includes overtones and combinations and therefore might actually be higher than the number of true peaks. A possible reason for detecting more IR peaks than Raman bands could lie in the better signal-to-noise ratio available through the Fourier-transform method.

As had been the case for the previous adamantane derivatives (except 1-$C_{10}H_{15}Br$), the room temperature spectra revealed many broad bands indicating that molecular motion is present, which is indicative of the plastic phase. As the sample is cooled, the peaks become sharper and narrower which can be attributed to a more ordered phase. Many of the bands are split into two components and, in both the IR and Raman spectra, there are some dramatic changes in relative peak intensities.

Consider the Raman spectra of uncycled 2-adamantanone. The room temperature Raman peaks (Figure 3.13a) as previously mentioned are rather broad. There is an absence of lattice modes below 100 $cm^{-1}$. As the sample is cooled down to 140 K (Figures 3.14a and 3.15b), a multitude of peaks appear below 100 $cm^{-1}$; some of which are broad (68 $cm^{-1}$) and others quite sharp (39 $cm^{-1}$). The broad 126 $cm^{-1}$ band present at room temperature remains broad but is shifted to 128 $cm^{-1}$. The 277 $cm^{-1}$ peak at 300 K is now observed at 282 $cm^{-1}$. The 372 $cm^{-1}$ envelope appears as four sharp peaks at 140 K. The same differences can be said about the majority of the peaks present at room temperature and 140 K. The 602 $cm^{-1}$ band (skeletal mode) which was of medium intensity at 300 K, is as intense as the 780 $cm^{-1}$ band. Interestingly, the 722 $cm^{-1}$ peak (C-C stretching) does not split at all; however, it does sharpen. The $CH_2$ wag and twisting modes as well as the CCH deformation modes also demonstrate some interesting changes; the 1210 $cm^{-1}$ peak and 1213 $cm^{-1}$ shoulder at 300 K, switch positions, i.e., the peak becomes a shoulder while the

shoulder becomes a peak. The 1270 $cm^{-1}$ (present at 140 K) is also of interest in that it is not even present at room temperature. Many of the other peaks which were barely detectable at room temperature are now clearly visible at 140 K. The C=O region is also of interest in that at both room temperature and 140 K (Figures 3.15a and b), it contains several peaks due to Fermi resonance as well as overtones and combinations; however, at 140 K many more peaks are detected. The exact number of bands present in that region is difficult to determine due to the weakness of the C=O band; even multi-scanning did not help improve the signal-to-noise ratio. Finally, the CH stretching region which is quite broad at room temperature, becomes better defined and contains more features than before. It is interesting to note that, compared to the other adamantane derivatives examined in this thesis, the CH stretching region of 2-adamantanone (Figure 3.14a) is still rather broad at low-temperature and resembles the semi-ordered phase of 1-bromoadamantane (Figure 3.5b). It is therefore very possible that this phase is actually a semi-ordered rather than an ordered phase.

The FT-IR spectra also display many interesting differences between the room temperature scans and those at 140 K (Figures 3.16 and 3.17). As observed in the Raman spectra, many peaks underwent splitting into two components and some bands showed changes in relative intensities. The majority of the observations made in the Raman spectra also hold for the IR spectra (with the exception of some bands which are $a_2$ modes and thus not IR active). There are two points of interest which should be noted. Firstly, the CH stretching region does not show much difference when the 2-$C_{10}H_{14}O$ molecule is cooled down from the plastic phase to the ordered phase. Although the number of peaks detected does not change enormously, the peaks do become much sharper and more shoulders appear. This could be due to the method IR used to study the compound; notably, the KBr technique, where the sample might be locked in a certain manner preventing it from moving freely. This had not been noticed for the other compounds, however, as will be

**Table 3.VIII** Vibrational data ($cm^{-1}$) for 2-adamantanone

| Phase I' (150 K) (after cycling) | | Phase I (150 K) (before cycling) | | Phase II (280 K) | | |
|---|---|---|---|---|---|---|
| Raman | IR | Raman | IR | Raman | IR | Assignments |
| | 3000sh | | 3000sh | | 3000sh | |
| 2950sh | 2949sh | 2950sh | 2949sh | | | CH and |
| | | 2941s | | 2942sh | | |
| 2936vs | 2936sh | | 2936sh | | | $CH_2$ |
| 2930s | | 2930vs | | | | |
| 2925s | 2921vs | 2925vs | 2921vs | 2923s,br | | symmetric |
| | 2916sh | | 2916sh | | 2918s | |
| | | | | 2903sh | | and |
| 2893vs | | 2893vs | | | | |
| 2879s | | 2884w,br | | | | anti-symmetric |
| 2864m | | 2862m | | | | |
| 2851m | 2853s | 2850m | 2853s | 2855m | 2853s | str. |
| | 2810sh | | 2810sh | | 2810sh | |
| | | | | | 1756sh | |
| | | 1740w | | 1745w,sh | 1744sh | C=O |
| 1730vw | 1730vs | 1730sh | 1730vs | 1729w | 1730s | |
| 1721sh | | 1725sh | | 1723w | 1725sh | str. |
| 1720sh | 1719vs | 1720m | 1719vs | | 1719vs | |
| 1718sh | | 1718m | | | | and |
| 1717m | 1716vs | 1714m,sh | 1716vs | | 1716vs | |
| | 1712vs | 1710w | 1712vs | 1712w,sh | | combinations |
| 1702w | 1705sh | 1700w | 1705sh | | | |
| | 1701s | | 1701s | | 1700s | and |
| | 1697vs | | 1697vs | 1699w | 1697s | |
| 1681vw | 1676s | 1682vw,br | 1676s | 1674w | 1673s | overtones |
| | 1653sh | | 1653sh | | | |
| 1477vw | 1477vw | 1477vw | 1477vw | 1478vw | | |
| | 1471vw | | 1471vw | | 1470w | |
| 1455w | 1455s,sh | | 1455s,sh | | | $CH_2$ |
| 1450w | 1452s | 1452w | 1452s | | 1452s | |
| | 1447m | | 1447m | | | def. |
| | 1442sh | 1442m | 1442sh | | | |
| 1437w | 1439w | | 1439w | 1440m,br | 1438sh | |
| | 1435w | 1435w | 1435w | | | |
| 1430w | 1430w | | 1430w | | | |
| | 1386vw | | 1386vw | | 1387vw | $CH_2$ |
| 1370vw | 1365vw | 1369vw,br | 1365vw | | 1362sh | |
| 1359w | 1359m | 1357w,br | 1359m | | | wag |
| 1355w | 1355w | | 1355w | 1355vw,br | 1354m | |
| | 1349w | | 1349w | | | and |
| | 1342w | | 1342w | | 1342sh | |
| | 1333vw | | 1333vw | | 1330vw | CCH |
| | 1317vw | 1317vw | 1317vw | | | def. |
| 1311vw | 1314vw | | 1314vw | | | CC str. |
| | 1307vw,sh | 1308vw | 1307vw,sh | | 1310m | and |
| | 1304vw | | 1304vw | | | $CH_2$ twist |
| 1290w | 1289s | 1290w | 1289s | 1289vw,br | 1291m | and |
| | 1285sh | | 1285sh | | | $CH_2$ wag |
| | 1282sh | | 1282sh | | | |
| | 1277w | | 1277w | | | |
| 1270m | 1267w,sh | 1270m | 1267w,sh | | | |
| | 1265vw | | 1265vw | | | |
| | 1262w | | 1262w | | 1261vw | |

**Table 3.VIII** Vibrational data ($cm^{-1}$) for 2-adamantanone

| Phase I' (150 K) (after cycling) | | Phase I (150 K) (before cycling) | | Phase II (280 K) | | |
|---|---|---|---|---|---|---|
| Raman | IR | Raman | IR | Raman | IR | Assignments |
| 1258m | | 1257s | | 1253s | | $CH_2$ |
| 1247w | 1248vw | 1247sh | 1248vw | | | |
| 1240w | 1244vw,br | 1240sh | 1244vw | 1239m | 1243sh | wag |
| | 1236sh | | 1236sh | | | |
| | 1233s | | 1233s | | 1233m | and |
| 1220sh | 1221vw | | 1221vw | | | |
| 1214m | 1214sh | 1213s | 1214sh | | | CCH |
| | 1209vw | 1209sh | 1209vw | 1210s | | |
| | | | | | 1203vw | def. |
| 1153w | | | | | | |
| 1146w | | 1146m | | 1145m,br | | |
| | | 1140sh | | | 1138vw | |
| 1131vw | | | | | | |
| 1122vw | 1121vw | | | | | and |
| | 1116w | | | | | |
| 1113w | 1113vw | | | | 1112vw | |
| 1109w | | 1109sh | | | | $CH_2$ |
| | | 1107m | | | | |
| | 1105w | 1105sh | | | | twist |
| 1099m | 1101vw | 1099m | 1101vw | 1102m | | |
| | 1094vw | 1097m | 1094vw | 1095m | | |
| 1071s | | 1072s | | | | |
| | 1066sh | 1070s | 1066sh | 1064m | | C-C |
| 1056vw | 1063sh | | 1063sh | | | str. |
| | 1058s | | 1058s | 1054w,sh | 1058s | $CH_2$ |
| 1042w | | 1042m | | 1039m | | twist |
| 1037sh | 1035m | 1035sh | 1035m | | | |
| | 1029sh | | 1029sh | | 1030w | CCH def. |
| | 1025sh | | 1025sh | | | |
| 1015w | | | | | | |
| 1010vw | | 1010m | | | | skeletal |
| | 1006m | 1005m | 1006m | | | |
| | 1000w,sh | | 1000w,sh | 1002m | 997w | def. |
| 969s | | 970s | | | | $CH_2$ rock |
| 961s | 963w | 961s | 963w | 961m | | and |
| | 955m | | 955m | | 954sh | CCC bend |
| | | | | | 952w | and |
| | | | | | 950sh | CC str. |
| 889w | 884m | | 884m | | | |
| 879w | | 881w | | 880vw | | $CH_2$ rock |
| | 874s | | 874s | | 875s | |
| 839w | 834w | 840w | 834w | 840vw | 835w | |
| | 831sh | | 831sh | | | C-C |
| | 807w | | 807w | | 804vw | |
| 786s | | 786s | | 783m | | str. |
| 775w | 771vw | 775w | 771vw | | 773vw | |

**Table 3.VIII** Vibrational data ($cm^{-1}$) for 2-adamantanone

| Phase I' (150 K) (after cycling) | | Phase I (150 K) (before cycling) | | Phase II (280 K) | | |
|---|---|---|---|---|---|---|
| Raman | IR | Raman | IR | Raman | IR | Assignments |
| 724vs | | 722vs | | 721s | | |
| | 717vw | | 717vw | | 714vw | |
| 620m | 616s | 620m | 616s | 620vw | 616w | |
| 602s | | 601s | | 602w | | |
| | 597w | | 597w | | 597w | |
| 471m | | 471m | | 471m | | |
| | 457m | | 457m | | 457m | |
| 440m | | 445w | | | | |
| | | 439m | | 437m | | |
| 392m | | 395m | | 394m | | skeletal |
| 391m | | | | | | |
| 380m | | 385m | | | | modes |
| 377m | | 378w | | | | |
| 370m | | 373m | | 372m | | |
| 366m | | | | 368w,sh | | |
| | | 360m | | | | |
| 285w | | | | | | |
| 283m | | 280w,br | | 277w | | |
| 275w | | | | 276w,sh | | |
| 140m | | | | | | |
| | | 130sh | | | | |
| | | 128m,br | | 126m,br | | |
| 81m | | 82m | | | | skeletal |
| 70w | | 68br,m | | | | def. |
| | | 50m | | | | involving |
| 45m | | 45m | | | | CO |
| | | 39m | | | | |

shown later, not all the compounds behave like 2-adamantanone. It is also possible that this region contains $a_2$ modes which are IR inactive and therefore would not be observed in the IR region. Secondly, the region showing the most dramatic changes is the region containing the $CH_2$ wagging and twisting modes as well as the CCH deformations. The room temperature IR spectrum shows some extremely weak and broad bands at 1080, 1095, 1100, and 1110 $cm^{-1}$. As the sample is cooled down towards its ordered phase, the peaks become more prominent and even display splitting. This effect had previously been observed by Harvey[31] except that these peaks were not observed at room temperature. At this point, a more detailed comparison between the data obtained in this study and those acquired by Harvey[31] is in order.

The previously published Raman data by Harvey[31] show many more tabulated peaks than that observed in the present study. Furthermore, the data differ by up to 5 $cm^{-1}$ with for the bands which do correspond. There are some possible explanations which can account for these differences. Firstly, impurities might have been present in the previous sample. This is a possible source of error since in the current study a higher resolution was employed than that used by Harvey and yet fewer peaks were detected. Secondly, although both investigations used the same Raman instrument (I.S.A. U-1000), the previous work states that the argon-ion laser line used was 514.5-nm rather than the actual value of 514.532-nm. Even though, at first sight, this difference appears to be negligible, it has been found to generate discrepancies in band position up to 4 $cm^{-1}$. It is also interesting to note that the band at 1270 $cm^{-1}$ (present at 140 K) was not detected by variable-temperature Raman spectroscopy, but Harvey *et al.*[29] did notice it using variable-pressure Raman spectroscopy at 1273 $cm^{-1}$ which is well within experimental error considering the diamond-anvil-cell setup and that a different Raman spectrometer was used. Lastly, the published data do not give information about the region below 100 $cm^{-1}$.

Comparison of the FT-IR data of Harvey[31] with those obtained in the present investigation also shows that fewer peaks were detected and that here too, the band positions vary. The argument that calibration is partly the cause of these differences does not apply here since both studies used FT-IR and hence all the bands are referenced to the helium-neon lines (Connes advantage). Once again the possibility of impurities being present does come to mind. It is also possible that the method of sample preparation for the IR studies might be the cause of the observed differences. In the present study, the sample was studied via the KBr pellet method whereas in the previous study the sample had been ground onto a KBr window. As previously mentioned, this might account for the presence of the bands centered at ~1105 $cm^{-1}$. Finally, as far as the CH stretching region (3000 - 2800 $cm^{-1}$) is concerned a more detailed comparison is difficult since selected spectral regions rather than the complete spectrum were published.

After cycling, no significant difference was observed in the IR region, the only notable dissimilarity was that the peaks were sharper and appeared more suddenly than prior to cycling.

The Raman spectra of 2-$C_{10}H_{14}O$ after cycling presented many important changes for the low-temperature phase but none for the room temperature phase. This corresponds very well with the DSC work of Butler *et al.*[32] which demonstrated that after cycling a different DSC curve was obtained. Upon examining the lattice region below 200 $cm^{-1}$ (Figure 3.15), it is immediately obvious that a different phase is present. In order to simplify the description of the new phase, the new phase will be referred to as phase I'. This region now contains fewer peaks in the low-temperature phase at 140 K but they are sharper than before cycling. The peaks appear at 47, 75, 85, 90 and 142 $cm^{-1}$. The most interesting peak from the phase I' spectrum is the 142 $cm^{-1}$ which is not only a sharper peak but also it is different from the peak at 130 $cm^{-1}$ found in phase I, since it is possible to trap the molecule as it is returning to phase I and at that point both peaks are present.

Many other regions display a sort of "cleaning up" in that the peaks are narrower and much sharper; for example, the broad 282 $cm^{-1}$ band in phase I appears as three very sharp and relatively intense bands in phase I'. The same applies to the quartet in phase I centered at 373 $cm^{-1}$ which in phase I' is still a quartet but not only are they sharper and better defined, but also, the relative intensities have changed. Interestingly, the phase I broad doublet at 439 $cm^{-1}$ and 445 $cm^{-1}$ (skeletal modes) have collapsed into a single, narrow band at 440 $cm^{-1}$. The same observation can be made with the 471, 1072, and 1097 $cm^{-1}$ doublets. The 1209 $cm^{-1}$ shoulder, on the peak at 1213 $cm^{-1}$, present in phase I, has disappeared in phase I', but a shoulder is still present on the 1214 $cm^{-1}$ peak at 1220 $cm^{-1}$. The 1270 $cm^{-1}$ peak of phase I is now a very strong peak in phase I'. The 1477 $cm^{-1}$, however, has gone from a definite peak to being almost noise in phase I'. Even the complicated C=O region (Figure 3.15b and c), seems less complicated in phase I' than in phase I. There are very sharp peaks at 1717 and 1702 $cm^{-1}$ as well as a weak broad peak at 1681 $cm^{-1}$. Finally, the CH stretching region in phase I' contains more well-defined and sharp peaks than in phase I. The overall shape of the region in phase I' resembles that of the other adamantane derivatives in the ordered phase.

Based on the presented data, it can be concluded that phase I' is the most ordered phase, with phase I being semi-ordered and since no differences were observed for phase II, it is still the plastic phase. Moreover, since phase I eventually changes to phase I', phase I is most likely a metastable phase. This is also supported by the DSC results of Butler and co-workers[32] which showed that the $\Delta S_t$ of I' to II was nearly twice as large as that of I to II.

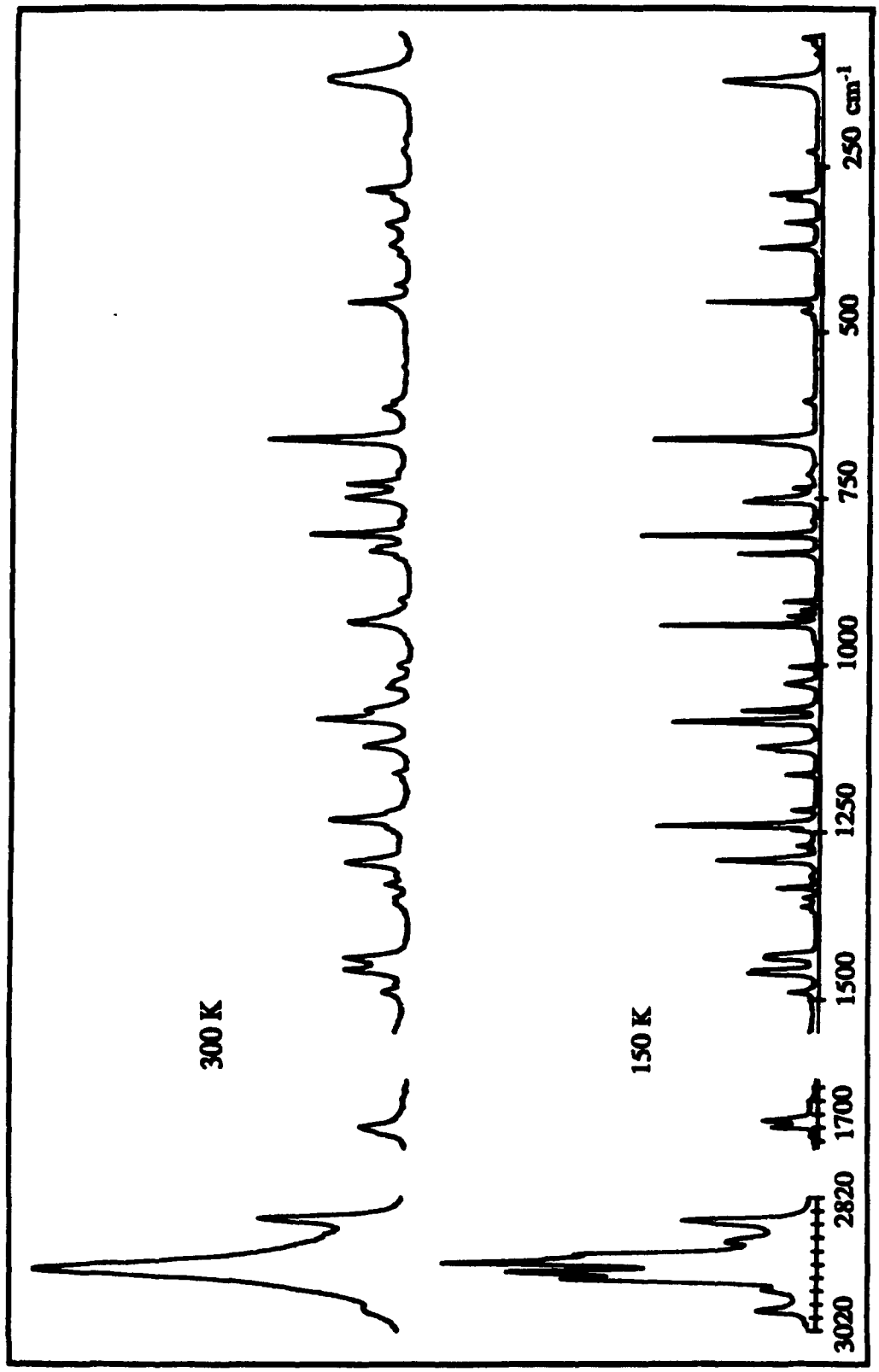


Figure 3.18 Raman spectra of bicyclononanone: phase I (150 K), and phase II (300 K).

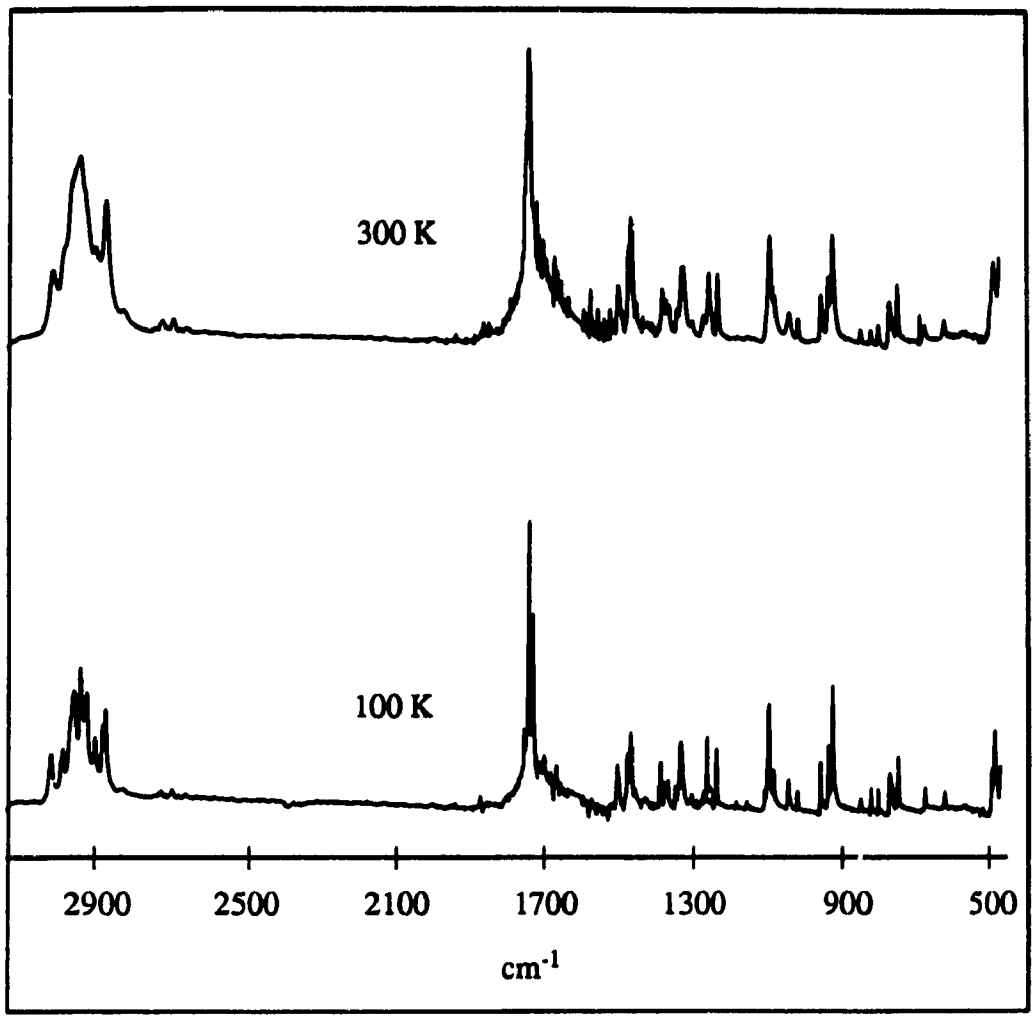


**Figure 3.19** IR spectra of bicyclononanone: phase I (100 K), and phase II (300 K).

### *vi. Bicyclo[3.3.1]nonan-9-one (9-$C_9H_{14}O$)*

A total of 66 Raman and 53 IR bands would be anticipated for this $C_{2v}$ molecule. The 66 normal modes of vibration can be broken down to yield $20a_1 + 13a_2 + 17b_1 + 16b_2$ for which $a_1$, $b_1$, and $b_2$ are both IR and Raman active, while $a_2$ is solely Raman active. Possibly due to band overlap and the presence of very weak bands hidden under the noise, only 40 Raman peaks and 36 IR bands were observed. The peak positions as well as their proposed assignments are presented in Table 3.IX.

At room temperature, the 9-$C_9H_{14}O$ molecule exhibited many broad vibrational peaks characteristic of an orientationally-disordered solid. Upon cooling, the Raman peaks became sharper and narrower and, at 150 K, many peaks split into two components (Figure 3.18). Furthermore, at 150 K, the lattice region which originally contained no peaks, is now comprised of three recognizable peaks. Similarly, the IR bands either became narrower or split into doublets as the sample was cooled down from 300 K to 150 K. These results parallel those obtained from the DSC measurements in that only two phases were detected. Phase I (the low-temperature phase) is the ordered phase, while phase II (the high-temperature phase) is the plastic phase.

In the Raman spectra, the 120 $cm^{-1}$ peak of phase II becomes narrower but does not split or shift by more than 1 $cm^{-1}$. The broad peaks present at 211 and 229 $cm^{-1}$ at 300 K, either disappear totally (211 $cm^{-1}$) or become much sharper (228 $cm^{-1}$). The same effect is encountered with the bands at 340, 370, 384, 430, 605, and 616 $cm^{-1}$ where the 340, 370, and 605 $cm^{-1}$ peaks become sharper and narrower at 150 K, whereas the 384, 430, and 616 $cm^{-1}$ bands disappear. The 456 $cm^{-1}$ peak gives rise to a very sharp band at 455 $cm^{-1}$ and a much weaker one at 470 $cm^{-1}$. Interestingly, the 661 $cm^{-1}$ band simply gets more intense but does not split or shift. Other peaks of interest are the 729 and 750 $cm^{-1}$ pair which in phase I undergo dramatic changes. For example, the 729 $cm^{-1}$ peak shifts to

**Table 3.IX** Vibrational data ($cm^{-1}$) for 9-bicyclononanone

| Phase I (150 K) | | Phase II (300 K) | | |
|---|---|---|---|---|
| Raman | IR | Raman | IR | Assignments |
| | 2995sh | | 2990sh | CH str. |
| 2989m | 2990vs | 2984m | 2988s | |
| | 2965sh | | | |
| 2958w | 2960s | | 2960sh | |
| 2941vs | 2940sh | | | |
| 2932s | 2932vs | | | |
| | | 2926vs | | |
| 2917vs | 2916vs | | 2920vs | |
| 2915sh | | | | |
| 2910vs | 2910sh | | 2910sh | |
| | 2900vs | | | |
| 2886m | | | | |
| 2880sh | 2879vs | | 2881vs | |
| 2865sh | 2860vs | | | |
| 2855s | 2853vs | 2852vs | 2854vs | |
| | 1733w | 1730sh,vw | 1730sh | C=O symmetric str. |
| 1719w | 1720vs | 1720w | 1722vs | |
| 1709w | 1710vs | | | |
| | 1700sh | | | |
| 1680br,vw | | | | |
| 1490vw | | 1490vw | 1496w | $CH_2$ Def. |
| | 1483m | | | |
| 1458w | 1457m | | 1456m | |
| 1455w | | 1455m | | |
| | 1447m | | 1448m | |
| 1440vw | | | | |
| 1436w | 1435vw | 1438m | 1436vw | $CH_2$ wag and CCH def. |
| 1430w | | | | |
| | 1408vw,br | | | |
| 1365sh | 1368w | | 1358w | |
| 1363vw | 1358vw | | | |
| | | 1356vw,br | | |
| 1349vw | 1349vw | | 1348w | |
| 1335vw | | | | |
| | 1328m | 1328vw | 1328vw | |
| | 1316m | | 1313vw | |
| 1292m | | 1295w | | CC str. |
| | 1287vw | | | |
| 1280vw | | | | |
| 1271vw | 1275vw | | | |
| | 1254vw | | 1257w | C-C str. $CH_2$ def. |
| 1245vw | 1247m | | 1244w | |
| 1240s | 1236w | 1235sh | 1240sh | |
| | | 1231m | | |
| | | 1228sh | | |
| 1218vw | 1220m | | 1218w | $CH_2$ twist and CCH def. |
| | | 1186sh | | |
| 1165w | 1165vw | 1162vw | | |
| | 1136vw | | | |
| 1125vw | | | | CCH def. |
| 1123w | | 1121vw | | |
| 1085s | 1088vw | 1081s | | |
| | 1078m | 1075m | 1076m | CCH def. |
| 1068m | 1068w | | 1070w | |
| 1029w | 1026vw | 1033w,br | 1025vw | |
| | 1020sh | | | |
| 1004w | 1001vw | 1001w,br | 1001vw | |

**Table 3.IX** Vibrational data ($cm^{-1}$) for 9-bicyclononanone

| Phase I (150 K) | | Phase II (300 K) | | |
|---|---|---|---|---|
| Raman | IR | Raman | IR | Assignments |
| 941s | 938w | 937m | 936w | CC str. |
| 929vw | 927vw | | | |
| 920vw | 915m | | 917w | |
| 907vw | 904s | 904vw | 904m | |
| 834w | 830sh | 830vw | 830sh | |
| | 829vw | 828vw | 829vw | |
| 807s | 804vw | 805s | 803vw | |
| 785vw | 784vw | | 783vw | C-C str. |
| 754w | 753w | | 752w,br | |
| 750w | 748vw | 750w | | |
| 735vw | 739vw | 729w | | |
| 714vw,br | | 714vw | | |
| 661s | 655vw | 661m | 655vw | C-C-C bending |
| | | 616vw | | |
| 605vw | 603vw | 605vw | 601vw | |
| 470vw | 474w | | | |
| | 466m | | 466vw | |
| 455m | 460w | 456w | | |
| | | 430vw | | skeletal modes |
| | | 384sh | | |
| 372w | | 370vw | | |
| 337vw | | 340vw | | |
| 305vw | | 300vw,br | | |
| 293vw | | 288vw | | |
| 228vw | | 228vw | | |
| | | 221vw | | |
| 121m | | 120m | | |
| 80vw | | | | lattice modes |
| 70vw,br | | | | |
| 55vw | | | | |

735 $cm^{-1}$ and loses considerable intensity, while the 750 $cm^{-1}$ splits into a peak at 750 and another one of slightly greater intensity at 754 $cm^{-1}$. The 805 $cm^{-1}$ band merely shifts to 807 $cm^{-1}$ in phase I, while the peaks at 830 and 828 $cm^{-1}$ collapse into one band at 834 $cm^{-1}$. The two peaks at 904 and 937 $cm^{-1}$ give rise to four very sharp peaks at 907, 920, 929, and 941 $cm^{-1}$, with the latter being the most intense. The peaks at 1438 and 1445 $cm^{-1}$, which are of equal intensity, diminish and split into two components. The carbonyl region is much cleaner than in the case of 2-adamantanone as only one band (1720 $cm^{-1}$) is visible in phase II (room-temperature). Upon cooling, the band is split into two narrower peaks at 1709 and 1719 $cm^{-1}$. Finally, as was the case for the adamantane derivatives, the ν(CH) region (3100-2800 $cm^{-1}$) explodes into 10 sharp and well-defined peaks and shoulders at 150 K from the three featureless and broad peaks at 300 K.

The FT-IR spectra (Figure 3.19) do not show as many changes as the Raman spectra. The bands that underwent splitting, did so into two components. The CH stretching region was one of the most interesting regions in that at 300 K (phase II) there were 11 peaks and shoulders while at 150 K (phase I), 17 bands and shoulders appeared. The C=O region was not very clean at either 300 K or 150 K. In phase II, a total of five bands and shoulders can be observed, however, there is only one strong, broad peak at 1722 $cm^{-1}$. As the sample is cooled down to phase I, five peaks can still be detected but there are three distinct, narrow and sharp bands at 1733, 1720, and 1710 $cm^{-1}$. The 1550-450 $cm^{-1}$ region contains many peaks which, upon cooling, become sharper, better defined, and narrower than the phase II spectra. For example, the peaks centered at 1078 $cm^{-1}$ go from two bands in phase II, to three narrow and well-resolved peaks in phase I. The intensity of the latter increases as well. There is one IR peak at 668 $cm^{-1}$ that disappears in phase I, as was also observed in the Raman spectra.

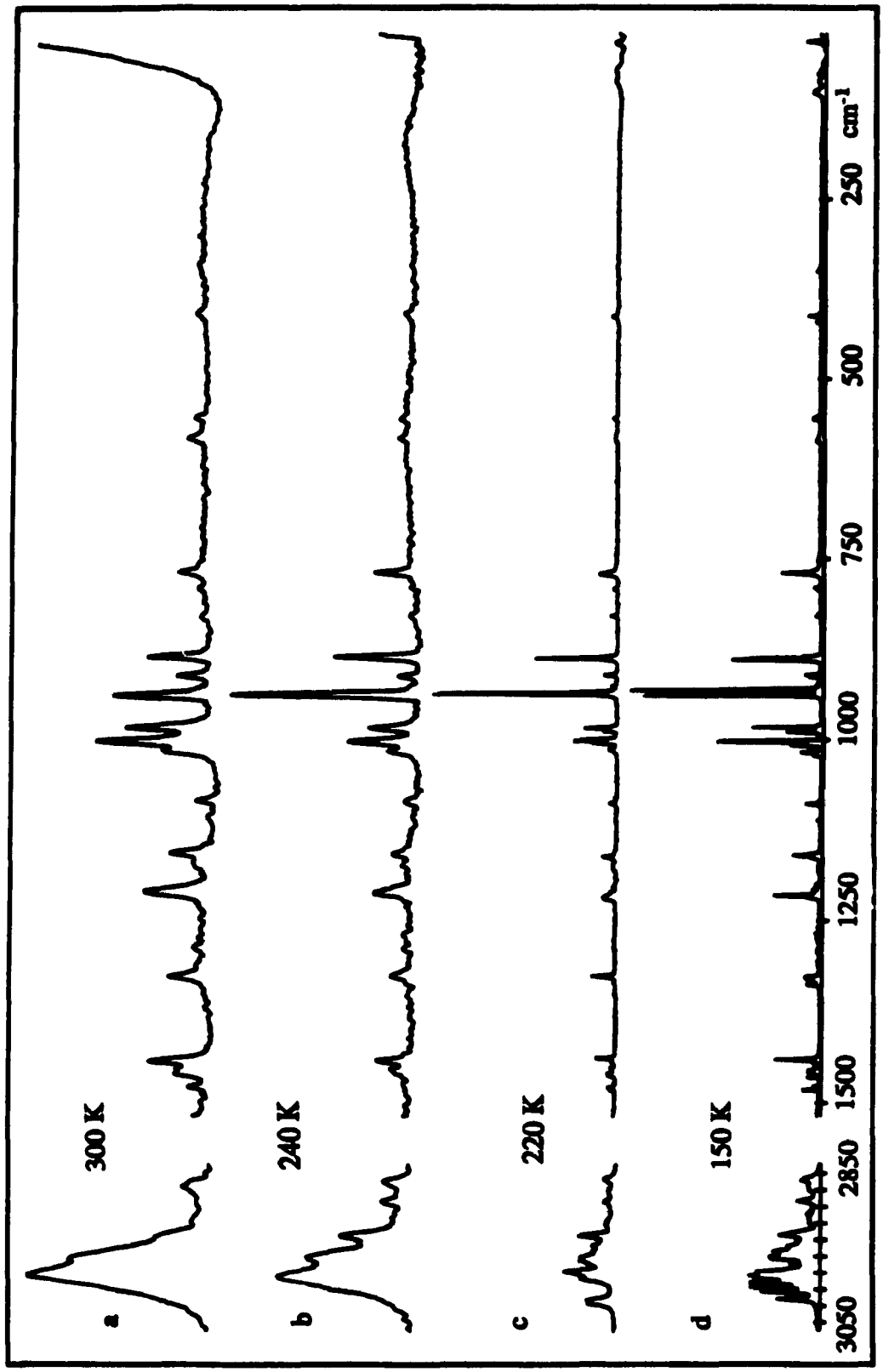


**Figure 3.20** Raman spectra of oxanorbornane: phase I (150 K), phase II (220 K), phase III (240 K), and and the liquid phase (300 K).

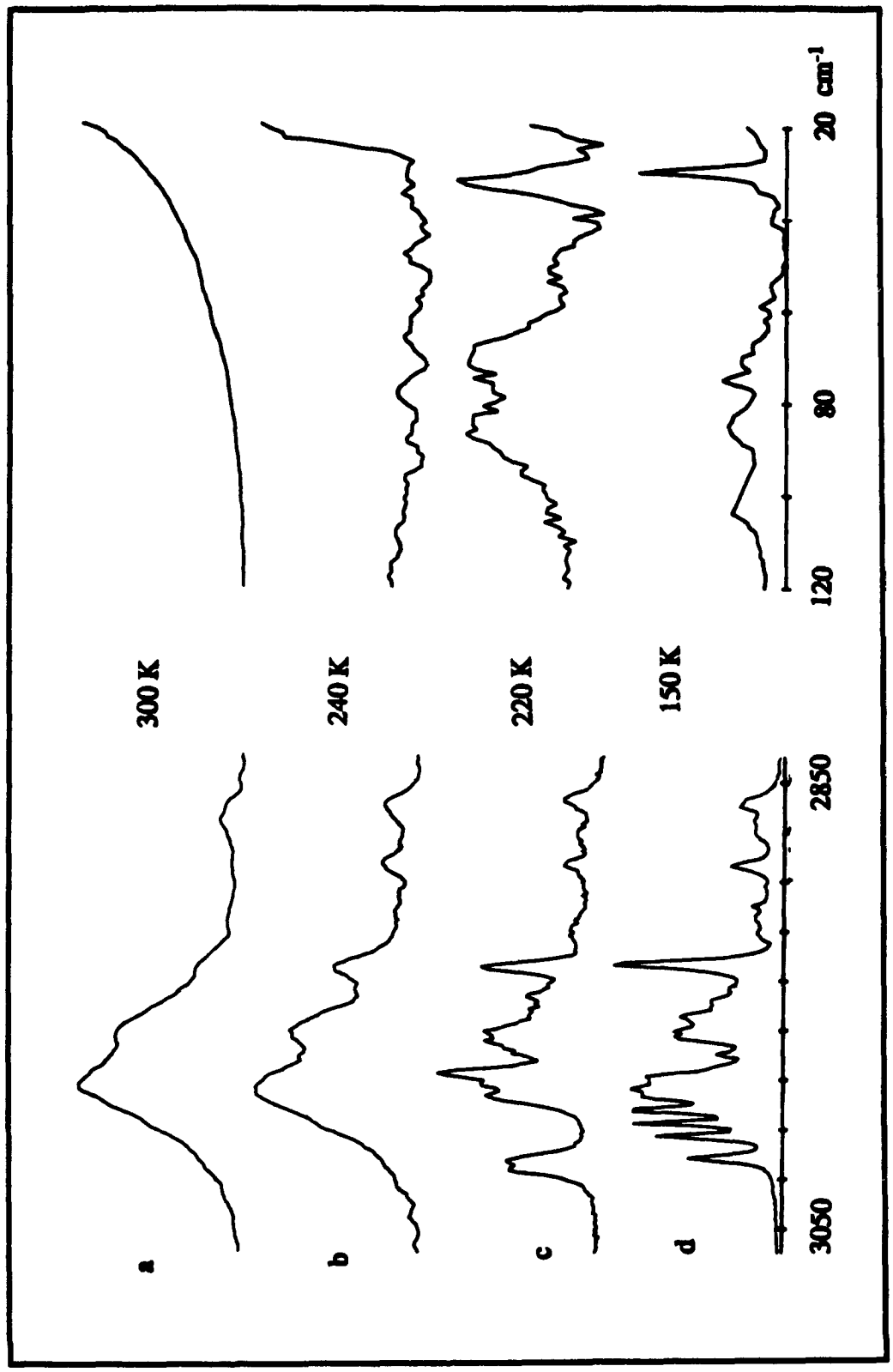


Figure 3.21 Raman spectra of the lattice region, and the CH region of oxanorbornane: phase I (150 K), phase II (220 K), phase III (240 K), and the liquid phase (300 K).

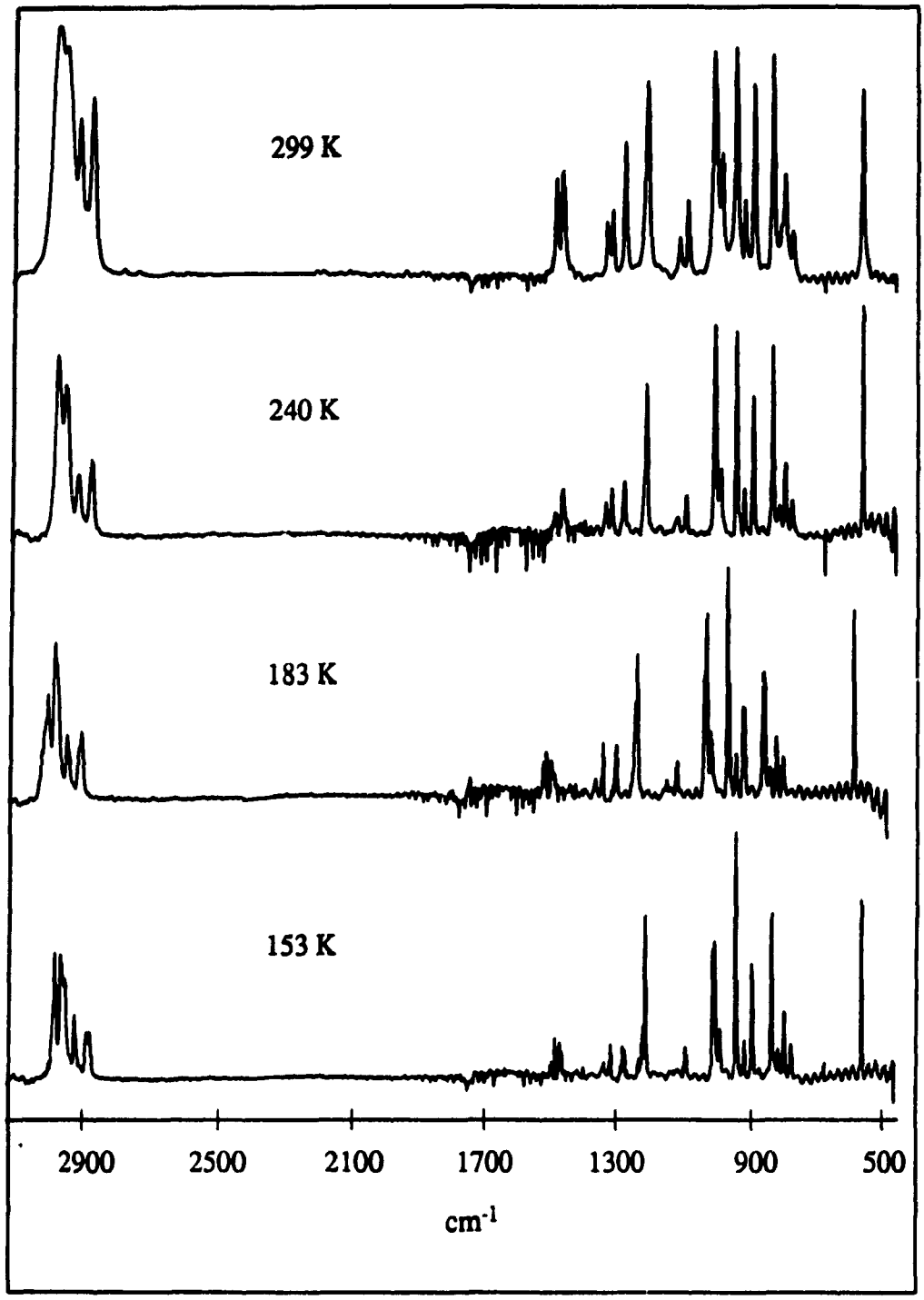


Figure 3.22 IR spectra of oxanorbornane: phase I (153 K), phase II (183 K), phase III (240 K) and liquid phase (299 K).

### *vii. 7-Oxabicyclo[2.2.1]heptane ($C_6H_{10}O$)*

The vibrational representation for the isolated oxanorbornane molecule of $C_{2v}$ symmetry reduces to $\Gamma_{vib} = 13a_1 + 10a_2 + 12b_1 + 10b_2$. Since $a_2$ modes are only Raman active while the others are both IR and Raman active, 35 IR and 45 Raman-active peaks are predicted. Furthermore, the $13a_1$ modes will be polarized in the Raman spectra. Surprisingly, only 23 Raman peaks were detected at 300 K and 25 IR bands were observed. It is possible to account for the observation of fewer peaks than expected by noting that many of them are broad and that they may be superposed on other peaks which are perhaps weaker and narrower. The tabulation of the observed IR and Raman peaks and their proposed assignments, based on published norbornane data, can be found in Table 3.X, while typical spectra are shown in Figures 3.20 and 3.22.

It is immediately evident from the Raman data for the liquid and phase III (Figures 3.20a and b, and 3.21a and b) that there is a direct correlation between the two. This is in good agreement with the DSC results which indicate the entropy of melting is approximately equal to the gas constant, and therefore, the only additional motion acquired is translational. The additional peaks observed in the Raman spectra of phase III can be attributed to solid-state splitting effects where extra splittings would be expected. Based on the Raman spectra of the liquid phase and of phase III, it is obvious that phase III is the disordered phase.

The Raman spectra are once again a good indicator of the type of phase present. For instance, consider the lattice region presented in Figure 3.21. In phase III, as in the liquid phase, there are no peaks, indicating a totally-disordered phase. As the sample is cooled down, phase II begins to appear, as evidenced by the appearance of four lattice modes. Finally, in phase I, seven lattice modes can be detected. It is therefore obvious that phase I is ordered, phase II semi-ordered, and phase III totally-disordered. The same

**Table 3.X** Vibrational data ($cm^{-1}$) for oxanorbornane

| Liquid (300 K) | Phase I (100 K) | | Phase II (220 K) | | Phase III (240 K) | | |
|---|---|---|---|---|---|---|---|
| Raman | Raman | IR | Raman | IR | Raman | IR | Assignments |
| | | | 3018w | | | | |
| | 3014w | | 3015w | | | | |
| | 3010m | | | | | | |
| | 3005m | | | | | | |
| | 2999m | | | | | | |
| | 2997m | 2997sh | | 2997sh | | 2995sh | |
| | 2990sh | | 2990sh | 2990sh | | | |
| 2984br,p | 2987m | 2985sh | 2985w | 2985sh | 2987br | | |
| | 2980sh | 2978vs | 2979m | 2978m,br | | 2977vs,br | |
| | 2970vw | | 2970w,sh | | | | |
| | 2963w | | 2964w | | | | |
| 2960s,p | 2961w | 2960s | 2961w | | 2960sh | | |
| | | 2955s | | 2954s,br | | | |
| | 2950sh | 2953sh | 2950br | 2953sh | | 2951br,vw | CH str. |
| | 2945sh | | 2945sh | | | | |
| 2940sh,p | 2935m | 2940s | 2936s | 2940s | 2936s | | |
| | 2930vw | | | | | | |
| | 2920vw | | 2921vw | | | | |
| | | 2914m | | 2915m,br | | | |
| | 2910vw | 2910sh | | 2911sh | | 2911s | |
| | 2895w | | 2894w | | 2894w | | |
| | 2888sh | | | | | | |
| | 2880sh | | 2882br | | | | |
| | | 2876m | | 2875sh | | 2871s | |
| 2873sh,p | 2870w | | | 2869m,br | 2871w | | |
| | | 2867m | 2868w | 2867sh | | 2867sh | |
| | | | 1490sh | | | | $CH_2$ |
| | 1483w | 1480vw | 1482w | 1479vw | | | str. |
| 1480vw | 1478vw | | | | 1479br | | |
| | 1475vw | | 1475vw | | | 1474vw | |
| | 1467w | 1470vw | 1465sh | 1470vw | | | |
| 1461w | 1460sh | | 1463vw | | 1462sh | | |
| | 1458w | | 1458vw | 1458vw | | | $CH_2$ |
| 1455sh | 1455vw | 1456vw | 1455sh | | | | def. |
| | 1452vw | 1450sh | 1452vw | | | 1452vw | |
| | 1445vw | | 1445vw | | 1443vw | | |
| 1443m,p | 1441m | | | | | | $CH_2$ def. |
| | 1439sh | | 1440m | | 1440sh | | |
| | 1340vw | | | | | | |
| | 1338vw | | | | | | |
| | 1332w | | | | | | |
| 1328w,p | 1329w | 1324vw | 1328w | 1324vw | 1329br,w | 1321vw | |
| | | 1305sh | | | | 1304vw | $CH_2$ |
| | | 1303vw | | 1302vw | | | |
| | | 1270vw | | | | | bend |
| | | 1266vw | | | | 1265vw | |
| | | 1260vw | | 1262vw | | | |
| | | 1250vw | | | | | |
| | 1220vw | 1218vw | | | | | $CH_2$ bend |
| | 1216m | | | | | | |
| 1210w | 1210vw | 1208sh | 1210sh | | 1210sh | | and |
| | 1205vw | 1204w | 1205vw | 1203w | 1205vw | | |
| | | 1197s | | 1197s | | 1197s | skeletal str. |
| | 1175vw | | 1175br | | 1175br | | |
| | 1170vw | | | | | | |
| | 1165sh | | 1163m | | | | COC |
| 1157w | 1161m | | | | 1159br | | str. |

**Table 3.X** Vibrational data ($cm^{-1}$) for oxanorbornane

| Liquid (300 K) | Phase I (100 K) | | Phase II (220 K) | | Phase III (240 K) | | |
|---|---|---|---|---|---|---|---|
| Raman | Raman | IR | Raman | IR | Raman | IR | Assignments |
| 1085m,p | 1090m | | 1089vw | | 1087vw | | |
| | | 1080vw | | 1080vw | | 1081vw | $CH_2$ |
| | 1023m | | | | | | |
| 1016m,p | 1019m | | 1015br,w | | 1017br,w | | |
| | | | 1013sh | | | | bend |
| | 1008m | | 1010m | | | | |
| 1003m,p | 1004m | 1001m | 1003m | | | | |
| | 990vw | 995m | 990vw | 996m | | 998m | |
| | 987sh | | 986m | | 986m | | skeletal str. |
| 984m,p | 983m | 981w | | 984w | 983sh | 981w | |
| 940vw,p | 939vs | | 937vs | | 939s | | and |
| | 932vs | 933vs | | 933vs | | 933vs | |
| | | 930sh | 930sh | 931sh | | 932sh | $CH_2$ bend |
| | 917vw | | | | | | |
| 913m,p | 913vw | | 912vw | | 914vw | | |
| | | 907sh | | 907sh | | 908w | $CH_2$ bend |
| | | 905w | | | | | |
| | 895w | | | | 890w | | |
| | 890w | | 888w | 885m | 888vw | | skeletal |
| 886vw | 885vw | 882m | | 882m | | 882m | |
| | 831vw | | 830vw | | | | str. |
| | | 824s | | 823s | | 824s | |
| | | 821sh | | 822sh | | 822sh | and |
| | | 805w | | 806w | | 803w | |
| 793vw | | | 793 | | | | bend |
| | | 787w | | 786w | | 787w | |
| 770vw | 771vw | 766w | 772vw | 766vw | 771vw | 766w | and |
| 584vw | | | 586vw | | 586vw | | |
| | 572vw | | | | | | $CH_2$ bend |
| 556vw | | 551s | 557 | 551s | 557 | 550s | |
| | 433vw | | | | | | |
| | | | 420sh | | | | |
| 411vw,p | 413w | | 415w | | 413w | | |
| | 353vw | | | | | | COC |
| | | | 346vw | | | | def. |
| | 105vw | | | | | | |
| | 103vw | | | | | | |
| | 93vw | | | | | | |
| | 89vw | | | | | | lattice |
| | 77vw | | 80vw | | | | |
| | 75vw | | | | | | modes |
| | | | 69vw | | | | |
| | 31vw | | 32vw | | | | |
| | | | 29vw | | | | |

conclusion is obtained from the CH stretching region (3050-2850 $cm^{-1}$) where only five broad peaks are present in the plastic phase, 15 relatively sharp peaks in the semi-ordered phase, and 21 sharp bands in the ordered phase (Figure 3.21). The 888 $cm^{-1}$ peak is intriguing in that it goes from a broad singlet in phase III to a sharp singlet in phase II to a triplet (885, 890, and 895 $cm^{-1}$) in phase I. Another peak of interest is the 933 $cm^{-1}$ which is a broad singlet in phase III, sharp singlet at 937 $cm^{-1}$ in phase II, and a sharp intense, doublet at 932 and 939 $cm^{-1}$ in phase I. The peaks centered at 1212 $cm^{-1}$ in phase III collapse into one broad peak at 1219 $cm^{-1}$ with shoulders in phase II and finally a very sharp peak at 1216 $cm^{-1}$ in phase I. Interestingly, the 1328 $cm^{-1}$ varies from a broad singlet with many shoulders in phase III to a very sharp and intense singlet in phase II to a quadruplet of weak intensity in phase I.

The FT-IR data (Figure 3.22) for oxanorbornane are not as informative as those obtained in Raman study. The ν(CH) region does undergo the same changes as was observed in the Raman spectra, most notably that the peak count goes from six very broad bands in phase III to 11 peaks and shoulders in phase I. The remaining peaks are split into two components except for the 1262 $cm^{-1}$ which splits into four peaks on going from phase II to phase I.

The previous DSC investigation had shown that cycling oxanorbornane at 20 K $min^{-1}$ yielded what appeared to be a new low-temperature phase labelled phase I'. It had also been shown that when the scan was done at 2.5 K $min^{-1}$ the new peak disappeared. Although oxanorbornane was cycled in the cryostat, through the phase transformation, the Raman spectrum at low-temperature after cycling did not differ from the spectrum prior to cycling. This could indicate that, as had been proposed in the previous chapter, the new peak detected by DSC was merely due to a different nucleation site rather than a different phase. Alternatively, the cycling and scanning in the Raman work were performed at a

much slower rates than those available for DSC. It was not possible to cycle in the IR region due to the type of cryostat used (see Section 3.III.ii).

### *viii. o-Carborane ($o$-$C_2B_{10}H_{12}$)*

The $o$-$C_2B_{10}H_{12}$ molecule has $C_{2v}$ point group symmetry and the 66 normal modes of vibration span the $21a_1 + 13a_2 + 16b_1 + 16b_2$ representations. All 66 modes are Raman active. Since the $a_2$ modes are IR-inactive, only 53 bands should be observed in the IR spectrum. In our spectra, a total of 43 bands were detected at 295 K: 30 IR and 30 Raman bands (Table 3.XI). The missing bands may either be too weak to be observed or buried beneath stronger peaks. The proposed vibrational assignments for the observed bands are presented in Table 3.XI. The assignments are based in part on the force field calculations for $o$- and $m$-carboranes reported by Klimova *et al.*[33]

The following scheme will be used to help in the discussion of the FT-IR and Raman spectra:

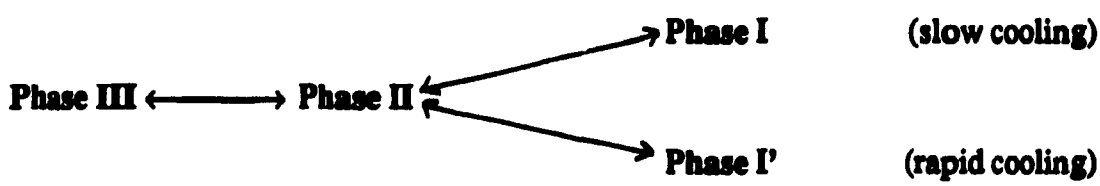


The behavior of the variable-temperature IR spectra was quite peculiar (Figure 3.23). When the sample was cooled rapidly (about 10 K $min^{-1}$) from either room temperature or 260 K (i.e., from phase III or phase II, respectively) to 39 K, a new phase I resulted, which exhibited more splittings than phase II (hence ruling out the possibility of a 'glassy' phase being formed). This new phase also displayed a very pronounced shoulder in the ν(CH) region, at 3061 $cm^{-1}$. When the sample was allowed to stand at 100 K for three days, the vibrational peaks became only slightly sharper. If the sample was cooled

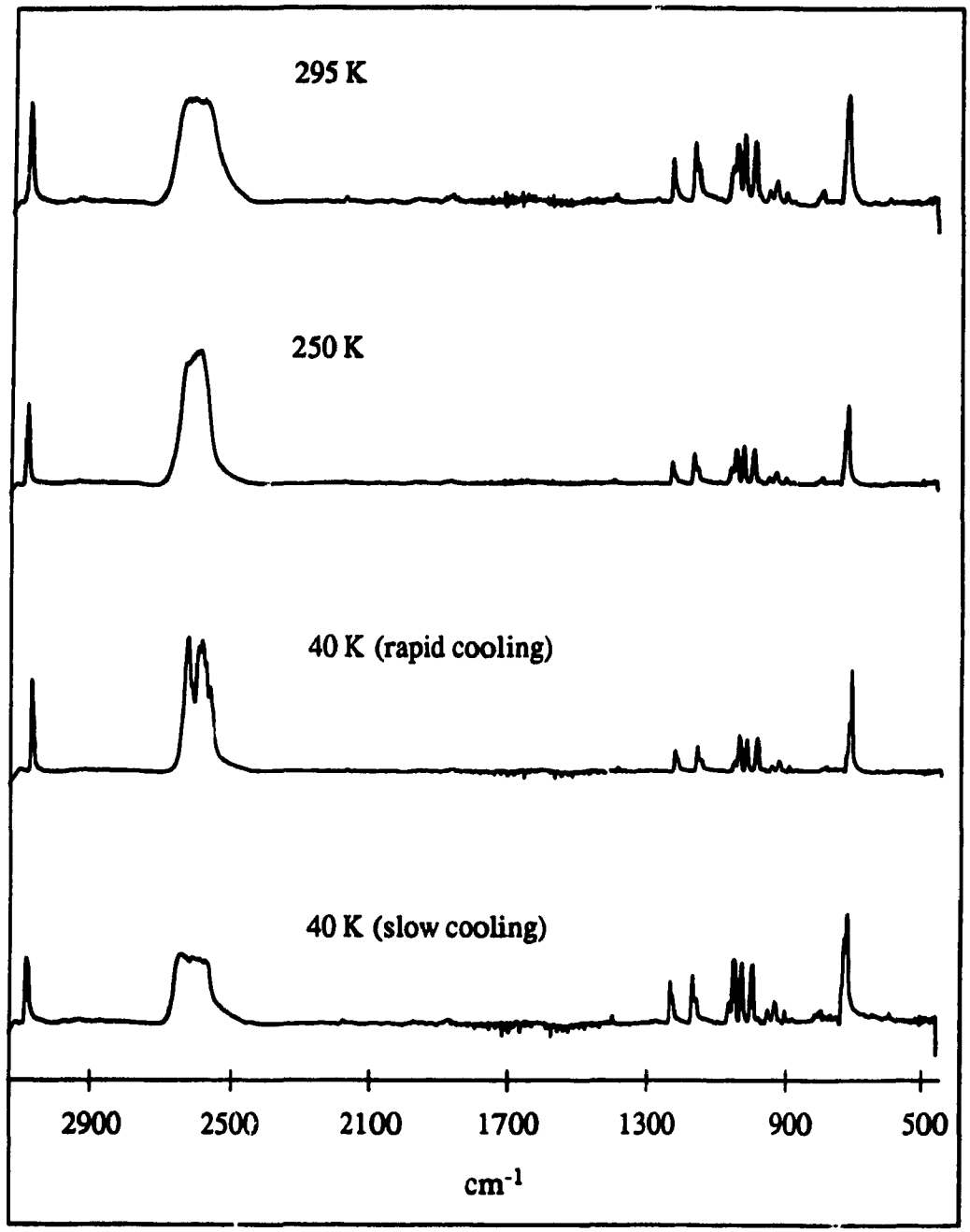


Figure 3.23 IR spectra of *o*-carborane: phase I (40 K, slow cooling), phase I' (40 K, rapid cooling), phase II (250 K) and phase III (295 K).

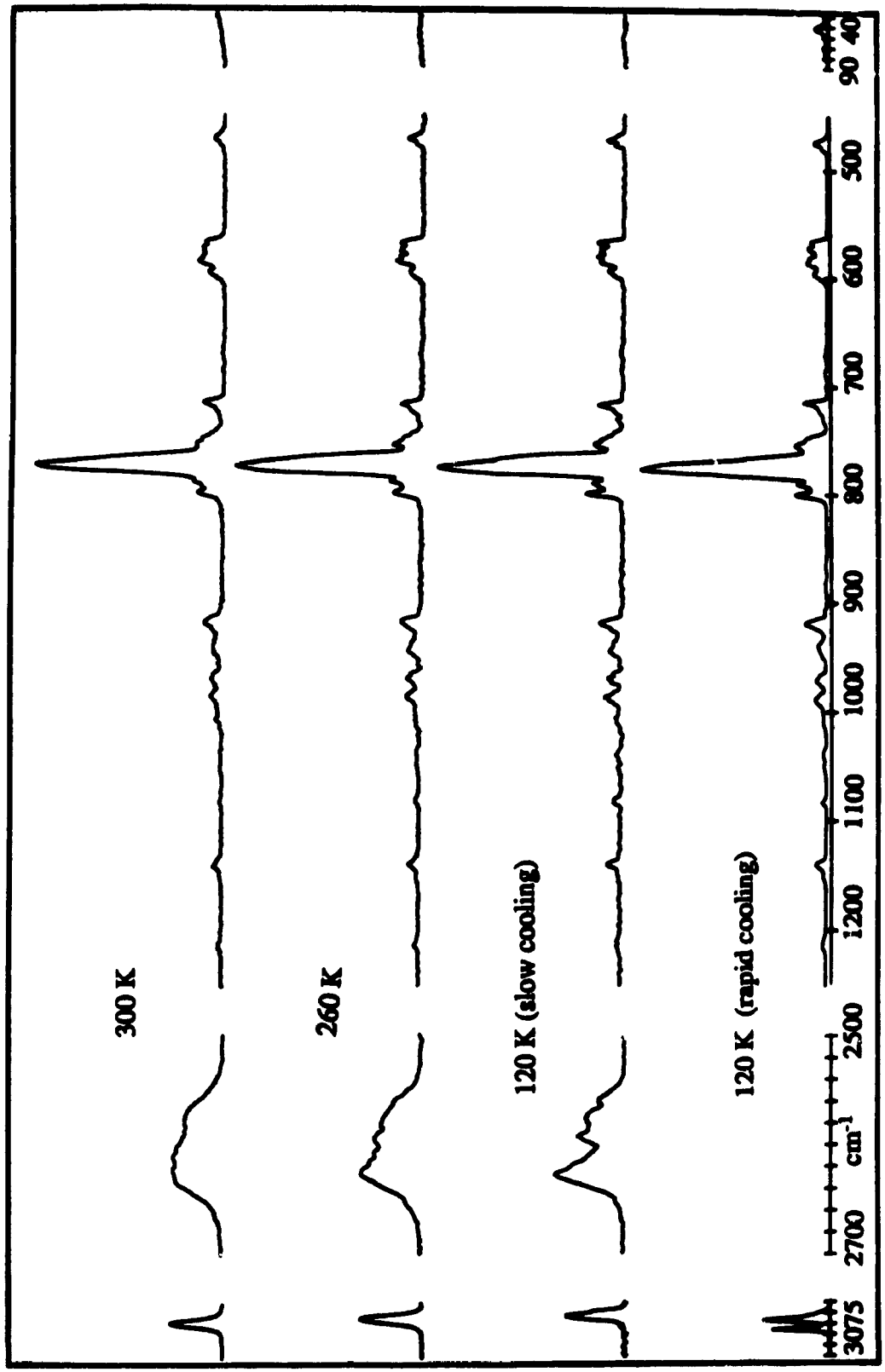


**Figure 3.24** Raman spectra of *o*-carborane: phase I '(120 K, rapid cooling), phase I (120 K, slow cooling), phase II (260 K), and phase III (300 K).

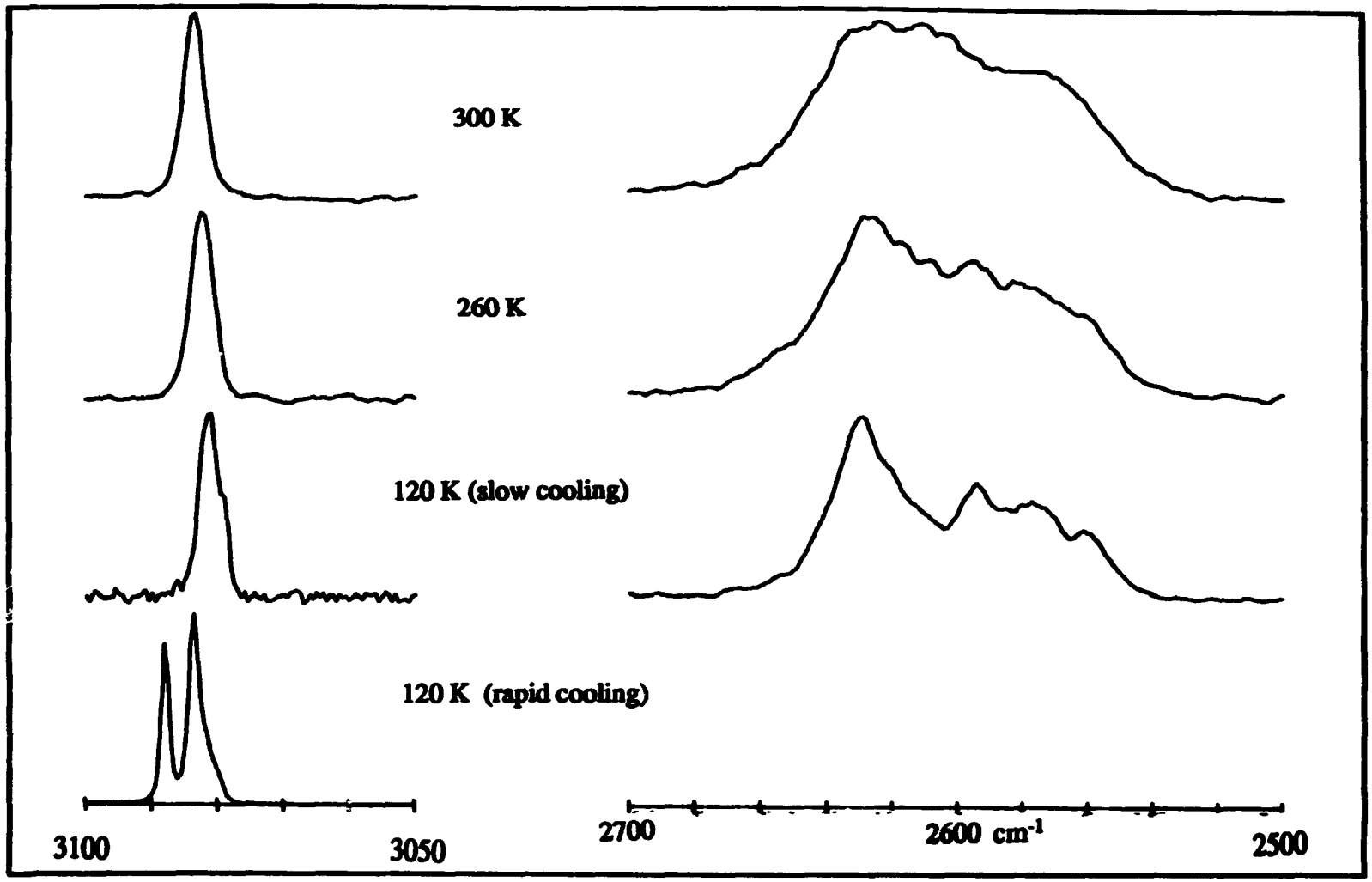


Figure 3.25 Raman spectra of the CH and BH regions of *o*-carborane: phase I '(120 K, rapid cooling), phase I (120 K, slow cooling), phase II (260 K), and phase III (300 K).

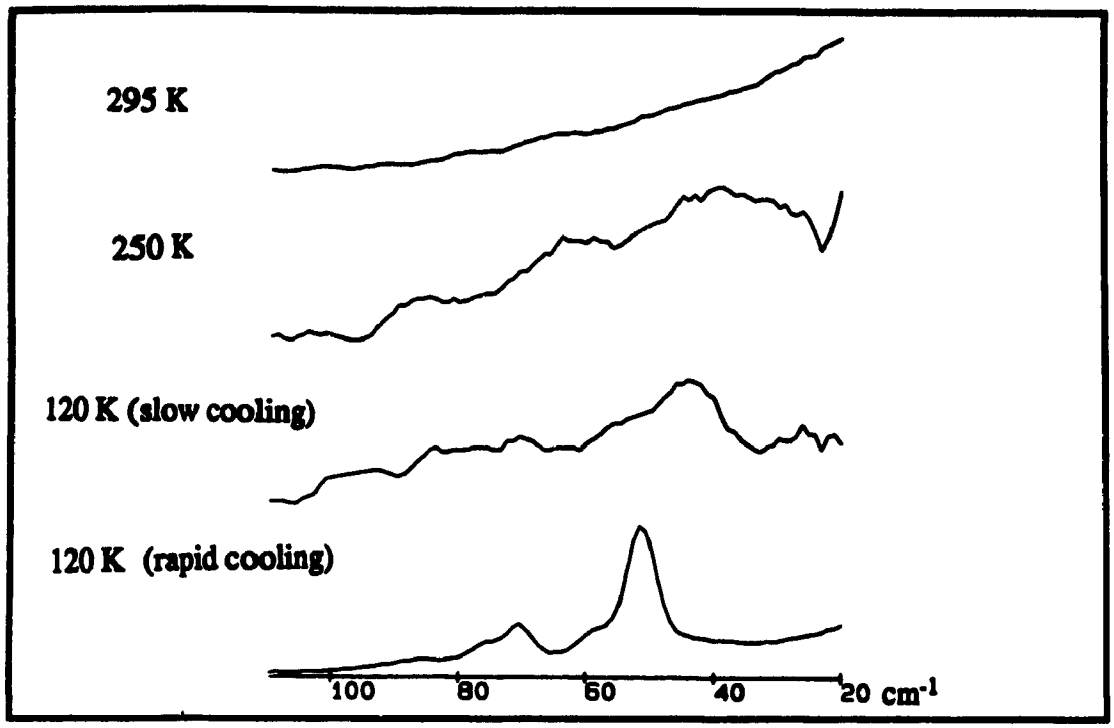


Figure 3.26 Raman spectra of the lattice region of *o*-carborane: phase I' (120 K, rapid cooling), phase I (120 K, slow cooling), phase II (250 K) and phase III (295 K).

slowly from room temperature (or from 260 K) to 39 K, however, fewer splittings were observed in the BH stretching region (2700-2500 $cm^{-1}$), and the shoulder at 3061 $cm^{-1}$ became a well-defined peak at 3062 $cm^{-1}$. No spectral changes were observed for this new phase I', even when the sample was maintained at 100 K for three days. It appears that upon slow cooling, the nucleation sites of the sample may have more time to equilibrate and only one crystal type is obtained. Upon rapid cooling, the nucleation sites do not reach equilibrium and, therefore, the formation of a metastable phase is more probable.

Some variable-temperature Raman data, using different experimental conditions, have been reported.[34-36] In the present work, the sample was cooled to 120 K and allowed to remain at that temperature. After 40 h, a new peak began to appear in the ν(CH) region at 3077 $cm^{-1}$ which, after nine days, ceased to grow in intensity. The lattice region

Table 3.XI Vibrational data ($cm^{-1}$) for *o*-carborane

| Phase I[a] (39 K) | | Phase II (260 K) | | Phase III (290 K) | | |
|---|---|---|---|---|---|---|
| Raman | IR | Raman | IR | Raman[b] | IR | Assignments[c] |
| 3073s | | | | | | |
| 3064s | 3064s | 3063s | 3064s | 3067s | 3070s | ν(CH) |
| | 3061s | | | | | |
| | | 2668sh | | 2668sh | | |
| | | 2630s | | 2632s | | |
| | 2623vs | 2623s | | 2621s | | |
| | 2612s,sh | | | | | |
| | | | | 2609s | | ν(BH) |
| | | | 2604vs,br | 2603s | 2604vs,br | |
| | 2593vs | 2594s | | | | |
| | | 2585s,sh | | | 2583vs | |
| | | 2578s | 2577vs,br | 2576s | | |
| | 2571vs | | | | 2573vs,br | |
| | 2559s | 2559s | | | | |
| | 1275vw | | 1270vw,br | | 1266vw,br | |
| | 1214w | | 1214w | | 1214w | |
| 1211w | | 1213w | 1213sh | 1212w | | |
| | 1209sh | | | | | δ(HCB) |
| 1200sh | | 1203sh | | | | |
| 1147vw | 1149w | 1148sh | 1149w | 1150sh | 1149w | $b_1$ (1150) |
| | 1140vw | | 1139vw | | 1140vw | |
| 1136m | 1138sh | 1138w | | 1138m | | |
| 1079w | 1082vw,br | 1080w | 1080vw,br | 1079w | 1080vw,br | |
| | 1051sh | | 1051sh | | | |
| 1046w | 1049vw | 1048w | 1047w | 1047w | 1047w | $a_1$ (1050) |
| | | | 1045sh | | 1045sh | |
| 1036w | 1037w | 1037w | 1036w | 1035w | 1035w | $b_1$ (1040) |
| 1032sh | 1034w | 1033sh | | | | |
| | 1015w | | 1015w | | | $b_2$ (1020) |
| 1003w | | 1004w | | 1002w | | |
| 996w | | 997w | | | | |
| 983m | 986w | 985m | 985w | 983m | 985w | $b_1$ (990) |
| | 972vw | | | | | |
| 967m | 968vw | 967m | 968sh | 966m | 968sh | δ(HBB) |
| 963sh | 964vw | 964sh | | | | |
| | 955vw | 953vw | | | | |
| | 949vw | | 949vw | | 949vw | |
| | 945sh | | | | | |
| 940m | 942w | 942m | 942w | 940m | 942w | |
| 937sh | | 937sh | | | | |
| | 921w | | 921sh | | 921sh | |
| 917s | 917sh | 917s | 917w | 916s | 917w | |
| 903vw | 906vw | 904vw | 906sh | | 906sh | |

Table 3.XI Vibrational data ($cm^{-1}$) for *o*-carborane

| Phase I[a] (39 K) | | Phase II (260 K) | | Phase III (290 K) | | |
|---|---|---|---|---|---|---|
| Raman | IR | Raman | IR | Raman[b] | IR | Assignments[c] |
| | 888w | | 887w | | 886w | |
| 876vw | 880vw | 878vw | 880sh | 877vw | 880sh | |
| 863vw | 865w | 864vw | 863w | 862vw | 863w | ν (BB), |
| 796s | 797vw | 797s | 797w | 795s | 797w | δ (CBB), |
| | 789sh | | 789sh | | 789sh | δ (BB) |
| 786s | 787w | 787s | 786w | | 786w | |
| | 777vw | | | | | |
| 772vs | 773sh | 773vs | | 770vs | 768vw | $a_1$ |
| 761s | 762vw | 763sh | 760vw | | | |
| 751s | 752vw | 752s | 750sh | 750s | 752br,vw | |
| 746sh | 746vw | | 744vw | | | |
| 728sh | 730sh | 730sh | | | | skeletal |
| | 724w | | 720sh | | 718sh | |
| 713s | 716s | 715s | 715m | 713s | 714sh | vibrations |
| | 638vw | | 638vw | | 638br,vw | |
| 594m | | 594m | | 590m | | $a_2$ (·) |
| 583s | 585vw | 583s | 585vw | 581s | 585vw | |
| 580s | | 580s | | | | |
| 570s | | 574s | | 570s | | |
| 560s | | 566s | | 562s | | |
| 476w | | 476w | | 480sh | | $a_2$ (·) |
| 472m | | 472m | | 470m | | |
| 70m | | | | | | |
| 50m | | | | | | |
| | | 38m | | | | |

a A fourth phase was found in the IR and Raman spectra which differs from phase I by the presence of a peak rather than a shoulder at 3062 $cm^{-1}$.

b No Raman spectral data were obtained in the ν(BH) region.

c Values shown in parentheses are those from the force field calculations in ref. 33.

(Figures 3.25 and 3.26), which in phase III, was featureless, and showed only a single peak in phase II at 38 $cm^{-1}$, now contained many distinct peaks which is indicative of a more ordered crystal. Upon slow cooling, however, ν(CH) does not undergo splitting, instead, as was seen in the IR spectra, a shoulder appears. This had been previously observed by Bukalov and Leites[35,36]. Clearly, kinetic effects are important since the new peak at 3077 cm-1 took longer to appear at 120 K (40 h) than at 168 K (15 h). We shall see that published results[37-40] will provide some clues as to why such an effect was observed.

All the NMR results in the literature dealing with the molecular dynamics of *o*-$C_2B_{10}H_{12}$ indicate that the motion is isotropic in phase III, but anisotropic in the low-temperature phases. The exact temperature for the transition from phase II to phase III and the nature of the motions in these phases has not been established. The reported NMR phase-transition temperatures vary from 165 K to 200 K, compared with 158 K from adiabatic calorimetry. The proton line width varies smoothly with changes in temperature from 120 to 250 K. This is a wide temperature range for a motional transition and might well be a factor accounting for the difficulties in interpreting the spin-lattice relaxation-time data.

The activation energy ($E_a$) determined for the isotropic phase III is about 12 kJ $mol^{-1}$, while that for the anisotropic phases lies in the 23-40 kJ $mol^{-1}$ range. Reynhardt and co-workers[40] suggested that the 23 kJ $mol^{-1}$ barrier might be due to rotation about a two-fold axis, a reasonable suggestion for the $C_{2v}$-symmetry reduction of the icosahedral cage. On the basis of this barrier, the correlation time for molecular reorientation, $\tau_c$, would vary from 5.9 ms at 165 K to 3 s at 120 K. The $E_a$ values reported by Beckmann and Leffler,[39] 27 kJ $mol^{-1}$ and 40 kJ $mol^{-1}$, were attributed to a temperature-dependent activation energy, since the high and low side of the $T_1$ plot produced different values. The 40 kJ $mol^{-1}$ value leads to a $\tau_c$ of 1.3 s at 165 K and ca. 20 h at 120 K. A

higher barrier would lead to an even longer $\tau_c$ value, as is suggested by our vibrational measurements.

Rapid quenching of the sample to low temperatures can freeze-in disorder. The potential function governing whole molecule rotation will depend on the orientation of neighboring molecules and, therefore, a distribution of barriers will exist. This would explain the observed temperature dependence of the barriers.

**Table 3.XII** Correlation diagram for 1-substituted adamantanes.

| Adamantane ($T_d$) | Adamantane ($C_{3v}$) | 1-$C_{10}H_{15}X$ ($C_{3v}$) |
|---|---|---|
| $5a_1$ (Raman) | $5a_1$ | $5a_1$ (IR*,Raman) |
| $a_2$ (-) | $a_2$ | $a_2$ (-) |
| 6e (Raman) | 6e | 6e (IR*,Raman) |
| $7t_1$ (-) | $7a_2$ | $7a_2$ (-) |
| | 7e | 7e (IR*,Raman*) |
| $11t_2$ (IR,Raman) | $11a_1$ | $11a_1$ (IR,Raman) |
| | 11e | 11e (IR,Raman) |

## II. Discussion

### *i. Adamantane derivatives*

Adamantane has been studied by vibrational spectroscopy and force field calculations. With the aid of these data and published data on adamantane derivatives, it has been possible to assign the vibrational modes shown in Tables 3.II, and 3.V-3.VIII. Lowering the symmetry of adamantane by replacing a hydrogen atom with a halogen, or by removal of a methylene group and introducing a carbonyl group, results in all of the e and t modes of adamantane being split to non-degenerate levels. Thus, 40, 69, and 72 IR/Raman peaks are expected for $C_{3v}$, $C_{2v}$, and $C_s$ symmetry, respectively, as opposed to merely 22 bands for adamantane ($T_d$-symmetry). As evidenced by the data presented in Tables 3.II and 3.V to 3.VIII, some peaks which were originally inactive or merely Raman active, become IR and/or Raman active, upon reduction of symmetry. These are denoted by an asterisk in Tables 3.XII to 3.XIV.

One of the most interesting regions in the substituted adamantanes is certainly the CH stretching region (3000-2800 $cm^{-1}$). It appears to be an excellent phase transformation indicator. In general, the Raman spectra of the plastic phases contain approximately four peaks, and as the sample is cooled towards its ordered phase, many more peaks appear. This is not simply a low-temperature effect where many sharp and well-defined bands would be expected Consider the adamantane derivatives which have more than one phase transition, more specifically, 1-bromoadamantane, 2-adamantanone and 2-chloroadamantane. In each of these cases, the first transition yields more ν(CH) peaks but not as many as when phase I is attained. This is regardless of the temperature at which the transition takes place. This is clearly seen with 2-adamantanone which, prior to cycling, exhibits six relatively broad peaks in the CH region. After cycling, however, the

**Table 3.XIII** Correlation diagram for adamantanone.

| Adamantane ($T_d$) | Adamantane ($C_{2v}$) | 2-$C_{10}H_{14}O$ ($C_{2v}$) |
|---|---|---|
| $5a_1$ (Raman) | $5a_1$ | $5a_1$ (IR*,Raman) |
| $a_2$ (-) | $a_2$ | $a_2$ (Raman*) |
| 6e (Raman) | $6a_1$ | $6a_1$ (IR*,Raman) |
| | $6a_2$ | $6a_2$ (Raman) |
| $7t_1$ (-) | $7a_2$ | $6a_2$ (R*) |
| | $7b_1$ | $7b_1$ (IR*,Raman*) |
| | $7b_2$ | $7b_2$ (IR*,Raman*) |
| $11t_2$ (IR,Raman) | $11a_1$ | $10a_1$ (IR,Raman) |
| | $11b_1$ | $11b_1$ (IR,Raman) |
| | $11b_2$ | $10b_2$ (IR,Raman) |

same region contains seven sharp and well-defined peaks. Bear in mind that both the phase I and the phase I' spectra are taken at the same temperature, thereby ruling out temperature effects. Since the DSC results for adamantanone showed that after cycling a new phase appeared, it is safe to say that the new peaks appearing in the CH stretching region are due a new phase. It can therefore be concluded that this region is a good indicator of an order-disorder transition. A possible explanation for this observation is that the C-H groups are protruding in all of the molecules studied, in other words they are like flagpoles. In such a case, they would be expected to be more sensitive to a change in

**Table 3.XIV** Correlation diagram for 2-substituted adamantanes having $C_s$ symmetry.

| Adamantane ($T_d$) | Adamantane ($C_s$) | 2-$C_{10}H_{15}X$ ($C_s$) |
|---|---|---|
| $5a_1$ (Raman) | 5a' | 5a' (IR*,Raman) |
| $a_2$ (-) | 5a'' | a' (IR*,Raman*) |
| 6e (Raman) | 6a' | 6a' (IR*,Raman) |
| | 6a'' | 6a'' (IR*,Raman) |
| $7t_1$ (-) | 7a' | 7a' (IR*,Raman*) |
| | 14a'' | 7a'' (IR*,Raman*) |
| $11t_2$ (IR,Raman) | 22a' | 22a' (IR,Raman) |
| | 7a'' | 7a'' (IR,Raman) |

environment or, in orientationally-disordered solids, highly sensitive to orientational changes.[41-43] The CH stretching region is not, however, the most ideal as far as interpretation is concerned since it is known to be highly degenerate.[31]

Another region which should be equally sensitive to orientational changes of the molecules is the C-X stretching region (X = Br, Cl, and O). Interestingly, the C=O stretching vibration does undergo modification as the sample is cooled from phase II to phase I. It had previously been shown that Fermi resonance was involved in this region, but this region still indicates that a phase transition occurs which, based on the same

argument as for ν(CH), most likely originates from an orientational change. After cycling, this region did not change very much thus implying that the phase I → phase I' transformation does not undergo a change in orientation. The carbon-halogen stretching mode is peculiar in that it does not appear to be sensitive to phase transitions. The bending modes, however, were susceptible to splitting as the sample went through a phase transition. As had been seen previously, lowering the temperature did not necessarily imply that more peaks would appear as the splitting took place only at the phase transformation.

### *ii. Others*

Similar effects to those described for the substituted adamantanes were observed for the other compounds studied in this thesis. As mentioned in the previous section, the ν(C-H) region is a good indicator of phase transformations. Consider the FT-IR and Raman spectra of *o*-carborane. Originally, only a single peak is observed in the ν(CH) region, however, after a certain time, a splitting occurs. The lattice region, also underwent changes and since it contained better defined peaks than originally, the splitting must be due to a phase change. As would be expected, the ν(B-H) modes also exhibited changes. In the case of bicyclononanone, splitting occurred in the C=O stretching region as well. It is therefore self-evident that flag-pole type moieties are very sensitive to phase transformations.

The lattice regions of *o*-$C_2B_{10}H_{12}$, 9-$C_9H_{14}O$, and $C_6H_{10}O$ always underwent changes as an order-to-disorder phase change occurred. The most conspicuous change took place in oxanorbornane for which both the liquid and plastic phase display no external modes. Upon cooling, peaks begin to appear but only in the most ordered phase (phase I) are they well-defined. As stated above, *o*-carborane also had changes occur to its lattice

modes but only after ~40 hours at 120 K, thus eliminating the possibility that this change is solely a temperature effect. Based on the data presented it is obvious that these external modes are excellent phase transformation indicators.

## D. CONCLUSION

It has been shown that variable-temperature IR and Raman are excellent complements to DSC in that they do give more information about the phase being probed. Also, due to the fact that commercial refrigeration systems allow the user to go to lower temperatures than that available from commercial DSC instruments, variable-temperature spectroscopy is sometimes the only possible method available to investigate possible phase transitions. It was also possible to detect another phase transformation in *o*-carborane which had gone undetected by DSC.

It can also be unquestionably stated that some vibrational modes such as the C-H, B-H, and C=O, as well as the external modes are very susceptible to orientational changes.

## E. REFERENCES


(1) R. J. Obremski, *Introduction to Raman Spectroscopy*, Beckman Instruments Inc., Fullerton, California, 1972.

(2) A. L. Smith, *Chemical Analysis, Vol. 54: Applied Infrared Spectroscopy*, John Wiley and Sons, Inc., U.S.A., 1979.

(3) R. G. J. Miller, B. C. Stace, *Laboratory Methods in Infrared Spectroscopy*, 2nd Edition, Heyden and Son, Ltd., Great Britain, 1979.

(4) J. G. Grasselli, M. K. Snavely, B. J. Bulkin, *Chemical Applications of Raman Spectroscopy*, John Wiley and Sons, U.S.A., 1981.

(5) W. G. Fateley, F. R. Dollish, N. T. McDevitt, F. F. Bentley, *Infrared and Raman Selection Rules for Molecular and Lattice Vibrations: The Correlation Method*, John Wiley and Sons, Inc., U.S.A., 1972.

(6) D. P. Strommen, K. Nakamoto, *Laboratory Raman Spectroscopy*, John Wiley and Sons, Inc., USA, 1984.

(7) D. M. Adams, "Vibrational Spectroscopy" in *Solid State Chemistry*, A. K. Chetham, P. Day, Eds., Oxford University Press, USA, 1987.

(8) W. F. Sherman, G. R. Wilkinson, "Raman and Infrared Studies of Crystals at Variable Pressure and Temperature", in *Advances in Infrared and Raman Spectroscopy*, Vol. 6, R. J. H. Clark, R. E. Hester, Eds., Heyden and Son, Ltd., Great Britain, 1980.

(9) Z. Iqbal, F. J. Owens, *Vibrational Spectroscopy of Phase Transitions*, Academic Press, Inc., USA, 1984.

(10) P. R. Griffiths, J. A. de Haseth, *Chemical Analysis, Vol. 83: Fourier Transform Infrared Spectroscopy*, John Wiley and Sons, Ltd., USA, 1986.

(11) D. L. Pavia, G. M. Lampman, G. S. Kriz, *Introduction to Spectroscopy*, W. B. Saunders Company, USA, 1979.

(12) H. A. Szymanski, *Raman Spectroscopy: Theory and Practice*, Plenum Press, New York, 1970.

(13) J. F. Scott, "Raman Studies of Structural Phase Transitions", in *Advances in Raman Spectroscopy*, Vol. 1, J. P. Mathieu, Ed., Heyden and Son, Ltd., Great Britain, 1973.

(14) T. Geisel, W. Duitz, W. Gebhardt "Raman Spectroscopy of Orientational Disorder", in *Advances in Raman Spectroscopy*, Vol. 1, J. P. Mathieu, Ed., Heyden and Son, Ltd., Great Britain, 1973.

(15) H. Baranska, A. Labudzinska, J. Terpinski, *Laser Raman Spectrometry: Analytical Applications*, John Wiley and Sons, Ltd., Poland, 1987.

(16) A. Cabana, "Vibrational Spectra and Structure of Plastic Crystals", in *Vibrational Spectra and Structure*, **4**, 39 (1975).

(17) S. B. Kim, R. M. Hammaker, W. G. Fateley, *Appl. Spectrosc.*, **40**, 412 (1986).

(18) R. M. Corn, V. L. Shannon, R. G. Snyder, H. L. Strauss, *J. Chem. Phys.*, **81**, 5231 (1984).

(19) B. A. Weinstein, *Rev. Sci. Instrum.*, **57**, 910 (1986).

(20) T. E. Jenkins, J. Lewis, *Spectrochim. Acta*, **36A**, 259 (1980).

(21) R. T. Bailey, *Spectrochim. Acta*, **27A**, 1447 (1971).

(22) E. N. Grishna, I. V. Aleksandrov, Y. M. Solobodin, R.R. Kostikov, *Zh. Prikl. Spektrosk.*, **32**, 664 (1980).

(23) S. Pal, Z. Zoltan, V. Gyorgy, *Magyar. Kem. Foly*, **75**, 432 (1969).

(24) T. J. Broxton, L. W. Deady, M. Kendall, R. D. Topsom, *Appl. Spectrosc.*, **25**, 600 (1971).

(25) R. G. Snyder, J. H. Schachtschneider, *Spectrochim. Acta*, **21**, 169 (1965).

(26) S. P. Srivastava, I. D. Singh, *Acta Phys. Acad. Hung.*, **47**, 275 (1979).

(27) P.-J. Wu, L. Hsu, D. A. Dows, *J. Chem. Phys.*, **54**, 2714 (1971).

(28) J. L. Sauvajol, M. Bee, J. P. Amoureux, *Molec. Phys.*, **46**, 811 (1982).

(29) P. D. Harvey, I. S. Butler, D. F. R. Gilson, P. T. T. Wong, *J. Phys. Chem.*, **90**, 4546 (1986).

(30) P. Zielinski, M. Foulon, "Phenomenological Description of Phase Transitions in Derivatives of Adamantane", in *Dynamics of Molecular Crystals*, J. Lascombe, Ed., Elsevier Science Publishers B. V., Amsterdam, 1987.

(31) P. D. Harvey, *Applications of Vibrational and NMR Spin-Lattice Relaxation Time Measurements to Organometallic and Organic Molecular Crystals*, PhD. Thesis, McGill University, 1985.

(32) I. S. Butler, H. B. R. Cole, D. F. R. Gilson, P. D. Harvey, J. D. McFarlane, *J. Chem. Soc., Farad. Trans.*, *2*, **82**, 535 (1986).

(33) T. P. Klimova, L. A. Gribov, and V. I. Stanko, *Opt. Spectrosc.*, **36**, 650 (1974).

(34) M. J. Hones, D. E. Shaw, F. J. Wunderlich, *Spectrosc. Lett.*, **6**, 483 (1973).

(35) S. S. Bukalov, L. A. Leites, *Chem. Phys. Lett.*, **87**, 327 (1982).

(36) S. S. Bukalov, L. A. Leites, *Proc. International Conf. Raman Spectrosc.*, **8**, 611 (1982).

(37) R. H. Baughmann, *J. Chem. Phys.*, **53**, 3781 (1970).

(38) A. J. Leffler, M. N. Alexander, P. L. Sagalyn, N. Walker, *J. Chem. Phys.*, **63**, 3971 (1975).

(39) P. Beckmann, A. J. Leffler, *J. Chem. Phys.*, **72**, 4600 (1980).

(40) E. C. Reynhardt, A. Watton, H. E. Petch, *J. Magn. Reson.*, **46**, 453 (1982).

(41) M. Debeau, Ph. Depondt, *J. Chim. Phys. (JCPBAN)*, **82**, 233 (1985).

(42) D. Cavagnat, *J. Chim. Phys. (JCPBAN)*, **82**, 239 (1985).

(43) J. L. Sauvajol, *J. Chim. Phys. (JCPBAN)*, **82**, 219 (1985).

# CHAPTER 4
# VARIABLE-PRESSURE MICRO-RAMAN STUDIES OF ORIENTATIONALLY-DISORDERED SOLIDS (PLASTIC CRYSTALS)

## A. INTRODUCTION

### I. General

In the preceding chapter, it was shown that spectral changes are encountered for orientationally-disordered solids as a function of temperature. It was also determined that these changes are due to phase changes rather than just temperature effects. One of the problems encountered with variable-temperature vibrational spectroscopy is the determination, with any degree of certainty, whether or not a spectral change observed at low or high temperature is in fact due to a phase transition or merely a temperature effect. There are times when the transformations are very subtle and it is therefore difficult to conclude that a phase change was indeed encountered. It is well known that variable-temperature measurements affect the thermal population and hence the vibrational energy levels more than the distance parameters, and, therefore, a good complementary technique would be one where the distance parameters predominate. Such a method is variable-pressure vibrational spectroscopy, where changes in volume occur isothermally and are

more easily observed because anharmonic effects are improbable and therefore will not obscure the decrease in volume.

Variable-pressure spectroscopic methods employing a diamond-anvil cell (DAC) have been in use for approximately 30 years. The DAC was developed at the National Bureau of Standards in the United States and was originally intended for IR spectroscopy up to 50 kbar or ~50 000 atm (1 bar = $10^5$ N $m^{-2}$ = 0.9869 atm).[1] Due to its small size and, more importantly, the interest in studying materials as a function of pressure, the DAC was adapted to other techniques such as x-ray and Raman spectroscopy. The usefulness of the DAC is immediately apparent from the number of publications appearing in the literature (697 from January 1967 to September 1988) in fields ranging from the physical to the health sciences and even in forensic science.

The diamond-anvil cell consists of two transparent diamond anvils mounted in opposition to one another. The size of the diamonds themselves vary from 1.2 mm (when studying pressures up to ~70 kbar) to ~0.3 mm (for pressures exceeding 400 kbar). There are four different types of diamonds available; types Ia and Ib contain nitrogen impurities, type IIa is pure diamond, and type IIb has boron impurities.[2] The determining factor as to which type should be used is dependent on the spectroscopic method employed and the cost. The cheapest diamonds are type Ia since they are the most abundant in nature; however, they are only practical for Raman spectroscopy, as Wong and Klug[2] have demonstrated that there is less fluorescence with type Ia diamonds than with type II diamonds when the 514.5 nm line of the argon-ion laser is used, and they absorb strongly in the mid-IR region (2700-300 $cm^{-1}$).[2] Type II diamonds are considered to be a compromise for those who want to perform pressure IR and Raman spectroscopy with the same cell. It is considered a compromise because type II diamonds are highly fluorescent when either the 488.0 nm or the 514.5 nm line of the argon-ion laser is used to execute the Raman spectrum. Adams *et al.*[3] have found that using the 632.8 nm (red) line of a He-Ne laser

allowed the DAC equipped with type II diamonds to be used from 0 $cm^{-1}$ up to, but not limited to, 4000 $cm^{-1}$. More recently, Hirsch and Holzapfel have established that the diamond overtone at 2500 $cm^{-1}$ can be used as a standard for the selection of diamonds for Raman spectroscopy.[4] They found that for diamonds to be useable for Raman spectroscopy, be they type I or type II, the intensity of the 2500 $cm^{-1}$ band should be three times greater than the background. There does not appear to be any criterion, however, for high pressure x-ray spectroscopy.[5] For a detailed review, comparison, and description of different types of diamond anvil cells, see references 2-18.

Although the DAC has been around since 1959, it was not until 1964 that this device could be used as a quantitative technique. This came about when Van Valkenburg started using a gasket between the two diamond anvils.[19] The purpose of the gasket is actually threefold; (1) to contain the sample, (2) to prevent the diamonds from coming into contact with each other thereby prolonging their working life, and (3) to help maintain hydrostatic pressure. The last purpose is debatable, however, and many workers still use a hydrostatic medium. The most popular media are a 4:1 methanol-ethanol mixture or a 16:3:1 water-methanol-ethanol mixture when pressures of less than 200 kbar are being employed.[20,21]

Pressure measurements are useless unless the pressure values are known with a high degree of certainty. Various methods exist that permit the calibration of pressure. Essentially, these can be broken down into two categories; (1) primary gauges and (2) secondary gauges. The primary scales comprise any device that measures pressure on the basis of fundamental equations, such as,

$$P = F/a \qquad [4.1]$$

where P is the pressure, F is the force, and a is the area. The mercury manometer is based on equation 4.1 and is therefore a primary scale. However, such scales are not always

practical and therefore some other scale, which has been calibrated against a primary gauge, is used. These are known as secondary scales and encompass well-known devices such as strain-gauges and electrical resistance devices. The criteria for a pressure calibrant include: reproducibility, temperature-independence, chemical inertness, lack of hysteresis, and well-characterized.[22] Prior to 1972, the calibration of the DAC was done using freezing-points of liquids and well-known solid-solid transitions. In 1972, however, Forman *et al.*[23] introduced a calibration technique (for measurements at that time up to 22 kbar) based on the fluorescence of ruby powder (0.5% $Cr^{3+}$-doped $Al_2O_3$). Theoretically, isolated $Cr^{3+}$ should show only one peak (due to the spin-forbidden transitions between the $^2E$ and $^4A_2$ states); however, since $Cr^{3+}$ can occupy one of the $Al^{3+}$ sites, spin-orbit coupling takes place, thereby removing the degeneracy of the $^2E$ level and generating two states (E and 2A). Consequently, two ruby fluorescence lines are observed at 694.2 nm or 14405 $cm^{-1}$ ($R_1$-line) and 692.7 nm or 14436 $cm^{-1}$ ($R_2$-line) at 0 kbar[23,24]. There are two important advantages to using the ruby gauge: (1) only a small chip is necessary and (2) it is chemically inert and, even from a spectroscopic point of view, it does not interfere with the majority of the internal or external modes. The pressure dependence of the ruby $R_1$ line was found to be -0.77 $cm^{-1}$ $kbar^{-1}$ while that of the $R_2$ line was observed to be -0.84 $cm^{-1}$ $kbar^{-1}$.[23] Presently, below 300 kbar, the accepted value of the $R_1$ line is now 0.753 $cm^{-1}$ kbar. The relation can be written as:

$$P = -1.328\Delta v \qquad [4.2a]$$

or

$$P = 2.740\Delta\lambda \qquad [4.2b]$$

where P is in kbar and $\Delta v$, $\Delta\lambda$ are the wavenumber and wavelength differences in peak position in $cm^{-1}$ and Å, respectively, measured at pressure P and ambient pressure. Above 300 kbar, and up to 1000 kbar, the accepted relation becomes:[29]

$$P = 3808[(\lambda/\lambda_0)^5 - 1] \qquad [4.2c]$$

where both $\lambda$ and $\lambda_0$ are in nm and are measured at pressure P and 0 kbar, respectively.

Unfortunately, the $R_1$ and $R_2$ lines of ruby are also temperature-dependent, -0.134 $cm^{-1}$ $K^{-1}$, and therefore care must be taken that the experimental temperature be known and since this dependence corresponds to 0.17 kbar $K^{-1}$, local heating must be avoided.[23,24] Another disadvantage is that the two ruby bands coalesce as the pressure is increased. Needless to say, as the years went by, the calibration has been improved and it

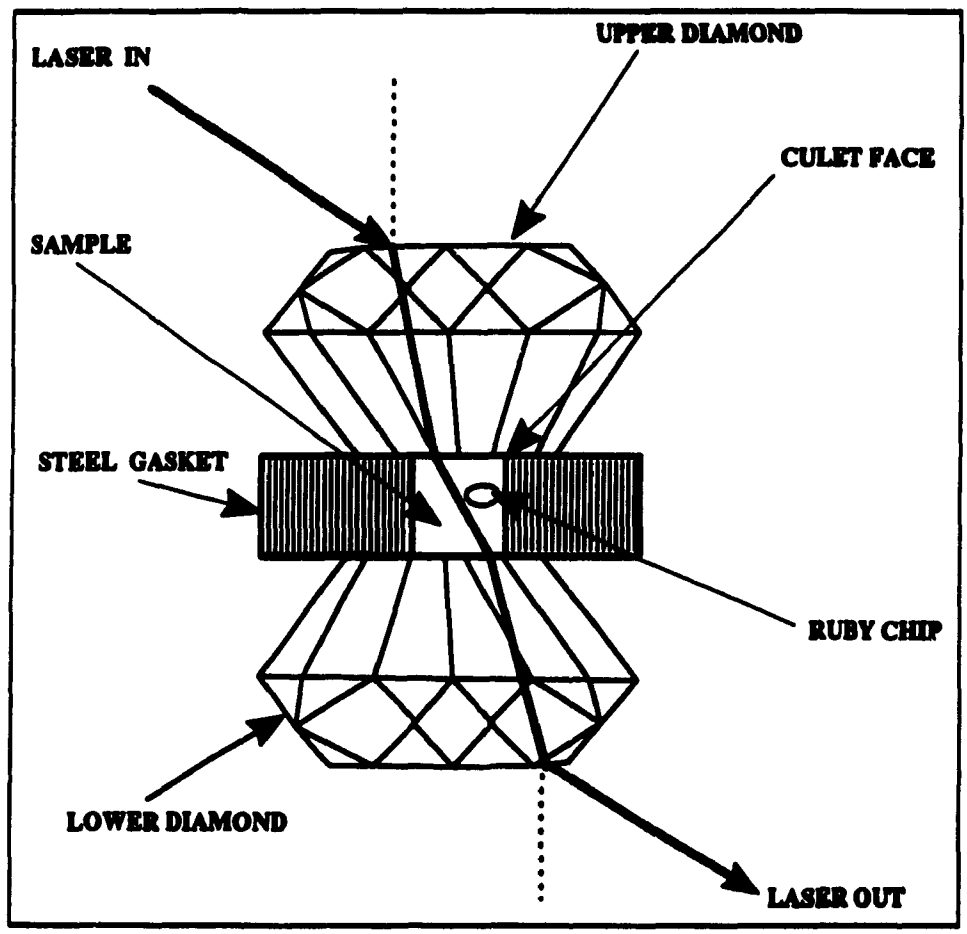


Figure 4.1 Schematic diagram of diamond set-up for scattering experiment.

has now been used up to 1000 kbar and at variable-temperature.[25-33] The ruby scale is very useful for Raman spectroscopy, but not very convenient for infrared spectroscopy since fluorescence measurements cannot be made on an FT-IR spectrometer without special equipment. It is for this reason that research has been done using other types of calibrants. For example, Klug and Whalley have suggested using nitrite and nitrate ions in the form of sodium salts, which have characteristic IR absorptions at 1279.0 and 1401.3 $cm^{-1}$ at zero-pressure, respectively.[34] For example, the pressure value can be obtained by monitoring the nitrite band at 1279.0 $cm^{-1}$ using eq. [4.2]:

$$P = 2.356\Delta\nu - 1.334\Delta\nu * \exp(-\Delta\nu/92) \qquad [4.2]$$

where P is the pressure in kbar, and $\Delta\nu$ is the difference between frequency values at pressure P and at atmospheric pressure, and is given in $cm^{-1}$. If the nitrate ion is used as the calibrant (1401.3 $cm^{-1}$), then the pressure is calculated from eq. [4.3]:

$$P = 1.775\Delta\nu - 0.7495\Delta\nu * \exp(-\Delta\nu/78) \qquad [4.3]$$

where the symbols are defined as in eq. [4.2]. Wong *et al.*[35] have found that nitrite and nitrate ions are not always convenient to use and proposed using the band at 801 $cm^{-1}$ of crystalline quartz as an internal calibrant. The relation used to determine the pressure (kbar) in this case is:

$$P = 0.0158\Delta\nu^2 + 1.168\Delta\nu - 0.1660 \qquad [4.4a]$$

More recently, Wong[13] has proposed using the 695.2 and 795.5 $cm^{-1}$ bands of $\alpha$-quartz; the associated pressure dependences are:

$$P = 0.1516\Delta\nu^2 + 1.2062\Delta\nu \qquad (695.2\ cm^{-1}) \qquad [4.4b]$$

$$P = 0.0138\Delta\nu^2 + 1.0752\Delta\nu \qquad (795.5\ cm^{-1}) \qquad [4.4c]$$

Over the last three years, attempts have been made to use the 1332.5 $cm^{-1}$ of diamond itself as the pressure calibrant for Raman experiments.[36-38] There are, however, problems that arise, and the diamond pressure scale will probably not be used, especially if FT-Raman spectroscopy is employed.

The micro-Raman (also known as MOLE or Raman microprobe) technique presents many advantages in studying phase transitions using a DAC.[36-43] The major advantage is its ability to focus on a particular position with a minimum amount of power. The collection efficiency is very high so that only small amounts of sample are required for analysis. The alignment of the DAC is facilitated by placing the DAC on an X-Y microscope stage and both the sample and the ruby chip can be observed on the microscope screen using white light.

## B. EXPERIMENTAL

### I. Raman Spectrometer

The Raman and ruby fluorescence spectra were recorded on an Instruments S.A. U-1000 Ramanor spectrometer equipped with a Nachet optical microscope and interfaced to a Columbia Commandor microcomputer (see Section 3.B.I).

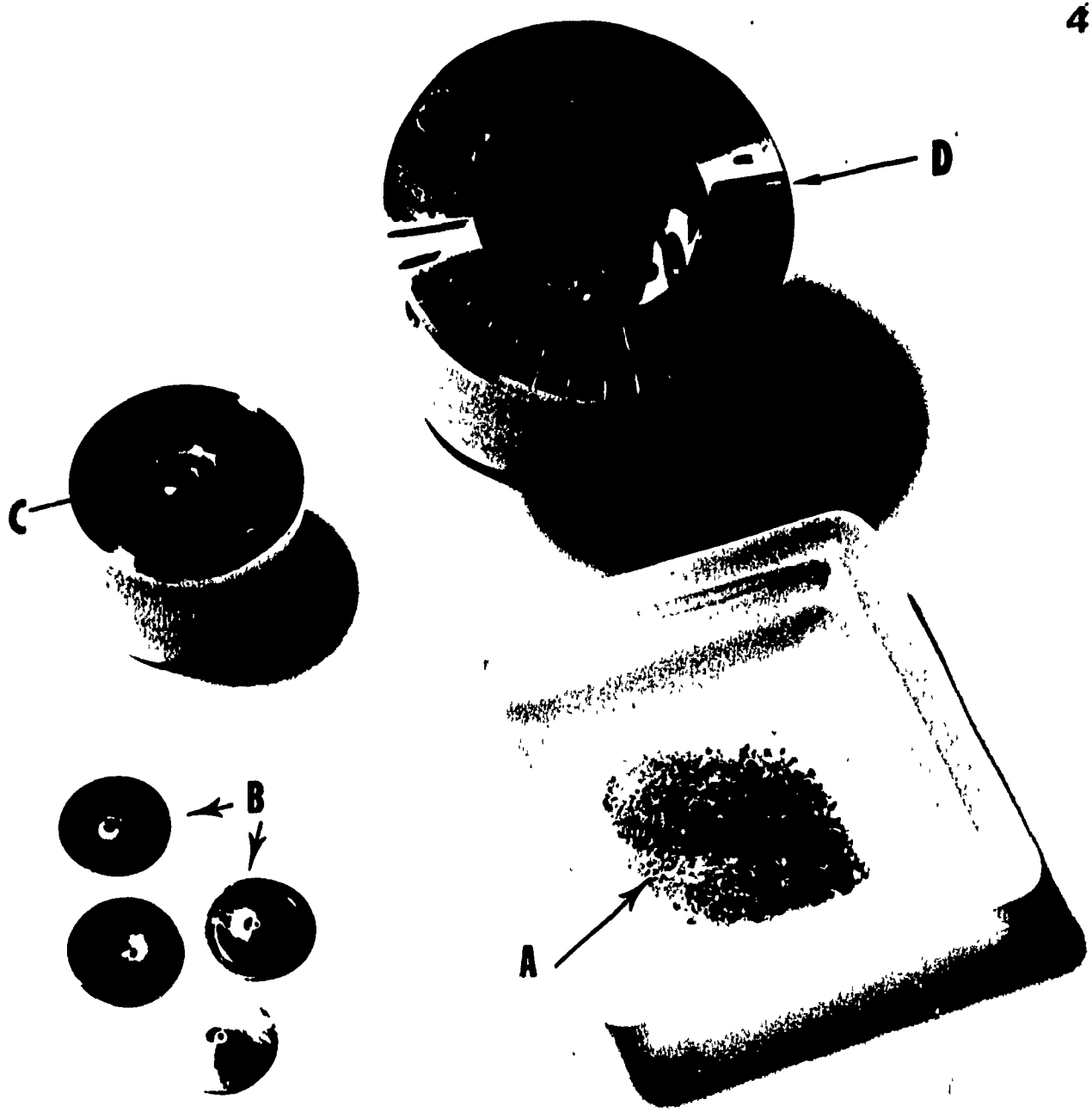


Figure 4.2 Main accessories used in pressure-Raman studies.
(a) Ruby powder
(b) Pre-compressed 200 μm thick stainless steel gaskets (200 μm hole)
(c) Diamond mounted on piston (lower diamond)
(d) Diamond mounted on cylinder (upper diamond)

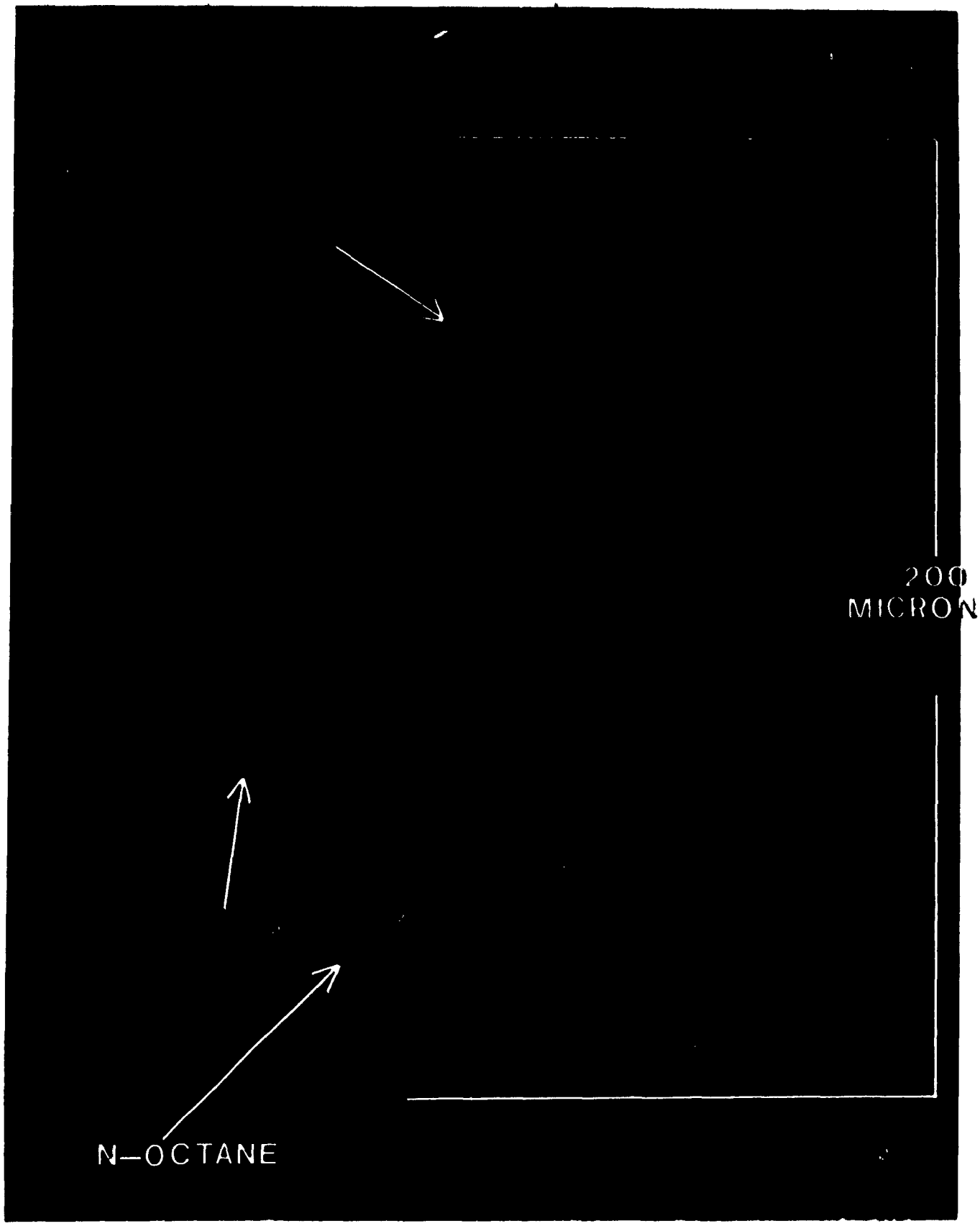


**Figure 4.3** Inside view of diamond anvil cell as seen through the microscope observation screen.

## II. Diamond Anvil Cell

A 400-μm thick gasket was mounted between the parallel surfaces of two type-IIa diamonds (whose alignment had been verified) of a diamond-anvil cell (Diacell Products, 54 Ash Tree Rd., OADBY, Leicester, LE2 5TD, England). The powdered ruby chip (internal pressure calibrant) and the sample were placed in the 300-μm hole of the stainless-steel gasket. Since the samples examined are plastic crystals at room temperature, it was difficult to introduce them into the gasket under normal conditions. This problem was surmounted by cooling the samples (with liquid nitrogen) into their ordered state, prior to placing them in the gasket. Moreover, due to the solubility of the samples studied (1-$C_{10}H_{15}Cl$, 2-$C_{10}H_{15}Cl$, and *o*-$C_2B_{10}H_{12}$), none of the conventional hydrostatic media could be used. The DAC was then mounted onto an X-Y microscope stage, and a 4X microscope objective was used to focus the laser beam onto the sample. The laser powers employed were approximately 20 mW for the sample and 10 mW for the ruby fluorescence (to avoid local heating effects). The following sequence was used when making spectral measurements at each pressure: (1) apply pressure, (2) wait 10 min to allow the sample and ruby to reach pressure equilibrium, (3) scan the ruby fluorescence, (4) scan the Raman spectrum of the sample, and (5) rescan the ruby fluorescence region. The pressure exerted on the sample was calculated using equation 4.2a.

Figure 4.4 View of the Raman microprobe coupled to the DAC.

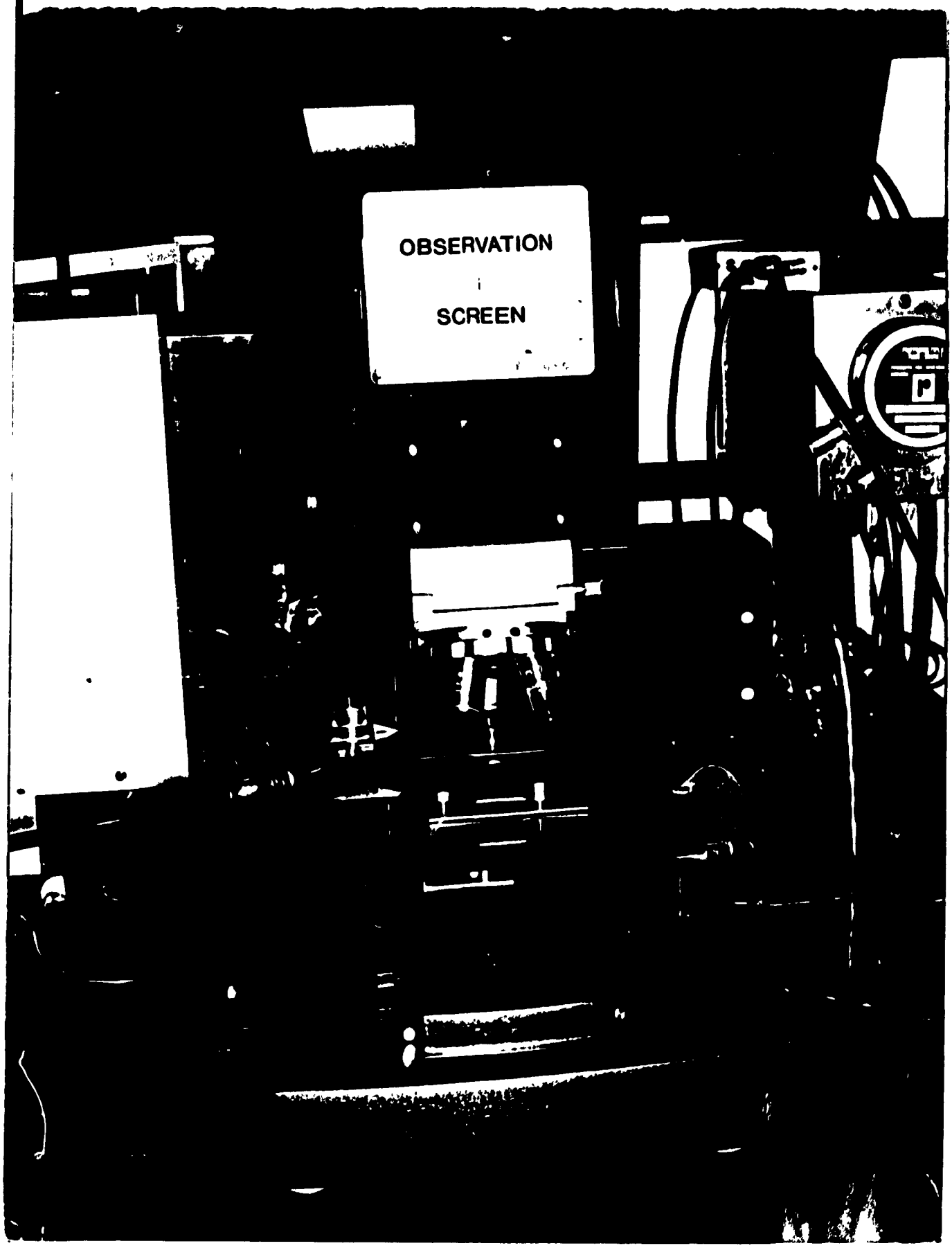

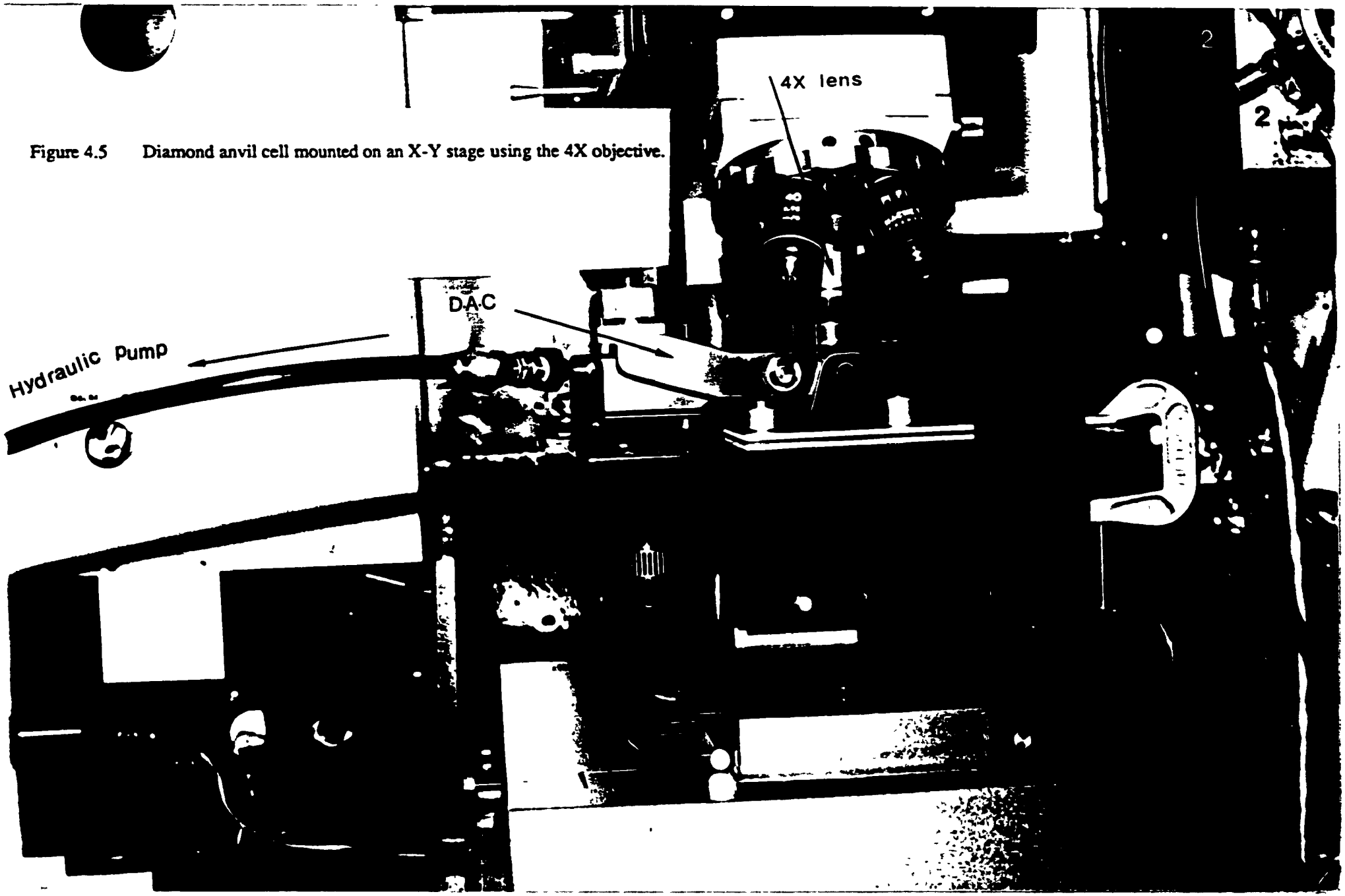


Figure 4.5 Diamond anvil cell mounted on an X-Y stage using the 4X objective.

## C. RESULTS AND DISCUSSION

### I. Results

#### *i. 1-Chloroadamantane, 1-$C_{10}H_{15}Cl$*

The pressure dependence of this compound was studied up to 55 kbar when, due to non-hydrostatic conditions, the bands became featureless. The regions studied were the ν(CH) region (3000-2800 $cm^{-1}$) and the fingerprint region (1500-400 $cm^{-1}$). However, due to the fluorescence of the diamonds only the 773 $cm^{-1}$ band could be easily monitored while the ν(CH) region was studied with difficulty. The 773 $cm^{-1}$ peak has been attributed to a mixture of the $a_1$ and e elements of the anti-symmetric $CH_2$ deformation modes (see Table 3.VI).

No dramatic changes were detected in the 773 $cm^{-1}$ region but a continuous shift towards higher wavenumber was observed. The peak went from 773 $cm^{-1}$ at ambient pressure to 800 $cm^{-1}$ at 53.6 kbar. There was also a loss of intensity which could possibly be explained by some peaks splitting into two or more components. This, however, was not observed due to the high background caused by the diamonds (see Figure 4.6). A plot of wavenumber vs. pressure for this region, Figure 4.7, does reveal that there is a change in slope occurring at ~4.6 kbar. Below 4.6 kbar the slope of the curve is 2.0 $cm^{-1}$ $kbar^{-1}$, while above, it decreases to 0.47 $cm^{-1}$ $kbar^{-1}$. The latter dν/dP value is similar to that obtained for adamantane[44] and adamantanone[45], where the values range between 0.4 and 1.0 $cm^{-1}$ $kbar^{-1}$. The low-pressure dν/dP value is much higher but it is only based on a few data points and therefore is most probably not very reliable.

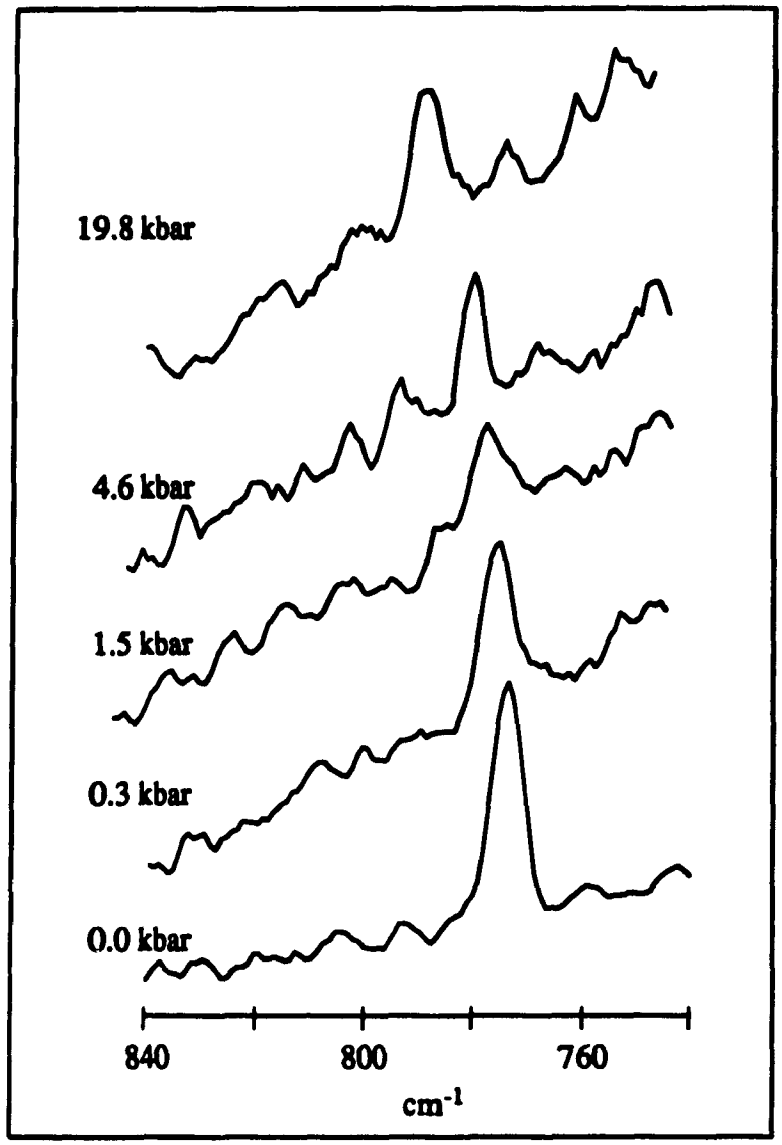


Figure 4.6 Variable-pressure Raman spectra of 1-$C_{10}H_{15}Cl$ in the 840-740 $cm^{-1}$ region.

Although more difficult to study, the 3000-2800 $cm^{-1}$ region does suggest more clearly that a phase transition occurs around 4.6 kbar. This is especially obvious from the dv/dP plot shown in Figure 4.8. The slope before and after the transition does not really change and is essentially zero if one takes into account the errors involved in peak measurements due to the broadness of the bands. There is, however, a definite shift in peak

position from 2929 $cm^{-1}$ at ambient pressure to 2940 $cm^{-1}$ at pressures greater than 4.6 kbar.

The data for both regions therefore indicate that a phase transition occurs around 4.6 kbar. This is in agreement with the number of phases found by variable temperature Raman and infrared spectroscopy as well as by DSC. Furthermore, based on the appearance of the ν(CH) region and the behaviour of the 773 $cm^{-1}$ peak, the phase produced at 4.6 kbar is the same as that formed at 245 K. This observation implies that the phase transition is dominated by a change in volume.

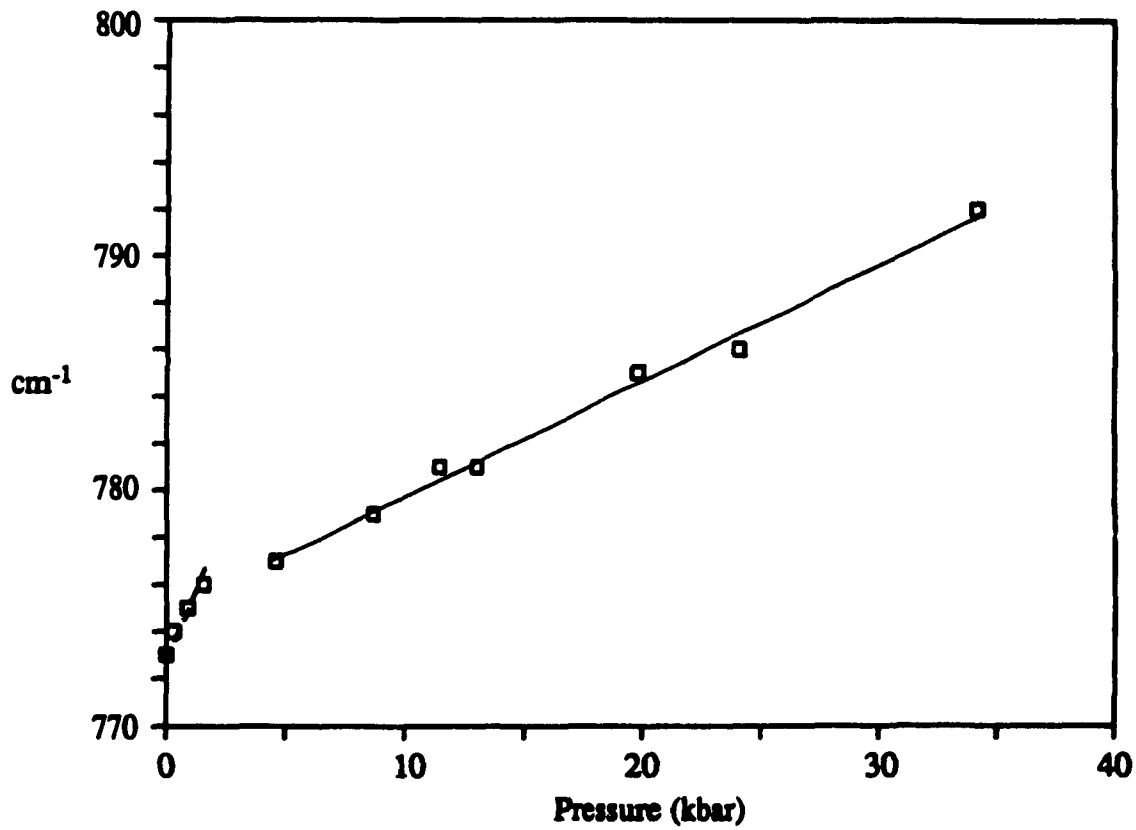


Figure 4.7 Pressure dependence of the 773 $cm^{-1}$ band of 1-$C_{10}H_{15}Cl$.

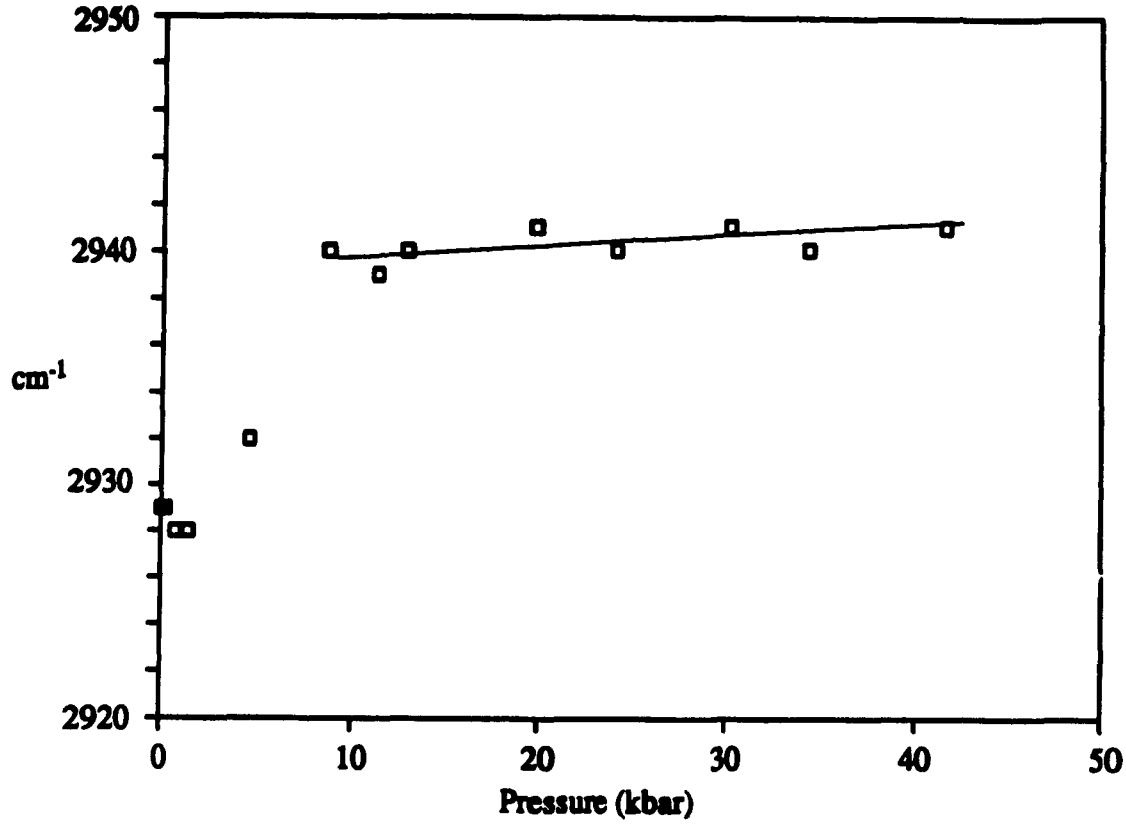


Figure 4.8 Pressure dependence of the 2929 $cm^{-1}$ ($\nu_{CH}$) band of 1-$C_{10}H_{15}Cl$.

### *ii. 2-Chloroadamantane, 2-$C_{10}H_{15}Cl$*

The compound, 2-$C_{10}H_{15}Cl$, was studied as function of pressure up to 35 kbar. Once again, the regions investigated were 3000-2800 and 1500-400 $cm^{-1}$, but due to the diamond fluorescence only the behaviour of the ν(CH) region and the 763 $cm^{-1}$ band (a', C-C stretching and C-C-C bending modes, see Table 3.VII) could be monitored with relative ease.

The ν(CH) region, Figure 4.9, proved to be the most pressure sensitive region. As had been observed by variable-temperature Raman and IR spectroscopy, the disordered phase at room temperature and ambient pressure, exhibited three featureless bands (2853,

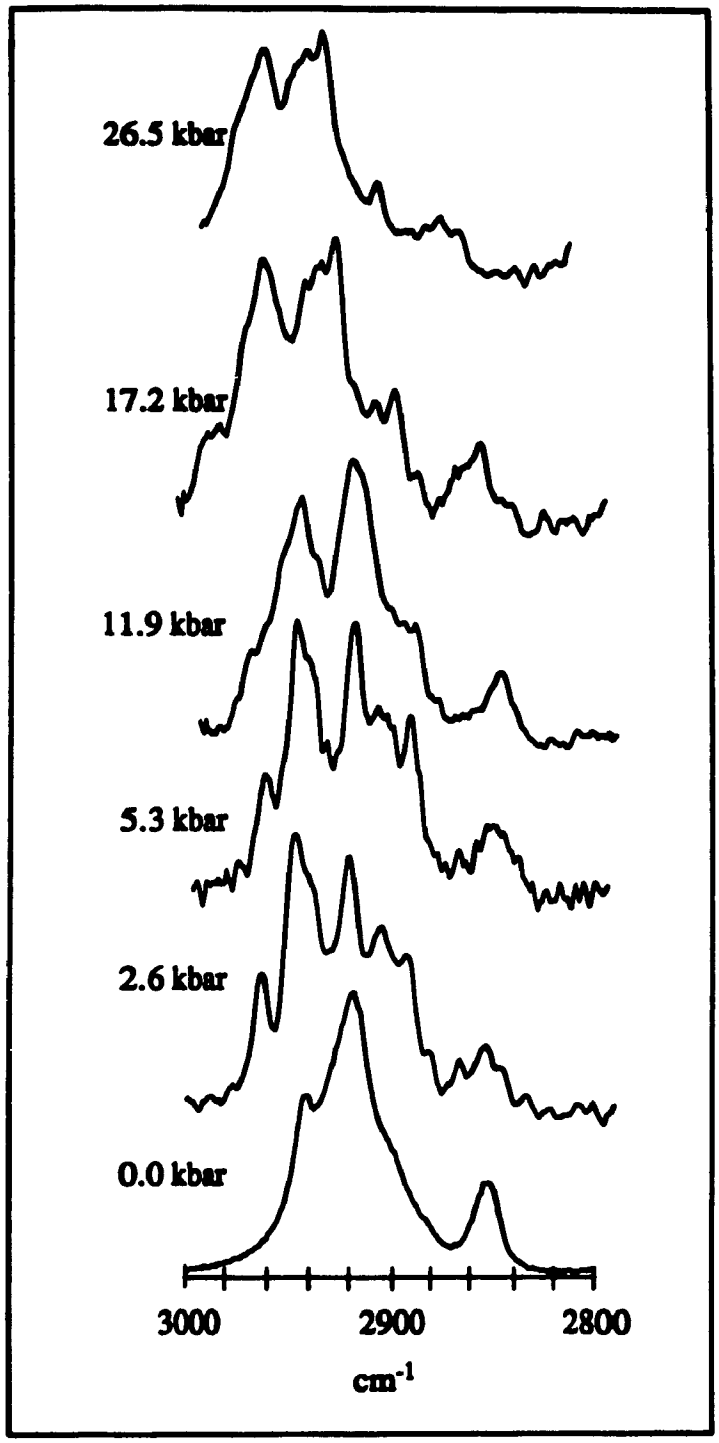


Figure 4.9 Variable-pressure Raman spectra of the CH stretching region (3000-2800 $cm^{-1}$) of 2-$C_{10}H_{15}Cl$.

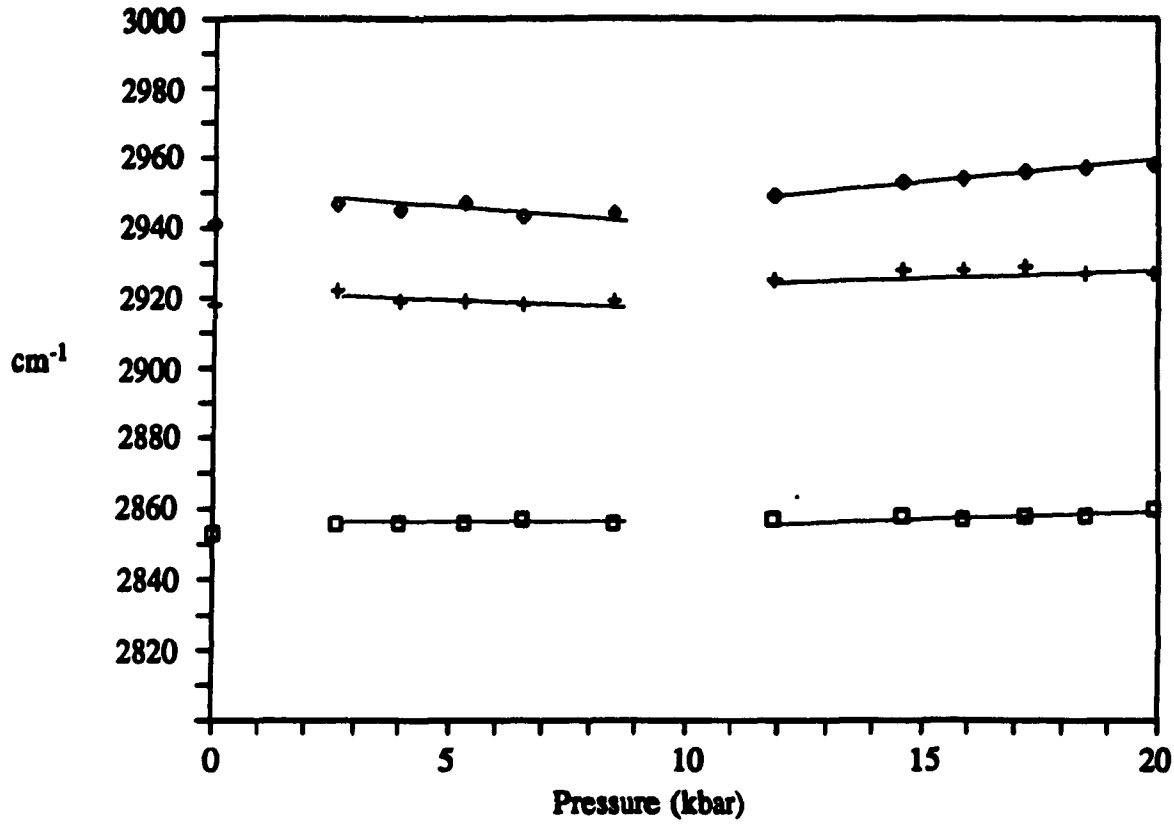


Figure 4.10 Pressure-dependences of the 2853, 2918, and 2941 $cm^{-1}$ bands of 2-chloroadamantane.

2918, and 2941 $cm^{-1}$). At 2.6 kbar, however, 10 peaks could be observed, the same number as observed at 242 K. The bands that had been observed at 0 kbar can now be seen at 2856, 2922, and 2947 $cm^{-1}$, respectively. Moreover, the band shapes at this pressure are identical to those obtained by variable-temperature Raman spectroscopy. As the pressure is increased, the bands begin to coalesce until about 11 kbar, but the previous bands are still noticeable at 2867, 2940, and 2963 $cm^{-1}$. The bands associated with this new phase do not appear to be the same as those observed by variable-temperature Raman spectroscopy. There are two possible reasons for this observation. Firstly, the phase transition involves more than a mere change in volume. Secondly, since the sample is now crystalline, non-

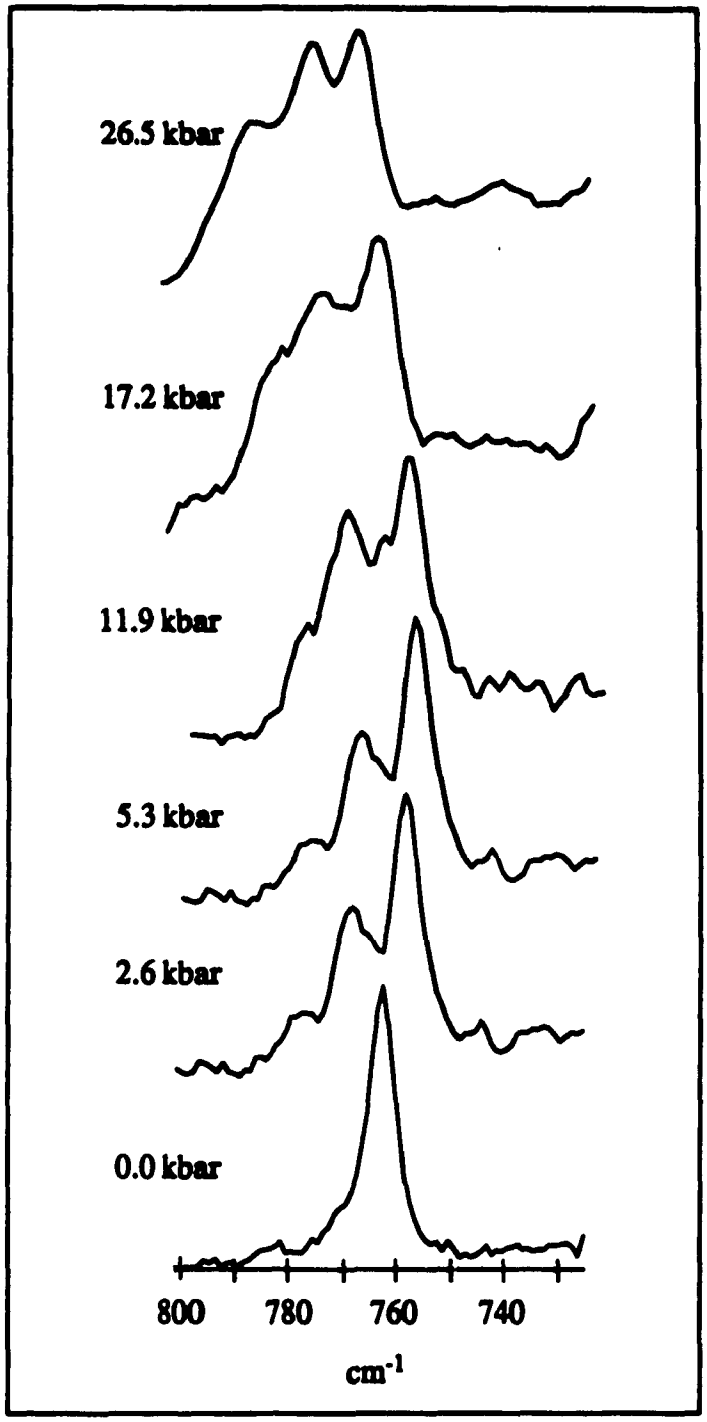


Figure 4.11 Variable-pressure Raman spectra of the a' mode of 2-$C_{10}H_{15}Cl$ (800-725 $cm^{-1}$ region).

hydrostatic effects become more important and the coalescence of the peaks is actually due to non-hydrostatic conditions. The dv/dP plot (Figure 4.10) for this region did not provide additional information except that it confirmed what had been observed from the spectra, i.e., a phase transition occurs between 0 and 2.6 kbar and another transformation takes place between 8.5 and 11.9 kbar. The calculated dv/dP values for the three major bands are 0.2, -0.9, and -0.8 $cm^{-1}$ $kbar^{-1}$ for phase II and 0.7, 0.9 and 0.7 $cm^{-1}$ $kbar^{-1}$ for phase I. The negative dv/dP values observed in phase II as well as the fact that they are smaller than those for the more ordered phase I, are rare occurrences and could possibly be attributed to some factor which inhibited the molecule from being compressed in phase II but is no longer present in phase I. No value could be obtained for phase III since only one point was measured.

The 763 $cm^{-1}$ peak (see Figure 4.11) also showed that a phase transition occurred between 0 and 2.6 kbar since it went from a singlet at 0 kbar to a doublet (759 and 768 $cm^{-1}$) at 2.6 kbar. Another change appears to take place at ~11.9 kbar, but, as can be seen from Figure 4.11, this region is quite noisy and thus it is difficult to determine whether or not a phase transformation does actually take place. Also, due to the noise, the band positions cannot be determined accurately; hence, a dv/dP plot does not reveal very much information.

### *iii. o-Carborane, o-$C_2B_{10}H_{12}$*

The effects of pressure on this compound were studied up to 70 kbar when the peaks became too broad to determine their positions with sufficient accuracy. The ν(CH) region (3100-3000 $cm^{-1}$) was investigated, but proved to be less pressure sensitive than the 840-740 $cm^{-1}$ region. Representative spectra in this latter range are shown in Figure 4.12.

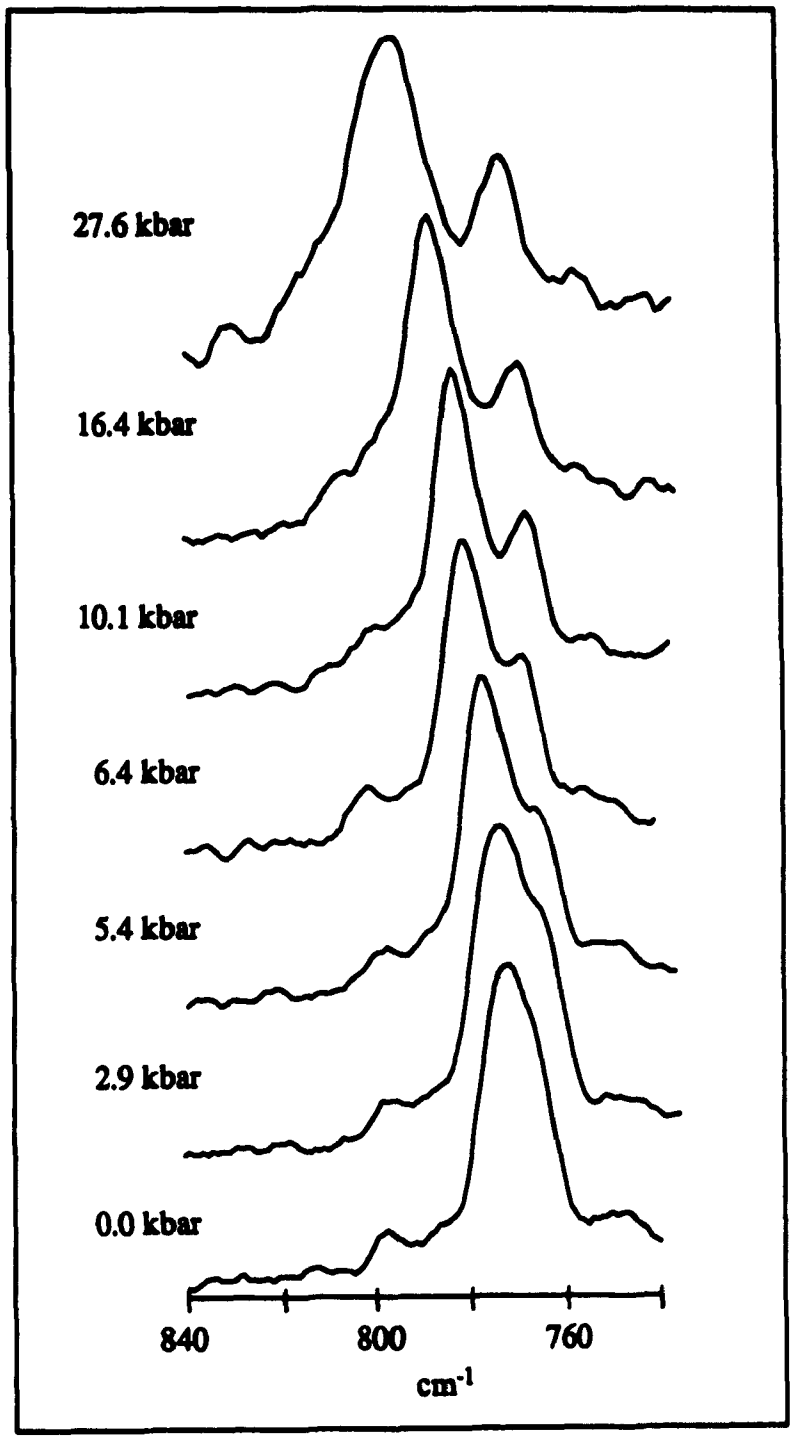


Figure 4.12 Variable-pressure Raman spectra of *o*-$C_2B_{10}H_{12}$ in the 840-740 $cm^{-1}$ region.

The 773 $cm^{-1}$ peak has been assigned to the in-phase B-B stretching mode ($a_1$) of the $C_{2v}$-symmetry icosahedral cage (see Table 3.XI).

Initially, the 773 $cm^{-1}$ peak was relatively symmetrical, with only an extremely weak shoulder at ~765 $cm^{-1}$, which developed into a separate peak at a pressure of 2.9 kbar. At 5.4 kbar, the original 773 $cm^{-1}$ peak shifted to 781 $cm^{-1}$ and the band became sharper. As the pressure was increased to 10.1 kbar, two distinct peaks could be seen, one at 771 $cm^{-1}$ and the other at 785 $cm^{-1}$. Both peaks continued to shift steadily to higher wavenumbers as the pressure was increased to 70 kbar, with the 785 $cm^{-1}$ peak being the more pressure sensitive. The pressure dependences (dv/dP) of these two bands are shown in Figure 4.13.

The data indicate that there is a phase transition in *o*-$C_2B_{10}H_{12}$ at about 10 kbar, from its disordered face-centered cubic lattice[46,47] to a more ordered, lower-symmetry lattice. The pressure coefficients for the 773 $cm^{-1}$ peak in the two phases are: 1.3 $cm^{-1}$ $kbar^{-1}$ (low-pressure phase) and 0.75 $cm^{-1}$ $kbar^{-1}$ (high-pressure phase). The pressure coefficient for the peak originating from the 765 $cm^{-1}$ shoulder and appearing at high pressure is 0.37 $cm^{-1}$ $kbar^{-1}$. These dv/dP values are smaller than those obtained for the cesium dodecahydroborate salt, $Cs_2[B_{12}H_{12}]$ (1.6 and 1.9 $cm^{-1}$ $kbar^{-1}$ for the low-pressure phase and 2.1 and 2.3 $cm^{-1}$ $kbar^{-1}$ for the high-pressure phase)[42], but are in the same range as those for smaller caged hydrocarbons, e.g., adamantane[44] ($C_{10}H_{16}$) and adamantanone[45] ($C_{10}H_{14}O$), 0.4-1.0 $cm^{-1}$ $kbar^{-1}$. The existence of a distinct discontinuity in the dv/dP plot for *o*-carborane suggests that the observed phase transition is first order.

Although there was no definitive spectral evidence for any further phase-transitions between 10 and 70 kbar, even when the sample was allowed to stand at 40 kbar for five days, there is a hint of a change in the dv/dP slope at about 35 kbar (Figure 4.13). This may possibly be due to either the II → III or the II → IV phase transformation and such a transition would be second-order. However, due to the uncertainty in peak position at

pressures greater than 35 kbar, it is difficult to claim that a phase transition does occur, especially since the spectral data did not reveal any major changes at higher pressures.

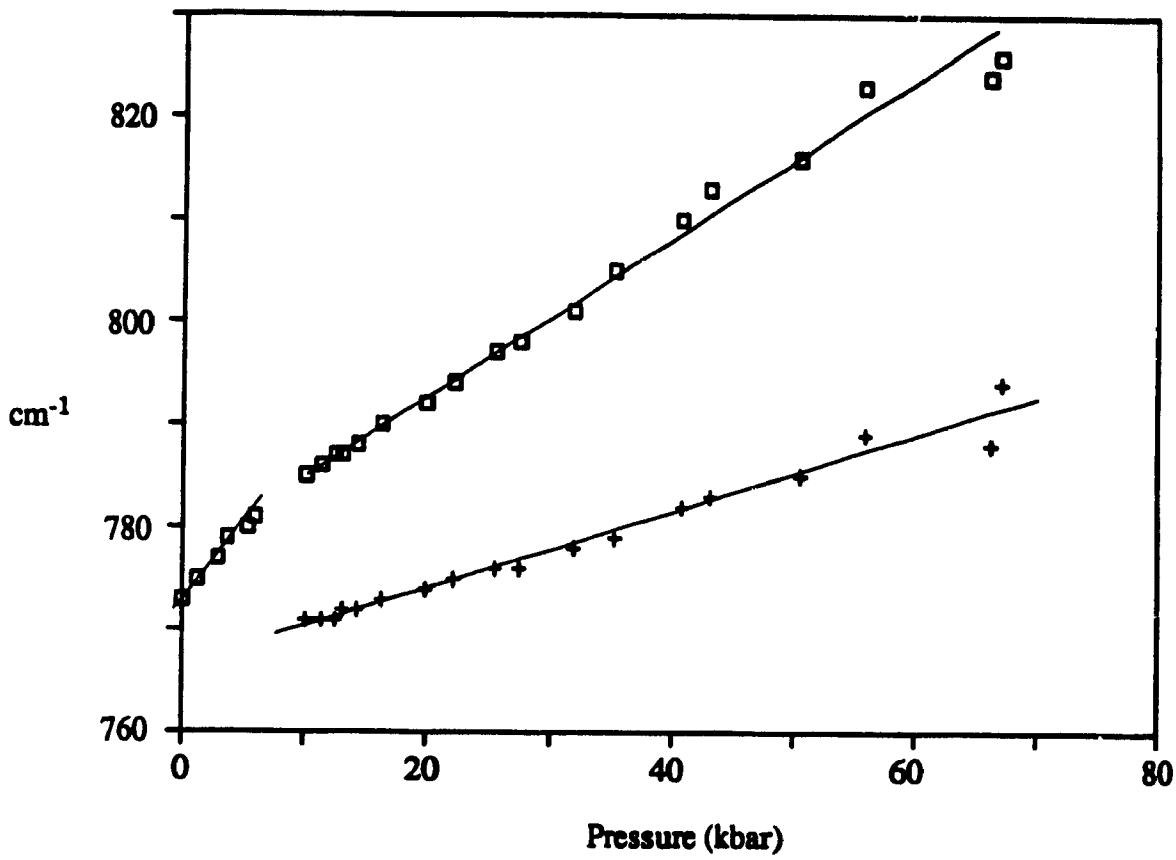


Figure 4.13 Pressure dependences of the 773 $cm^{-1}$ and 765 $cm^{-1}$ bands of *o*-carborane.

## II. Discussion

The volume dependence of a given vibrational frequency is related to the dimensionless quantity known as the mode Grüneisen parameter, $\gamma_i$, which is given by eq. [4.5a]:

$$\gamma_i = -d(\ln\nu_i)/d(\ln V) \qquad [4.5a]$$

or

$$\gamma_i = (d\nu_i/\nu_i)(-V/dV) \qquad [4.5b]$$

where $\nu_i$ is the position of a given vibration at ambient pressure, and V is the volume. Since the bulk modulus, B, is defined as:

$$B = 1/\kappa = (-V/dV)dP \qquad [4.6]$$

where $\kappa$ is the compressibility of the molecule, and P is the pressure, it is possible to re-write eq. [4.5b] as,

$$\gamma_i = (1/\{\kappa\nu_i\})(d\nu_i/dP) \qquad [4.7]$$

The value of $\gamma_i$ is usually positive since the vibrational frequency generally increases as the pressure is increased and as the name implies, i.e., *mode*, each vibration can have different Grüneisen parameters. Moreover, it has been found that for molecular crystals the external modes have values, $2 < \gamma_i < 5$, while for the internal modes, $0.02 < \gamma_i < 0.1$.[10-12] The much smaller values of the mode Grüneisen parameter for internal modes has been attributed to the fact that the large volume changes, observed as a function of pressure are caused by the contraction of one specific intermolecular bond (lattice mode) having a certain force constant while the intramolecular bonds are barely affected by changes in pressure because many other factors have to be taken into account, such as different types of bond as well as

**Table 4.I** Pressure dependences for 1-$C_{10}H_{15}Cl$, 2-$C_{10}H_{15}Cl$, and *o*-$C_2B_{10}H_{12}$

| Compound | Phase | $\nu^o_i$ $cm^{-1}$ | $d\nu_i/dP$ $cm^{-1}$ $kbar^{-1}$ | $\gamma_i$ |
|---|---|---|---|---|
| 1-$C_{10}H_{15}Cl$ | | 773 | | |
| | I | | 0.47 | 0.2 |
| | II | | 2.0 | 0.06 |
| 2-$C_{10}H_{15}Cl$ | | 2853 | | |
| | I | | 0.7 | 0.03 |
| | II | | 0.2 | 0.008 |
| | III | | * | * |
| | | 2918 | | |
| | I | | 0.9 | 0.03 |
| | II | | -0.9 | -0.3 |
| | III | | * | * |
| | | 2941 | | |
| | I | | 0.7 | 0.02 |
| | II | | -0.8 | -0.02 |
| | III | | * | * |
| *o*-$C_2B_{10}H_{12}$ | | 773 | | |
| | I | | 0.37 | 0.05 |
| | II | | 1.3 | 0.2 |

* No data available.

bond-bending and bond-stretching vibrations.[10] Although the compressibilities of *o*-$C_2B_{10}H_{12}$, 1-$C_{10}H_{15}Cl$, and 2-$C_{10}H_{15}Cl$ are not known, molecular crystals are known to have values of $\kappa$ in the range of 0.01 $kbar^{-1}$.[48] Assuming compressibility values of 0.01 $kbar^{-1}$ for the above three compounds, then the $\gamma_i$ values can be calculated. In the case of 1-$C_{10}H_{15}Cl$, $\gamma$(773 $cm^{-1}$) for the low-pressure phase (phase II) is 0.2 while that of the

high-pressure phase, phase I, is 0.06. The $\gamma(773\ cm^{-1})$ value for *o*-$C_2B_{10}H_{12}$, was found to be 0.2 in the low-pressure phase and 0.05 in the high-pressure one. The values obtained for 2-$C_{10}H_{15}Cl$ are peculiar in that the phase II Grüneisen parameters for the 2918 and 2941 $cm^{-1}$ peaks are negative. This situation arises because the dv/dP values are also negative. The calculated Grüneisen parameters for phase II are 0.008 for $\gamma(2853\ cm^{-1})$, -0.03 for $\gamma(2918\ cm^{-1})$ and -0.02 for $\gamma(2941\ cm^{-1})$. In phase I, these values become 0.03, 0.03, and 0.02 for $\gamma(2853\ cm^{-1})$, $\gamma(2918\ cm^{-1})$, and $\gamma(2941\ cm^{-1})$, respectively.

**Table 4.II** Experimental data for the temperature- and pressure-induced phase transitions in 1-$C_{10}H_{15}Cl$, 2-$C_{10}H_{15}Cl$, and *o*-$C_2B_{10}H_{12}$

| | Transition | | |
|---|---|---|---|
| | DSC at 1.01 bar | | DAC at 298 K |
| Compound and Transition | Temperature K | ΔH kJ $mol^{-1}$ | Pressure kbar |
| 1-$C_{10}H_{15}Cl$ | | | |
| Phase I→II | 245 | 5.35 | 4.6 |
| 2-$C_{10}H_{15}Cl$ | | | |
| Phase I→II | 227 | 0.470 | 2.6 |
| Phase II→III | 242 | 8.31 | 11 |
| *o*-$C_2B_{10}H_{12}$ | | | |
| Phase I→II | 274 | 3.88 | 10 |

From equation 4.7, it can be seen that the compressibility of a molecule is directly proportional to dv/dP. It is therefore possible to state that, as expected, based on the vibrational data, the low-pressure, disordered phases of both *o*-$C_2B_{10}H_{12}$ and 1-$C_{10}H_{15}Cl$ are more compressible than the ordered, high-pressure phases. Surprisingly, however, this is not the case for 2-$C_{10}H_{15}Cl$, where phase II appears to be less compressible than phase I. As had previously been pointed out, it is possible that even though phase II is less ordered than phase I, there are certain factors present which restrict its movements. In phase I, these obstacles are removed and thus, a different compression mechanism is present; hence, phase I is more compressible than phase II.[49-51] This higher value of dv/dP for the ordered phase had also been observed by Harvey *et al.* for 2-$C_{10}H_{14}O$.[45] They proposed that the increase in dv/dP values for the ordered phase relative to the disordered phase was due to an increase in crystal density. This, however, is not likely since it is to be expected that an increase in density should yield a less compressible material and if the values of dv/dP increase than so should the compressibility. It is therefore not surprising that Hara *et al.* observed this situation when they studied the compressibility and density of adamantane, 2-adamantanone, and 2-methyladamantane.[52] Hazen and co-workers[51], have argued that the increase in compressibility found in some molecular solids could also be due a decrease in symmetry and that what is actually observed is possibly a distortional phase transition. This latter argument might very well be applicable in our case since, as was previously noted, phase I observed by pressure-Raman spectroscopy is not the same as that observed by variable-temperature Raman spectroscopy.

## D. REFERENCES


(1) C. E. Weir, E. R. Lippincott, A. Van Valkenburg, E. N. Bunting, *J. Res. Natl. Bur. Stand. (U.S.)*, **A63**, 55 (1959).

(2) P. T. T. Wong, D. D. Klug, *Appl. Spectrosc.*, **37**, 284 (1983).

(3) D. M. Adams, S. J. Payne, K. Martin, *Appl. Spectrosc.*, **27**, 377 (1973).

(4) K. R. Hirsch, W. B. Holzapfel, *Rev. Sci. Instrum.*, **52**, 52 (1981).

(5) A. Jayaraman, *Rev. Mod. Phys.*, **55**, 65 (1983).

(6) A. Jayaraman, *J. Phys., Colloq.*, **C8**, 355 (1984).

(7) A. Jayaraman, *Physica B+C*, **139-140**, 464 (1986).

(8) A. Jayaraman, *Trans. Indian Inst. Met.*, **39**, 187 (1986).

(9) A. Jayaraman, *Indian J. Pure Appl. Phys.*, **26**, 163 (1988).

(10) W. F. Sherman, G. R. Wilkinson, "Raman and Infrared Studies of Crystals at Variable Pressure and Temperature" in *Advances in Infrared and Raman Spectroscopy*, vol. 6, Eds., R. J. H. Clark and R. E. Hester, Heyden and Son, Ltd., London, 1980.

(11) J. R. Ferraro, *Vibrational Spectroscopy at High External Pressures: The Diamond Anvil Cell*, Academic Press, Inc., U.S.A., 1984.

(12) W. F. Sherman, *J. Mol. Struct.*, **113**, 101 (1984).

(13) P. T. T. Wong, "Vibrational Spectroscopy Under High Pressures", in *Vibrational Spectra and Structure: A Series of Advances*, Vol. 16, Ed., J. R. Durig, Elsevier, New York, 1987.

(14) J. R. Ferraro, L. J. Basile, *Appl. Spectrosc.*, **28**, 505 (1974).

(15) P. T. T. Wong, E. Whalley, *Rev. Sci. Instrum.*, **45**, 904 (1974).

(16) P. T. T. Wong, D. J. Moffatt, *Appl. Spectrosc.*, **38**, 599 (1984).

(17) D. M. Adams and S. K. Sharma, *J. Phys. E.:Sci. Instrum.*, **10**, 10 (1977).

(18) H. Kawamura, K. Tachikawa, O. Shimomura, *Rev. Sci. Instrum.*, **56**, 1903 (1985).

(19) A. Van Valkenburg, *Ind. Diamond Rev.*, **24**, 17 (1964).

(20) G. J. Piermarini, S. Block, and J. D. Barnett, *J. Appl. Phys.*, **44**, 5377 (1973).

(21) I. Fujishiro, G. J. Piermarini, S. Block, R. G. Munro, *High Pressure in Research in Industry: 8th AIRAPT Conf.*, **2**, 608 (1982).

(22) I. L. Spain, J. Paauwe, "The measurement of Pressure and Temperature in High Pressure Systems", in *High Pressure Technology*, Vol. I, eds., I. L. Spain, J. Paauwe, Marcel Dekker, Inc., New York, 1977.

(23) R. A. Forman, G. J. Piermarini, J. D. Barnett, S. Block, *Science*, **176**, 284 (1972).

(24) D. M. Adams, R. Appleby, S. K. Sharma, *J. Phys. E.: Sci. Instrum.*, **9**, 1140 (1976).

(25) G. J. Piermarini, S. Block, and R. A. Forman, *J. Appl. Phys.*, **46**, 2774 (1975).

(26) G. J. Piermarini, S. Block, *Rev. Sci. Instrum.*, **46**, 973 (1975).

(27) H. K. Mao, P. M. Bell, *Science*, **191**, 851 (1976).

(28) H. K. Mao, P. M. Bell, *Science*, **200**, 1145 (1978).

(29) H. K. Mao, P. M. Bell, J. W. Shaner, D. J. Steinberg, *J. Appl. Phys.*, **49**, 3276 (1978).

(30) H. K. Mao, P. M. Bell, *Science*, **203**, 1004 (1979).

(31) H. E. King, C. T. Prewitt, *Rev. Sci. Instrum.*, **51**, 1073 (1980).

(32) S. L. Wunder, P. E. Schoen, *J. Appl. Phys.*, **52**, 3772 (1981).

(33) B. A. Weinstein, *Rev. Sci. Instrum.*, **57**, 910 (1986)

(34) D. D. Klug, E. Whalley, *Rev. Sci. Instrum.*, **54**, 1205 (1983).

(35) P. T. T. Wong, D. J. Moffat, F. L. Baudais, *Appl. Spectrosc.*, **39**, 733 (1985).

(36) D. J. Gardiner, M. Bowden, J. Daymond, A. C. Gorvin, M. P. Dare-Edwards, *Appl. Spectrosc.*, **38**, 282 (1984).

(37) S. K. Sharma, H. K. Mao, P. M. Bell, J. A. Xu, *J. Raman Spectrosc.*, **16**, 350 (1985).

(38) H. Boppart, J. Van Straaten, I. F. Silvera, *Phys. Rev. B.*, **32**, 1423 (1985).

(39) M. Hanfland, K. Syassen, S. Fahy, S. G. Louie, M. L. Cohen, *Physica*, **139-140B**, 516 (1986).

(40) C. J. Sandroff, L. A. Farrow, *Chem. Phys. Lett.*, **130**, 458 (1986).

(41) L. A. Farrow, C. J. Sandroff, *Microbeam Analysis-1986*, Eds., A. D. Romig and W. F. Chambers, p. 22 (1986).

(42) V. Benham, G. Lord, I. S. Butler, D. F. R. Gilson, *Appl. Spectrosc.*, **41**, 915 (1987).

(43) P. Gillet, J. M. Malezieux, M. C. Dhamelincourt, *Bull. Minéral.*, **111**, 1 (1988).

(44) G. Burns, F. H. Dacol, B. Weber, *Solid. State Commun.*, **32**, 151 (1979).

(45) P. D. Harvey, I. S. Butler, D. F. R. Gilson, P. T. T. Wong, *J. Phys. Chem.*, **90**, 4546 (1986).

(46) R. H. Baughmann, *J. Chem. Phys.*, **53**, 3781 (1970).

(47) T. J. Klingen, J. H. Kindsvater, *Mol. Cryst. Liq. Cryst*, **26**, 365 (1974).

(48) D. M. Adams, I. O. C. Ekejiuba, *J. Chem. Phys.*, **77**, 4793 (1982).

(49) J. E. Schirber, B. Morosin, *Phys. Rev. Lett.*, **42**, 1485 (1979).

(50) J. E. Schirber, B. Morosin, R. W. Alkire, A. C. Lawson, P. J. Vergamini, *Phys. Rev. B: Condens. Matter*, **29**, 4150 (1984).

(51) R. M. Hazen, T. C. Hoering, A. M. Hofmeister, *J. Phys. Chem.*, **91**, 5042 (1987).

(52) K. Hara, Y. Katou, J. Osugi, *Bull. Chem. Soc., Jpn.*, **54**, 687 (1981).

# CHAPTER 5
# SUMMARY
# AND
# CONTRIBUTIONS TO KNOWLEDGE

(1) The solid-solid phase transformations of various 1- and 2-haloadamantane derivatives have been investigated by differential scanning calorimetry and variable-temperature vibrational spectroscopy. Only one phase transition was found for 1-chloro- and 2-bromoadamantane, while two solid-solid phase changes were detected for the related 1-bromo- and 2-chloroadamantane derivatives. All four compounds were established as being orientationally-disordered and assignments have been proposed for the vibrational spectra of all the phases.

(2) The effect of cycling 2-adamantanone through its phase transition has been studied by variable-temperature IR and Raman spectroscopy. The low-temperature phase after cycling is more ordered than that prior to cycling, while the high-temperature phase is unchanged by cycling.

(3) The phase transitions of the caged hydrocarbons, bicyclononanone and oxanorbornane, were studied by DSC, variable-temperature -IR and -Raman spectroscopy. While bicyclononanone only exhibits one phase transition, oxanorbornane has three such transformations. In the case of the latter, it was shown that the spectra of the liquid and plastic phases are essentially the same. It was also shown that oxanorbornane has a metastable phase.

(4) A method has been developed to study the phase transitions of plastic crystals by variable-pressure micro-raman spectroscopy. *o*-Carborane, 1-chloroadamantane, and 2-chloroadamantane were studied with the aid of this technique; one phase transition was found for *o*-carborane at 10 kbar, one phase transition were observed for 1-chloroadamantane at 4.6 kbar and two phase transformations were found for 2-chloroadamantane at 2.6 and 11 kbar. In all three cases, the phases are believed to be isostructural with the phases detected by variable-temperature Raman spectroscopy, except possibly for the 11 kbar phase transformation for 2-chloroadamantane.

(5) A calibration curve has been constructed which relates the resolution of the I.S.A. U-1000 Raman spectrometer to both the slit-width and the wavelength of the excitation line.

(6) A cryostat has been designed and constructed for low-temperature FT-IR spectroscopy which has the advantage of having a very small volume and therefore requiring minimal evacuation time. This allows it to be used on volatile liquids, such as oxanorbornane.

# CHAPTER 6
# SUGGESTIONS FOR FUTURE WORK

## I. High-Pressure Raman Spectroscopy

One of the major problems encountered in the pressure-Raman spectroscopic studies described in this thesis was the diamond fluorescence. Although type II diamonds were used, the fluorescence was still sufficiently intense to obscure many of the peaks and even precluded us from studying the lattice region. The latter in itself was disappointing because the Grüneisen parameter really applies only to that region. It would therefore be valuable to eliminate the fluorescence problem. Suggestions are given below that could possibly eliminate or at least reduce the fluorescence effects:

(a) Using the macrochamber rather than the microscope will permit the excitation of the sample with more laser power. This will be necessary since the light collection is less efficient than when using the microscope. The particular advantage, however, will be that the steering optics for the macrochamber are more easily aligned than the microscope and hence, more signal should be captured. Some preliminary work has been done with the help of Mr. A. Kluck (McGill University) to enable the DAC to be mounted on the same X-Y-Z stage as used for the cryostat. One of the difficulties which is yet to be surmounted is the need to bring the DAC closer to the mirror chip while at the same time maintaining X-Y-Z freedom for both the mirror and DAC (see Figure 6.1).

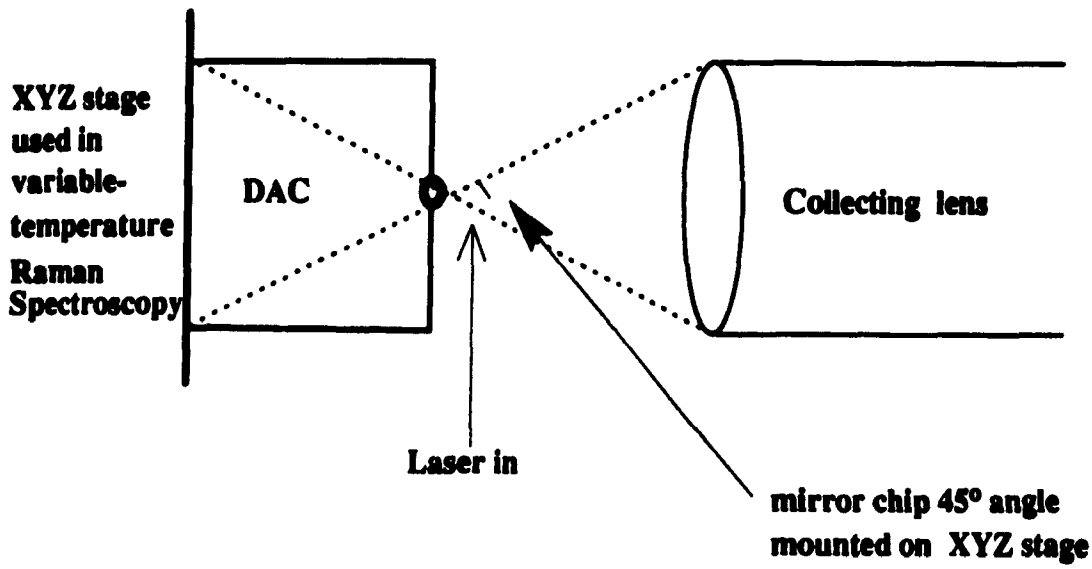


**Top view of macrochamber**

Figure 6.1 Proposed set-up for DAC in macrochamber.

(b) The use of longer wavelengths such as those available in the krypton-ion laser should also reduce the fluorescence. As mentioned previously, Adams *et al.*[1] have found that the 632.8 nm He-Ne line permitted the use of type II diamonds in the 4000 to 0 $cm^{-1}$ region. Schoen and co-workers[2] have discovered that the 752.8 nm line of the $Kr^+$ laser greatly reduces diamond fluorescence and has allowed poor scatterers to be studied by pressure-Raman spectroscopy. This approach would probably still require the use of the microscope since these same researchers have also found that using the 647.1 nm $Kr^+$ line generated interference from the ruby fluorescence.

(c) Gardiner and his colleagues[3] have used a 40X long-range (18 mm) microscope objective coupled to a DAC in order to study liquids and were successful in reducing the fluorescence caused by type II diamonds, even when using the 514.5 nm line of the $Ar^+$ ion laser for excitation. An 80X objective should be even better since a reduction in fluorescence could be obtained by focusing the beam directly on to the sample rather than a combination of diamond and sample.

(d) Using type I diamonds should dramatically reduce fluorescence; however, this would prevent the same cell from being used in pressure-IR spectroscopy.

## II. DSC-FTIR AND -RAMAN SPECTROSCOPY

The data presented in this thesis were obtained using DSC, variable-temperature FT-IR spectroscopy (where the sample was in a KBr matrix), and variable-temperature Raman spectroscopy where the sample was studied in a capillary tube. Can we be absolutely sure, however, that data obtained from the three methods are for the same phase? Based on the observations for the compounds in this thesis, the answer is yes. However, it would be a great deal simpler if we could simultaneously obtain the DSC and vibrational-temperature Raman or IR data, i.e., use the DSC apparatus as a cryostat. The following are therefore proposed as possible solutions to this problem:

(a) Variable-temperature diffuse reflectance IR could be used. Although this would not solve the simultaneous acquisition of the DSC data, it would at least permit us to obtain the IR and Raman data under similar conditions. In other words, we would be capable of studying samples in their "as is" form without subjecting them to any form of sample preparation.

(b) Mirabella and Shankernayaranan[4] have recently built a DSC-FTIR which requires a microscope; this is an expensive proposition that is useful above ambient temperature only. A less expensive option would be to try to couple a DSC instrument with a diffuse reflectance unit to obtain variable-temperature -IR measurements. With the progress currently being made in fibre optics, it might be possible to bring the signal to the IR detector with the aid of such optics.

(c) As far as DSC-Raman is concerned, it would actually be an easier method than DSC-IR since we would have access to both a macrochamber and a microprobe. Use of the micro-raman technique would actually be quite simple since all that would be required is a long-view objective for the microprobe and a glass cover for the DSC chamber through which nitrogen gas could flow. The same system could be used in the macrochamber by simply using a similar approach to that proposed for pressure Raman spectroscopy

## III. Baselines as Phase Detectors

If one looks at uncorrected IR baselines, it appears to be possible to detect the presence of different phases. This should not be surprising since it can easily be imagined that as molecules become more ordered, more scattering will occur thereby changing the baselines. The reason for specifying uncorrected baselines is merely due to the fact that with the advent of FT-IR spectroscopy, baseline correction is very common. The function of baseline correction is to correct using zero absorbance as the minimum value, thus destroying baseline effects due to phase changes.

## III. Variable-Temperature-Variable-Pressure- IR and Raman Spectroscopy

The studies using variable-pressure IR and Raman spectroscopy at ambient temperature, or variable-temperature IR and Raman spectroscopy, limit us to the analysis of just two points on a phase diagram. In other words, we know, for example, that a given phase transformation occurs at 240 K and 1 bar or 295 K and 10 000 bar. To better characterize the materials it would be preferable to vary both temperature and pressure simultaneously, i.e., vary the pressure, then vary the temperature at pressure P, and, in another experiment, vary the temperature and then study the phase transition as a function of pressure at temperature T.

## IV. References

(1) D. M. Adams, S. J. Payne, K. Martin, *Appl. Spectrosc.*, **27**, 377 (1973)

(2) P. E. Schoen, J. M. Schnur, J. P. Sheridan, *Appl. Spectrosc.*, **31**, 337 (1977)

(3) D. J. Gardiner, M. Bowden, J. Daymond, A. C. Gorvin, M. P. Dare-Edwards, *Appl. Spectrosc.*, **38**, 282 (1984)

(4) F. M. Mirabella, M. J. Shankernarayanan, *Microbeam Analysis-1988*, D. E. Newbury, Ed., San Francisco Press, San Francisco, p. 233 (1988)